Title
GPR35 on Vagal Afferent Neurons as a Peripheral Drug Target for Treating Diet-Induced Obesity

Author
Zumpano-Brucia, Danielle Lorena

Publication Date
2023

Peer reviewed|Thesis/dissertation

GPR35 on Vagal Afferent Neurons as a Peripheral Drug Target
for Treating Diet-Induced Obesity

By

DANIELLE LORENA ZUMPANO-BRUCIA
DISSERTATION

Submitted in partial satisfaction of the requirements for the degree of

DOCTOR OF PHILOSOPHY

in

Molecular, Cellular, and Integrative Physiology

in the

OFFICE OF GRADUATE STUDIES

of the

UNIVERSITY OF CALIFORNIA

DAVIS

Approved:

Helen Raybould, Chair

Bethany Cummings

Erkin Şeker

Committee in Charge

2023

Acknowledgments

My research and dissertation would not have been possible without the support and encouragement of my mentors, family, friends, and especially my husband.

Thank you to my advisor, Helen Raybould, for her thoughtful guidance and mentorship over the years. I am sincerely grateful for her patience and for guiding my development as a scientist.

My research would not have been accomplished without the physical assistance and mental support of the Raybould lab: the fearless Michael Goodson, Wendie Vang, Trina Knotts, Kuei-Pin Huang, Sunhye Lee, Amy Ehrlich, Annabella Rodriguez, Lauren Farley, and Julia and Angela deJesus. Thank you to my diversity mentor, Mariana Barboza-Gardner, for your confidence in me and for helping me reach the impossible.

Thank you to my thesis committee members, Drs. Bethany Cummings and Erkin Şeker, for your careful guidance and support. Thank you for making me a better scientist.

Thank you to the writing communities at UC Davis, including program leaders, Kirsten Asher (Got an F) and Marit Macarthur (UWP 298) for guiding me in my writing journey. Thank you for helping me identify and overcome my creative barriers.

Thank you to the entire team at the UC Davis Innovation Institute for Food and Health for your mentorship, support, and advocacy. Thank you to Dr. Emily Aston and Brian Frank for your invaluable mentorship in the world of venture capital.

Thank you to Connie Champagne and Heather Lawrence and the UC Davis Biology Undergraduate Scholars Program (BUSP) for granting me professional development opportunities in my larval stage to pursue scientific research. When I trace back every accomplishment in the past decade, you are at the center of the nexus, along with the honorable Barbara Horwitz. Thank you all for believing in me, especially when I did not.

Thank you to my parents for your support, encouragement, and prayers from my very first steps, to each milestone, and now to this finish line. Thank you to my mother for her quiet strength, wisdom, and fierce protection. I cannot thank you enough for your walks of Jericho and for re-lighting my lamp whenever I lost my way. Thank you to my father for planting the seed of my passion for chemistry and physiology. Thank you for showing me how to maintain my focus in the midst of the storm, my hope in the tumult, and joy in every battle.

Thank you to my chiropractor (seriously), Dr. David Atkinson, for fixing me when I was physically broken and for keeping me going for all these years. I told you that I would thank you after I thanked my parents. Thank you for your support all these years.

Thank you to my grandparents. You were my best friends growing up and have gently shepherded me through the most tender times of my life. It has been an honor to help care for you as you enter delicate times of your own. I will never regret the time I took to honor you and care for you while you were present.

Thank you to my Uncle Greg and Auntie Franca for your relentless encouragement and for opening your home to Eric and me. Thank you to Auntie Betsey and Uncle Rod for your prayers and encouraging words throughout this process. Thank you to my Auntie Sandy and Uncle David for motivating me to pursue my curiosities from the very beginning. Thank you to my dear great Auntie Janet and Uncle Bob for fanning the flames of my fascination with life.

Thank you to my siblings, Mike and Omega, for preparing me for some of the most challenging hurdles in my life and for always being there to strengthen and encourage me. Thank you for giving me perspective and for keeping me humble.

Thank you to my writing partner, Sudikshya Bhandari for walking with me through the many creative battles and for your encouragement every single day. Thank you for helping me prune ideas. Thank you to UC Davis GradPathways for catalyzing this partnership.

Thank you to my sister, Erica Dellenbach, for your fire spirit and encouragement all these years. Thank you to my sister, Paige Hamilton-Conaty, for your inspiration to persevere through all of life's storms. Thank you to my dear friends, Pia and Klaus Van Benthem; I don't know where I would be without your "juice". Thank you to the Genetos Lab: Damian Genetos and Kristina Wells, for your unquenchable, magical dark sparkle. Thank you to Crystal Rogers for reviving my passion for my research when I needed it most. Thank you to the Reardon Lab: Valerie Ramirez, Katie Murray, Emmy Tay, Sierra Schreiber, Michael Cremin, and Tina Sanchez. Thank you to Ingrid for your help and patience in teaching me the ins-and-outs of microscopy. Thank you to the Gareau Lab: Ciara Keough, Jelissa Reynoso Garcia, Carly Hennessey, and Jess Sladek. Thank you for the camaraderie catalyzed in "Poo Corner".

To the ones we lost along the way: Grace Meschendorf, Kate Oswald Hildebrand, Stan Fogle, and our sweet Soleil. I have carried the precious memories of you all with me throughout this journey. Thank you for the joy and hope you instilled in me at the beginning of this voyage. It is painful to cross this finish line without you. Soleil, your memory is always within my reach.

Thank you to Papa Dr. Frank Brucia. Your encouragement, wisdom, and enthusiasm for learning have inspired me since my embarkation. Crossing this finish line without you is especially difficult. I will be faithful in caring for this magical life and family you helped create. Ti voglio un mondo di bellezza, Papa.

To my husband, Eric, a mighty man of valor. Your friendship has been the greatest blessing of my life. You have been my catalyst, fuel, and have kept the fire lit for the past 17 years. Thank you for being my anchor and the voice of reason in every one of life's storms. God's not done…

"For since the creation of the world, God's invisible qualities—his eternal power and divine nature—have been clearly seen, being understood from what has been made, so that we are without excuse."
Romans 1:20

Table of Contents

Dissertation Abstract

The vagus nerve is a neurochemical expressway that carries sensory and motor signals between the viscera and central nervous system and represents an important metabolic actuator. Vagal sensory neurons (VANs) densely innervate the wall of the GI tract and relay visceral and chemical sensory information from the gut to the brain, coordinate digestion, and regulate food intake and metabolism. Short-lived peptide enteroendocrine hormones are released from the gut wall and act upon receptors located on VANs to regulate satiety. Chronic consumption of calorie-dense foods reduces the sensitivity of VANs to satiety hormones, leading to excessive eating and weight gain. In addition to sensing peripheral peptide hormones, VANs also express receptors for dietary and microbial metabolites, such as tryptophan derivatives. Recent evidence suggests that these microbiota-derived byproducts may act directly on VANs to alter satiety signaling. However, the role of these microbial metabolites on VAN activity is unknown. Previous work shows that one of the microbial metabolite receptors, GPR35, is co-expressed with CCK_AR, the cognate receptor for CCK, a key peripheral satiety signal. However, the role of GPR35 on VANs in peripheral satiety signaling has not been studied.

The first two data chapters of the dissertation show that natural and synthetic GPR35 agonists activate VANs *in vitro* and reduce food intake *in vivo*. We also demonstrate that GPR35 and CCKAR interact on VANs *in vitro*, which is also reflected in our feeding behavior studies using short hairpin-RNA-mediated knockdown of GPR35 in VANs. The last section of this dissertation introduces a new *in vitro* model for a gut-brain axis on-a-

chip, which demonstrates primary VAN cultures can be used as a “living” biosensor for screening neuroactive metabolites that are produced in the gut.

Taken together, the data show that GPR35 activation on VANs increases satiety signaling and reduces food intake in mice. Furthermore, this dissertation details the first studies demonstrating that the deorphaned receptor GPR35 may modulate the activity of CCK_AR on VANs. This work is impactful for the field by revealing a potential new peripheral target for treating and perhaps preventing diet-induced hyperphagia and subsequent weight gain.

Abbreviations

2’-FL	2’-fucosyl lactose
3HK	3-hydroxykynurenine
6’-SL	6’-sialyl lactose
AhR	Aryl hydrocarbon receptor
Ca^{2+}_i	Intracellular calcium
CCK	Cholecystokinin
CNS	Central nervous system
DIM	3,3’-diindolylmethane
DMV	Dorsal motor nucleus of the vagus
EEC	Enteroendocrine cells
FFAR2	Free-fatty acid receptor 2 (i.e., GPR43)
FFAR3	Free-fatty acid receptor 3 (i.e., GPR41)
GBA	Gut-brain axis
GI(T)	Gastrointestinal/gastrointestinal tract
GLP-1	Glucagon-like peptide-1
GPR35	G-protein coupled receptor 35
GPR41	G-protein coupled receptor 41 (i.e., FFAR3)
GPR43	G-protein coupled receptor 43 (i.e., FFAR2)
HFD	High-fat diet
HMO	Human milk oligosaccharide(s)
I3A	Indole-3-aldehyde
I3C	Indole-3-carbinol
IDO1	Indoleamine-2,3-deoxygenase

IGLE	Intraganglionic laminar endings
IMA	Intramuscular arrays
IPA	Indole-3-propionic acid
KP	Kynurenine pathway
KYNA	Kynurenic acid
LFD	Low-fat diet
LNT	L-N-tetraose
LPS	Lipopolysaccharide
MA	Mucosal afferent endings
MGBA	Microbiota-gut-brain axis
MPF	Murine-pathogen-free
NTS	Nucleus tractus solitarius (nucleus of the solitary tract)
PDMS	Poly(dimethyl)-siloxane
PYY	Peptide YY
QA	Quinolinic acid
SCFA	Short-chain fatty acids
SGC	Satellite glial cell(s)
SPF	Specific-pathogen-free
TDO	Tryptophan deoxygenase
TLR-4	Toll-like receptor 4
VAN	Vagal afferent neuron(s)

Chapter 1:
Peripheral Targets of Microbial Metabolites and Gut Hormones on the Gut-Brain Axis in the Treatment of Diet-Induced Obesity

The goals of this introductory chapter are (1) to provide an overview of the targets of enteroendocrine hormones and microbial metabolites on vagal afferent neurons (VANs), and (2) to discuss the evidence demonstrating how microbial metabolites change the sensitivity to satiety hormones by altering VAN signaling and thereby influence feeding behavior and diet-induced weight gain. This introductory chapter is divided into four sections. Section 1.1 discusses the roles of VANs in regulating digestion and feeding behavior. Section 1.2 provides an overview of gut-derived hormones and their cognate receptors on VANs, their role in the regulation of food intake, and how they are dysregulated in diet-induced obesity. Section 1.3 discusses microbial metabolites, their molecular targets on VANs, and their association with changes in feeding behavior and metabolism. Finally, section 1.4 summarizes the current literature on diet-induced dysregulation of gut hormone signaling and microbial metabolites production and how these peripheral disturbances reduce VAN excitability and increase food intake. Investigating the synergy between gut-derived hormones and microbial metabolites and understanding the interacting mechanisms between these two classes of effectors could be used to develop new therapies for treating diet-induced hyperphagia and consequent weight gain and metabolic disease.

The scope of this review will be limited to discussing the evidence of the interaction between gut-derived enteroendocrine hormones and microbiota-derived metabolites to alter vagal afferent signaling. Although we recognize that these effectors play an important role in CNS regulation of energy balance, this will not be discussed here but is available elsewhere[1–5]. This review will not discuss the incretin action of

enteroendocrine hormones to increase insulin release and prevent glucose excursions, which has been extensively reviewed elsewhere[6–9].

1.1: The Vagal Pathway in the Regulation of Digestion and Satiety

The vagus nerve is a key bidirectional neural pathway between visceral organs and the brain. The vagus nerve is largely responsible for coordinating gastrointestinal function and feeding behavior. Therefore, it represents a critical node in the regulation of energy balance. The vagus nerve ensheaths extrinsic pseudounipolar sensory neurons (afferent fibers and neuronal soma) and motor (efferent) neurons; the majority of the vagus nerve is comprised of afferent fibers[10]. The cell bodies of vagal afferent neurons (VANs) are located within the nodose ganglion, found at the base of the skull within the jugular foramen. Focusing on gastrointestinal (GI) innervation, the peripheral sensory termini of the vagus nerve are embedded within the wall of the GI tract and relay visceral and chemical sensory information from the gut to the brain and coordinate digestion and regulate food intake and metabolism.

VAN sensory endings densely innervate the wall of the stomach and proximal intestine[11–15]. Even though the prevalence of VAN fibers decreases distally[12], recent mouse studies using retrograde tracers have shown that VANs also innervate the proximal colon whereas spinal afferents predominately relay sensory information from the distal colon[15–17]. Indeed, there is considerable overlap in innervation between these two families of sensory afferent fibers, and it is proposed that VANs relay chemosensory signals whereas spinal afferents relay noxious stimuli, such as pain[16,18,19].

VANs are key regulators of post-prandial metabolism and feeding behavior. Vagal afferent fibers relay sensory information from the gut to the caudal nucleus of the solitary tract (NTS), the primary site of vagal afferent termination in the brain. Cell bodies of vagal efferent neurons are located immediately superior to the NTS in the dorsal motor nucleus of the vagus nerve (DMV). Vagal motor neurons provide the

majority of parasympathetic innervation to the visceral organs. Via the vago-vagal reflex[20–22], sensory information conducted by VANs directly influences the electrical activity of vagal motor neurons to modulate virtually all aspects of gastrointestinal function, including but not limited to rates of gastric emptying, gastrointestinal motility and secretory activity, pancreatic secretions, and bile synthesis and release. Neurons originating from the NTS also project to mesolimbic and mesocortical regions in the brain to integrate nutritional signals from the periphery to regulate energy expenditure and energy intake[23,24]. For these reasons, recent innovations in obesity treatment have targeted the vagal pathway to increase satiety signaling, reduce food intake, and alter energy balance.

VANs do not project into the GI lumen[12,25,26]. Instead, during meal ingestion, VANs monitor nutritional status by detecting mechanical and chemosensory signals in the form of distention/tension[12,25–27] and chemical stimuli[18,23,26,28,29], respectively, to regulate digestion and feeding behavior[27]. However, discrete classes of VANs differ in their ability to detect various sensory cues.

Volumetric distension/tension of the stomach and GI tract activate a subset of mechanosensitive VANs[12,25–27]. Vagal afferent intraganglionic laminar endings (IGLEs) and intramuscular arrays (IMAs) within the GI muscularis detect mechanosensory changes, which influence VAN-mediated suppression of gastric emptying and food intake. In addition, stretch induces the release of serotonin from enterochromaffin cells located in the gastrointestinal epithelium, which activates ionotropic serotonin receptors (5-HT_3R) located on IGLE and IMA terminals[25]. Mechanosensitive VANs are also present in the mucosa (i.e., mucosal afferents) and detect stroking (e.g., ingested food

particles). In addition to mechanosensation, mucosal afferents (MAs) are critical for detecting chemical stimuli. Mucosal vagal afferents (MAs) are responsible for detecting chemical stimuli, such as pH, osmolality, absorbed nutrients (i.e., glucose and metabolites), and gut-derived hormones (enteroendocrine hormones)[14]. MAs are embedded in the lamina propria and lie near the basolateral membrane of epithelium cells and enteroendocrine cells[12,30]. VAN mucosal afferents are critical for detecting enteroendocrine hormones[31,32]. Therefore, MAs represent a unique and integral node of peripheral sensory signaling and can sense multiple indicators of nutritional status, and are critical for regulating GI motility, digestion, and feeding behaviors[11,12].

1.2: Gut-Derived Enteroendocrine Hormones and Their Peripheral Targets on VANs in Regulating Food Intake

Enteroendocrine hormones are peptide hormones generated from specialized epithelial cells in the gut, termed enteroendocrine cells (EECs). Some of these peptide hormones are also produced in and act within the brain[4,33], but this discussion is beyond the scope of this introductory chapter and is reviewed elsewhere[34–37]. These gut-derived hormones are crucial for coordinating digestion by increasing pancreatic enzyme secretion and modifying gastric emptying and intestinal motility. In addition to modulating digestion, peptide hormones, such as cholecystokinin (CCK), glucagon-like peptide-1 (GLP-1), and peptide YY (PYY), are also important for regulating feeding behaviors. Considering VANs lie in close proximity to EECs within the gut wall and that also express the cognate receptors for these peptide hormones[18,29], VANs are proposed

to be the primary targets for mediating the effects of most of these satiating peptide hormones.

Cholecystokinin

Cholecystokinin (CCK) is a key gut-derived satiety signal and is a hallmark regulator of food intake. CCK is a peptide hormone released in many forms that vary in length and post-translational modifications of the prohormone precursor, procholecystokinin[38]. While most forms of CCK can reduce food intake, post-translational sulfation of a tyrosine moiety near the C-terminus is essential for its physiological activity and is also an important distinguishing factor in the effects of CCK on GI secretion, digestion, and satiety[38–40]; little is known about the physiological role of un/desulfated CCK. Therefore, the following discussion of CCK refers to the sulfated form of CCK.

CCK has a short-half life in serum in humans (<1 hour) and in rodent models (~20 minutes)[41]. Therefore, peripheral CCK induces satiation likely through a paracrine mechanism. Studies have shown that CCK released or exogenously administered in the periphery reduces food intake[31,32]. Previous work shows that CCK-induced reduction in food intake is due to CCK binding to CCK_AR on peripheral terminals of chemosensitive VANs, which depolarizes VANs and activates central nuclei that inhibit food intake[31,32,40,42–44].

The most potent nutritional stimulus for CCK is fat and protein[11,40]. CCK-induced activation of VANs inhibits food intake[45,42,40,46] and reduces gastric emptying[47,11,48], which made it an attractive target for the treatment of diet-induced obesity. CCK also increases bile synthesis[49], stimulates the release of bile from the gall bladder[50], and increases pancreatic secretions[49,51]. CCK is also produced in the CNS[52,53], but the

actions of CCK in the brain are beyond the scope of this introductory chapter and have been discussed elswhere[54].

In the context of managing weight gain and feeding behavior in humans, CCK_AR agonists were initially proposed as attractive weight loss drugs because CCK is a potent stimulator of satiety and reduces gastric emptying. Previous studies in humans have shown that postprandial levels of CCK are reduced in patients with diabetes[55]. In addition, chronic ingestion of a high-fat diet reduces CCK-induced satiety in animal models of obesity, leading to diet-induced hyperphagia[56–58]. Diet-induced hyperphagia occurs when calorie intake exceeds energetic demand and contributes to increased weight gain. Therefore, studies were undertaken to determine if pharmacologically activating CCK_AR could reduce diet-induced hyperphagia. However, clinical studies showed that CCK_AR agonist monotherapy not only failed to reduce body weight but also induced pancreatitis and other adverse gastrointestinal symptoms, which resulted in the discontinuation of treatment[59]. The study concluded that CCKAR agonists may have been made more effective by co-administration with a synergistic therapy, such as leptin. Leptin improves CCK signaling in VANs *in vitro*[60,61], and leptin and CCK-coadministration enhances satiety in animal models[42,62]. Although there are currently no active drug development programs for CCK_AR agonist monotherapy, ongoing research includes CCK_AR as a potential enteroendocrine target to treat obesity[63].

Glucagon-like peptide-1

Glucagon-like peptide-1 (GLP-1) is a satiating peptide released from L cells in the small intestine and proximal colon[6,64] . Like CCK, GLP-1 levels rise in response to ingestion of a meal[4,33,65,66]. Its primary stimuli are glucose, carbohydrate, and fatty

acids. The GLP-1 receptor (GLP1R) is the only known receptor for GLP-1[67]. Studies in rodent models demonstrate that peripheral GLP-1 and peripherally-administered GLP1R agonists primarily act on GLP1R expressed on VANs to reduce gastric emptying and food[43,46,68–70]. Nonetheless, two studies using vagotomy[71] and genetic deletion of GLP1R on VANs in mice[72] show that VAN-GLP1R is not essential for the anorectic effects of GLP1R agonist liraglutide; these studies attribute the satiety-inducing effects of GLP1R agonists to GLP1R activation in the CNS. However, unlike the other studies that demonstrate VAN-GLP1R is an important peripheral target of GLP1R agonists, these two studies may have reached these conclusions due to (1) subcutaneous vs intraperitoneal administration of GLP1R agonists (≥ 200 µg/kg), (2) low-resolution food intake analysis (≥ 1-hour measurements), and (3) no measurement of meal microstructure. These differences in administration could certainly have led to pharmacodynamic variations in agonist exposure to VANs (e.g., slow absorption and excretion. Furthermore, methods for measuring food intake in these studies may lack the resolution required to evaluate VAN integrity. Considering these limitations, mounting evidence supports the hypothesis that endogenous, gut-derived GLP-1 and peripherally administered GLP1R agonists reduce food intake and gastric emptying by activating GLP1R expressed by VANs.

GLP1R agonists and drugs to increase endogenous GLP-1 currently represent the most promising pharmaceutical approaches to enhance satiety signaling and reduce body weight in humans, especially since patients with obesity maintain their sensitivity to exogenous GLP-1 and GLP1R agonists. Previous data demonstrate that high-fat feeding and obesity are associated with a reduction in enteroendocrine L cell

abundance and GLP-1 production, but the sensitivity to exogenous GLP-1 is maintained[73,74]. These observations motivated, in part, the development of dipeptidyl peptidase 4 (DPP-4) inhibitors, which increase the half-life of endogenous GLP-1 by reducing its proteolytic degradation. DPP-4 inhibitors have been shown to modestly increase circulating GLP-1 and improve blood glucose management in humans, but do not significantly reduce gastric emptying nor food intake in humans [75–77]**.** On the other hand, GLP1R agonists, such as semaglutide and liraglutide, significantly reduce gastric emptying and food intake in obese subjects [63,67,78], and represent one of the most effective drug classes for the long-term maintenance of body weight in humans[78,79]. At the time of this review article, tirzepatide, a GLP1R/GIP receptor dual agonist, is the most successful pharmaceutical treatment on the market for the long-term maintenance of weight loss[80]. GIP, glucose-dependent insulinotropic polypeptide, produced by enteroendocrine L[81] and K cells[82], is recognized for its role in mediating glucose-dependent insulin secretion, but it is not associated with enhanced satiety[83–85]. Correspondingly, evidence suggests that GIP receptors are not expressed by chemosensory VANs that predominately mediate satiety induced by the anorectic enteroendocrine hormones[29]. Although GLP1R is abundant in the brain and is critical for regulating glucose homeostasis and feeding behavior, VANs represent an important tissue target in mediating GLP1-R agonist-induced restorations in feeding behavior[63,68,70]**.**

Peptide YY

Peptide YY (PYY) is a 36-amino acid peptide hormone predominately produced by enteroendocrine L cells in the distal intestine. Although PYY is also produced within and

acts on the CNS, the central effects of PYY on satiety signaling are beyond the scope of this review. Ingestion of dietary fiber, fat, fatty acids, and protein increase PYY secretion[86–88]. Levels of PYY rise shortly after ingestion (~15 minutes) before macronutrients enter the distal intestine, which suggests neural or hormonal mechanisms regulate its release[86,88]. PYY3-36, the most abundant form of endogenous PYY[88], has a high affinity for neuropeptide Y receptor type 2 (NPY2R), which is highly expressed by chemosensory VANs[29]. PYY inhibits gastrointestinal motility and reduces food intake, in part, by activating NPY2R on VANs[89–91].

Evidence shows that circulating levels of PYY are also affected by diet. Increased intake of dietary protein is positively associated with PYY levels in rodent models and humans[88,92,93]. This is one proposed mechanism by which high-protein diets can improve weight loss by stimulating the production of gut-derived satiety hormones. As previously discussed, chronic consumption of a high-fat diet decreases the abundance of enteroendocrine L cell abundance and the production of PYY[88]. Since PYY is associated with enhanced satiety, potential interventions that increase or preserve the production of PYY may help reduce diet-induced hyperphagia.

Similar to GLP-1, sensitivity to exogenous PYY is maintained in obese humans[86,88,94]. Therefore, current pharmacotherapies aim to activate NPY2R or increase circulating PYY[86,88,95,96]. Injections of PYY have been shown to increase weight loss by significantly reducing food intake in humans without major adverse effects[86,88,94,97,98]. Others have shown that NPY2R agonists can be paired with GLP-1 agonists to further increase satiety in non-human primate models[95,96]**.**

Pharmacotherapies are currently being developed to target peripheral NPY2R activation as a new weight loss strategy[95,99].

Taken together, vagal afferent neurons represent major sites of action by which endogenous, gut-derived enteroendocrine hormones coordinate gastrointestinal activity and feeding behavior. Chronic consumption of a high-fat diet has been shown to reduce levels of satiety-inducing peptide hormones. Based on clinical evidence demonstrating that the sensitivity to these hormones is maintained in obesity, current weight loss drugs aim to increase the activity of their cognate receptors using hormone analogs (e.g., GLP-1, PYY receptor agonists); VANs are likely important players in mediating the therapeutic effects of these pharmacotherapies. However, considering VANs are also activated by microbiota-derived products [25,24,23,100,101], non-pharmaceutical strategies to increase satiety signaling include increasing the abundance of beneficial microbial metabolites.

1.3: Microbial Metabolites and Their Peripheral Targets on VANs Regulating Satiety Signaling

Mounting evidence demonstrates the role of the gut microbiota in modulating virtually all aspects of physiology, including but not limited to behavior, immune function, and metabolism[102–107]. The host can directly sense the gastrointestinal microbiota via pattern recognition receptors (PRRs), expressed by resident immune cells, intestinal epithelial cells, and visceral sensory neurons[104,108,109]. However, in the context of satiety signaling, recent work in our lab and others suggests that the gut microbiota influences VAN signaling primarily through indirect mechanisms by detecting microbial metabolites[108–114].

Microbial metabolites are small molecules that are produced by viable microorganisms inhabiting the gut. These microbial metabolites are byproducts of fermentation or transformed from host-derived products [115]. The abundance of microorganisms increases along the length of the gastrointestinal tract (GIT) as does the concentration of important metabolites, such as short-chain fatty acids (SCFAs) and tryptophan metabolites, in mice and humans[103,116,117]. Relative to murine-pathogen-free mice (MPF), previous work has shown that the abundance of numerous metabolite classes, including tryptophan metabolites, is reduced in germ-free mice[118].This section will discuss anorectic and obesogenic microbial metabolites, their molecular targets on VANs, and the mechanisms of their impact on satiety signaling and feeding behavior.

Short-Chain Fatty Acids (SCFAs)

Short-chain fatty acids (SCFAs) are among the most well-characterized microbiota-derived metabolites. SCFAs, such as acetate, propionate, and butyrate are produced by the fermentation of dietary fiber by microorganisms within the gut and are found in millimolar quantities (20-100 mM) in the GI lumen in humans[119,120]. Approximately 95% of SCFAs are absorbed in the large intestine and is a crucial energy source for colonocytes[110].

Recent work has highlighted the anorectic activity of SCFA butyrate and has shown that butyrate may act directly on GPR41/FFAR3 expressed on enteric neurons and VANs to increase satiety signaling and reduce food intake[121] and weight gain in diet-induced obese mice[113]. Cook *et al.* used VAN-specific FFAR3 knockout mice to show that FFAR3 may modulate short-term feeding behavior and CCK-induced activation of VANs ($p<0.06$)[113]. Peripherally-generated SCFAs are efficiently absorbed, present in

systemic circulation, and can cross the blood-brain barrier, which presents another mechanism by which SCFAs can activate receptors in the hypothalamus to induce satiety[119,122–124]. Although evidence supports that SCFAs may enhance satiety signaling by acting upon VANs, a technical consideration in the study by Cook *et al.* is that it does not isolate the effects of SCFA-induced activation or modulation of CNS satiety circuitry and inflammation; SCFA activation of VANs is only one mechanism by which SCFAs may alter feeding behaviors.

Tryptophan Metabolites

In addition to short-chain fatty acids, the gut microbiota can generate metabolites from dietary amino acids, such as tryptophan, which can profoundly impact host physiology, metabolism, and behavior. The gut microbiota has been shown to play an important role in host tryptophan homeostasis and regulate immune function and gastrointestinal function[103,125,126]. Tryptophan is an essential amino acid, but it is also important for generating molecules that are used for communication by the host and the microbiota. Bacteria within the intestine generate indoles from unabsorbed tryptophan, which are important for modulating the host's immune response to inflammation and metabolism[103,125]. However, most of the dietary tryptophan is absorbed in the small intestine and degraded via the host kynurenine pathway.

In the host, the majority (~95%) of dietary tryptophan is metabolized via the kynurenine pathway (KP); the remaining is metabolized via the serotonin pathway[103,117,125]. The rate-limiting enzymes of the kynurenine pathway are indoleamine-2,3-deoxygenase (IDO1) and tryptophan deoxygenase (TDO) generate L-kynurenine from tryptophan. TDO primarily dictates plasma levels of tryptophan and L-

kynurenine in the host[127,128]. IDO1 is ubiquitously expressed in the host, whereas TDO is predominately expressed in the liver. L-kynurenine is further metabolized to kynurenine-3-monooxygenase, kynureninase, and kynurenine aminotransferase to generate important bioactive end-products, including quinolinic (QA) and kynurenic acid (KYNA).

L-kynurenine has also been shown to act via the aryl hydrocarbon receptor (AhR), which plays an important role in intestinal homeostasis[129]. Studies evaluating the role of AhR in energy balance compared diet-induced weight gain in wild-type C57BL6/J mice to B6.D2 mice, which harbor AhR with a lower ligand-binding affinity, showed that B6.D2 mice were significantly leaner and consumed fewer calories than WT counterparts[130]. These and other studies suggest that AhR may be involved in energy homeostasis[102,103,131].

Neuroactive and immune-modulatory metabolites are generated by the metabolism of L-kynurenine through the KP. The neuroactive end-products of the kynurenine pathway include quinolinic acid (QA), 3-hydroxykynurenine (3HK), and kynurenic acid (KYNA)[132]. QA and 3HK act in concert as NMDA agonists and are indicated as neurotoxic agents. KYNA has been shown to counteract the neurotoxic effects of the other KP metabolites by acting as an NMDA antagonist and is indicated as the only anti-inflammatory product of the KP[133–135].

Studies suggest that the effects of the KP-generated metabolites may be attributed to where they are generated and accumulate. Experiments measuring the rates of cerebral uptake and mechanisms of blood-brain barrier (BBB) transport demonstrate that L-kynurenine is transported via the large neutral amino acid carrier, whereas other

products of the KP, such as QA and KYNA, are limited to passive diffusion[126,136]. Although peripheral levels of KP byproducts are associated with concentrations in the CNS and enzymes of the KP are ubiquitously expressed, this evidence may suggest that the peripherally generated KP products with limited BBB permeability may exert their anti-inflammatory effects in the periphery. Previous work supports this hypothesis and shows that GI hypermotility in inflammatory conditions is associated with a reduction in KP activation and is normalized by KYNA administration[137]. Although systemic levels of KYNA are dictated by the host kynurenine pathway activity, evidence suggests that the gut microbiota can modulate the KP pathway and generate KYNA[138,139]. This evidence further strengthens the link between the gut microbiota and tryptophan homeostasis of the host.

In addition to modulating the host's immune response, KYNA has been implicated in influencing host energy balance by acting in peripheral tissues[135,140–142]. Although both L-kynurenine and KYNA have been shown to activate AhR, *in vitro* studies demonstrate that L-kynurenine, but not KYNA, activates AhR in hepatocytes at physiological levels, which is indicated in liver steatosis[143]. Previous studies have shown that chronic consumption of a high-fat diet alters the composition of microbial metabolites[102,144] and also reduces systemic KYNA[142,145]. Administration of KYNA high-fat diet-induced obese mice reduces diet-induced weight gain and this effect is eliminated in GPR35 knockout animals relative to controls, demonstrating KYNA is a ligand for GPR35[140]. Considering work by Egerod *et al.* showing that GPR35 is highly expressed on CCK-sensing, $Na_V1.8$-positive VANs[29], data in the following chapters seek to advance the current

understanding of how KYNA and other GPR35 agonists act via VANs to enhance satiety signaling and improve metabolic phenotype.

Obesogenic Metabolites

The gut microbiota can also negatively impact host physiology, metabolism, and behavior by generating proinflammatory metabolites that are linked to diet-induced weight gain; evidence suggests that these effects can be mediated by VANs[108,109,146,147]. In the context of diet-induced obesity, HFD may induce metabolic diseases not only by decreasing the abundance of beneficial microorganisms and their associated anti-inflammatory metabolites, such as SCFAs and KYNA, but also by increasing the abundance of obesity-associated microorganisms and metabolites, such as bacterial lipopolysaccharide[148–151]. Work in our lab and others have demonstrated that HFD-induced disturbances in the composition of the gut microbiota and associated metabolites is associated with early metabolic and behavioral changes in obesity[108,118,148,149,152,153].

Lipopolysaccharide (LPS) is a component of the outer membrane of Gram-negative bacteria and is shed from bacteria throughout their life cycle[154,155]. LPS, also known as endotoxin, is associated with septic shock and can stimulate a strong immune response via the pattern recognition receptor (PRR) Toll-like receptor 4 (TLR-4), which is expressed on immune cells, such as macrophages, as well as endothelial cells and neurons, including VANs[154,155]. Circulating LPS binds to LPS-binding protein and, with CD14, binds to TLR-4, which induces a classical molecular inflammatory cascade, including the activation of the transcription factor nuclear factor kappa beta (NF-KB).

Our group and others have demonstrated that consumption of a high-fat diet is associated with moderately elevated levels of LPS in the plasma of mice and in humans, which has been termed metabolic endotoxemia[156–158]. Previous clinical studies show that even a single lipid-enriched meal can significantly alter postprandial plasma levels of LPS[158] and that these levels are positively correlated with energy intake[156,158]. Previous work shows that whole body knockout of TLR-4 prevents HFD-induced inflammation in peripheral tissues in mice relative to wild-type controls[159], suggesting that HFD-induced metabolic perturbations may be partly attributed to TLR-4. Other studies have clearly demonstrated an association between chronic HFD-feeding, hypothalamic inflammation, and alterations in central neuronal circuits that govern feeding behavior and metabolism[160–162]. Our group has previously shown that diet-induced weight gain is associated with increased plasma levels of LPS in rodent models of obesity[163]. Other work from our lab and others have shown that chronic low-dose infusions of LPS increase weight gain in animal models[108,157]. Our group has shown that increases in plasma LPS help drive hyperphagia, in part, by interfering with VAN-mediated satiety signaling and induce weight gain in animals on a normal diet[108,163,164]. Although HFD-induced increases in LPS may not cause obesity, this work demonstrates that bacterial-derived LPS can alter homeostatic circuitry that alter feeding behavior and promotes hyperphagia.

Recent studies from our laboratory and others have demonstrated that supplementation with anorectic microbial metabolites, such as SCFAs, may help restore diet-induced disturbances in microbiota diversity and energy homeostasis[152,153]. For example, experiments by Li et al. demonstrated that SCFA supplementation of HFD-fed

mice reduced diet-induced hyperglycemia and hyperinsulinemia, as well as plasma levels of inflammatory cytokines, IL-1β, IL-6 and MCP-1[165]. Lu et al. also demonstrated that SCFA administration to HFD-fed animals partially restored the gut microbiota[165], which was also observed by our group[152]. In vitro experiments by Li et al. mechanistically demonstrated that SCFAs could reduce HFD-induced atherosclerosis by inhibiting LPS-induced inflammation in endothelial cells via GPR41/FFAR3[166]. These data support the hypothesis that SCFAs may reduce diet-induced inflammation systemically and may help restore gut microbiota composition and metabolic homeostasis.

This work shows that energy-dense diets can negatively impact the gut microenvironment and increase the production of proinflammatory metabolites, which drive changes in satiety signaling and energy homeostasis and contribute to diet-induced obesity. This and other work illustrate the critical role of the microbiota in generating neuroactive metabolites that can modulate feeding behavior and metabolism[108,152,153]. Therefore, manipulating the gut microbiota and associated metabolites presents a prime point of intervention for managing obesity and metabolic disease.

1.4: Interaction of Gut-Derived Satiety Hormones and Microbial Metabolites on Peripheral Targets in Regulating Satiety Signaling

Early behavioral changes in diet-induced obesity, such as hyperphagia, are associated with peripheral changes in gut hormone signaling, the composition of the gut microbiota, and the profile of microbial metabolites[108,148,149]. Short-term high-fat feeding also increases the abundance of pro-inflammatory metabolites and induces systemic

inflammation *in vivo*, which is accompanied by hyperphagia[102,108]**.** Researchers in the field are enthusiastic to identify the cause of these early changes in HFD-induced metabolic disease in order to create new and accessible treatment options, especially as the global obesity epidemic grows annually[167,168]. However, the literature suggests that early diet-induced changes in enteroendocrine signaling and changes in the profile of gut microbiota and their secreted metabolites are not only concomitant but interconnected.

Currently, the most successful strategy for treating obesity is bariatric surgery, which has been shown to increase satiety and increase the abundance of beneficial microbial metabolites, including tryptophan metabolites and short-chain fatty acids[169,170]. The most successful pharmaceutical treatments for obesity are gut hormone mimetics, which reduce energy intake[80]. Cumulating evidence suggests that the gut microbiota may sensitize VANs to enteroendocrine satiety hormones to help restore satiety signaling and improve metabolic outcomes[171–174]. Taking an integrative approach to understanding how satiety hormone receptor agonists alter the gut microbiota and secreted products may reveal more effective strategies to restore early peripheral changes before they impose lasting effects on satiety signaling and feeding behavior.

Microbial Metabolites and Satiety Hormone Production

Previously mentioned data show that SCFAs activate FFARs expressed on VANs to increase satiety signaling and reduce food intake[113]. However, bacterial-derived SCFAs produced in the gut lumen also enhance satiety signaling by increasing the production and release of GLP-1 from enteroendocrine L cells in the colon[171,175]. In addition to GLP-1, SCFA treatment of primary murine enteroendocrine L cells and intracolonic

administration of SCFAs in rodent models increase PYY secretion[176]. In accordance with this, Samuel *et al.* showed that global knockout of SCFA-receptor FFAR3 (i.e., Gpr41) decreases PYY production in mice[177]. Although studies utilizing global knockout animal models and other SCFA supplementation studies have generated conflicting data[152,177], most of the literature shows that SCFAs generated by the gut microbiota enhance satiety hormone secretion[113,120,122,174,176,178]. Increases in satiety hormone release may also explain how SCFAs enhance VAN satiety signaling and energy homeostasis observed by our laboratory and others[129,132,180].

SCFAs are not the only microbial metabolites that can increase satiety hormone secretion. Evidence indicates that the tryptophan metabolite, indole-3-propionic acid (IPA), increases GLP-1 secretion from colonic L cells[179] and is partly responsible for its association with reduced risk of metabolic disease [180,181]. In addition, a byproduct of the microbial-derived indole-3-carbinol (I3C), 3,3'-diindolylmethane (DIM), was shown to increase PYY production in mouse enteroendocrine cells *in vitro*[182]. Taken together, these data suggest that select microbial metabolites produced within the gut can increase the production of satiety hormones and thereby enhance satiety signaling by activating their cognate receptors on VANs.

Microbial Metabolites and Enteroendocrine Hormone Receptor Function

While anorectic microbial metabolites can indirectly increase VAN signaling by enhancing satiety hormone production, evidence shows that microbial metabolites, such as SCFAs, can act locally to enhance the sensitivity of satiety hormone receptors[113,173]. Recent data from Cook *et al.* show that SCFA treatment of VANs *in vitro* increases CCK-induced signaling pathways[60] and that this was mediated at least in part by

FFAR3[113]. Additionally, other data shows that FFAR3 gene expression in VANs overlaps with that of the oxytocin receptor (OXTR), which is involved in regulating feeding and drinking behaviors[18]. Cook *et al*. suggests that short-term, SCFA-induced changes in feeding and drinking behavior observed in their studies may be attributed to synergistic intracellular signaling of these two receptors within VANs.

Indeed, Egerod *et al*. also showed that the microbial metabolite receptor GPR35, which senses the tryptophan metabolite KYNA, is also highly expressed in the same class of chemosensory VANs responsible for detecting the satiety hormone, CCK[29]. Although KYNA has also been shown to improve glucose homeostasis in diet-induced obese mice[140] perhaps by protecting insulin-producing beta cells[183] and reduce diet-induced weight gain in mouse models of obesity[140], its role in altering VAN sensitivity to satiety hormones has not been studied.

Conversely, our lab has shown that chronic exposure to the proinflammatory bacterial component, LPS, impairs normal satiety signaling by desensitizing VANs to leptin, a key peripheral satiety hormone[108]. Taken together, these data show (1) beneficial metabolites, such as SCFAs and select tryptophan metabolites, are more abundant in lean than obese subjects and are associated with the restoration of a lean phenotype, and (2) that chronic low levels of proinflammatory bacterial metabolites, such as LPS, are associated with poor metabolic outcomes. Together, these findings suggest that microbial metabolites are likely involved in altering the sensitivity of VANs to peripheral satiety hormones, which alters the integration of satiety cues and consequently, feeding behavior.

1.5: Conclusions

The focus of this introductory chapter was to review the role of VANs in sensing peripheral satiety hormones and metabolites and the modulation of feeding behavior. However, we recognize that VANs represent just one tissue upon which these signaling molecules act. While VANs predominately mediate the effects of short-lived enteroendocrine peptide hormones and microbial metabolites generated within the gastrointestinal lumen, many of these signaling molecules can also cross the blood-brain barrier or are generated within the brain to alter satiety signaling, which is beyond the scope of this discussion and is described elsewhere. Nevertheless, VANs represent the dominant pathway by which the vast majority of peripherally produced peptide hormones mediate their effects. Ultimately, VANs represent the common sensory path by which hormones and the gut microbiota can directly influence host behavior. Therefore, investigating the synergy between gut-derived hormones and microbial metabolites and understanding the interacting mechanisms between these two classes of effectors could help generate new therapies for treating diet-induced hyperphagia and consequent metabolic disease.

1.6: References

1. Rui, L. Brain regulation of energy balance and body weight. *Rev. Endocr. Metab. Disord.* **14**, 387–407 (2013).
2. Browning, K. N. & Carson, K. E. Central Neurocircuits Regulating Food Intake in Response to Gut Inputs—Preclinical Evidence. *Nutrients* **13**, 908 (2021).
3. Lenard, N. R. & Berthoud, H. Central and Peripheral Regulation of Food Intake and Physical Activity : Pathways and Genes. **16**, 11–22 (2008).
4. Sandoval, D. CNS GLP-1 regulation of peripheral glucose homeostasis. *Physiol. Behav.* **94**, 670–674 (2008).
5. Elmquist, J. K. CNS regulation of energy balance and body weight: insights from rodent models. *Lab. Anim. Sci.* **48**, 630–637 (1998).
6. Hjørne, A. P., Modvig, I. M. & Holst, J. J. The Sensory Mechanisms of Nutrient-Induced GLP-1 Secretion. *Metabolites* **12**, 420 (2022).
7. Danowitz, M. & De Leon, D. D. The Role of GLP-1 Signaling in Hypoglycemia due to Hyperinsulinism. *Front. Endocrinol.* **13**, 863184 (2022).
8. Yanagisawa, Y. How dietary amino acids and high protein diets influence insulin secretion. *Physiol. Rep.* **11**, e15577 (2023).
9. Hyun, U. & Sohn, J.-W. Autonomic control of energy balance and glucose homeostasis. *Exp. Mol. Med.* **54**, 370–376 (2022).
10. Prechtl, J. C. & Powley, T. L. The fiber composition of the abdominal vagus of the rat. *Anat. Embryol. (Berl.)* **181**, 101–115 (1990).
11. Raybould, H. E. *et al.* Vagal Afferent Innervation and Regulation of Gastric Function. in *Sensory Nerves and Neuropeptides in Gastroenterology: From Basic Science to Clinical Perspectives* (eds. Costa, M., Surrenti, C., Gorini, S., Maggi, C.

A. & Meli, A.) 109–127 (Springer US, 1991). doi:10.1007/978-1-4899-0744-8_10.

12. Berthoud, H. R. & Neuhuber, W. L. Functional and chemical anatomy of the afferent vagal system. *Auton. Neurosci. Basic Clin.* **85**, 1–17 (2000).
13. Berthoud, H. R. & Neuhuber, W. L. Vagal mechanisms as neuromodulatory targets for the treatment of metabolic disease. *Ann. N. Y. Acad. Sci.* **1454**, 42–55 (2019).
14. Powley, T. L., Spaulding, R. A. & Haglof, S. A. Vagal Afferent Innervation of the Proximal Gastrointestinal Tract Mucosa: Chemoreceptor and Mechanoreceptor Architecture. *J. Comp. Neurol.* **519**, 644–660 (2011).
15. Osman, S., Tashtush, A., Reed, D. E. & Lomax, A. E. Analysis of the spinal and vagal afferent innervation of the mouse colon using neuronal retrograde tracers. *Cell Tissue Res.* (2023) doi:10.1007/s00441-023-03769-3.
16. Meerschaert, K. A. *et al.* Unique Molecular Characteristics of Visceral Afferents Arising from Different Levels of the Neuraxis: Location of Afferent Somata Predicts Function and Stimulus Detection Modalities. *J. Neurosci.* **40**, 7216–7228 (2020).
17. Muller, P. A. *et al.* Microbiota modulate sympathetic neurons via a gut–brain circuit. *Nature* **583**, 441–446 (2020).
18. Bai, L. *et al.* Genetic Identification of Vagal Sensory Neurons That Control Feeding. *Cell* **179**, 1129-1143.e23 (2019).
19. Kupari, J., Hä Ring, M., Agirre, E., Alo Castelo-Branco, G. & Ernfors, P. An Atlas of Vagal Sensory Neurons and Their Molecular Specialization Cell Reports Resource An Atlas of Vagal Sensory Neurons and Their Molecular Specialization. *CellReports* **27**, 2508-2523.e4 (2019).
20. AbuAlrob, M. A. & Tadi, P. Neuroanatomy, Nucleus Solitarius. in *StatPearls*

(StatPearls Publishing, 2022).

21. Grill, H. J. & Hayes, M. R. Hindbrain Neurons as an Essential Hub in the Neuroanatomically Distributed Control of Energy Balance. *Cell Metab.* **16**, 296–309 (2012).
22. Maniscalco, J. W. & Rinaman, L. Vagal Interoceptive Modulation of Motivated Behavior. *PHYSIOLOGY* **33**, 151–167 (2018).
23. Kaelberer, M. M. *et al.* A gut-brain neural circuit for nutrient sensory transduction. *Science* **361**, (2018).
24. Han, W. *et al.* A Neural Circuit for Gut-Induced Reward. *Cell* 1–14 (2018) doi:10.1016/j.cell.2018.08.049.
25. Williams, E. K. K. *et al.* Sensory Neurons that Detect Stretch and Nutrients in the Digestive System. *Cell* (2016) doi:10.1016/j.cell.2016.05.011.
26. Wang, Y. B., de Lartigue, G. & Page, A. J. Dissecting the Role of Subtypes of Gastrointestinal Vagal Afferents. *Front. Physiol.* **11**, (2020).
27. Browning, K. N. Relieving tension: effects of cannabinoids on vagal afferent sensitivity. *J. Physiol.* JP279173 (2019) doi:10.1113/JP279173.
28. Pizarroso, N. A., Fuciños, P., Gonçalves, C., Pastrana, L. & Amado, I. R. A Review on the Role of Food-Derived Bioactive Molecules and the Microbiota–Gut–Brain Axis in Satiety Regulation. *Nutr. 2021 Vol 13 Page 632* **13**, 632 (2021).
29. Egerod, K. L. *et al.* Profiling of G protein-coupled receptors in vagal afferents reveals novel gut-to-brain sensing mechanisms. *Mol. Metab.* **12**, 62–75 (2018).
30. Raybould, H. E. Gut chemosensing: Interactions between gut endocrine cells and visceral afferents. *Auton. Neurosci. Basic Clin.* **153**, 41–46 (2010).

31. Serlin, H. K. & Fox, E. A. Abdominal vagotomy reveals majority of small intestinal mucosal afferents labeled in nav1.8cre-rosa26tdTomato mice are vagal in origin. *J. Comp. Neurol.* **528**, 816–839 (2020).
32. de Lartigue, G., Ronveaux, C. C. & Raybould, H. E. Deletion of leptin signaling in vagal afferent neurons results in hyperphagia and obesity. *Mol. Metab.* **3**, 595–607 (2014).
33. Brierley, D. I. *et al.* Central and peripheral GLP-1 systems independently suppress eating. *Nat. Metab.* **3**, 258–273 (2021).
34. Boer, G. A., Hay, D. L. & Tups, A. Obesity pharmacotherapy: incretin action in the central nervous system. *Trends Pharmacol. Sci.* **44**, 50–63 (2023).
35. Davis, E. A. *et al.* Ghrelin signaling regulates feeding behavior, metabolism, and memory through the vagus nerve. doi:10.1101/2020.06.16.155762.
36. Lau, S. H., Young, C. H., Zheng, Y. & Chen, X. The potential role of the cholecystokinin system in declarative memory. *Neurochem. Int.* **162**, 105440 (2023).
37. Till, A., Fries, C. & Fenske, W. K. Brain-to-BAT - and Back?: Crosstalk between the Central Nervous System and Thermogenic Adipose Tissue in Development and Therapy of Obesity. *Brain Sci.* **12**, 1646 (2022).
38. Beinfeld, M. C. Inhibition of pro-cholecystokinin (CCK) sulfation by treatment with sodium chlorate alters its processing and decreases cellular content and secretion of CCK 8. *Neuropeptides* **26**, 195–200 (1994).
39. Huang, S. C. *et al.* Importance of sulfation of gastrin or cholecystokinin (CCK) on affinity for gastrin and CCK receptors. *Peptides* **10**, 785–789 (1989).

40. Rogers, R. C. & Hermann, G. E. Mechanisms of action of CCK to activate central vagal afferent terminals. *Peptides* **29**, 1716–1725 (2008).
41. Koulischer, D., Moroder, L. & Deschodt-Lanckman, M. Degradation of cholecystokinin octapeptide, related fragments and analogs by human and rat plasma in vitro. *Regul. Pept.* **4**, 127–139 (1982).
42. Wang, L., Martínez, V., Barrachina, M. D. & Taché, Y. Fos expression in the brain induced by peripheral injection of CCK or leptin plus CCK in fasted lean mice. *Brain Res.* **791**, 157–166 (1998).
43. Diepenbroek, C. *et al.* Validation and characterization of a novel method for selective vagal deafferentation of the gut. *Am J Physiol Gastrointest Liver Physiol* **313**, 342–352 (2017).
44. Huang, K. P. *et al.* Leptin signaling in vagal afferent neurons supports the absorption and storage of nutrients from high-fat diet. *Int. J. Obes.* **45**, 348–357 (2021).
45. Gibbs, J., Young, R. C. & Smith, G. P. Cholecystokinin decreases food intake in rats. *J Comp Physiol Psychol* **5**, 284–290 (1997).
46. McDougle, M. *et al.* Intact vagal gut-brain signalling prevents hyperphagia and excessive weight gain in response to high-fat high-sugar diet. *Acta Physiol.* **00**, (2020).
47. Raybould, H. E. & Tache, Y. Cholecystokinin inhibits gastric motility and emptying via a capsaicin-sensitive vagal pathway in rats. *Am. J. Physiol.-Gastrointest. Liver Physiol.* **255**, G242–G246 (1988).
48. Yamagishi, T. & Debas, H. T. Cholecystokinin inhibits gastric emptying by acting on

both proximal stomach and pylorus. *Am. J. Physiol.-Endocrinol. Metab.* **234**, E375 (1978).

49. Koop, I. *et al.* Physiological control of cholecystokinin release and pancreatic enzyme secretion by intraduodenal bile acids. *Gut* **39**, 661–667 (1996).
50. Froehlich, F., Gonvers, J. J. & Fried, M. Role of nutrient fat and cholecystokinin in regulation of gallbladder emptying in man. *Dig. Dis. Sci.* **40**, 529–533 (1995).
51. Chandra, R. & Liddle, R. A. Neural and Hormonal Regulation of Pancreatic Secretion. *Curr. Opin. Gastroenterol.* **25**, 441–446 (2009).
52. Rehfeld, J. F. Immunochemical studies on cholecystokinin. II. Distribution and molecular heterogeneity in the central nervous system and small intestine of man and hog. *J. Biol. Chem.* **253**, 4022–4030 (1978).
53. Larsson, L.-I. & Rehfeld, J. F. Localization and molecular heterogeneity of cholecystokinin in the central and peripheral nervous system. *Brain Res.* **165**, 201–218 (1979).
54. Rehfeld, J. F. Cholecystokinin—From Local Gut Hormone to Ubiquitous Messenger. *Front. Endocrinol.* **8**, (2017).
55. Rushakoff, R. A. *et al.* Reduced postprandial cholecystokinin (CCK) secretion in patients with noninsulin-dependent diabetes mellitus: evidence for a role for CCK in regulating postprandial hyperglycemia. *J. Clin. Endocrinol. Metab.* **76**, 489–493 (1993).
56. Covasa, M. & Ritter, R. C. Adaptation to high-fat diet reduces inhibition of gastric emptying by CCK and intestinal oleate. *Am J Physiol Regul. Integr. Comp Physiol* **278**, 166–170 (2000).

57. Covasa, M., Grahn, J. & Ritter, R. C. High fat maintenance diet attenuates hindbrain neuronal response to CCK. *Regul. Pept.* **86**, 83–88 (2000).
58. Donovan, M. J., Paulino, G. & Raybould, H. E. CCK1 receptor is essential for normal meal patterning in mice fed high fat diet. *Physiol. Behav.* **92**, 969–974 (2007).
59. Jordan, J. *et al.* Stimulation of Cholecystokinin-A Receptors With GI181771X does not Cause Weight Loss in Overweight or Obese Patients. *Clin. Pharmacol. Ther.* **83**, 281–287 (2008).
60. de Lartigue, G. *et al.* EGR1 Is a target for cooperative interactions between cholecystokinin and leptin, and inhibition by ghrelin, in vagal afferent neurons. *Endocrinology* **151**, 3589–99 (2010).
61. Peters, J. H., Ritter, R. C. & Simasko, S. M. Leptin and CCK modulate complementary background conductances to depolarize cultured nodose neurons. *Am J Physiol Cell Physiol* **290**, 427–432 (2006).
62. Matson, C. A., Reid, D. F. & Ritter, R. C. Daily CCK injection enhances reduction of body weight by chronic intracerebroventricular leptin infusion. *Am. J. Physiol.-Regul. Integr. Comp. Physiol.* **282**, R1368–R1373 (2002).
63. Wang, J.-Y. *et al.* GLP－1 receptor agonists for the treatment of obesity: Role as a promising approach. *Front. Endocrinol.* **14**, (2023).
64. Yang, M. *et al.* Duodenal GLP-1 signaling regulates hepatic glucose production through a PKC-δ-dependent neurocircuitry. *Cell Death Dis.* **8**, e2609 (2017).
65. Deacon, C. F. What do we know about the secretion and degradation of incretin hormones? *Regul. Pept.* **128**, 117–124 (2005).

66. Pannacciulli, N. *et al.* Postprandial glucagon-like peptide-1 (GLP-1) response is positively associated with changes in neuronal activity of brain areas implicated in satiety and food intake regulation in humans. *NeuroImage* **35**, 511–517 (2007).
67. Zhao, X. *et al.* GLP-1 Receptor Agonists: Beyond Their Pancreatic Effects. *Front. Endocrinol.* **12**, (2021).
68. Iwasaki, Y. *et al.* GLP-1 release and vagal afferent activation mediate the beneficial metabolic and chronotherapeutic effects of D-allulose. *Nat. Commun.* **9**, 113 (2018).
69. Abbott, C. R. *et al.* The inhibitory effects of peripheral administration of peptide YY 3-36 and glucagon-like peptide-1 on food intake are attenuated by ablation of the vagal-brainstem-hypothalamic pathway. *Brain Res.* **1044**, 127–131 (2005).
70. Krieger, J.-P. *et al.* Knockdown of GLP-1 Receptors in Vagal Afferents Affects Normal Food Intake and Glycemia. *Diabetes* **65**, 34–43 (2016).
71. Secher, A. *et al.* The arcuate nucleus mediates GLP-1 receptor agonist liraglutide-dependent weight loss. *J. Clin. Invest.* **124**, 4473–4488 (2014).
72. Sisley, S. *et al.* Neuronal GLP1R mediates liraglutide's anorectic but not glucose-lowering effect. *J. Clin. Invest.* **124**, 2456–2463 (2014).
73. Mul, J. D. *et al.* High-fat diet changes the temporal profile of GLP-1 receptor-mediated hypophagia in rats. *Am. J. Physiol. - Regul. Integr. Comp. Physiol.* **305**, R68–R77 (2013).
74. Richards, P. *et al.* High fat diet impairs the function of glucagon-like peptide-1 producing L-cells. *Peptides* **77**, 21–27 (2016).
75. Vella, A. *et al.* The effect of dipeptidyl peptidase-4 inhibition on gastric volume,

satiation and enteroendocrine secretion in type 2 diabetes: a double-blind, placebo-controlled crossover study. *Clin. Endocrinol. (Oxf.)* **69**, 737–744 (2008).

76. Wong, M. C. S. *et al.* Comparative Effectiveness of Dipeptidyl Peptidase-4 (DPP-4) Inhibitors and Human Glucagon-Like Peptide-1 (GLP-1) Analogue as Add-On Therapies to Sulphonylurea among Diabetes Patients in the Asia-Pacific Region: A Systematic Review. *PLOS ONE* **9**, e90963 (2014).
77. Deacon, C. F. Physiology and Pharmacology of DPP-4 in Glucose Homeostasis and the Treatment of Type 2 Diabetes. *Front. Endocrinol.* **10**, (2019).
78. Jensterle, M., Rizzo, M., Haluzík, M. & Janež, A. Efficacy of GLP-1 RA Approved for Weight Management in Patients With or Without Diabetes: A Narrative Review. *Adv. Ther.* **39**, 2452–2467 (2022).
79. Vilsbøll, T., Christensen, M., Junker, A. E., Knop, F. K. & Gluud, L. L. Effects of glucagon-like peptide-1 receptor agonists on weight loss: systematic review and meta-analyses of randomised controlled trials. *BMJ* **344**, d7771 (2012).
80. HEISE, T. *et al.* 338-OR: Tirzepatide Reduces Appetite, Energy Intake, and Fat Mass in People with T2D. *Diabetes* **71**, 338-OR (2022).
81. Mortensen, K., Christensen, L. L., Holst, J. J. & Orskov, C. GLP-1 and GIP are colocalized in a subset of endocrine cells in the small intestine. *Regul. Pept.* **114**, 189–196 (2003).
82. Baggio, L. L. & Drucker, D. J. Biology of incretins: GLP-1 and GIP. *Gastroenterology* **132**, 2131–2157 (2007).
83. Asmar, M. *et al.* On the role of glucose-dependent insulintropic polypeptide in postprandial metabolism in humans. *Am. J. Physiol.-Endocrinol. Metab.* **298**,

E614–E621 (2010).

84. Holst, J. J. & Rosenkilde, M. M. GIP as a Therapeutic Target in Diabetes and Obesity: Insight From Incretin Co-agonists. *J. Clin. Endocrinol. Metab.* **105**, e2710–e2716 (2020).
85. Zhang, Q. *et al.* The glucose-dependent insulinotropic polypeptide (GIP) regulates body weight and food intake via CNS-GIPR signaling. *Cell Metab.* **33**, 833-844.e5 (2021).
86. Batterham, R. L. *et al.* Gut hormone PYY(3-36) physiologically inhibits food intake. *Nature* **418**, 650–654 (2002).
87. Savage, A. P., Adrian, T. E., Carolan, G., Chatterjee, V. K. & Bloom, S. R. *Effects of peptide YY (PYY) on mouth to caecum intestinal transit time and on the rate of gastric emptying in healthy volunteers*. *Gut* vol. 28 166–170 (1987).
88. Batterham, R. L. *et al.* Critical role for peptide YY in protein-mediated satiation and body-weight regulation. *Cell Metab.* **4**, 223–233 (2006).
89. Alonso, A. M. *et al.* The Vagus Nerve Mediates the Physiological but not Pharmacological Effects of PYY3-36 on Food Intake. 2020.08.07.241851 Preprint at https://doi.org/10.1101/2020.08.07.241851 (2020).
90. Karra, E., Chandarana, K. & Batterham, R. L. The role of peptide YY in appetite regulation and obesity. *J. Physiol.* **587**, 19–25 (2009).
91. Koda, S. *et al.* The role of the vagal nerve in peripheral PYY3-36-induced feeding reduction in rats. *Endocrinology* **146**, 2369–2375 (2005).
92. van der Klaauw, A. A. *et al.* High Protein Intake Stimulates Postprandial GLP1 and PYY Release. *Obes. Silver Spring Md* **21**, 1602–1607 (2013).

93. Zapata, R. C., Singh, A. & Chelikani, P. K. Peptide YY mediates the satiety effects of diets enriched with whey protein fractions in male rats. *FASEB J. Off. Publ. Fed. Am. Soc. Exp. Biol.* **32**, 850–861 (2018).
94. Batterham, R. L. *et al.* Inhibition of food intake in obese subjects by peptide YY3-36. *N. Engl. J. Med.* **349**, 941–948 (2003).
95. Rangwala, S. M. *et al.* A Long-Acting PYY3–36 Analog Mediates Robust Anorectic Efficacy with Minimal Emesis in Nonhuman Primates. *Cell Metab.* **29**, 837-843.e5 (2019).
96. Lear, S. *et al.* Engineering of a Potent, Long-Acting NPY2R Agonist for Combination with a GLP-1R Agonist as a Multi-Hormonal Treatment for Obesity. *J. Med. Chem.* **63**, 9660–9671 (2020).
97. Batterham, R. L. *et al.* PYY modulation of cortical and hypothalamic brain areas predicts feeding behaviour in humans. *Nature* **450**, 106–109 (2007).
98. Tan, T. M.-M. *et al.* Safety and efficacy of an extended-release peptide YY analogue for obesity: A randomized, placebo-controlled, phase 1 trial. *Diabetes Obes. Metab.* **23**, 1471–1483 (2021).
99. Østergaard, S., Paulsson, J. F., Kjærgaard Gerstenberg, M. & Wulff, B. S. The Design of a GLP-1/PYY Dual Acting Agonist. *Angew. Chem. Int. Ed.* **60**, 8268–8275 (2021).
100. De Vadder, F. *et al.* Microbiota-generated metabolites promote metabolic benefits via gut-brain neural circuits. *Cell* **156**, 84–96 (2014).
101. Bellono, N. W. *et al.* Enterochromaffin Cells Are Gut Chemosensors that Couple to Sensory Neural Pathways. *Cell* **170**, 185-198.e16 (2017).

102. Agus, A., Clément, K. & Sokol, H. Gut microbiota-derived metabolites as central regulators in metabolic disorders. *Gut* **0**, 1–9 (2020).
103. Agus, A., Planchais, J. & Sokol, H. Gut Microbiota Regulation of Tryptophan Metabolism in Health and Disease. (2018) doi:10.1016/j.chom.2018.05.003.
104. Bliss, E. S. & Whiteside, E. The gut-brain axis, the human gut microbiota and their integration in the development of obesity. *Front. Physiol.* **9**, (2018).
105. Clarke, G. *et al.* The microbiome-gut-brain axis during early life regulates the hippocampal serotonergic system in a sex-dependent manner. *Mol. Psychiatry 2013 186* **18**, 666–673 (2012).
106. Cryan, J. F. *et al.* The Microbiota-Gut-Brain Axis. *Physiol Rev* **99**, 1877–2013 (2019).
107. Mu, C. *et al.* Seizure modulation by the gut microbiota and tryptophan-kynurenine metabolism in an animal model of infantile spasms. *eBioMedicine* **76**, 103833 (2022).
108. de La Serre, C. B., de Lartigue, G. & Raybould, H. E. Chronic exposure to Low dose bacterial lipopolysaccharide inhibits leptin signaling in vagal afferent neurons. *Physiol. Behav.* **139**, 188–194 (2015).
109. Hosoi, T., Okuma, Y., Matsuda, T. & Nomura, Y. Novel pathway for LPS-induced afferent vagus nerve activation: Possible role of nodose ganglion. *Auton. Neurosci.* **120**, 104–107 (2005).
110. Blaak, E. E. *et al.* Short chain fatty acids in human gut and metabolic health. *Benef. Microbes* **11**, 411–455 (2020).
111. Colosimo, D. A. *et al.* Mapping Interactions of Microbial Metabolites with Human G-

Protein-Coupled Receptors. *Cell Host Microbe* **26**, 273-282.e7 (2019).

112. Raybould, H. E. & Zumpano, D. L. Microbial metabolites and the vagal afferent pathway in the control of food intake. *Physiol. Behav.* **240**, (2021).
113. Cook, T. M. *et al.* Vagal neuron expression of the microbiota-derived metabolite receptor, free fatty acid receptor (FFAR3), is necessary for normal feeding behavior. *Mol. Metab.* **54**, 101350 (2021).
114. Nøhr, M. K., Egerod, K. L., Christiansen, S. H., Gille, A., Offermanns, S., Schwartz, T. W., & Møller, M. Expression of the short chain fatty acid receptor GPR41/FFAR3 in autonomic and somatic sensory ganglia. *Neuroscience* **290**, 126–137 (2015).
115. Guzior, D. V. & Quinn, R. A. Review: microbial transformations of human bile acids. *Microbiome* **9**, 140 (2021).
116. Su, X., Gao, Y. & Yang, R. Gut Microbiota-Derived Tryptophan Metabolites Maintain Gut and Systemic Homeostasis. *Cells* **11**, 2296 (2022).
117. Dehhaghi, M., Kazemi Shariat Panahi, H. & Guillemin, G. Microorganisms, Tryptophan Metabolism, and Kynurenine Pathway: A Complex Interconnected Loop Influencing Human Health Status. *Int. J. Tryptophan Res.* **12**, 1–10 (2019).
118. Zarei, I. *et al.* Tissue-wide metabolomics reveals wide impact of gut microbiota on mice metabolite composition. *Sci. Rep.* **12**, 15018 (2022).
119. Brown, A. J. *et al.* The Orphan G Protein-coupled Receptors GPR41 and GPR43 Are Activated by Propionate and Other Short Chain Carboxylic Acids*. *J. Biol. Chem.* **278**, 11312–11319 (2003).
120. Nøhr, M. K. *et al.* GPR41/FFAR3 and GPR43/FFAR2 as cosensors for short-chain fatty acids in enteroendocrine cells vs FFAR3 in enteric neurons and FFAR2 in

enteric leukocytes. *Endocrinology* **154**, 3552–3564 (2013).

121. Goswami, C., Iwasaki, Y. & Yada, T. Short-chain fatty acids suppress food intake by activating vagal afferent neurons. *J. Nutr. Biochem.* **57**, 130–135 (2018).
122. Frost, G. *et al.* The short-chain fatty acid acetate reduces appetite via a central homeostatic mechanism. *Nat. Commun.* **5**, 1–11 (2014).
123. Wang, C., Zheng, D., Weng, F., Jin, Y. & He, L. Sodium butyrate ameliorates the cognitive impairment of Alzheimer's disease by regulating the metabolism of astrocytes. *Psychopharmacology (Berl.)* **239**, 215–227 (2022).
124. Keogh, C. E. *et al.* Myelin as a regulator of development of the microbiota-gut-brain axis. *Brain. Behav. Immun.* **91**, 437–450 (2021).
125. Gao, J. *et al.* Impact of the Gut Microbiota on Intestinal Immunity Mediated by Tryptophan Metabolism. *Front. Cell. Infect. Microbiol.* **8**, 13 (2018).
126. Hyland, N. P., Cavanaugh, C. R. & Hornby, P. J. Emerging effects of tryptophan pathway metabolites and intestinal microbiota on metabolism and intestinal function. *Amino Acids* **54**, 57–70 (2022).
127. Kanai, M. *et al.* Tryptophan 2,3-dioxygenase is a key modulator of physiological neurogenesis and anxiety-related behavior in mice. *Mol. Brain* **2**, 8 (2009).
128. Larkin, P. B. *et al.* Tryptophan 2,3-dioxygenase and indoleamine 2,3-dioxygenase 1 make separate, tissue-specific contributions to basal and inflammation-induced kynurenine pathway metabolism in mice. *Biochim. Biophys. Acta* **1860**, 2345–2354 (2016).
129. Moyer, B. J. *et al.* Inhibition of the aryl hydrocarbon receptor prevents Western diet-induced obesity. Model for AHR activation by kynurenine via oxidized-LDL, TLR2/4,

TGFβ, and IDO1. *Toxicol. Appl. Pharmacol.* **300**, 13–24 (2016).

130. Oshida, K. *et al.* Screening a mouse liver gene expression compendium identifies modulators of the aryl hydrocarbon receptor (AhR). *Toxicology* **336**, 99–112 (2015).

131. Lamas, B. *et al.* CARD9 impacts colitis by altering gut microbiota metabolism of tryptophan into aryl hydrocarbon receptor ligands. *Nat. Med.* **22**, 598–605 (2016).

132. Favennec, M. *et al.* Post-Bariatric Surgery Changes in Quinolinic and Xanthurenic Acid Concentrations Are Associated with Glucose Homeostasis. (2016) doi:10.1371/journal.pone.0158051.

133. Berlinguer-Palmini, R. *et al.* GPR35 Activation Reduces Ca2+ Transients and Contributes to the Kynurenic Acid-Dependent Reduction of Synaptic Activity at CA3-CA1 Synapses. *PLoS ONE* **8**, e82180 (2013).

134. Zarnowski, T. *et al.* Ketogenic diet increases concentrations of kynurenic acid in discrete brain structures of young and adult rats. *J. Neural Transm.* **119**, 679–684 (2012).

135. Zheng, X. *et al.* Kynurenic acid/GPR35 axis restricts NLRP3 inflammasome activation and exacerbates colitis in mice with social stress. *Brain. Behav. Immun.* **79**, 244–255 (2019).

136. Fukui, S., Schwarcz, R., Rapoport, S. I., Takada, Y. & Smith, Q. R. Blood-Brain Barrier Transport of Kynurenines: Implications for Brain Synthesis and Metabolism. *J. Neurochem.* **56**, 2007–2017 (1991).

137. Kaszaki, J. *et al.* Kynurenines and intestinal neurotransmission: the role of N-methyl-d-aspartate receptors. *J. Neural Transm.* **119**, 211–223 (2012).

138. Foata, F., Sprenger, N., Rochat, F. & Damak, S. Activation of the G-protein coupled receptor GPR35 by human milk oligosaccharides through different pathways. *Sci. Rep.* **10**, 1–9 (2020).
139. Desbonnet, L., Garrett, L., Clarke, G., Bienenstock, J. & Dinan, T. G. The probiotic Bifidobacteria infantis: An assessment of potential antidepressant properties in the rat. *J. Psychiatr. Res.* **43**, 164–174 (2008).
140. Agudelo, L. Z. *et al.* Kynurenic Acid and Gpr35 Regulate Adipose Tissue Energy Homeostasis and Inflammation. *Cell Metab.* **27**, 378-392.e5 (2018).
141. Agudelo, L. Z. *et al.* Skeletal Muscle PGC-1α1 Modulates Kynurenine Metabolism and Mediates Resilience to Stress-Induced Depression. (2014) doi:10.1016/j.cell.2014.07.051.
142. Pyun, D. H. *et al.* Endogenous metabolite, kynurenic acid, attenuates nonalcoholic fatty liver disease via AMPK/autophagy- and AMPK/ORP150-mediated signaling. *J. Cell. Physiol.* **236**, 4902–4912 (2021).
143. Rojas, I. Y. *et al.* Kynurenine-Induced Aryl Hydrocarbon Receptor Signaling in Mice Causes Body Mass Gain, Liver Steatosis, and Hyperglycemia. *Obes. Silver Spring Md* **29**, 337–349 (2021).
144. Liu, R. *et al.* Gut microbiome and serum metabolome alterations in obesity and after weight-loss intervention. *Nat. Med.* **23**, 859–868 (2017).
145. Li, J. *et al.* The Beneficial Effects of Edible Kynurenic Acid from Marine Horseshoe Crab (Tachypleus tridentatus) on Obesity, Hyperlipidemia, and Gut Microbiota in High-Fat Diet-Fed Mice. *Oxid. Med. Cell. Longev.* **2021**, (2021).
146. de Lartigue, G. Role of the vagus nerve in the development and treatment of diet-

induced obesity. *J. Physiol.* **594**, 5791–5815 (2016).

147. Siopi, E. *et al.* Gut microbiota changes require vagus nerve integrity to promote depressive-like behaviors in mice. *Mol. Psychiatry* 1–11 (2023) doi:10.1038/s41380-023-02071-6.

148. Zhang, S. & Dang, Y. Roles of gut microbiota and metabolites in overweight and obesity of children. *Front. Endocrinol.* **13**, (2022).

149. Torres-Sánchez, A., Ruiz-Rodríguez, A., Ortiz, P. & Aguilera, M. Key Stratification of Microbiota Taxa and Metabolites in the Host Metabolic Health–Disease Balance. *Int. J. Mol. Sci.* **24**, 4519 (2023).

150. Hernandez-Vargas, E. A. *et al.* Function of Akkermansia muciniphila in Obesity: Interactions With Lipid Metabolism, Immune Response and Gut Systems. *Front Microbiol* **11**, 219 (2020).

151. Maioli, T. U. *et al.* Possible Benefits of Faecalibacterium prausnitzii for Obesity-Associated Gut Disorders. *Front. Pharmacol.* **12**, (2021).

152. Lee, S. *et al.* Metabolic Responses to Butyrate Supplementation in LF-and HF-Fed Mice Are Cohort-Dependent and Associated with Changes in Composition and Function of the Gut Microbiota. *Nutrients* **12**, 3524 (2020).

153. Lee, S. *et al.* 2'-Fucosyllactose Supplementation Improves Gut-Brain Signaling and Diet-Induced Obese Phenotype and Changes the Gut Microbiota in High Fat-Fed Mice. *Nutrients* **12**, (2020).

154. Wassenaar, T. M. & Zimmermann, K. Lipopolysaccharides in food, food supplements, and probiotics: should we be worried? *Eur. J. Microbiol. Immunol.* **8**, 63–69 (2018).

155. Mohr, A. E., Crawford, M., Jasbi, P., Fessler, S. & Sweazea, K. L. Lipopolysaccharide and the gut microbiota: considering structural variation. *FEBS Lett.* **596**, 849–875 (2022).

156. Amar, J. *et al.* Energy intake is associated with endotoxemia in apparently healthy men. *Am. J. Clin. Nutr.* **87**, 1219–1223 (2008).

157. Cani, P. D. *et al.* Metabolic Endotoxemia Initiates Obesity and Insulin Resistance. *Diabetes* **56**, 1761–1772 (2007).

158. Laugerette, F. *et al.* Emulsified lipids increase endotoxemia: possible role in early postprandial low-grade inflammation. *J. Nutr. Biochem.* **22**, 53–59 (2011).

159. Shi, H. *et al.* TLR4 links innate immunity and fatty acid-induced insulin resistance. *J. Clin. Invest.* **116**, 3015–3025 (2006).

160. Souza, G. F. P. *et al.* Defective regulation of POMC precedes hypothalamic inflammation in diet-induced obesity. *Sci. Rep.* **6**, 1–9 (2016).

161. Maric, T., Woodside, B. & Luheshi, G. N. The effects of dietary saturated fat on basal hypothalamic neuroinflammation in rats. *Brain. Behav. Immun.* **36**, 35–45 (2014).

162. Valdearcos, M. *et al.* Microglia Dictate the Impact of Saturated Fat Consumption on Hypothalamic Inflammation and Neuronal Function. *Cell Rep.* **9**, 2124–2139 (2014).

163. de La Serre, C. B. *et al.* Propensity to high-fat diet-induced obesity in rats is associated with changes in the gut microbiota and gut inflammation. *AJP Gastrointest. Liver Physiol.* **299**, G440–G448 (2010).

164. De Lartigue, G., Barbier De La Serre, C., Espero, E., Lee, J. & Raybould, H. E.

Leptin Resistance in Vagal Afferent Neurons Inhibits Cholecystokinin Signaling and Satiation in Diet Induced Obese Rats. *PLoS ONE* **7**, (2012).

165. Lu, Y. *et al.* Short Chain Fatty Acids Prevent High-fat-diet-induced Obesity in Mice by Regulating G Protein-coupled Receptors and Gut Microbiota. *Sci. Rep.* **6**, 37589 (2016).
166. Li, M., van Esch, B. C. A. M., Henricks, P. A. J., Folkerts, G. & Garssen, J. The Anti-inflammatory Effects of Short Chain Fatty Acids on Lipopolysaccharide- or Tumor Necrosis Factor α-Stimulated Endothelial Cells via Activation of GPR41/43 and Inhibition of HDACs. *Front. Pharmacol.* **9**, (2018).
167. Hall, K. D. Did the Food Environment Cause the Obesity Epidemic? *Obesity* **26**, 11–13 (2018).
168. Abarca-GÃ, L. *et al.* Worldwide trends in body-mass index, underweight, overweight, and obesity from 1975 to 2016: a pooled analysis of 2416 population-based measurement studies in 128·9 million children, adolescents, and adults NCD Risk Factor Collaboration (NCD-RisC)*. *The Lancet* **390**, 2627–2642 (2017).
169. Yeung, K. T. D. *et al.* The impact of bariatric surgery on serum tryptophan–kynurenine pathway metabolites. *Sci. Rep.* **12**, 294 (2022).
170. Paganelli, F. L. *et al.* Roux-Y Gastric Bypass and Sleeve Gastrectomy directly change gut microbiota composition independent of surgery type. *Sci. Rep.* **9**, 10979 (2019).
171. Greiner, T. U. & Bäckhed, F. Microbial regulation of GLP-1 and L-cell biology. *Mol. Metab.* **5**, 753–758 (2016).
172. Gao, Z. *et al.* Butyrate improves insulin sensitivity and increases energy

expenditure in mice. *Diabetes* **58**, 1509–1517 (2009).

173. Li, Z. *et al.* Butyrate reduces appetite and activates brown adipose tissue via the gut-brain neural circuit. *Gut* **67**, 1269–1279 (2018).

174. Christiansen, C. B. *et al.* The impact of short-chain fatty acids on GLP-1 and PYY secretion from the isolated perfused rat colon. *Am. J. Physiol.-Gastrointest. Liver Physiol.* **315**, G53–G65 (2018).

175. Christensen, L. W., Kuhre, R. E., Janus, C., Svendsen, B. & Holst, J. J. Vascular, but not luminal, activation of FFAR1 (GPR40) stimulates GLP-1 secretion from isolated perfused rat small intestine. *Physiol. Rep.* **3**, e12551 (2015).

176. Psichas, A. *et al.* The short chain fatty acid propionate stimulates GLP-1 and PYY secretion via free fatty acid receptor 2 in rodents. *Int. J. Obes.* **39**, 424–429 (2015).

177. Samuel, B. S. *et al.* Effects of the gut microbiota on host adiposity are modulated by the short-chain fatty-acid binding G protein-coupled receptor, Gpr41. *Proc. Natl. Acad. Sci.* **105**, 16767–16772 (2008).

178. Larraufie, P. *et al.* SCFAs strongly stimulate PYY production in human enteroendocrine cells. *Sci. Rep.* **8**, 1–9 (2018).

179. Chimerel, C. *et al.* Bacterial Metabolite Indole Modulates Incretin Secretion from Intestinal Enteroendocrine L Cells. *Cell Rep.* **9**, 1202–1208 (2014).

180. van de Wouw, M., Schellekens, H., Dinan, T. G. & Cryan, J. F. Microbiota-Gut-Brain Axis: Modulator of Host Metabolism and Appetite. *J. Nutr.* **147**, 727–745 (2017).

181. Zhang, B. *et al.* The Mechanism Underlying the Influence of Indole-3-Propionic Acid: A Relevance to Metabolic Disorders. *Front. Endocrinol.* **13**, 841703 (2022).

182. Peiris, M. *et al.* Decoy bypass for appetite suppression in obese adults: role of synergistic nutrient sensing receptors GPR84 and FFAR4 on colonic endocrine cells. *Gut* **71**, 928–937 (2022).
183. Scholz, O., Welters, A. & Lammert, E. Role of NMDA Receptors in Pancreatic Islets. in *The NMDA Receptors* (ed. Hashimoto, K.) 121–134 (Springer International Publishing, 2017). doi:10.1007/978-3-319-49795-2_7.

Chapter 2:
GPR35 Agonists Activate Vagal Afferent Neurons and Reduce Diet-Induced Hyperphagia in Obese Mice

2.1. Abstract

Vagal afferent neurons (VANs) are key sensory neurons that project from the gut to the brain and relay peripheral cues of nutritional status to regulate feeding behavior and metabolism. VANs express receptors for enteroendocrine hormones, neurotransmitters, and dietary metabolites. Recent evidence shows that weight loss is associated with increased production of satiety peptide hormones and a shift in serum tryptophan metabolites. Kynurenic acid (KYNA) is an end-product of tryptophan metabolism and an endogenous agonist for GPR35. GPR35 is a metabolite receptor highly expressed by VANs and co-expressed with CCK_AR, a receptor for a key satiety hormone, cholecystokinin (CCK). There is evidence to suggest that a high-fat diet (HFD) reduces plasma levels of KYNA and that acute administration of KYNA increases weight loss. We report here that synthetic and naturally occurring GPR35 agonists activate VANs *in vitro*, likely through direct activation of GPR35 expressed by VANs. The synthetic GPR35 ligand zaprinast decreases food intake and activates the vagal afferent pathway in diet-induced obese mice, but not in lean mice. HFD had no effect on the gene expression of GPR35 in VANs. These data suggest that acute administration of the GPR35 agonist zaprinast restores normal feeding behavior in obese mice relative to lean mice and that this diet-dependent effect may be mediated via GPR35 on VANs. Furthermore, our group has previously shown that human milk oligosaccharides (HMOs), such as 2'-fucosyllactose and L-N-tetraose, partially restore satiety signaling and reduce diet-induced hyperphagia in diet-induced obese mice. These HMOs have also been shown to engage with GPR35 through direct and indirect mechanisms; LNT has been shown to be a direct agonist of GPR35. We report here that LNT activates

VANs *in vitro* via GPR35. These data suggest that GPR35 ligands may be involved in the modulation of satiety signaling revealing a novel peripheral target on VANs for treating diet-induced hyperphagia and weight gain.

2.2. Introduction

Vagal afferent neurons (VANs) innervate the gut and relay peripheral chemosensory signals in the form of enteroendocrine hormones to the brain to regulate appetite and feeding behavior[1–4]. Chronic consumption of a high-fat diet (HFD) desensitizes VANs to peripheral satiety signals and leads to aberrant signaling of VANs[5,6] and hyperphagia[7–13]. Diet-induced hyperphagia is considered an early physiologic adaptation to an HFD and precedes weight gain in diet-induced obese (DIO) rodent models[7,14–18] and there is evidence for altered gut-brain signaling in obese humans[19–21]. Mounting evidence suggests preventing diet-induced desensitization of VANs significantly reduces diet-induced hyperphagia in rodent models of obesity[15,22,23]. Successful therapies for maintaining weight loss in obese humans also alter the sensitivity of VANs to peripheral satiety signals[19,20]. Taken together, this evidence suggests that restoring the sensitivity of VANs to peripheral satiety hormones is a therapeutic target for treating obesity[24,25].

In addition to expressing receptors for satiety hormones, VANs innervating the gastrointestinal tract also express a plethora of receptors for microbial metabolites[26–28]. Kynurenic acid (KYNA) is a neuroactive tryptophan metabolite produced by both the host and gut microbiota[21–24] and is abundant in the lumen of the gastrointestinal tract, where its concentration increases distally[25]. Systemic and oral administration of KYNA to animal models of obesity reduces weight gain on a high-fat diet[29–31]. KYNA is an endogenous ligand for GPR35[29,32,33], which is a deorphaned G-protein coupled receptor (GPCR) and is highly expressed by VANs[26], which have been shown to innervate the proximal large intestine (i.e., proximal colon) where microorganisms are abundant[34,35].

Global knockout of GPR35 in mice increases body mass on a normal chow diet, indicating a potential role of GPR35 in energy homeostasis[27]. Furthermore, chronic consumption of a high-fat diet reduces plasma KYNA in humans and rodent models of obesity[36,37]. Ingestion of high-fat diets is associated with chronic inflammation and there is evidence to suggest that KYNA may suppress inflammation by inhibiting Nod-like receptor protein 3 (NLRP3)-induced activation of macrophages[33]. However, the role of GPR35 and its ligands on VAN-mediated satiety signaling has not been investigated.

CCK_AR expressed on VAN sensory terminals mediate endogenous CCK-induced satiety[38–40]. Double chromogenic *in situ* hybridization experiments using mouse nodose ganglia have shown that GPR35 is co-expressed with CCK_AR[26]. Studies using a Cre-DTA (diphtheria toxin fragment A) mouse model resulting in ablation of $Na_V1.8$-expressing neurons revealed that GPR35 is among the most highly expressed microbial metabolite GPCR on unmyelinated $Na_V1.8$ neurons[26], suggesting that GPR35 ligands generated within the gut lumen could act directly on VAN sensory terminals to alter satiety signaling.

This work was undertaken to determine whether GPR35 agonists activate vagal afferent neurons and affect feeding behavior in an animal model of obesity. We tested the hypothesis that GPR35 agonists activate VANs and reduce diet-induced hyperphagia. This hypothesis was tested with the following aims: (1) to demonstrate that synthetic and naturally occurring GPR35 agonists activate VANs *in vitro* and to show this is mediated via GPR35 and (2) to show that administration of GPR35 agonists increase satiety signaling and reduce food intake in a mouse model of HF diet-induced obesity. To address these aims, we used an established model of short-term culture of

nodose ganglia to test the effects of the synthetic GPR35 agonist zaprinast and naturally occurring agonists, KYNA and LNT[29,32,33,41], respectively, on VAN activity *in vitro*. Activation of VANs *in vivo* was determined in LF- and HF-diet-fed mice by measurement of *fos* expression in the nodose ganglia and in the nucleus of the solitary tract (NTS), the primary central termination site of VANs in the brainstem, after administration of zaprinast. Stimulation of VANs via the CCK or via electric vagal nerve stimulation terminates feeding, in part, by activating the NTS[2,37,49–51]. Finally, we determined the effects of acute administration of zaprinast on food intake and meal patterns in lean and HF diet-induced obese mice.

2.3. Methods

Animals and Housing

All experiments were approved by the University of California Davis Institutional Animal Care and Use Committees. All animals were maintained at 25 °C under a 12-h:12-h light-dark cycle (light 7 AM to 7 PM) with ad libitum access to water and food. C57BL6/J (Jackson Laboratories, Sacramento, California, USA) male/female? mice were individually housed in standard cages containing paper bedding before initiating feeding studies and provided standard chow (LabDiet 5001, St Louis, Missouri, USA) and water ad libitum. After 1 week of acclimation on a custom low-fat diet (LF, 10% kcal; matching composition of D12450J, Research Diets), mice were counter-balanced and maintained on either an LF or custom high-fat diet (HF, 45% fat kcal; matching composition of D08091803B, Research Diets) for 8 weeks. Food intake was measured twice per week to calculate the average food intake per animal (kcal/day) prior to

initiating feeding behavior studies in the BioDAQ food intake monitoring system (BioDAQ v 2.2, Research Diets, New Brunswick, New Jersey, USA).

For nodose cultures, 4-8-week-old adult male Wistar rats (Envigo, Hayward, California, USA) were housed in pairs in a separate facility and were provided ad libitum access to water and chow (Teklad #2018, Envigo, Indianapolis, Indiana, USA). Rats were chosen over mice to reduce the number of animals required to achieve statistical significance and experimental requirements for robustness and reproducibility.

Nodose Ganglia Dissection and Primary Cultures

We used an established model of primary VAN cultures[23,42,43]. Rat nodose ganglia were identified by following the vagus nerve to the jugular foramen and dissected under aseptic conditions. Nodose ganglia were collected into sterile calcium- and magnesium-free ice-cold Hanks Buffered Saline Solution (HBSS) (Corning, 21-022; Corning, New York, USA). Nerve fibers were cut away and unsheathed using sterile Dumont forceps and scalpel. The ganglia were pre-digested with 2 mg/ml collagenase type 4 (LS004188, Worthington-Biochem, Lakewood, New Jersey) and 2.4 mg/ml dispase II (4942078001, Roche, Penzberg, Germany) for 5 minutes at 37 °C. Following pre-digestion, ganglia were incubated in 22 U/mL papain (LS003126, Worthington-Biochem) resuspended in a solution of HBSS, L-cysteine (0.4 mg/mL, C6852, Sigma), 0.5 mM EDTA, and 1.5 mM CaCl2 for 30 minutes at 37 °C in a 5 cm Petri dish. Dissociated ganglia were transferred to a 15 mL centrifuge tube and centrifuged at 400 x g for 3 minutes before final digestion in collagenase (1 mg/mL) and dispase (1.2 mg/ml) for 30 minutes at 37 °C in a 5 cm Petri dish. Ganglia were mechanically dissociated before final centrifugation at 500 x g for 5 minutes. Nodose cultures were resuspended in 300

µL media consisting of DMEM base media (D5030, Sigma-Aldrich) supplemented with 0.5 mM L-glutamine, 10mM HEPES, 2.2g/L sodium bicarbonate, 0.227 mM sodium pyruvate, 5 mM glucose, 10% heat-inactivated rat serum (method included below). Cultures were equally distributed onto 8-chamber Millicell EZ Slides (PEZGS0416, Millipore, Burlington, Massachusetts, USA) and Matrigel (150 µg/ml, 354262, Corning). Nodose cultures were maintained at 37 °C, 5% CO2 for 24-48 hours prior to experiments. Each nodose culture consisted of pooled nodose ganglia (left and right) collected from two rats.

Generation of Heat-Inactivated Rat Serum

Wistar rats were euthanized by carbon dioxide asphyxiation. The ventral surface of the animal was sterilized and the skin was transected directly beneath the xiphoid process to expose the heart. Approximately 5 mL of blood was collected via cardiac puncture and centrifuged at 1,500 x g for 15 minutes at 4 °C to separate serum from whole blood and transferred to a Class II biosafety cabinet. Under sterile conditions, serum was collected and centrifuged for an additional 10 minutes at 20,000 x g at 4 °C to remove any remaining cell debris. The remaining 2 mL serum was distributed to 1.5 mL microcentrifuge tubes and heat-inactivated for 30 minutes at 56 °C in a heating block. Following heat inactivation, the serum was incubated in ice for 10 minutes to complete heat inactivation. The final serum was centrifuged for 10 minutes at 20,000x g before sterile filtration using a 0.2 µm syringe filter.

Sources of Chemical Treatments for Studies

CCK-8S (CCK) was sourced from either Bachem (Batch 1062975) or Tocris (#1166, Batch 19). Zaprinast was also sourced from Tocris (#0947; Batches 246356, 244357). Kynurenic acid (KYNA, K3375) and phorbol-12-myristate-13-acetate (PMA, P8139) were purchased from Sigma-Aldrich. Purified LNT was graciously provided to us by our collaborator, Daniela Barile, Ph.D. (Department of Food Science and Technology, University of California, Davis).

In Vitro VAN Treatments

All *in vitro* experiments were conducted 24-48 hours after plating. Nodose cultures were serum starved for 2 hours before all treatments. Working solutions of treatments were resuspended in either 0.9% normal saline (CCK, LNT, D-lactose) or 0.1-1% DMSO (KYNA, zaprinast, PMA, as dictated by solubility properties). Vehicle controls and PMA (100 nM), a positive control for ERK activation, were included for all experiments. The duration of all treatments was 15 minutes. To terminate treatments, cultures were washed with cold PBS and harvested in RIPA buffer containing 1% PMSF (Sigma, P7626), 1% protease inhibitor (Sigma, P8340), and 1% phosphatase inhibitor Cocktail 2 and 3 (Sigma, #5726 and #00444C respectively). Samples were flash-frozen on dry ice before storing at -80 °C until western blotting. Each experiment contained two technical replicates per treatment and each experiment was repeated in triplicate.

Western Blotting

Individual samples were denatured and reduced at 80 °C for 10 minutes and resolved using SDS-PAGE as per the manufacturer's standard protocol (Invitrogen, Mini Gel Tank). Two identical gels were run simultaneously to enable the probing of phosphorylated and total ERK protein. Following electrophoresis (100 V for 60 minutes), protein was transferred onto a poly(vinylidene fluoride) (PVDF) membrane (Bio-Rad, #1620264) according to the manufacturer's recommendations (Invitrogen, Mini Gel Tank) for 90 minutes at 20 V. Membranes were stained for total protein using No-Stain™ total protein stain reagent (Thermo Fisher, A44449) according to the manufacturer's recommendations. Membranes were washed in 1X TBST after visualizing total protein and blocked in 5% BSA in 1X TBST for 1 hour on a gyratory rocker at room temperature. All primary antibodies were purchased from Cell Signaling. Primary antibody solutions were resuspended in blocking buffer according to the following dilutions: pErk (1:500, 9101), Erk (1:1000, 9102). Membranes were incubated in the antibody solutions overnight at 4 °C on a gyratory rocker. On the following day, the membranes were incubated in secondary antibody solutions (HRP anti-rabbit IgG, 1:2000, Cell Signaling, 7074) and (HRP anti-mouse IgG, 1:4000, Cell Signaling, 7076) for 1 hour at room temperature. Chemiluminescence was used to detect proteins of interest (SuperSignal™ West Femto Maximum Sensitivity Substrate, ThermoFisher, 34096), and multiple exposures were taken to confirm that all samples were in the dynamic range. Total protein and antibody detection were analyzed using Bio-Rad Imager (Bio-Rad, Hercules, CA) and samples were normalized to total protein staining. Data are reported as the mean densitometry normalized to vehicle control ± SEM.

cFos Immunohistochemistry

Mice were euthanized via carbon dioxide asphyxiation. Upon termination, mice were exsanguinated. A scalp vein set (21-gauge needle) was used to perfuse 10 mL 0.9% saline into the left ventricle. Brains were collected and post-fixed in 4% paraformaldehyde in normal PBS for 24 hours, then transferred to 30% sucrose. Brains were separated at (~Bregma -3 mm) and hindbrains were frozen in OCT (Fisher, 23-730-571) in embedding molds. Brains were sectioned at 30 uM and mounted onto SuperFrost Plus microscope slides (Fisher, #12-550-15). Mounted cryosections were stored at -20 °C until immunostaining. Tissue was rehydrated in 1X TBS-Tween (0.1%) (TBST) before blocking in 10% normal goat serum (JacksonImmunoResearch Laboratories, 005-000-121) in 1X TBST + TritonX-100 (0.2%) for 1 hour at room temperature. After blocking, tissues were incubated overnight at 4 °C in a staining solution containing anti-cFos primary antibody (Cell Signaling, #2250) (1:500) and isolectin GS-IB4, Alexa Fluor™ 594 conjugate (Invitrogen, I21413) (1:500) resuspended in 10% normal goat serum in 1X TBST. The following day, slides were washed three times in 1X TBST for 5 mins/wash. The secondary antibody solution consisted of Alexa Fluor 647-conjugated goat anti-rabbit antibody (1:500) (Invitrogen, A21244, Lot 1834794) resuspended in 10% normal goat serum in 1X TBST for 1 hour at room temperature. Nuclei were stained with DAPI (1 µg/mL in 1X TBS) (Invitrogen, D1306) for 3 minutes at room temperature. Slides were treated with ProLong Diamond Antifade (Invitrogen, P36970) before mounting with rectangular #1.5 coverslips (Fisher, #NC1034527). Confocal images were acquired with a Leica TCS SP8 STED microscope using a 20X/0.75 oil lens. Bitplane Imaris software was used to analyze

cFos-positive neurons within the nucleus tractus solitarius, indicated by isolectin-IB4 stain[44,45]. cFos measurements were normalized by unit volume and were conducted using a single-blinded study design.

Automated Food Intake Monitoring

Mice were acclimated to food-monitoring Allentown cages (BioDAQ, v 2.2, Research Diets, New Brunswick, NJ) for 7 days prior to feeding experiments. For all feeding behavior studies, mice were fasted for 6 hours prior to the onset of the dark phase. Mice were injected with CCK-8S or vehicle (0.9% saline) or zaprinast or vehicle (4% DMSO, 2% Tween-80 in saline) (10 µL/g BW). Food was returned to mice immediately after CCK injections and 30 minutes after zaprinast injections. All feeding behavior studies were paired; treatments were randomized, and each animal received either vehicle or treatment 48 hours apart.

Analysis of Meal Microstructure

Feeding events were defined as “meals” if one or more feeding bouts were separated by 5 minutes or less and their sum was at least 0.02 g. If two feeding events were separated by more than 5 minutes, they were considered separate meals. Meal parameters included cumulative calorie intake, meal size, meal duration, meal number, rate of ingestion, and latency to eat. Latency to eat was measured as the time between gate opening and the initiation of the first meal. Energy intake is reported in kcal.

Quantitative PCR

Except for nodose ganglia, all tissues harvested for gene expression analyses were flash-frozen at necropsy. Total RNA was extracted using TRIzol (Life Technologies, Grand Island, NY, USA). Left and right nodose ganglia from euthanized animals were pooled per animal into RNA Later (Invitrogen, AM7021, Waltham, Massachusetts, USA) and RNA was extracted using Qiagen RNEasy Micro Plus Kit (Qiagen, Cat #74034, Germantown, Maryland, USA). All purified RNA from all samples was reverse transcribed using the High-Capacity cDNA Reverse Transcription Kit (Applied Biosystems, Cat # 4368814, Waltham, Massachusetts, USA) according to the manufacturer's instructions. Real-time PCR was performed using the QuantStudio 6 Flex Real-Time PCR system (Thermo Fisher Scientific, Waltham, MA, USA) and SyberGreen PowerUp (Life Technologies, Cat #A25778) using custom primers (Table 2.1). The qPCR cycling conditions included an initial denaturation step at 95 °C for 10 minutes followed by 40 cycles consisting of a 95 °C-step for 15 seconds and a 60 °C-step for 30 seconds. Control samples included "no RNA template control" and "no reverse transcriptase control". Data were analyzed using the $2^{-\Delta\Delta CT}$ method[46]. Target gene expression for all data is expressed as the ratio to housekeeping gene expression (RPLP0)[47].

Statistical Analysis

Randomization and blinding were used in the experimental design for all animal studies,imaging analysis, and analytical measurements. Differences between two groups were analyzed using GraphPad Prism using a two-tailed Student's t-test (e.g.,. paired for feeding studies, unpaired for endpoint studies). Differences among groups were analyzed by one- or two-way ANOVA as indicated in figure legends. Multiple comparisons tests for dose-response *in vitro* experiments were made using Dunnett's post hoc tests. Other multiple comparisons tests were made using Tukey's or Sidak's post hoc tests where appropriate. Data are presented ±SEM unless indicated otherwise. *P*-values less than 0.05 were considered statistically significant.

2.4. Experimental Protocols

GPR35 Expression in Mouse Tissues

8-week-old male C57BL6/J mice were used to verify the expression of GPR35 in nodose ganglia relative to other tissues. Liver, duodenum, proximal colon, and nodose ganglia were collected and RNA was harvested for qPCR. qPCR was conducted as described in the previous section.

Separation and Validation of Nodose Neurons from Glia

Percoll gradient protocol was used to separate nodose neurons from glial cells and axonal debris[48,49]. After nodose ganglia digestion, we layered 1 mL cell suspension onto a Percoll gradient consisting of 2 mL 50% Percoll, 2 mL 25% Percoll, and DMEM base media + 10% rat serum. The layered suspension was centrifuged for 10 minutes at 4 °C at 800 xg. The non-neuronal fraction (top) was separated from the neuronal fraction

(bottom) and the two populations were diluted in 4 mL DMEM base media + 10% rat serum before final centrifugation for 10 minutes at 4 °C at 800 x g.

This protocol was validated for separating rat VANs from glia using a viable fluorescent neuronal stain, NeuroFluorTM NeuO stain[50] (StemCell Technologies, #01801, Vancouver, British Columbia, Canada). After centrifugation, the two pelleted populations were resuspended separately in DMEM base media + 10% rat serum containing 1 µM NeuroFluorTM NeuO stain (0.2% DMSO) or vehicle control. Cells were incubated in cell staining solutions for 30 minutes at 37 °C then centrifuged for 4 minutes at 4 °C at 500 xg. Media was gently aspirated from pelleted cells and populations were separately filtered using 200 µm strainers and resuspended in HBSS + 10% rat serum. 10 µL of each cell suspension was pipetted onto SuperFrost microscope slides (Fisher, #12-550-15, ThermoFisher, Waltham, Massachusetts, USA), and circular #1.5 coverslips (Thomas Scientific, 1217N79, Swedesboro, New Jersey, USA) were mounted over each sample. Confocal images were acquired immediately with a Leica TCS SP8 STED microscope using a 40X/1.1 water lens. Brightfield microscopy was also used to verify morphology and the presence of cells in both fractions.

Following validation, we used this protocol to determine differences in gene expression between neuronal and non-neuronal populations within rat nodose ganglia. RNA was extracted from the sorted populations immediately following Percoll gradient separation (Qiagen, #74034). These samples were processed alongside unseparated rat nodose ganglion cultures. cDNA was generated from the extracted RNA, according to the manufacturer's recommendations (Applied Biosystems, #4368814). Differential

gene expression of GPR35, neuronal marker TUBB3, and glial marker IBA-1 were determined by quantitative real-time PCR (QuantStudio 6 Flex; Applied Biosystems) with SyberGreen PowerUp (Life Technologies, Cat #A25778) using custom primers (Table 2.2). The qPCR cycling conditions included an initial denaturation step at 95 °C for 10 minutes followed by 40 cycles consisting of 95 °C step for 15 seconds and 60 °C step for 30 seconds. Control samples included “no RNA template control” and “no reverse transcriptase control”. Data were analyzed using the $2^{-\Delta\Delta CT}$ method[46] with RPLP0 as the reference gene. Data are presented as fold changes relative to unsorted populations, which were normalized to 1.0.

Dose-Dependent Response *In Vitro* Studies

Dose-dependent responses of VANs *in vitro* were determined for each treatment tested. The duration of all treatments was 15 minutes. We had previously determined this treatment duration to induce peak activation of pERK/ERK in VANs in preliminary studies with a variety of treatments (e.g.,., CCK, PMA, ZAP, etc.). According to the available literature, we tested the following concentrations of proposed GPR35 agonists on nodose cultures to determine peak pERK/ERK activation: zaprinast (ZAP): 10^{-8}, 10^{-6}, 10^{-5}, 10^{-3} M; kynurenic acid (KYNA): 2, 20, 200, 2000 µM; L-N-tetraose (LNT): 0.5, 5, 10, 20, 50 mM. All dose response studies were carried out with negative control (e.g.,., saline or DMSO vehicle) and positive control samples (PMA, 100 nM).

GPR35 Antagonist *In Vitro* Studies

For VAN *in vitro* experiments including the GPR35 antagonist (CID-2745687, Tocris, 4293, Minneapolis, Minnesota), nodose cultures were pre-treated with either the

antagonist or vehicle (1% DMSO) during the last hour of serum starvation. The following treatments were suspended in the same pre-treatment solution.

Zaprinast-Induced *Fos* Expression in NTS

To measure *fos* expression in the hindbrain, mice were fasted overnight prior to intraperitoneal injection of zaprinast or vehicle (4% DMSO, 2% Tween-80 in saline) (10 mg/kg, 10 µL/g body weight; Tocris, #0947; Batch 246356). Mice were euthanized via carbon dioxide asphyxiation 90 minutes after injection, exsanguinated, and flushed with 1X PBS. Brains were harvested and post-fixed in 4% PFA according to the method described above and in previously published work from our lab[22,51].

Validation of Vagal Afferent Activation *In Vivo* Using Nodose *Fos* Expression

CCK activates VAN peripheral termini and terminates feeding, in part, by activating the NTS[2,37,49–51]. Activation of the NTS via VAN stimulation is associated with an increase in the expression of the early immediate gene, *c-fos*[36,37,51–54], which can be inhibited via pharmacological inhibition[36,55–57] or vagotomy[15,58,59]. A quantitative method for detecting VAN activation using qPCR was used to measure CCK-induced *fos* gene expression in nodose ganglia, which houses VAN soma. After validating this method, we applied this procedure to determine whether zaprinast-induced satiety is associated with an increase in VAN activation. To determine if CCK increased *fos* gene expression relative to vehicle control, chow-fed male and female C57BL6/J mice were injected with CCK (30 µg/kg, IP) or vehicle (0.9% saline). Nodose ganglia were harvested 2 hours after intraperitoneal injection. RNA was harvested from nodose ganglia as described in the previous section and processed for qPCR to measure relative changes in *fos* gene

expression, a marker for neuronal activation. The procedure was repeated in male and female mice using zaprinast (10 mg/kg) or vehicle.

2.5. Results

GPR35 Gene Expression in Mouse Nodose Ganglia

GPR35 mRNA expression in mouse nodose ganglia was measured and compared to GPR35 gene expression in the gastrointestinal tract (GIT). Gene expression of GPR35 in nodose ganglia was significantly higher in mice than liver, duodenum, or proximal colon (Figure 2.1, N=5, *p<0.05).

Figure 2.1: Gene expression of GPR35 in nodose ganglia relative to gastrointestinal tissue in mice. GPR35 gene expression in liver, duodenum, colon, and nodose in male C57BL6/J mice. N=5 per group. Data are presented as ±SEM. Different letters indicate $p<0.05$.

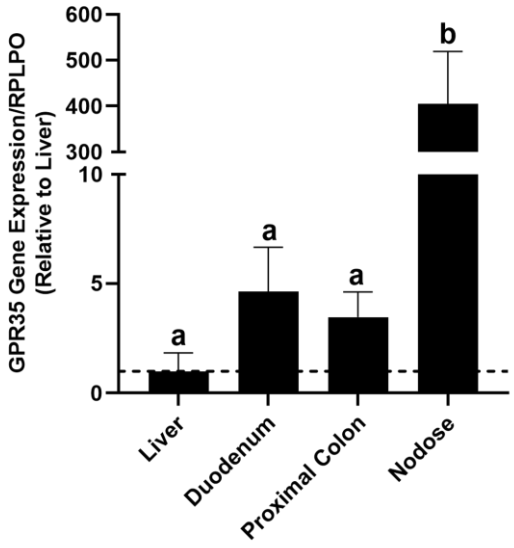

GPR35 Gene Expression in Rat Vagal Afferent Neurons Relative to Glia in Nodose

After separating VANs from non-neuronal cells by Percoll gradient, the VAN fraction of the nodose ganglia separated by Percoll gradient positively stained with the neuron-specific fluorescent probe, NeuO (Figure 2.2.A, N=4). In contrast, the top fraction containing glia and other supporting cells excluded NeuO (not shown). Brightfield microscopy revealed that cells were present in both fractions and that the top fraction was dominated by non-neuronal cells and axonal debris (Figure 2.2B). These data demonstrate that the Percoll gradient protocol effectively separated VANs from non-neuronal cells.

qPCR revealed that gene expression of GPR35 in VAN fractions is not significantly different relative to whole nodose cultures (Figure 2.2C, N=4). However, gene expression of GPR35 was not detected in glia fractions. Gene expression of the neuronal marker β-tubulin III (TUBB3) in the VAN fractions was not different from the whole nodose culture (Figure 2.2D). However, expression of TUBB3 in the glia fractions was significantly lower relative to the unseparated nodose culture (Figure 2.2D, N=4, $p<0.05$), supporting the fluorescent microscopy data showing that the glia fraction is predominantly free of neurons. Gene expression of the glial marker IBA-1 in the VAN fractions was significantly lower compared to whole nodose cultures (Figure 2.2E, N=4, $p<0.05$). The expression of IBA-1 in the glia fraction was not significantly different from the whole nodose culture nor the VAN fraction (Figure 2.2E). Together, these data suggest that GPR35 is likely expressed in VANs. Therefore, the potential effects of GPR35 agonists on VANs *in vivo* may be due to the direct activation of GPR35 on VANs.

Figure 2.2: GPR35 gene expression in VANs vs glia in rat nodose ganglia.

A) NeuO-stained live VAN fraction of gradient-separated rat nodose ganglia cultures.

B) Image of Percoll gradient-separated VANs and glia fractions. Scale bars = 20 µm.

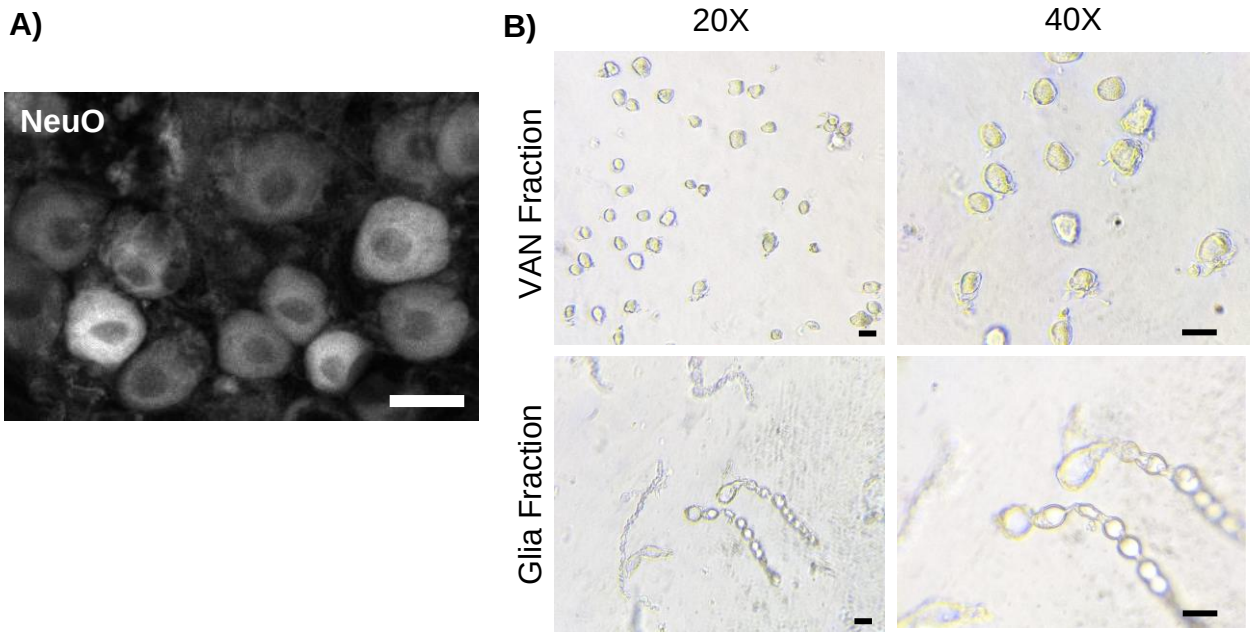

Figure 2.2: GPR35 gene expression in VANs vs glia in rat nodose ganglia.

Gene expression of C) GPR35, D) neuronal marker β-tubulin III (TUBB3), and E) glial marker IBA-1 in VAN and glia fractions. Data are presented as ±SEM. N=4/group. Different letters indicate $p<0.05$.

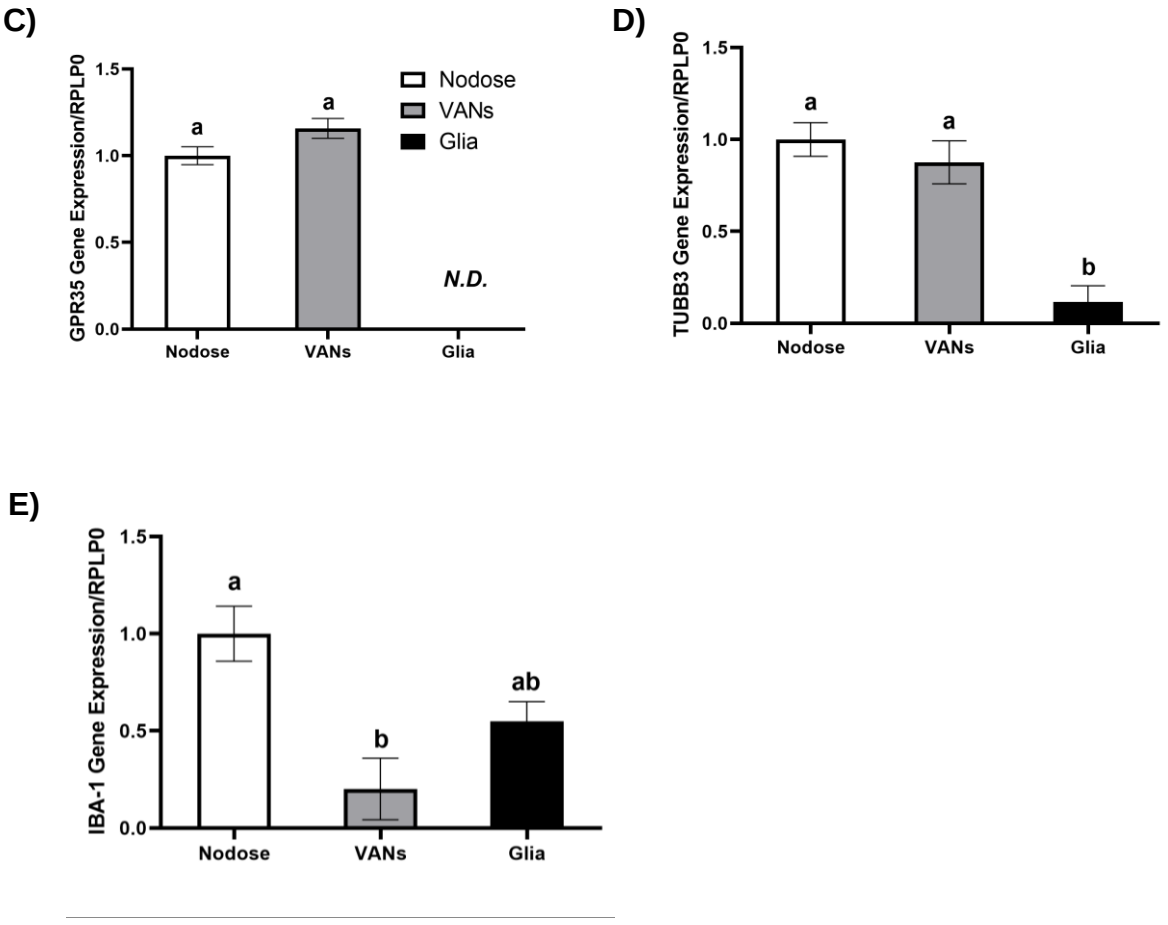

Effect of GPR35 Agonists on Vagal Afferent Neurons *In Vitro*

The dose-dependent response of VANs to GPR35 agonists was used to determine the range of concentrations that activate VANs *in vitro*; these western blot experiments were performed on crude protein extracts of cultured whole nodose ganglia. The GPR35 agonist zaprinast (10^{-5} M) significantly increased VAN activation relative to vehicle control, as measured by phosphorylation of ERK relative to total ERK (Figure 2.3A and 2.3B, *p<0.05, N=3). CCK (10 nM), also increased pERK/ERK relative to vehicle control, but this did not reach statistical significance (Figure 2.3B, p = 0.08, N=3). Treatment with the GPR35 antagonist CID-245687 (CID; 50-100 µM) had no significant effect on basal expression of pERK in VANs but significantly reduced zaprinast-induced expression of pERK/ERK relative to vehicle control, suggesting that zaprinast activates VANs via GPR35 (Figure 2.3C and 2.3D, *p<0.05, N=4). The positive control for ERK phosphorylation, PMA (100 nM) also significantly increased pERK/ERK relative to vehicle control (p<0.05, N=4). The competitive GPR35 antagonist CID (50 µM) had no effect on PMA-induced pERK/ERK (p=0.81, N=4), suggesting that CID specifically inhibits GPR35.

Figure 2.3: Effect of GPR35 agonist zaprinast on vagal afferent neurons (VANs) *in vitro.* Neuronal activation as measured by phosphorylation of ERK relative to total ERK (pERK/ERK). A) Representative western blot of dose response to GPR35 agonist zaprinast (0.01 - 1000 µM) on pERK/ERK. Positive controls of VAN and pERK/ERK activation are included (CCK and PMA, respectively). B) Quantification of dose response of zaprinast on pERK/ERK in VANs (Dunnett's multiple comparisons test; *p <0.05, **p<0.005 from control), N=3).

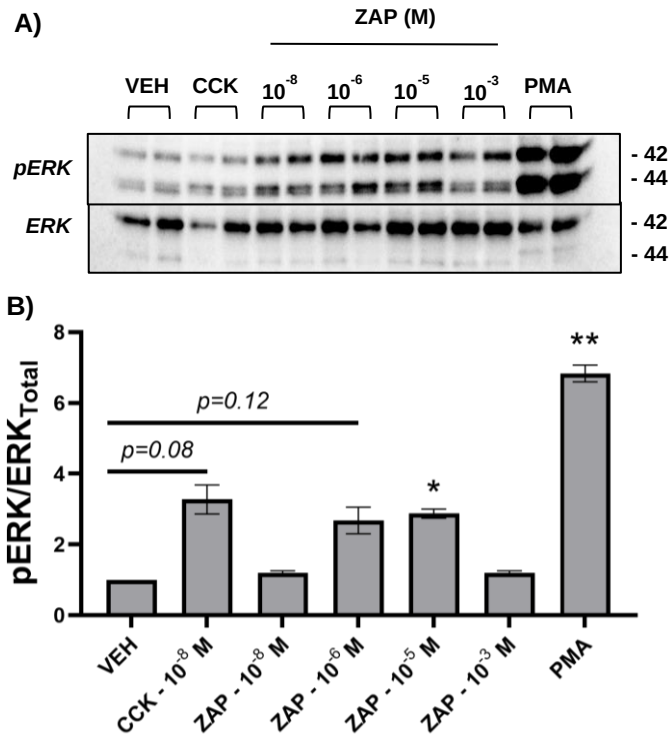

Figure 2.3: Effect of GPR35 agonist zaprinast on vagal afferent neurons (VANs) *in vitro.* C) Representative western blot of GPR35 antagonist CID-2745687 (CID; 50-100 µM) inhibition of zaprinast (10 µM)-induced pERK/ERK of VANs *in* vitro. D) Quantification of inhibition by CID (50 µM) on zaprinast- or PMA-induced-activation of VANs (N=4-5). Different letters indicate statistically significant differences ($p < 0.05$). All samples normalized to VEH control. Data are presented as ±SEM. VEH, vehicle. CCK, cholecystokinin. ZAP, zaprinast. CID, CID-2745687. PMA, phorbol 12-myristate 13-acetate**.**

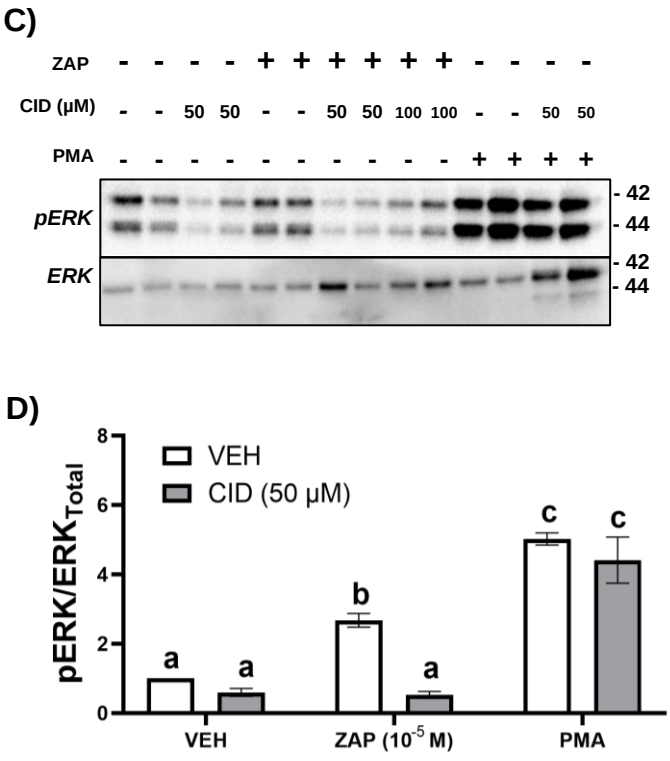

KYNA (2-20 µM) significantly increased pERK/ERK relative to vehicle control in cultures of the nodose ganglion (Figure 2.4A and 2.4B, *p<0.05, N=3). CCK (10 nM) significantly increased pERK/ERK relative to controls (Figure 2.4A, *p<0.05, N=3). The GPR35 antagonist CID-245687 (CID; 50-100 µM) significantly reduced KYNA-induced activation of pERK/ERK relative to vehicle control, indicating that KYNA activates VANs via GPR35 (Figure 2.4C and 2.4D, *p<0.05, N=3). PMA (100 nM) significantly increased pERK/ERK relative to vehicle control (p<0.05, N=3); PMA-induced phosphorylation of ERK was unaffected by the GPR35 antagonist CID (50 µM; p=0.89, N=3).

Figure 2.4: Effect of GPR35 agonist kynurenic acid (KYNA) on activating GPR35 on vagal afferent neurons (VANs) *in vitro*, as measured by phosphorylation of ERK relative to total ERK (pERK/ERK). A) Representative western blot of dose response to GPR35 agonist KYNA (2-2000 µM) on pERK/ERK. Positive controls of VAN and pERK/ERK activation are included (CCK and PMA, respectively).
B) Quantification of dose response of KYNA (1 µM - 2 mM) on pERK/ERK in VANs (Dunnett's multiple comparisons test; *p <0.05, ****p <0.0001 from control, N=3).

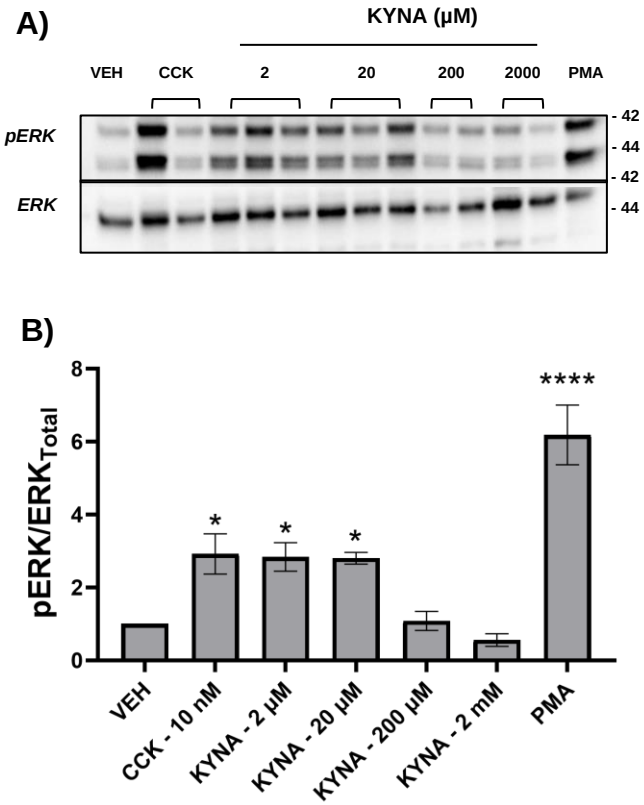

Figure 2.4: Effect of GPR35 agonist kynurenic acid (KYNA) on activating GPR35 on vagal afferent neurons (VANs) *in vitro*, as measured by phosphorylation of ERK relative to total ERK (pERK/ERK). C) Representative western blot of GPR35 antagonist CID-2745687 (CID; 50-100 µM) inhibition of KYNA (10 µM)-induced pERK/ERK of VANs *in* vitro. D) Quantification of inhibition by CID (50 µM) on KYNA- or PMA-induced-activation of VANs (N=3). Different letters indicate statistically significant differences ($p < 0.05$). All samples normalized to VEH control. Data are presented as ±SEM. VEH, vehicle. CCK, cholecystokinin. CID, CID-2745687. KYNA, kynurenic acid. PMA, phorbol 12-myristate 13-acetate.

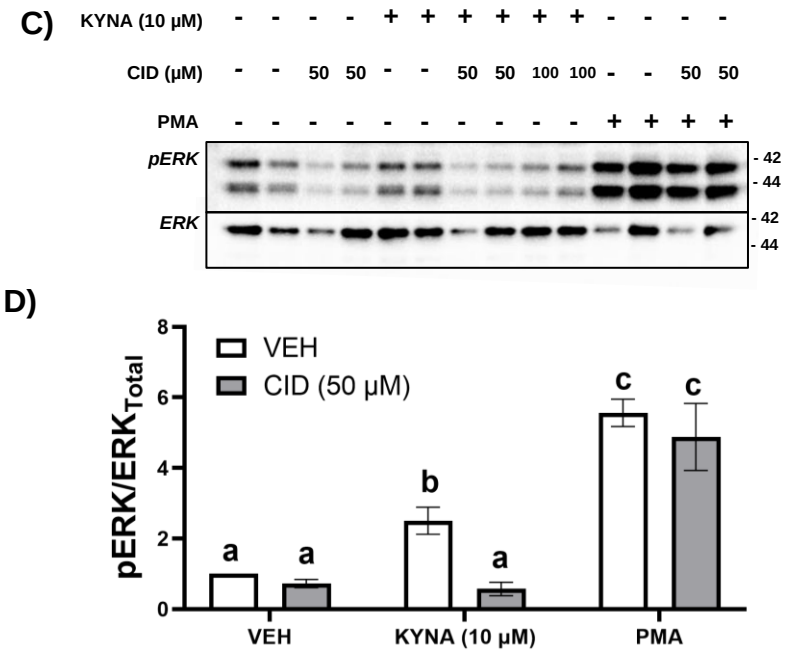

A previous study revealed that select human milk oligosaccharides (HMOs), such as L-N-tetraose (LNT), are naturally occurring GPR35 agonists[41]. Here, the effect of LNT (0.5-50 mM) on VANs was determined. LNT (10 mM) significantly increased pERK/ERK relative to vehicle control (Figure 2.5A and 2.5B, *p<0.05, N=3). The GPR35 antagonist CID-245687 (CID; 50-100 µM) significantly reduced LNT-induced pERK/ERK relative to saline control (Figure 2.5C and 2.5D, *p<0.05, N=3). The response of VANs to a component of LNT, D-lactose, was determined to confirm that the observed LNT-induced pERK/ERK was not due to hyperosmotic stress[44–46]. Equimolar D-lactose (10 mM) increased pERK/ERK relative to saline control but this did not reach statistical significance (Figure 2.5D, p=0.47, N=3). Furthermore, inhibiting GPR35 did not affect the observed lactose-induced activation (Figure 2.5D, p>0.99, N=3), indicating that the ability of lactose to increase pERK/ERK in VAN cultures is not mediated via GPR35. These data suggest that the human milk oligosaccharide, LNT, activates GPR35 expressed by VANs.

Figure 2.5: Effect of GPR35 agonist L-n-tetraose (LNT) on activating GPR35 on vagal afferent neurons (VANs) *in vitro*, as measured by phosphorylation of ERK relative to total ERK (pERK/ERK). A) Representative western blot of dose response to GPR35 agonist LNT (0.5-50 mM) on pERK/ERK. PMA was used as a positive control for pERK/ERK activation. B) Quantification of dose response of LNT (0.5-50mM) on pERK/ERK in VANs (Dunnett's multiple comparisons test; **p* <0.05, ****p* <0.001 from control, N=3).

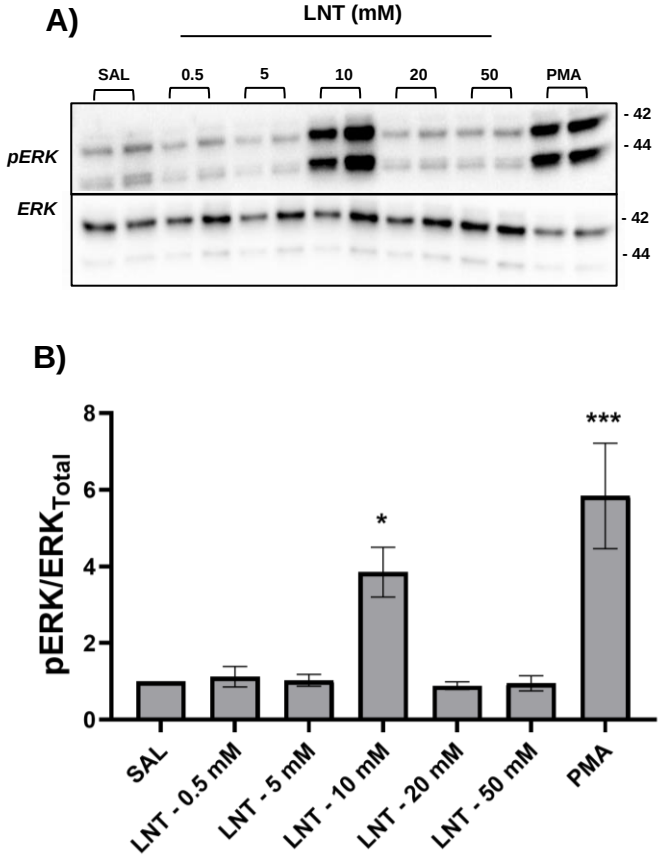

Figure 2.5: Effect of GPR35 agonist L-n-tetraose (LNT) on activating GPR35 on vagal afferent neurons (VANs) *in vitro*, as measured by phosphorylation of ERK relative to total ERK (pERK/ERK). C) Representative western blot of GPR35 antagonist CID-2745687 (CID; 50-100 µM) inhibition of LNT (10 mM)- or equimolar LAC-induced pERK/ERK of VANs. D) Quantification of inhibition by CID (50 µM) on LNT- or LAC-induced-activation of VANs (N=3). Different letters indicate statistically significant differences ($p < 0.05$). All samples normalized to VEH control. Data are presented as mean ± SEM. SAL, saline. LNT, lacto-N-tetraose. LAC, lactose. PMA, phorbol 12-myristate 13-acetate.

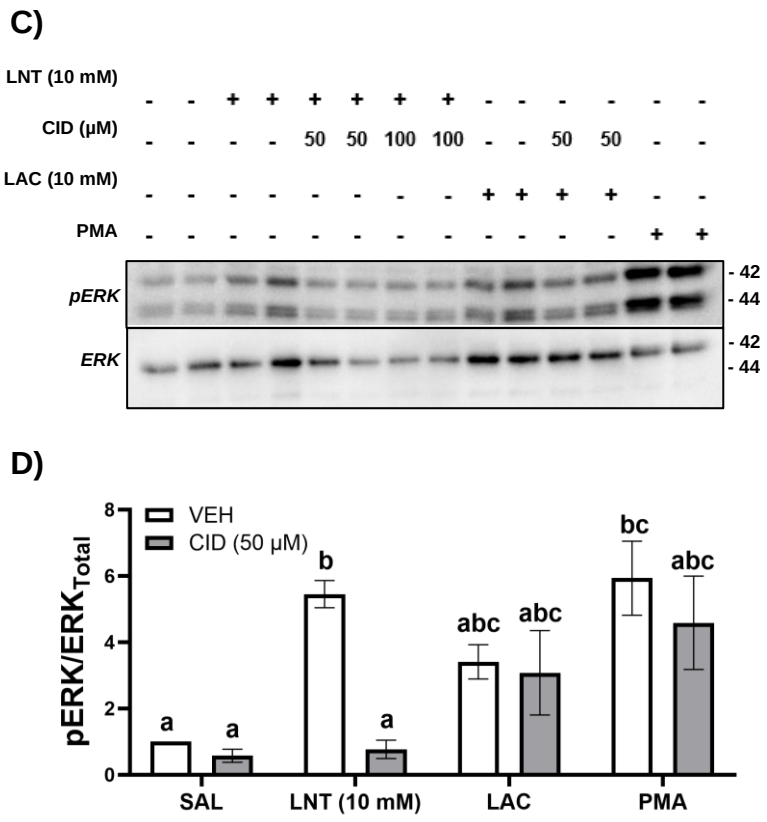

Effect of Acute Administration of the Synthetic GPR35 Agonist Zaprinast on Feeding Behavior and Satiety Signaling in Diet-Induced Obese Mice

The results from the *in vitro* studies suggest that GPR35 agonists directly activate vagal afferent neurons. Therefore, we determined the effects of acute administration of the GPR35 agonist zaprinast on food intake in mice. Study 1 included only male mice. Study 2 included male and age-matched female mice to determine if biological sex has a significant effect on zaprinast-induced changes in feeding behavior.

Study 1: Effect of Acute Administration of the Synthetic GPR35 Agonist Zaprinast on Feeding Behavior in Diet-Induced Obese Male Mice

In Study 1, zaprinast (10 mg/kg, IP) had no significant effect on cumulative diet intake relative to vehicle control throughout the 3-hour time course in LF-fed male mice (Figure 2.6A). Zaprinast had no significant effect on meal size, number or duration, ingestion rate, or latency to eat relative to vehicle controls in LF-fed male mice (Figures 2.7A-F). However, in HF-fed male mice, zaprinast significantly reduced cumulative diet intake relative to vehicle control (Figure 2.6A and 2.7A, N=6-8/group, $*p<0.05$). Zaprinast-induced reduction in diet intake in HF-fed males was associated with a significant reduction in average meal size (Figure 2.7B, N=6-8/group, $p<0.05$). Zaprinast also decreased meal number in HF-fed males, but this difference did not reach statistical significance (Figure 2.7C, N=6-8/group, $p=0.13$). Zaprinast did not affect average meal duration (Figure 2.7D) nor ingestion rate (Figure 2.7E) in HF-fed male mice relative to vehicle control. Surprisingly, zaprinast decreased the latency to eat in HF-fed male mice relative to vehicle controls (Figure 2.7F, $p=0.06$), but this difference did not reach statistical significance.

Figure 2.6: Effect of acute GPR35 agonist zaprinast (10 mg/kg, IP) or vehicle on cumulative food intake (kcal) up to 3 hours in LF- and HF-fed male (A-B) and female (C) mice. Each mouse received both treatments (vehicle or zaprinast, 10 mg/kg, IP) 48 hours apart. *p<0.05, **p< 0.005, ***p<0.001.

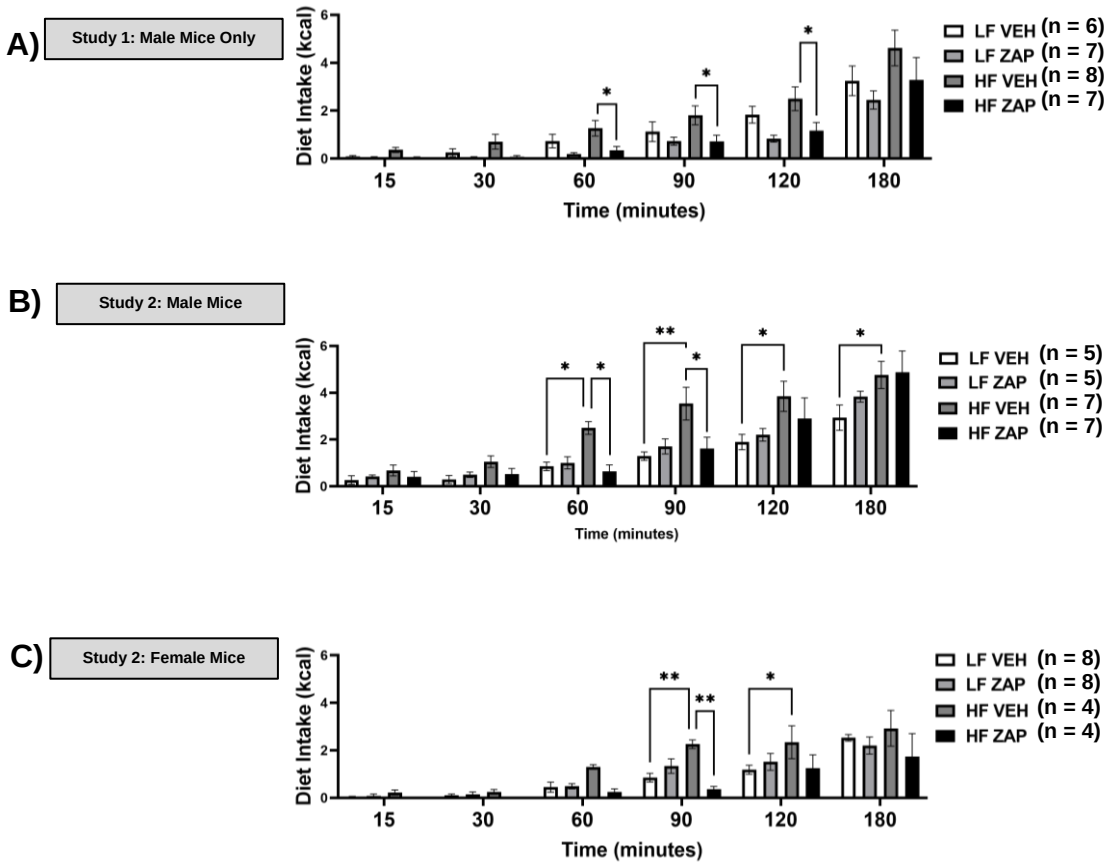

Figure 2.7: Effect of acute GPR35 agonist zaprinast (10 mg/kg, IP) or vehicle on feeding behavior at 60 minutes in LF- and HF-fed male mice (Study 1). Effect of zaprinast relative to vehicle on A) cumulative diet intake and meal parameters: B) meal size, C) meal number, D) meal duration, E) ingestion rat, and F) latency to eat. Each mouse received both treatments (vehicle or zaprinast, 10 mg/kg, IP) 48 hours apart. * $p<0.05$, ** $p<0.005$. N=6-8/group.

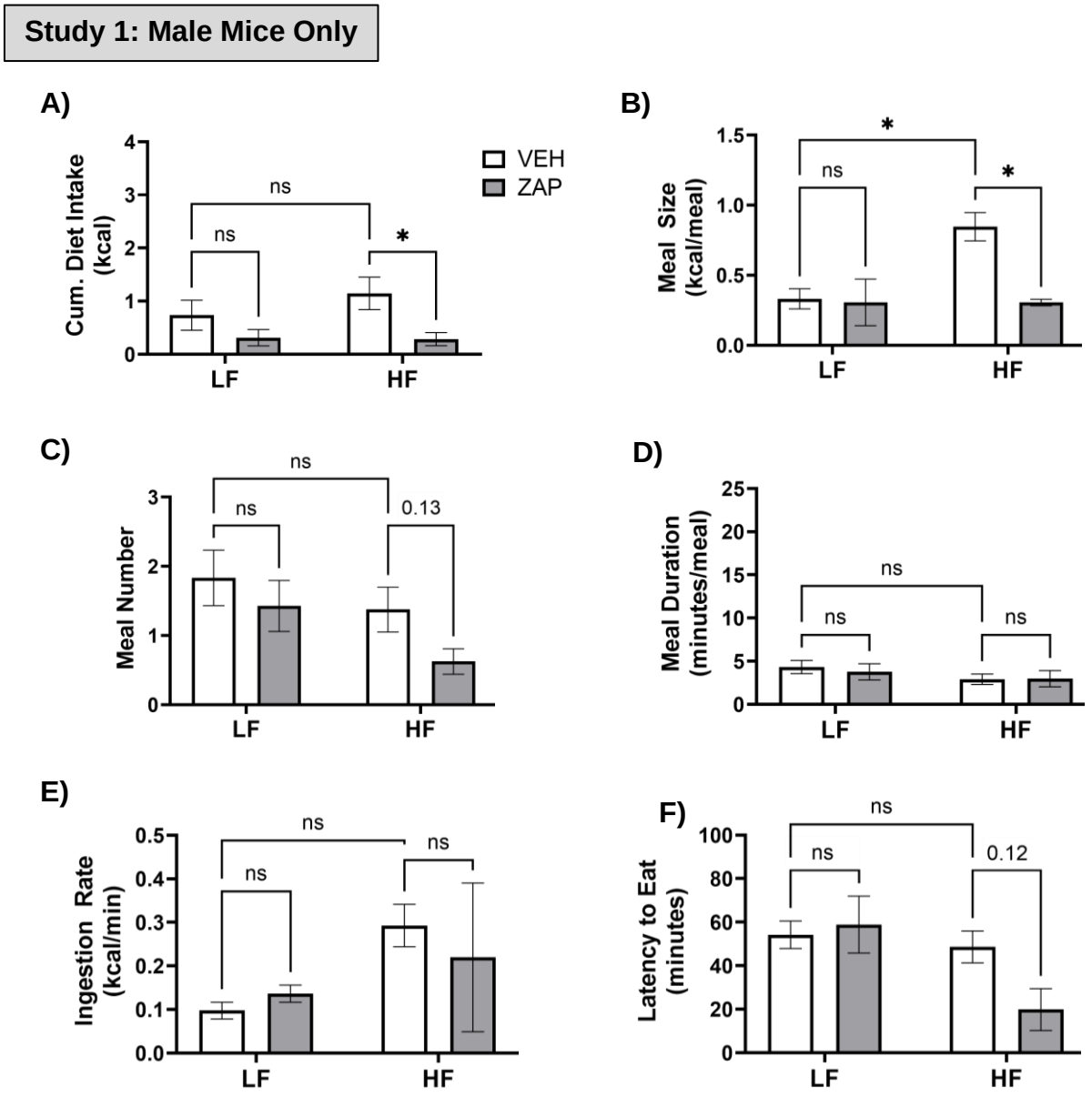

Study 1: Effect of Zaprinast on *c-fos* Expression in Nucleus of the Solitary Tract in Mouse Model of Obesity

In Study 1, zaprinast (10 mg/kg, IP) tended to increase *c-fos* expression in the NTS of LF-fed and HF-fed male mice relative to vehicle control (data not shown), but these differences from vehicle in either group did not reach statistical significance. We suspect this was due to poor sample integrity, which increased variance in this measurement in the pilot study.

Study 1: Effect of Zaprinast on VAN Activation *In Vivo*, as Measured by *Fos* Gene Expression in Nodose Ganglia of Male Mice

Previous work has shown that CCK-8S significantly increases *c-fos* gene expression in the NTS and reduces food intake by activating CCK_AR on VANs[15,43]. Here we show that CCK-8S (30 µg/kg, IP) significantly increases *fos* gene expression in the nodose ganglia of chow-fed male and female mice relative to saline control (Figure 2.8, N=3-7/group, *$p<0.05$). This data validates this qPCR method for quantifying VAN activation as measured by *fos* gene expression in nodose ganglia.

Figure 2.8: Effect of acute administration of CCK-8S (30 µg/kg, IP) on *fos* expression in nodose ganglia in male and female mice relative to vehicle. *Fos* gene expression in the nodose ganglion following acute injection of CCK-8S (30 µg/kg, IP) or saline control (0.9% v/v) in fasted male and female mice (N=3-7 per group). Data are presented as ±SEM. Different letters indicate $p<0.05$. CCK, cholecystokinin.

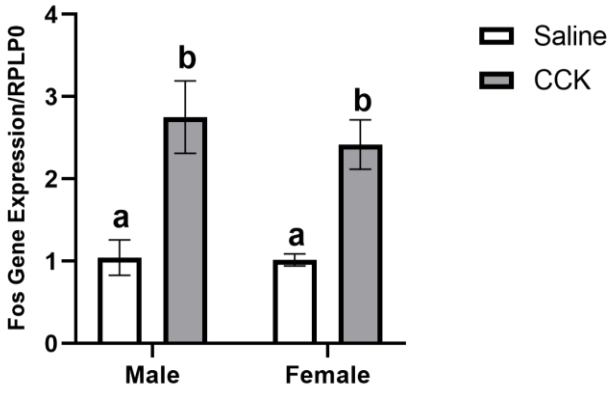

In Study 1, acute administration of zaprinast did not increase *fos* gene expression in the nodose ganglia of LF-fed male mice relative to vehicle control. However, in HF-fed males, zaprinast significantly increased *fos* gene expression in nodose of HF-fed male relative to vehicle control (Figure 2.9A, N=3-4/group, $*p<0.05$). Zaprinast increased *fos* expression in the nodose of diet-induced obese mice despite an HFD-induced increase in gene expression of *KCNK3*, which has been implicated in diet-induced desensitization of VANs to peripheral satiety signals[52] (Figure 2.9C, N=3-4/group, $p=0.0072$). Acute administration of zaprinast had no significant effect on gene expression of *GPR35* in nodose ganglion of male mice relative to vehicle control in either diet group (Figure 2.9B).

Figure 2.9: Effect of acute administration of GPR35 agonist zaprinast (10 mg/kg) on gene expression in nodose ganglia of LF- or HF-fed male mice (Study 1). A) Relative gene expression of A) *Fos* (marker of VAN activation), B) *GPR35*, and C) *KCNK3.* (N=3-4/group). Data are presented as ±SEM (*P<0.05). VEH, vehicle. ZAP, zaprinast.

Study 1: Male Mice Only

A)

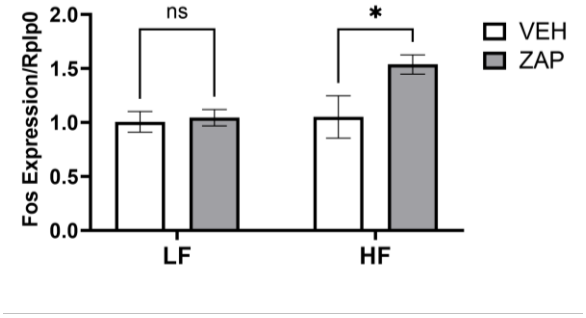

B)

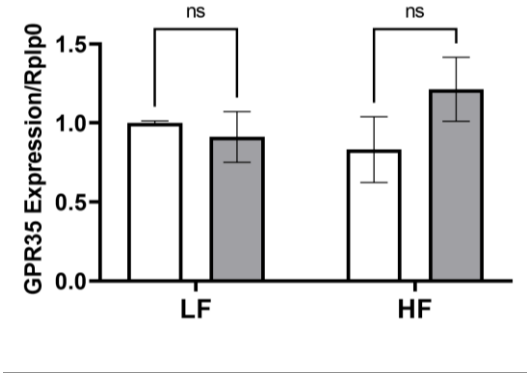

C)

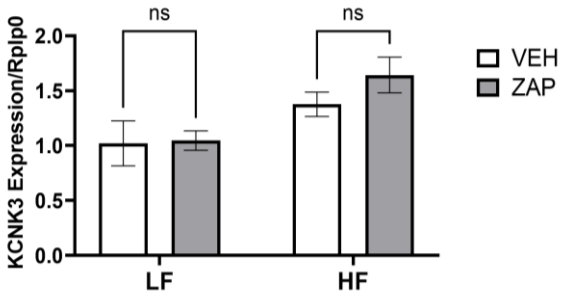

ANOVA - Fixed Effects	P value
Zaprinast	0.3273
Diet	0.0072
Zaprinast x Diet	0.4159

Study 2: Effect of Acute Administration of the Synthetic GPR35 Agonist Zaprinast on Feeding Behavior in Diet-Induced Obese Male and Female Mice

In study 2, zaprinast (10 mg/kg, IP) had no significant effect on cumulative food intake in LF-fed male mice relative to vehicle controls during the 3-hour time course (Figure 2.6B). Zaprinast had no significant effect on meal size, number or duration, ingestion rate, or latency to eat relative to vehicle controls at the 60-minute timepoint in LF-fed male mice (Figures 2.10B-F). However, as in Study 1, zaprinast significantly reduced cumulative food intake relative to vehicle control in HF-fed male mice (Figure 2.6B and 2.10A, N=5-7/group, *p<0.05). Similar to Study 1, zaprinast significantly reduced average meal size (Figure 2.10B, p<0.01). Zaprinast had no significant effect on average meal number (Figure 2.10C), meal duration (Figure 2.10D), nor ingestion rate (Figure 2.10E) in male HF-fed mice relative to vehicle. Zaprinast tended to decrease the latency to eat in HF-fed male mice relative to vehicle controls (Figure 2.10F), but this difference did not reach statistical significance.

Figure 2.10: Effect of acute GPR35 agonist zaprinast (10 mg/kg, IP) or vehicle on feeding behavior at 60 minutes in LF- and HF-fed male mice (Study 2). Effect of zaprinast on A) cumulative diet intake and meal parameters: B) meal size, C) meal number, D) meal duration, E) ingestion rat, and F) latency to eat. Each mouse received both treatments (vehicle or zaprinast, 10 mg/kg, IP) 48 hours apart. * $p<0.05$, ** $p<0.005$, *** $p<0.001$. N=5-7/group.

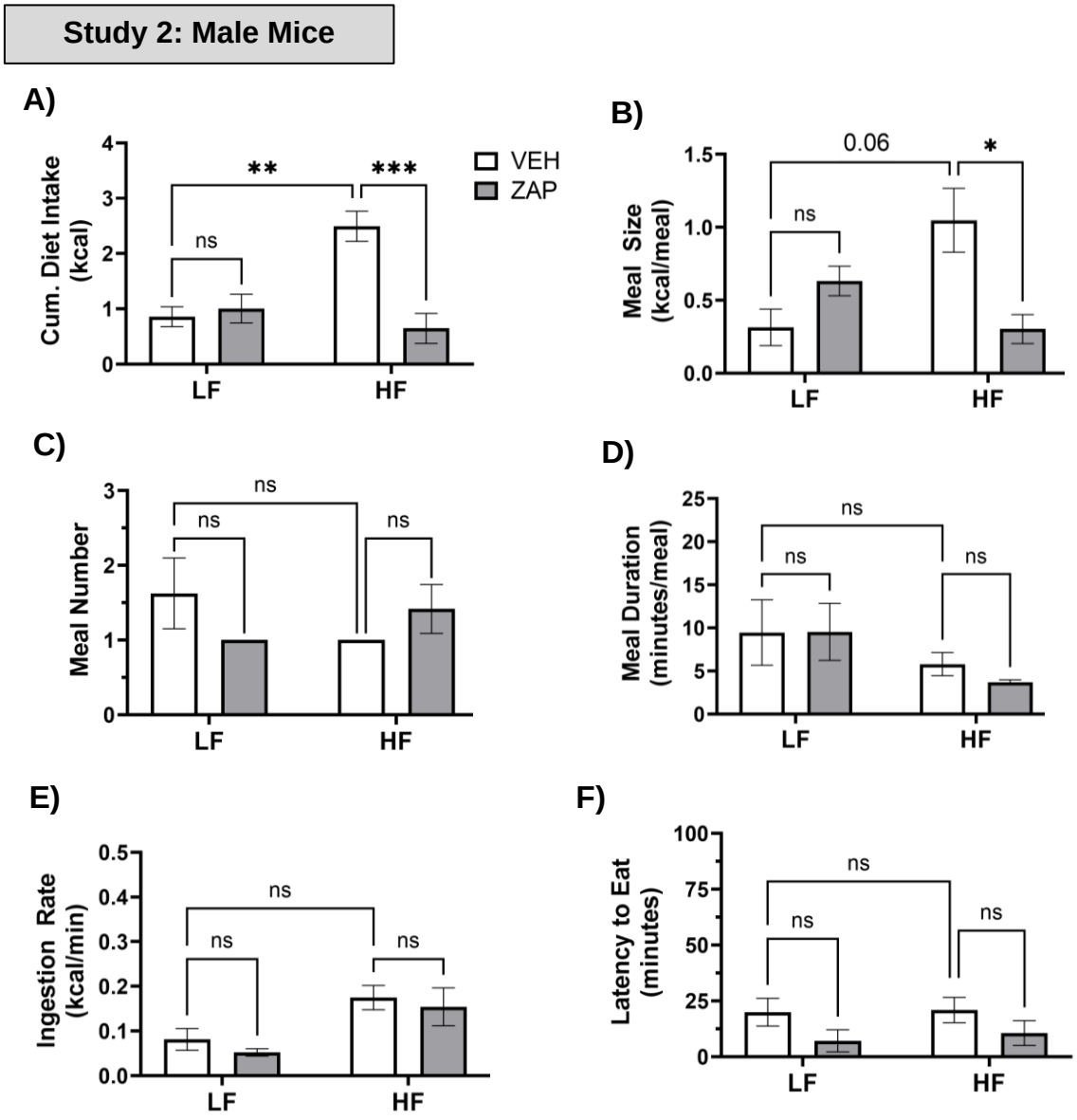

One striking difference between the feeding patterns of male and female mice was the difference in cumulative food intake across the 3-hour time course (Figure 2.6C). The 90-minute timepoint was the first timepoint at which zaprinast had a significant effect on feeding behavior in female mice. Zaprinast had no significant effect on cumulative food intake, meal size, number, or duration in LF-fed female mice relative to vehicle controls (Figures 2.11A-F), similar to observations in male mice. HF-fed female mice ate significantly more calories in the 90-minute period relative to their LF-fed counterparts, indicating the HF-fed female mice were hyperphagic (Figure 2.11A, N=4-8/group, *p<0.05). Zaprinast significantly reduced cumulative food intake in HF-fed female mice relative to vehicle controls (Figure 2.11A, N=4-8/group, *p<0.05), similar to the effect of zaprinast on feeding behavior in male mice. Zaprinast reduced meal size in HF-fed female mice relative to vehicle-treated controls (Figure 2.11B, p=0.35), but this difference did not reach statistical significance. Zaprinst did not affect meal number (Figure 2.11C) or meal duration (Figure 2.11D). There was a trend for zaprinast to reduce the rate of ingestion in both LF- and HF-fed female mice relative to vehicle controls (Figure 2.11E), but these differences did not reach statistical significance. Zaprinast also increased the latency to eat in female HF-fed mice relative to vehicle (Figure 2.11F, p=0.18) but this difference did not reach statistical significance.

Figure 2.11: Effect of acute GPR35 agonist zaprinast (10 mg/kg, IP) or vehicle on feeding behavior at 90 minutes in LF- and HF-fed female mice. Effect of zaprinast relative to vehicle on A) cumulative diet intake and meal parameters: B) meal size, C) meal number, D) meal duration, E) ingestion rat, and F) latency to eat. Each mouse received both treatments (vehicle or zaprinast, 10 mg/kg, IP) 48 hours apart. *p<0.05, **p<0.005. N=4-8/group.

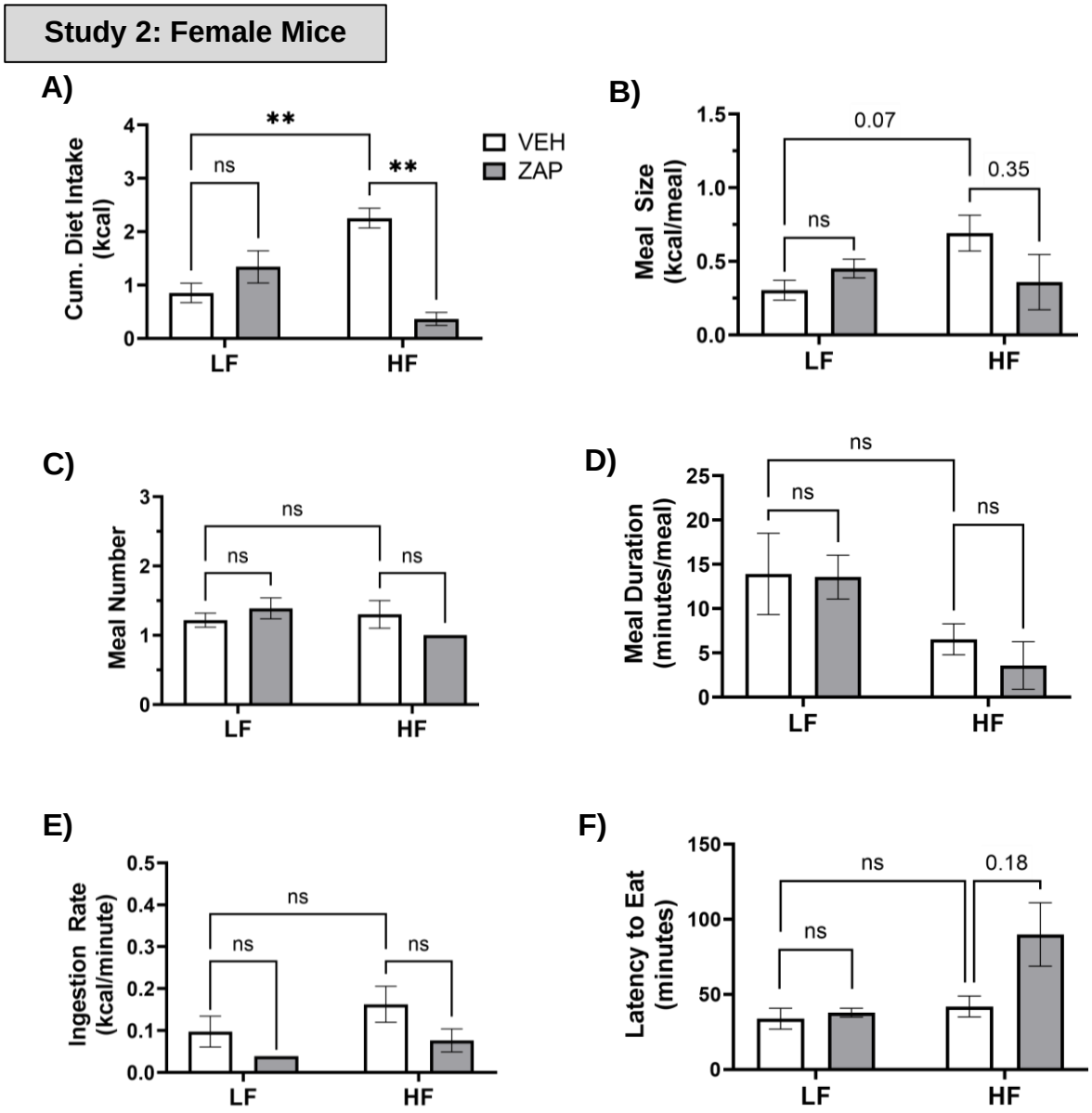

Study 2: Effect of Zaprinast on *C-fos* Expression in Nucleus of the Solitary Tract of Diet-Induced Obese Male and Female Mice

In Study 2, zaprinast had no significant effect on *c-fos* expression in the NTS of LF-fed male mice. However, in HF-fed male mice, zaprinast significantly increased *c-fos* expression in the NTS relative to vehicle controls (Figure 2.12, N=3-4/group, *p<0.05).

Similar to male counterparts, zaprinast had no significant effect on *c-fos* expression in the NTS of LF-fed female mice. Zaprinast significantly increased *c-fos* expression in the NTS of HF-fed female mice relative to vehicle controls (Figure 2.13, N=3-4/group, *p<0.05).

Figure 2.12: Effect of acute administration of GPR35 agonist zaprinast (10 mg/kg) on *c-fos protein* expression in nucleus of the solitary tract (NTS) in male mice. A) Quantitation of *c-fos* expression in NTS of LF- or HF-fed male mice treated with zaprinast or vehicle 2 hours before termination. B) Representative images of NTS from HF- or LF-fed mice injected with zaprinast or vehicle (N=3-4/group), **p*<0.05.

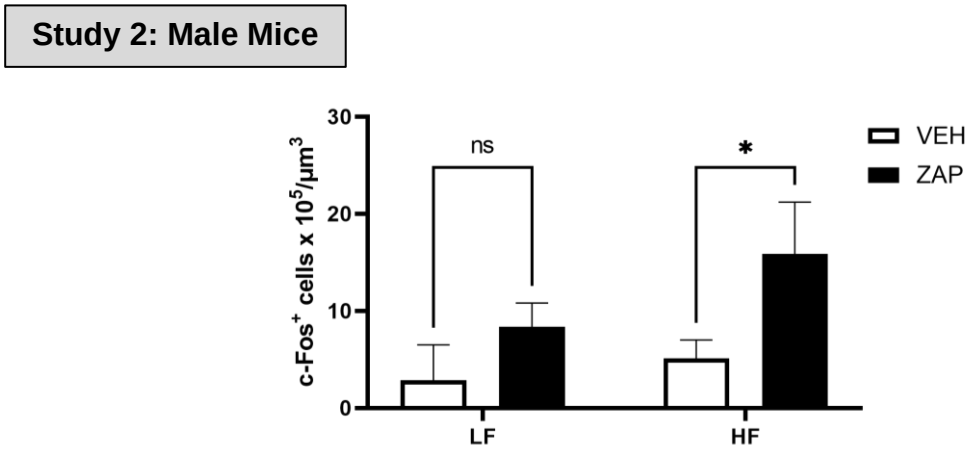

Figure 2.13: Effect of acute administration of GPR35 agonist zaprinast (10 mg/kg) on *c-fos protein* expression in nucleus of the solitary tract (NTS) in male and female mice. Quantitation of *c-fos* expression in NTS of LF- or HF-fed male mice treated with zaprinast or vehicle 2 hours before termination. (N=3-4/group). *p<0.05., **p<0.01.

Study 2: Female Mice

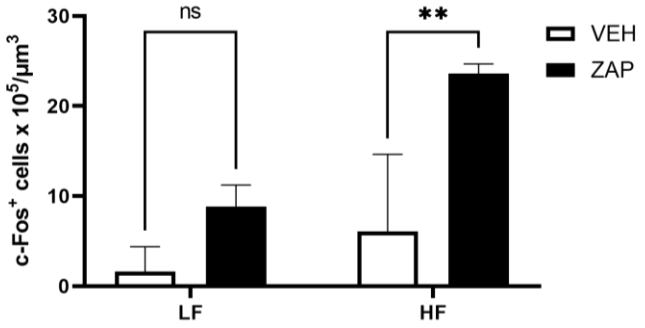

Study 2: Effect of Zaprinast on VAN Activation *In Vivo*, as Measured by *Fos* Gene Expression in Nodose Ganglia of Male and Female Mice

In Study 2, zaprinast did not increase *fos* gene expression in nodose of LF-fed nor HF-fed male mice relative to vehicle control (Figure 2.14A, N=3-4/group). Similar to Study 1, HF-feeding increased gene expression of *KCNK3* relative to LF-fed controls (Figure 2.14B, N=3-4/group, p=0.0078). Zaprinast had no significant effect on gene expression of *GPR35* (Figure 2.14B) nor *KCNK3* (Figure 2.14C) in nodose of male mice relative to vehicle control in either diet group.

Figure 2.14: Effect of acute administration of GPR35 agonist zaprinast (10 mg/kg) on gene expression in nodose ganglia of LF- or HF-fed male mice (Study 2). A) Relative gene expression of A) *Fos* (marker of VAN activation), B) *GPR35*, C) and *KCNK3* (N=3-4/group). Data are presented as ±SEM (*P<0.05). VEH, vehicle. ZAP, zaprinast.

Study 2: Male Mice

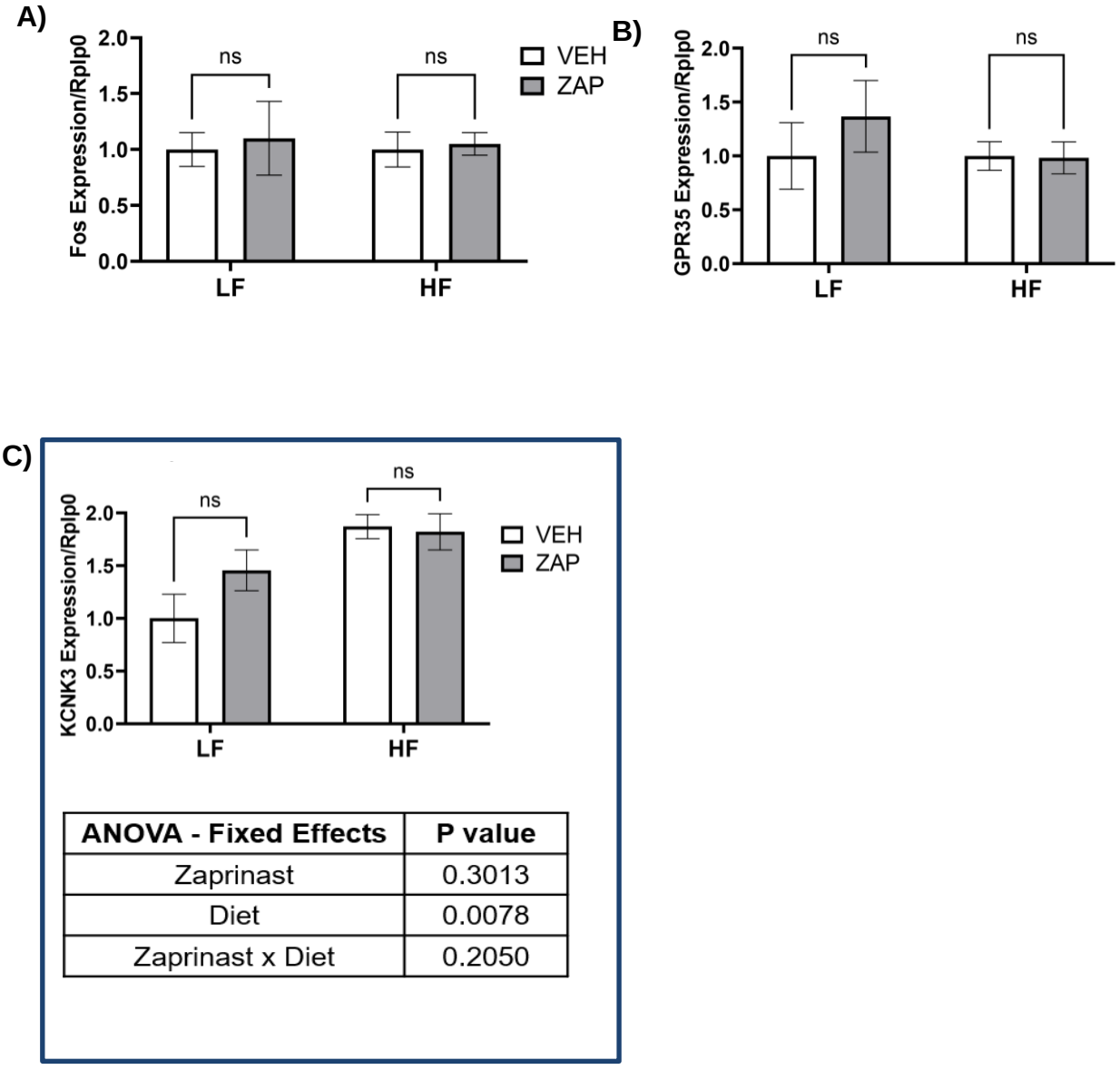

ANOVA - Fixed Effects	P value
Zaprinast	0.3013
Diet	0.0078
Zaprinast x Diet	0.2050

Similar to Study 1, zaprinast did not increase *fos* gene expression in the nodose ganglia of LF-fed female mice relative to vehicle control (Figure 2.15A, N=3-4/group). However, zaprinast significantly increased *fos* gene expression in nodose of HF-fed female mice relative to vehicle controls (Figure 2.15A, N=3-4/group, $*p<0.05$). Similar to Study 1, zaprinast increased *fos* expression in nodose from female mice despite an HFD-induced increase in gene expression of *KCNK3* relative to LF-fed controls (Figure 2.15C, N=3-4/group, $p=0.0171$). Acute administration of zaprinast did not significantly affect gene expression of *GPR35* (Figure 2.14B) nor *KCNK3* (Figure 2.14C) in nodose of female mice relative to vehicle control in either group.

Figure 2.15: Effect of acute administration of GPR35 agonist zaprinast (10 mg/kg) on gene expression in nodose ganglia of LF- or HF-fed female mice (Study 2). A) Relative gene expression of A) *Fos* (marker of VAN activation), B) *GPR35*, C) and *KCNK3* (N=3-4/group). Data are presented as ±SEM (*P<0.05). VEH, vehicle. ZAP, zaprinast.

Study 2: Female Mice

A)

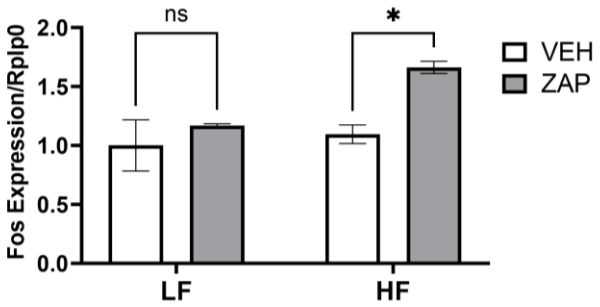

B)

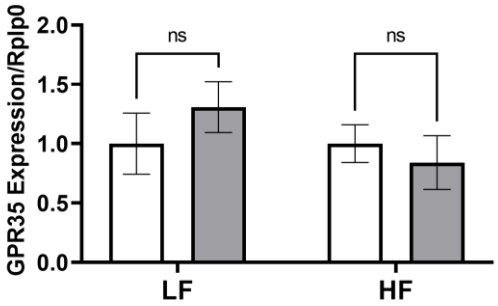

C)

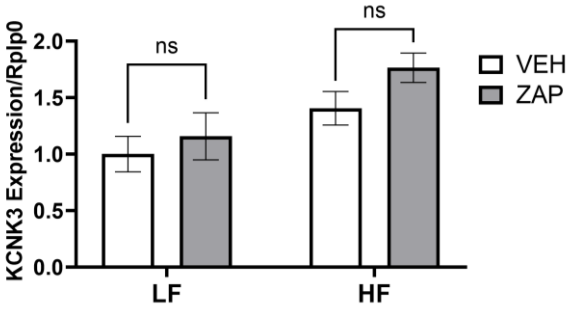

ANOVA - Fixed Effects	P value
Zaprinast	0.1718
Diet	0.0171
Zaprinast x Diet	0.5780

Table 2.1 Table of qPCR Primers

Species	Gene	Forward (5'→ 3')	Reverse (3' → 5')
Mouse	*GPR35*	AAGGCCCACCTGGAGTAGA	GAAGAAGTTGTTGACGGAAGCA
Mouse	*Fos*	GGCTCTCCTGTCAACACACA	CCGTGGGGATAAAGTTGGCA
Mouse	*KCNK3.1*	ACTTCGCCATCACCGTCATCA	AACATGACTAGTGTGAGCGGGA
Mouse	*KCNK9.1*	CTTCGCCATCACTGTCATCAC	GATACCCAGCACAGCGTAGAA
Mouse	*TDO2*	TGGCAATTACTTGCAGTTGGA	GTGCTCGTCATGGATTTTGTTC
Mouse	*KATI*	CGAAGGCTGGAAGGGATCG	GCGGTGAGAAGTCAGGGAA
Mouse	*KATII*	ATGAATTACTCACGGTTCCTCAC	AACATGCTCGGGTTTGGAGAT
Mouse	*KYAT3*	GTGCATCAGCGATGAGGTTTA	GTTCTCTCCCACATACCTGGAA
Mouse	*RPLP0*	AGATTCGGGATATGCTGTTGGC	TCGGGTCCTAGACCAGTGTTC
Rat	*GPR35*	AAGGCCAGCCTGGAGTAGAA	TGGTGAAGACGTGGTTGACTG
Rat	*TUBB3*	GAGCCTGGAACCATGGACAG	TGTATAGTGCCCTTTGGCCC
Rat	*IBA1*	CTGGAGGCCTTCAAGACGAA	TGGGAACCCCAAGTTTCTCC
Rat	*RPLP0*	TCGCTTCCTAGAGGGTGTCC	ACTGAGGCAACAGTCGGGTA

2.6. Discussion

Obesity is a leading risk factor for life-threatening diseases and its increasing prevalence parallels the over-consumption of calorically-dense foods[53–55]. Innovations in obesity research include neuromodulation of vagal afferent sensitivity using bioelectrical[56,57], pharmacological[58–60], or nutraceutical solutions to restore satiety signaling. Previous work shows that the success of effective weight loss strategies is associated with the increased production of anorectic microbial metabolites, such as short-chain fatty acids (SCFAs), bile acids (BAs), and tryptophan metabolites[61–63]. Recent work suggests that these metabolites may increase vagal afferent sensitivity to endogenous satiety hormones and may contribute to enhanced satiety[64,65]. A recent study showed that GPR35, the receptor for the microbial metabolite KYNA, is highly expressed by VANs and co-expressed with CCK_AR in the mouse[26]. The function of GPR35 expression on VANs is not known. Therefore, the goal of the present study was to determine whether GPR35 agonists activate VANs and reduce food intake in mice. The data here show that endogenous and synthetic GPR35 agonists directly activate VANs *in vitro* via GPR35 and that GPR35 agonists can activate the vagal afferent pathway *in vivo*. Acute administration of the synthetic GPR35 agonist zaprinast decreases food intake up to 2 hours post-injection in HF-fed, but not LF-fed, mice by reducing meal size. Taken together, this data suggests that GPR35 expressed by VAN may play a role in the regulation of food intake, potentially by inducing satiety.

Previous research on GPR35 has been focused on its potential role in tissues in which it is highly expressed including the gastrointestinal tract, liver (hepatosteatosis), and immune cell function [32,33,66–69]. Recent evidence has also demonstrated the potential role of GPR35 in energy balance[29,70,71] but its effect on satiety signaling at the

level of vagal afferent neurons (VANs) has yet to be studied. GPR35 is co-expressed with CCKAR on VANs[26], and our data show that GPR35 expression is 100-fold higher than in gastrointestinal tissue. It has been shown that KYNA, an endogenous GPR35 agonist, is generated in the gut lumen[72,73]. Therefore, KYNA in the gut could act directly on GPR35 expressed on VAN terminals located within the wall of the gastrointestinal tract. However, it is unknown whether GPR35 agonists directly activate VANs.

The nodose ganglia house vagal afferent neurons and peripheral glia. Previous work shows that GPR35 is expressed by macrophages[33]. Our work and others show that GPR35 is highly expressed in VANs within the nodose ganglia[26]. However, glia could mediate the effects of GPR35 agonists to alter VAN activity. Therefore, we sought to determine whether GPR35 agonists activate VANs via direct or indirect mechanisms. Neurons were separated from glia in extracts of the rat nodose ganglia using a low viscosity density gradient medium. Fluorescent and brightfield microscopy and qPCR verified that the method effectively separated the two cell populations. Furthermore, qPCR data showed that the neuronal, but not the glial fraction, expressed GPR35. These data suggest that VANs express GPR35 and that GPR35 agonists may activate VANs by direct activation of GPR35 expressed on sensory terminals of the neurons that are normally located in the gut wall.

Previous work shows that phosphorylation of extracellular regulated kinase (pERK) is necessary for peripheral CCK to suppress food intake in rats and that this is mediated via intact vagal nerves[15,74,75] In the context of the present experiments, pERK/ERK served as a measurement of VAN activation, as previously published[18,42,76]. Zaprinast is a synthetic agonist for GPR35 with a high affinity for murine and human orthologues[70].

Zaprinast has also been shown to act as a phosphodiesterase 5 (PDE) inhibitor at the concentrations used in this data chapter. However, previous work has demonstrated that PDE5 inhibitors decrease the sensitivity of VANs to peripheral satiety signals[26]. The data demonstrate that zaprinast activates VANs *in vitro*. The GPR35 antagonist CID-2754687 prevented zaprinast-induced activation of VANs suggesting that zaprinast-induced pERK/ERK is mediated via GPR35. Furthermore, this data also demonstrates that zaprinast is acting as a GPR35 agonist and not as a PDE5 inhibitor. This data indicates that GPR35 on cultured rat VANs is a functional receptor and that the synthetic GPR35 agonist zaprinast can activate VANs via GPR35. The data also show that endogenous GPR35 agonist, KYNA activates VANs *in vitro* and this effect is mediated via GPR35. Interestingly, KYNA increased pERK/ERK within the range of KYNA concentration found in the lumen of the gastrointestinal tract of rats[72]. Previous unpublished *in vitro* work in our lab demonstrated KYNA increases leptin signaling in VANs as measured by pERK relative to controls, although the mechanism had not been determined (Ehrlich and Raybould, unpublished observations). However, previous studies from our lab demonstrated that leptin increases the expression of an important immediate early gene, early growth response factor-1 (EGR1), and CCK induces the nuclear localization of EGR1 to upregulate the expression of important targets[77,78] involved in regulating VAN activation[42]. We did not investigate the mechanistic interaction of GPR35 and CCK_AR in the present studies. However, considering the previous work from our lab and published literature demonstrating GPR35 and CCK_AR are co-expressed on VANs[26], these data suggest that endogenous GPR35 agonists at physiologically relevant levels are capable of activating VANs via GPR35 and may alter

signaling in response to CCK or leptin. This may represent a potential mechanism by which the microbial metabolite KYNA generated at the level of vagal sensory terminals can increase satiety signaling. Although previous *in vitro* work has demonstrated that GPR35 activation reduces energy balance by increasing energy expenditure by activating brown adipose tissue (BAT)[29], these data suggest a new role for KYNA and GPR35 on VANs in the context of satiety signaling.

LNT is a milk oligosaccharide abundant in human breast milk[79]. The literature demonstrates these milk oligosaccharides are metabolized by commensal bacteria within the infant gut[79–81] to help establish a “healthy” microbiome in early life. In addition, HMOs act as important signaling molecules to regulate inflammatory responses[82–84]. Recent *in vitro* work using β-arrestin assays demonstrate that LNT is an agonist for GPR35 and hydrolysis of LNT eliminates this response, indicating intact LNT activates GPR35[41]. Our *in vitro* data using nodose ganglia cultures shows that LNT can activate VANs. This is likely to be a specific GPR35-mediated effect as it was inhibited by the GPR35 antagonist. In contrast, the activation of VANs by lactose was unaffected by GPR35 inhibition. These data support observations reported by Foata *et al.* where LNT, but not lactose, was shown to be an agonist for GPR35[41] and importantly, provide evidence for a functional response to GPR35 activation in a non-transformed cell. These data suggest a novel mechanism by which HMOs, such as LNT, may interact with the host to alter peripheral satiety signaling and feeding behavior.

Zaprinast significantly reduced cumulative food intake in HF-fed, but not LF-fed animals, regardless of sex. HF-fed mice ate larger meals consistent with many prior studies, likely to be due to decreased satiation. Zaprinast reduced food intake in HF-fed

male mice by reducing meal size, a marker of enhanced satiety. Zaprinast decreased meal size to a level not significantly different from that seen in LF fed mice, suggesting that acute administration of zaprinast may restore normal VAN satiety signaling in obese animals. There was a trend of zaprinast to reduce meal size in HF-fed female mice, but this difference did not reach statistical significance. Although this could be addressed in future studies by increasing the sample size, the data still suggest that acute administration of synthetic GPR35 agonists reduces diet-induced hyperphagia in males and females via VANs but perhaps through slightly different mechanisms. The data show that there was no difference in the gene expression of GPR35 between male and female mice.

The mechanisms by which zaprinast increases VAN satiety signaling may differ between male and female mice. Interestingly, zaprinast tended to reduce latency to eat, indicating increased urgency to feed, and although this effect was not significant, it was reproducible in both Study 1 and 2. This is an unexpected finding because this phenotype has been observed in CCK_AR global knockout mice[38] and would likewise be expected with inhibition of GPR35 if it is involved in enhancing the sensitivity of VANs to peripheral satiety signals, such as CCK. In contrast, zaprinast tended to increase meal latency in female HF-fed mice relative to vehicle control, albeit this effect was not significant. Since the stress of injection and acclimation were controlled in these feeding behavior experiments[85,86], this data may suggest there is a sex-dependent difference in VAN sensitivity to GPR35 agonists. Indeed, our lab has previously shown that disrupting satiety signaling in VANs in female mice reduces expression of the nuclear estrogen receptor, Esr1, and thereby reduces sensitivity to CCK[16,51]. Future studies should

investigate sex-dependent differences in signaling between CCK_AR and GPR35 at the level of vagal sensory neurons.

CCK stimulates VANs and increases *c-fos* expression, a marker of neuronal activation, in the NTS and decreases food intake. In Study 2, zaprinast significantly increased *c-fos* expression in the NTS of HF-fed mice relative to vehicle control, regardless of sex. Zaprinast had no significant effect on *c-fos* immunoreactivity in the NTS of LF-fed animals in either Study 1 or 2. In Study 1, although there was a trend of zaprinast to increase *c-fos* staining in the NTS relative to vehicle in both diet groups, this difference did not reach statistical significance and was insufficiently powered (N=2-4/group). These data support our hypothesis that zaprinast increases satiety signaling to the NTS and suggests that zaprinast-induced reductions in food intake mediated by VANs are also diet-dependent.

Relative to vehicle controls, zaprinast increased *fos* gene expression in nodose ganglia in HF-fed but not LF-fed males (Study 1) and female mice (Study 2) supporting the hypothesis that GPR35 agonists activate VANs and increase satiety signaling. However, zaprinast did not significantly increase *fos* gene expression in HF-fed male mice in Study 1 relative to vehicle controls. Considering the data shows that zaprinast significantly reduced cumulative food intake in these animals at earlier time points and also significantly increased zaprinast-induced activation of *c-fos* in the NTS of these mice relative to vehicle controls, we expect there was a technical error during tissue harvest or qPCR of nodose from male mice in Study 2.

Zaprinast administration did not significantly affect gene expression of GPR35 in nodose ganglia. Similarly, diet also did not significantly affect GPR35 gene expression

in the nodose ganglion, suggesting that HF-feeding reduces the activation of GPR35 on VANs but not its gene expression.

Recent work has shown that HFD may alter VAN sensitivity by increasing gene expression of two-pore potassium channels in VANs leading to increasing potassium conductance thereby reducing VAN excitability and sensitivity to peripheral satiety factors[17,52]. In our zaprinast feeding behavior study (Study 2), HF feeding increased gene expression of *KCNK3* in both male and female animals. This data suggests that zaprinast can induce satiety in both male and female mice despite HFD-induced increases in potassium conductance in VANs.

2.7. Conclusion

This *in vitro* and *in vivo* work shows that synthetic and naturally occurring GPR35 agonists increase VAN satiety signaling by direct activation of GPR35 on VANs. Importantly, this work shows that acute administration of a GPR35 agonist reduces diet-induced hyperphagia and that this effect was dependent on diet, but independent of sex. These data demonstrate a role for GPR35 on VANs and reveals a potential peripheral target for modifying feeding behavior in the context of diet-induced obesity. Future work could employ VAN-specific GPR35 knockout animals, vagotomy models, and/or chemogenetic tools to determine the mechanism by which GPR35 activation on VANs mediates satiety.

2.8. References

1. Bai, L. *et al.* Genetic Identification of Vagal Sensory Neurons That Control Feeding. *Cell* **179**, 1129-1143.e23 (2019).
2. Berthoud, H. R. & Neuhuber, W. L. Functional and chemical anatomy of the afferent vagal system. *Auton. Neurosci. Basic Clin.* **85**, 1–17 (2000).
3. Han, W. *et al.* A Neural Circuit for Gut-Induced Reward. *Cell* 1–14 (2018) doi:10.1016/j.cell.2018.08.049.
4. Wang, Y. B., de Lartigue, G. & Page, A. J. Dissecting the Role of Subtypes of Gastrointestinal Vagal Afferents. *Front. Physiol.* **11**, (2020).
5. Grabauskas, G. & Owyang, C. Plasticity of vagal afferent signaling in the gut. *Medicina (Mex.)* (2017).
6. Loper, H. *et al.* Both high fat and high carbohydrate diets impair vagus nerve signaling of satiety. *Sci. Rep.* **11**, 10394 (2021).
7. De Lartigue, G., Barbier, C., Serre, L. & Raybould, H. E. Vagal afferent neurons in high fat diet-induced obesity; intestinal microflora, gut inflammation and cholecystokinin. *Physiol. Behav.* **105**, 100–5 (2011).
8. De Lartigue, G., Barbier De La Serre, C., Espero, E., Lee, J. & Raybould, H. E. Diet-induced obesity leads to the development of leptin resistance in vagal afferent neurons. *Am J Physiol Endocrinol Metab* **301**, 187–195 (2011).
9. Little, T. J., Horowitz, M. & Feinle-Bisset, C. Modulation by high-fat diets of gastrointestinal function and hormones associated with the regulation of energy intake: Implications for the pathophysiology of obesity. *Am. J. Clin. Nutr.* **86**, 531–541 (2007).
10. Covasa, M. & Ritter, R. C. Adaptation to high-fat diet reduces inhibition of gastric

emptying by CCK and intestinal oleate. *Am J Physiol Regul. Integr. Comp Physiol* **278**, 166–170 (2000).

11. Covasa, M., Grahn, J. & Ritter, R. C. High fat maintenance diet attenuates hindbrain neuronal response to CCK. *Regul. Pept.* **86**, 83–88 (2000).
12. de La Serre, C. B. *et al.* Propensity to high-fat diet-induced obesity in rats is associated with changes in the gut microbiota and gut inflammation. *AJP Gastrointest. Liver Physiol.* **299**, G440–G448 (2010).
13. Madden, C. J. & Morrison, S. F. A high-fat diet impairs cooling-evoked brown adipose tissue activation via a vagal afferent mechanism. *Am. J. Physiol. - Endocrinol. Metab.* **311**, E287–E292 (2016).
14. de Lartigue, G., Ronveaux, C. C. & Raybould, H. E. Deletion of leptin signaling in vagal afferent neurons results in hyperphagia and obesity. *Mol. Metab.* **3**, 595–607 (2014).
15. McDougle, M. *et al.* Intact vagal gut-brain signalling prevents hyperphagia and excessive weight gain in response to high-fat high-sugar diet. *Acta Physiol.* **00**, (2020).
16. Huang, K. P. *et al.* Sex differences in response to short-term high fat diet in mice. *Physiol. Behav.* **221**, 112894 (2020).
17. Grabauskas, G. *et al.* High-fat diet-induced vagal afferent dysfunction via upregulation of 2-pore domain potassium TRESK channel. *JCI Insight* **4**, (2019).
18. de La Serre, C. B., de Lartigue, G. & Raybould, H. E. Chronic exposure to Low dose bacterial lipopolysaccharide inhibits leptin signaling in vagal afferent neurons. *Physiol. Behav.* **139**, 188–194 (2015).

19. Kim, D.-Y. *et al.* Is There a Role for Gastric Accommodation and Satiety in Asymptomatic Obese People? *Obes. Res.* **9**, 655–661 (2001).
20. Goldstein, D. J. *The management of eating disorders and obesity*. (Humana Press, 2005).
21. Stopyra, M. A. *et al.* Homeostasis and food craving in obesity: a functional MRI study. *Int. J. Obes.* **45**, 2464–2470 (2021).
22. Lee, S. *et al.* 2'-Fucosyllactose Supplementation Improves Gut-Brain Signaling and Diet-Induced Obese Phenotype and Changes the Gut Microbiota in High Fat-Fed Mice. *Nutrients* **12**, (2020).
23. Frost, G. *et al.* The short-chain fatty acid acetate reduces appetite via a central homeostatic mechanism. *Nat. Commun.* **5**, 1–11 (2014).
24. Berthoud, H. R. & Neuhuber, W. L. Vagal mechanisms as neuromodulatory targets for the treatment of metabolic disease. *Ann. N. Y. Acad. Sci.* **1454**, 42–55 (2019).
25. Gautron, L. The Phantom Satiation Hypothesis of Bariatric Surgery. *Front. Neurosci.* **15**, 22 (2021).
26. Egerod, K. L. *et al.* Profiling of G protein-coupled receptors in vagal afferents reveals novel gut-to-brain sensing mechanisms. *Mol. Metab.* **12**, 62–75 (2018).
27. Lund, M. L. *et al.* Enterochromaffin 5-HT cells – A major target for GLP-1 and gut microbial metabolites. *Mol. Metab.* **11**, 70–83 (2018).
28. Kupari, J., Hä Ring, M., Agirre, E., Alo Castelo-Branco, G. & Ernfors, P. An Atlas of Vagal Sensory Neurons and Their Molecular Specialization Cell Reports Resource An Atlas of Vagal Sensory Neurons and Their Molecular Specialization. *CellReports* **27**, 2508-2523.e4 (2019).

29. Agudelo, L. Z. *et al.* Kynurenic Acid and Gpr35 Regulate Adipose Tissue Energy Homeostasis and Inflammation. *Cell Metab.* **27**, 378-392.e5 (2018).
30. Turski, M. P., Turska, M., Paluszkiewicz, P., Parada-Turska, J. & Oxenkrug, G. F. Kynurenic Acid in the Digestive system-new Facts, new challenges. *Int. J. Tryptophan Res.* **6**, 47–55 (2013).
31. Turska, M., Paluszkiewicz, P., Turski, W. A. & Parada-Turska, J. A Review of the Health Benefits of Food Enriched with Kynurenic Acid. *Nutrients* **14**, (2022).
32. Wang, D. *et al. GPR35-mediated Kynurenic Acid Sensing Acts as a Defender Against Gut Microbiota Disorder in Ulcerative Colitis*. https://www.researchsquare.com/article/rs-2162768/v1 (2022) doi:10.21203/rs.3.rs-2162768/v1.
33. Zheng, X. *et al.* Kynurenic acid/GPR35 axis restricts NLRP3 inflammasome activation and exacerbates colitis in mice with social stress. *Brain. Behav. Immun.* **79**, 244–255 (2019).
34. Osman, S., Tashtush, A., Reed, D. E. & Lomax, A. E. Analysis of the spinal and vagal afferent innervation of the mouse colon using neuronal retrograde tracers. *Cell Tissue Res.* (2023) doi:10.1007/s00441-023-03769-3.
35. Meerschaert, K. A. *et al.* Unique Molecular Characteristics of Visceral Afferents Arising from Different Levels of the Neuraxis: Location of Afferent Somata Predicts Function and Stimulus Detection Modalities. *J. Neurosci.* **40**, 7216–7228 (2020).
36. Pyun, D. H. *et al.* Endogenous metabolite, kynurenic acid, attenuates nonalcoholic fatty liver disease via AMPK/autophagy- and AMPK/ORP150-mediated signaling. *J. Cell. Physiol.* **236**, 4902–4912 (2021).

37. Zhen, D., Liu, J., Zhang, X. D. & Song, Z. Kynurenic Acid Acts as a Signaling Molecule Regulating Energy Expenditure and Is Closely Associated With Metabolic Diseases. *Front. Endocrinol.* **13**, 187 (2022).
38. Donovan, M. J., Paulino, G. & Raybould, H. E. CCK1 receptor is essential for normal meal patterning in mice fed high fat diet. *Physiol. Behav.* **92**, 969–974 (2007).
39. Raybould, H. E. & Tache, Y. Cholecystokinin inhibits gastric motility and emptying via a capsaicin-sensitive vagal pathway in rats. *Am. J. Physiol.-Gastrointest. Liver Physiol.* **255**, G242–G246 (1988).
40. Lo, C.-M. *et al.* Cholecystokinin Knockout Mice Are Resistant to High-Fat Diet-Induced Obesity. *YGAST* **138**, 1997–2005 (2010).
41. Foata, F., Sprenger, N., Rochat, F. & Damak, S. Activation of the G-protein coupled receptor GPR35 by human milk oligosaccharides through different pathways. *Sci. Rep.* **10**, 1–9 (2020).
42. de Lartigue, G. *et al.* EGR1 Is a target for cooperative interactions between cholecystokinin and leptin, and inhibition by ghrelin, in vagal afferent neurons. *Endocrinology* **151**, 3589–99 (2010).
43. Diepenbroek, C. *et al.* Validation and characterization of a novel method for selective vagal deafferentation of the gut. *Am J Physiol Gastrointest Liver Physiol* **313**, 342–352 (2017).
44. Wang, L., Martínez, V., Barrachina, M. D. & Taché, Y. Fos expression in the brain induced by peripheral injection of CCK or leptin plus CCK in fasted lean mice. *Brain Res.* **791**, 157–166 (1998).
45. Fraser, K. A. & Davison, J. S. Cholecystokinin-induced c-fos expression in the rat

brain stem is influenced by vagal nerve integrity. *Exp. Physiol.* **77**, 225–228 (1992).

46. Livak, K. J. & Schmittgen, T. D. Analysis of Relative Gene Expression Data Using Real-Time Quantitative PCR and the 2−ΔΔCT Method. *Methods* **25**, 402–408 (2001).
47. Fan, X. *et al.* High-Fat Diet Alters the Expression of Reference Genes in Male Mice. *Front. Nutr.* **7**, (2020).
48. Häring, M., Fatt, M. & Kupari, J. Protocol to Prepare Single-Cell Suspensions from Mouse Vagal Sensory Ganglia for Transcriptomic Studies. *STAR Protoc.* **1**, (2020).
49. Malin, S. A., Davis, B. M. & Molliver, D. C. Production of dissociated sensory neuron cultures and considerations for their use in studying neuronal function and plasticity. *Nat. Protoc.* **2**, 152–160 (2007).
50. Er, J. C. *et al.* Neuo: A fluorescent chemical probe for live neuron labeling. *Angew. Chem. - Int. Ed.* **54**, 2442–2446 (2015).
51. Huang, K.-P. *et al.* Deletion of leptin receptors in vagal afferent neurons disrupts estrogen signaling, body weight, food intake and hormonal controls of feeding in female mice. *Am J Physiol Endocrinol Metab* **316**, 568–577 (2019).
52. Park, S. J. *et al.* Increased TASK channel-mediated currents underlie high-fat diet induced vagal afferent dysfunction. *Am. J. Physiol.-Gastrointest. Liver Physiol.* **315**, G592–G601 (2018).
53. Hales, C. M., Fryar, C. D., Carroll, M. D., Freedman, D. S. & Ogden, C. L. Trends in Obesity and Severe Obesity Prevalence in US Youth and Adults by Sex and Age, 2007-2008 to 2015-2016. *J. Am. Med. Assoc.* **319**, 1723–1725 (2018).
54. Abarca-GÃ, L. *et al.* Worldwide trends in body-mass index, underweight, overweight,

and obesity from 1975 to 2016: a pooled analysis of 2416 population-based measurement studies in 128·9 million children, adolescents, and adults NCD Risk Factor Collaboration (NCD-RisC)*. *The Lancet* **390**, 2627–2642 (2017).

55. Warren, M. *et al. The State of Obesity: Better Policies For a Healthier America 2020 - With Special Feature on Food Insecurity and its Connection to Obesity*. (2020).
56. Beaumont, E. *et al.* Cervical vagus nerve stimulation augments spontaneous discharge in second- and higher-order sensory neurons in the rat nucleus of the solitary tract. *Am. J. Physiol.-Heart Circ. Physiol.* **313**, H354–H367 (2017).
57. Hwang, S. S., Takata, M. C., Fujioka, K. & Fuller, W. Update on bariatric surgical procedures and an introduction to the implantable weight loss device: the Maestro Rechargeable System. (2016) doi:10.2147/MDER.S106223.
58. Iwasaki, Y. *et al.* GLP-1 release and vagal afferent activation mediate the beneficial metabolic and chronotherapeutic effects of D-allulose. *Nat. Commun.* **9**, 113 (2018).
59. Herman, G. A. *et al.* Effect of single oral doses of sitagliptin, a dipeptidyl peptidase-4 inhibitor, on incretin and plasma glucose levels after an oral glucose tolerance test in patients with type 2 diabetes. *J. Clin. Endocrinol. Metab.* **91**, 4612–4619 (2006).
60. Vilsbøll, T., Christensen, M., Junker, A. E., Knop, F. K. & Gluud, L. L. Effects of glucagon-like peptide-1 receptor agonists on weight loss: systematic review and meta-analyses of randomised controlled trials. *BMJ* **344**, d7771 (2012).
61. Dalile, B., Van Oudenhove, L., Vervliet, B. & Verbeke, K. The role of short-chain fatty acids in microbiota–gut–brain communication. *Nat. Rev. Gastroenterol. Hepatol.* **16**, 461–478 (2019).
62. Christiansen, C. B. *et al.* The impact of short-chain fatty acids on GLP-1 and PYY

secretion from the isolated perfused rat colon. *Am. J. Physiol.-Gastrointest. Liver Physiol.* **315**, G53–G65 (2018).

63. Paganelli, F. L. *et al.* Roux-Y Gastric Bypass and Sleeve Gastrectomy directly change gut microbiota composition independent of surgery type. *Sci. Rep.* **9**, 10979 (2019).
64. Cook, T. M. *et al.* Vagal neuron expression of the microbiota-derived metabolite receptor, free fatty acid receptor (FFAR3), is necessary for normal feeding behavior. *Mol. Metab.* **54**, 101350 (2021).
65. Li, Z. *et al.* Butyrate reduces appetite and activates brown adipose tissue via the gut-brain neural circuit. *Gut* **67**, 1269–1279 (2018).
66. Kim, M.-J., Park, S.-J., Nam, S.-Y. & Im, D.-S. Lodoxamide Attenuates Hepatic Fibrosis in Mice: Involvement of GPR35. https://www.ncbi.nlm.nih.gov/pmc/articles/PMC6939691/pdf/bt-28-092.pdf.
67. Nam, S.-Y., Park, S.-J. & Im, D.-S. Protective effect of lodoxamide on hepatic steatosis through GPR35. *Cell. Signal.* **53**, 190–200 (2019).
68. Wirthgen, E., Hoeflich, A., Rebl, A. & Günther, J. Kynurenic Acid: The Janus-Faced Role of an Immunomodulatory Tryptophan Metabolite and Its Link to Pathological Conditions. *Front. Immunol.* **8**, 1957 (2018).
69. Keszthelyi, D. *et al.* Decreased levels of kynurenic acid in the intestinal mucosa of IBS patients: Relation to serotonin and psychological state. *J. Psychosom. Res.* **74**, 501–504 (2013).
70. Lemieux, G. A. *et al.* Kynurenic Acid Is a Nutritional Cue that Enables Behavioral Plasticity. *Cell* **160**, 119–131 (2015).

71. Schlittler, M. *et al.* Endurance exercise increases skeletal muscle kynurenine aminotransferases and plasma kynurenic acid in humans. *Am. J. Physiol. - Cell Physiol.* **310**, C836–C840 (2016).
72. Kuc, D., Zgrajka, W., Parada-Turska, J., Urbanik-Sypniewska, T. & Turski, W. A. Micromolar concentration of kynurenic acid in rat small intestine. *Amino Acids* **35**, 503–505 (2008).
73. Moloney, G. M. *et al.* Microbial regulation of hippocampal miRNA expression: Implications for transcription of kynurenine pathway enzymes. *Behav. Brain Res.* **334**, 50–54 (2017).
74. Sutton, G. M., Duos, B., Patterson, L. M. & Berthoud, H.-R. Melanocortinergic Modulation of Cholecystokinin-Induced Suppression of Feeding through Extracellular Signal-Regulated Kinase Signaling in Rat Solitary Nucleus. *Endocrinology* **146**, 3739–3747 (2005).
75. Sutton, G. M., Patterson, L. M. & Berthoud, H.-R. Extracellular Signal-Regulated Kinase 1/2 Signaling Pathway in Solitary Nucleus Mediates Cholecystokinin-Induced Suppression of Food Intake in Rats. *J. Neurosci.* **24**, 10240–10247 (2004).
76. Ehrlich, A. M. *et al.* Indole-3-lactic acid associated with Bifidobacterium-dominated microbiota significantly decreases inflammation in intestinal epithelial cells. *BMC Microbiol.* (2020).
77. De Lartigue, G. Putative roles of neuropeptides in vagal afferent signaling. doi:10.1016/j.physbeh.2014.03.011.
78. De Lartigue, G., Dimaline, R., Varro, A. & Dockray, G. J. Cocaine-and Amphetamine-Regulated Transcript: Stimulation of Expression in Rat Vagal Afferent

Neurons by Cholecystokinin and Suppression by Ghrelin. (2007) doi:10.1523/JNEUROSCI.5508-06.2007.

79. Lawson, M. A. E. *et al.* Breast milk-derived human milk oligosaccharides promote Bifidobacterium interactions within a single ecosystem. *ISME J.* **14**, 635–648 (2020).
80. Chichlowski, M., De Lartigue, G., German, J. B., Raybould, H. E. & Mills, D. A. Bifidobacteria isolated from infants and cultured on human milk oligosaccharides affect intestinal epithelial function. doi:10.1097/MPG.0b013e31824fb899.
81. James, K., Motherway, M. O., Bottacini, F. & van Sinderen, D. Bifidobacterium breve UCC2003 metabolises the human milk oligosaccharides lacto-N-tetraose and lacto-N-neo-tetraose through overlapping, yet distinct pathways. *Sci. Rep.* **6**, 38560 (2016).
82. Noll, A. J. *et al.* Human DC-SIGN binds specific human milk glycans. *Biochem. J.* **473**, 1343–1353 (2016).
83. Autran, C. A., Schoterman, M. H. C., Jantscher-Krenn, E., Kamerling, J. P. & Bode, L. Sialylated galacto-oligosaccharides and 2′-fucosyllactose reduce necrotising enterocolitis in neonatal rats. *Br. J. Nutr.* **116**, 294–299 (2016).
84. He, Y., Lawlor, N. T. & Newburg, D. S. Human Milk Components Modulate Toll-Like Receptor–Mediated Inflammation. *Adv. Nutr.* **7**, 102–111 (2016).
85. Francois, M., Canal Delgado, I., Shargorodsky, N., Leu, C.-S. & Zeltser, L. Assessing the effects of stress on feeding behaviors in laboratory mice. *eLife* **11**, e70271.
86. Rathod, Y. D. & Di Fulvio, M. The feeding microstructure of male and female mice. *PLoS ONE* **16**, e0246569 (2021).

Chapter 3:
GPR35 Inhibition on Vagal Afferent Neurons Impairs CCK_AR Signaling

3.1: Abstract

GPR35 is a metabolite receptor highly expressed by vagal afferent neurons (VANs) and co-expressed with CCK_AR, a receptor for the satiety peptide hormone, cholecystokinin (CCK). VANs are sensory neurons embedded within the gastrointestinal tract wall that relay peripheral cues of nutritional status to regulate feeding behavior and metabolism. However, our understanding of the role of GPR35 on VAN-mediated satiety signaling is lacking. Global knockout of GPR35 increases body weight and increases susceptibility to diet-induced weight gain in mice. Administration of kynurenic acid (KYNA), a tryptophan metabolite and endogenous agonist for GPR35, reduces weight gain and improves insulin signaling in mice. There is growing evidence showing that beneficial microbial metabolites, such as short-chain fatty acids and tryptophan metabolites, may increase peripheral satiety signaling. However, research investigating the interactions of enteroendocrine receptors and microbial metabolite receptors on VANs is lacking. We report here that synthetic and naturally occurring GPR35 agonists increase the sensitivity of VANs to CCK *in vitro.* Likewise, inhibition of GPR35 on VANs reduces their sensitivity to CCK *in vitro*. Ablation of VANs expressing CCK_AR in mice using CCK-conjugated saporin significantly reduces GPR35 expression in the nodose ganglia, which house the neuronal soma of VANs. We also show that shRNA-mediated knockdown of GPR35 reduces GPR35 gene expression in VANs, although the efficacy the knockdown varied with time. GPR35 knockdown on VANs impaired hyperphagia and gastric emptying induced by CCK_AR blockade. However, GPR35 knockdown on VANs had an inconsistent effect on cumulative food intake, weight gain, and adiposity in LF-fed mice. Knockdown of GPR35 in VANs using sh-GPR35 had no significant effect on HFD-induced weight gain. Nevertheless, these data demonstrate that GPR35 is

expressed on CCK_AR-positive VANs in mice and show that GPR35 agonists increase the sensitivity of VANs to CCK *in vitro.* Furthermore, the data show that GPR35 inhibition *in vitro* and *in vivo* disrupts CCK_AR signaling in VAN and blocks endogenous CCK sensing *in vivo*. Although nodose microinjection with sh-GPR35 was not sufficient to increase cumulative food intake in LF-fed male mice, we have demonstrated that gene expression of GPR35 in nodose ganglia is negatively correlated with ingestion rate in low-fat (LF)-fed mice. These data suggest that GPR35 may be involved in CCK_AR signaling of VANs. GPR35 could present a novel peripheral target for increasing the sensitivity of VANs to endogenous CCK.

3.2: Introduction

Vagal afferent neurons (VANs) innervate the walls of the gastrointestinal tract and transmit chemosensory signals in the form of enteroendocrine hormones to the brain to regulate post-prandial metabolism, appetite, and feeding behavior[1–4]. A high-fat diet (HFD) promotes the development of obesity in part by desensitizing VANs to peripheral satiety hormones, which leads to aberrant signaling of VANs[5,6] and hyperphagia[7–13]. Methods to prevent diet-induced desensitization of VANs in mice or restore VAN signaling improves metabolic outcomes in rodent models of obesity[14–16].

Currently, the most successful pharmaceutical therapies for reducing body weight and improving glucose homeostasis in humans are enteroendocrine hormone analogs[17]; the success of these drugs is largely due to reducing energy intake by acting in part through increasing VAN activation[19,20]. This evidence suggests that increasing peripheral satiety signaling via or restoring VAN activation to satiety hormones is a promising therapeutic target for treating obesity[18,19].

VANs innervating the gastrointestinal tract also express receptors for dietary and microbial metabolites[20–22]. Other studies have shown microbial metabolites, such as short-chain fatty acids (SCFAs), activate VANs and influence satiety signaling pathways *in vivo* via the G-protein coupled receptor (GPCR) FFAR3/GPR41[23,24]. A study by Egerod *et al.* revealed that VANs also highly express the metabolite GPCR GPR35, which senses kynurenic acid (KYNA)[20], a tryptophan metabolite generated by the host and gut microbiota[25,26]. Furthermore, Egerod *et al.* showed that the gene expression of GPR35 in VANs is significantly higher than the gene expression of FFAR3/GPR41. Both SCFAs and kynurenic acid are abundant in the lumen of the intestine[27–29]; their concentrations increase distally, and evidence shows that both their production is

heavily influenced by the gut microbiota[27,29,30]. However, our understanding of the role of GPR35 on VAN-mediated satiety signaling is lacking. These studies reveal a gap in our understanding of how microbial metabolite receptors can modulate the function of enteroendocrine hormone receptors on VANs and impact satiety signaling.

KYNA is an ended-product of tryptophan metabolism and is generated by both the host, via the kynurenine pathway, and gut microbiota[25,26,31,32]. Chronic ingestion of a HFD reduces the sensitivity of VANs to gut-derived satiety hormones, which promotes hyperphagia and diet-induced weight gain[12,14,33]. Previous studies have also demonstrated that HFD reduces plasma levels of KYNA[31,34,35]. Evidence suggests that HFD reduces KYNA production in part by shifting kynurenine metabolism in the host[36] and perhaps also by reducing either the abundance of KYNA-producing microbiota, such as *Bacteroidetes*[37–40]. Global knockout of GPR35 in mice increases body mass on a normal chow diet[37] and exacerbates HFD-induced hepatosteatosis in mice[39]. Recent studies have shown that administration of KYNA to diet-induced obese mice reduces HFD-induced weight gain, insulin resistance, and hyperlipidemia[31,41,42]. However, the mechanism by which KYNA improves metabolic outcomes on a HFD is unknown.

Experiments by Egerod *et al.* revealed that GPR35, the receptor for KYNA, on VANs is co-expressed with CCK_AR, the cognate receptor for CCK[20]. One study has shown that acute treatment of VANs with KYNA at concentrations similar to the gastrointestinal lumen[29] activates VANs, as measured by calcium imaging[43]. However, the role of GPR35 on CCK_AR activity on VANs has not been investigated.

This data may suggest that endogenous GPR35 ligands may influence CCK_AR signaling on VANs and satiety signaling, but this has not been tested directly. This work was undertaken to test the hypothesis that GPR35 affects CCKAR signaling on vagal afferent neurons. This hypothesis was tested using the following aims: (1) to demonstrate that synthetic and naturally occurring GPR35 agonists increase the sensitivity of VANs *in vitro* and (2) to show that inhibition of GPR35, using antagonists or VAN-specific knockdown of GPR35, reduces CCKAR signaling and exacerbates food intake in mouse model of diet-induced obesity. To address these aims, we used an established model of short-term culture of VANs to test the sensitizing effects of the synthetic GPR35 agonist zaprinast and naturally occurring agonists, KYNA and L-N-tetraose (LNT), on CCK-induced activation of VANs. Alternately, we used this *in vitro* model to determine if GPR35 inhibition reduced VAN activation by CCK. To examine the effects of GPR35 inhibition on VANs *in vivo*, we used shRNA microinjection to knock down GPR35 in VANs and determined its effects on feeding behavior, glucose homeostasis, and propensity to increase diet-induced weight gain.

These data demonstrate that GPR35 agonists increase CCK-induced activation *in vitro*, suggesting that GPR35 signaling may sensitize CCK_AR to endogenous CCK. In addition, we confirmed that GPR35 is expressed on CCK_AR-expressing VANs using CCK-conjugated saporin, as previously demonstrated by others[14,44]. Our *in vitro* data also support previous findings showing the human milk oligosaccharide LNT is an agonist for GPR35[26]. Conversely, our data also support the hypothesis that reducing GPR35 signaling on VANs interferes with CCK_AR signaling *in vitro* and impairs endogenous CCK-induced satiety in mice. These studies are the first to demonstrate

that GPR35 and CCK_AR on VANs may be functionally linked to influence satiety signaling. Although GPR35 knockdown in VANs did not exacerbate diet-induced obesity as expected, this may be due to the knockdown efficiency and could be addressed using a VAN-specific knockdown model, as demonstrated by others[24]. Therefore, targeting GPR35 on VANs may present a novel peripheral target for enhancing the sensitivity of VANs to endogenous CCK and restoring normal satiety signaling.

3.3: Methods

Animals and Housing

All experiments were approved by the University of California Davis Institutional Animal Care and Use Committees. All animals were maintained at 25 °C under a 12-h:12-h light-dark cycle (light 7 AM to 7 PM) with ad libitum access to water and food. C57BL6/J (Jackson Laboratories, Sacramento, California, USA) mice were individually-housed in standard cages containing paper bedding before initiating feeding studies and provided standard chow (LabDiet, #5001; St Louis, Missouri, USA) and water *ad libitum*. After 1 week of acclimation on a custom low-fat diet (LF, 10% kcal; matching composition of D12450J, Research Diets), mice were counter-balanced and maintained on either an LF or custom high-fat diet (HF, 45% fat kcal; matching composition of D08091803B, Research Diets) for 8-10 weeks. Food intake was measured twice per week to calculate average food intake per animals (kcal/day) prior to initiating feeding behavior studies in the BioDAQ food intake monitoring system (BioDAQ, version 3; Research Diets, New Brunswick, NJ, USA. After housing mice in BioDAQ cages for 10 days, mice were returned to standard Allentown cages for the remaining feeding studies.

For nodose cultures, 4-8-week-old adult male Wistar rats (Envigo, Hayward, CA, USA) were housed in pairs in a separate facility and were provided ad libitum access to water and chow (#2018, Teklad, Envigo, Indianapolis, Indiana, USA). Rats were chosen over mice to reduce the number of animals required to achieve statistical significance and experimental requirements for robustness and reproducibility.

Nodose Ganglia Dissection and Primary Cultures

We used an established model of primary VAN cultures[44–46] to determine the effects of GPR35 on CCK signaling *in vitro***.** Rat nodose ganglia were identified by following the vagus nerve to the jugular foramen and dissected under aseptic conditions. Nodose ganglia were collected into sterile calcium- and magnesium-free ice-cold Hanks Buffered Saline Solution (HBSS) (# 21-022, Corning; Corning, New York, USA). Nerve fibers were cut away and desheathed using sterile Dumont forceps and scalpel. The ganglia were pre-digested with 2 mg/ml collagenase type 4 (LS004188, Worthington-Biochem, Lakewood, New Jersey) and 2.4 mg/ml dispase II (4942078001, Roche, Penzberg, Germany) for 5 minutes at 37 °C. Following pre-digestion, ganglia were incubated in 22 U/mL papain (LS003126, Worthington-Biochem; Lakewood, New Jersey, USA) resuspended in a solution of HBSS, L-cysteine (0.4 mg/mL; C6852, Sigma-Aldrich; St. Louis, Missouri, USA), 0.5 mM EDTA, and 1.5 mM CaCl2 for 30 minutes at 37 °C in a 5 cm Petri dish. Dissociated ganglia were transferred to a 15 mL centrifuge tube and centrifuged at 400 x g for 3 minutes before final digestion in collagenase (1 mg/mL) and dispase (1.2 mg/ml) for 30 minutes at 37 °C in a 5 cm Petri dish. Ganglia were mechanically dissociated before final centrifugation at 500 x g for 5 minutes. Nodose cultures were resuspended in 300 µL media consisting of DMEM base

media (D5030, Sigma-Aldrich) supplemented with 0.5 mM L-glutamine, 10mM HEPES, 2.2g/L sodium bicarbonate, 0.227 mM sodium pyruvate, 5 mM glucose, 10% heat-inactivated rat serum (method included below). Cultures were equally distributed onto 8-chamber Millicell EZ Slides (PEZGS0416, Millipore; Burlington, MA) and Matrigel (150 µg/ml, 354262, Corning). Nodose cultures were maintained at 37 °C, 5% CO2 for 24-48 hours prior to experiments. Each nodose culture consisted of pooled nodose ganglia (left and right) collected from two rats.

Generation of Heat-Inactivated Rat Serum

Wistar rats were euthanized by carbon dioxide asphyxiation. The ventral surface of the animal was sterilized, and the skin was transected directly beneath the xiphoid process to expose the heart. Approximately 5 mL of blood was collected via cardiac puncture and centrifuged at 1,500 x g for 15 minutes at 4 °C to separate serum from whole blood and transferred to a Class II biosafety cabinet. Under sterile conditions, serum was collected and centrifuged for an additional 10 minutes at 20,000 x g at 4 °C to remove any remaining cell debris. The remaining 2 mL serum was distributed to 1.5 mL microcentrifuge tubes and heat-inactivated for 30 minutes at 56 °C in a heating block. Following heat inactivation, the serum was incubated in ice for 10 minutes to complete heat inactivation. The final serum was centrifuged for 10 minutes at 20,000x g before sterile filtration using a 0.2 µm syringe filter.

Sources of Chemical Treatments for Studies

CCK-8S (CCK) was sourced from either Bachem (Batch 1062975) or Tocris (#1166, Batch 19). Zaprinast was also sourced from Tocris (#0947; Batches 246356, 244357).

Kynurenic acid (KYNA, K3375) and phorbol-12-myristate-13-acetate (PMA, P8139) were purchased from Sigma-Aldrich. Purified LNT was graciously provided to us by our collaborator, Daniela Barile, Ph.D. (Department of Food Science and Technology, University of California, Davis).

In Vitro VAN Treatments

All *in vitro* experiments were conducted 24-48 hours after plating. Nodose cultures were serum starved for 2 hours before all treatments. Working solutions of CCK (Bachem, H-2080; or Tocris, 11668), LNT (graciously provided by our collaborator, Dr. Daniela Barile; UC Davis), or D-lactose (6PNC2, Spectrum) were resuspended in 0.9% normal saline. Treatment solutions of KYNA (K3375, Sigma-Aldrich), zaprinast (#0947, Tocris), PMA (P8139, Sigma-Aldrich) were resuspended in 0.1-1% DMSO (as dictated by solubility properties). Vehicle controls and PMA (100 nM), a positive control for ERK activation, were included in all experiments. The duration of all treatments was 15 minutes. For experiments including the GPR35 antagonist (CID-2745687, #4293, Tocris), nodose cultures were pre-treated with either the antagonist or vehicle (1% DMSO) during the last hour of serum starvation. To terminate treatments, cultures were washed with cold PBS and harvested in RIPA buffer containing 1% PMSF (P7626, Sigma), 1% protease inhibitor (P8340, Sigma), and 1% phosphatase inhibitor Cocktail 2 and 3 (#5726 and #00444C, Sigma, respectively). Samples were flash-frozen on dry ice before storing at -80 °C until western blotting. Each experiment contained two technical replicates per treatment and each experiment was repeated in triplicate.

Western Blotting

Individual samples were denatured and reduced at 80 °C for 10 minutes and resolved using SDS-PAGE as per the manufacturer's standard protocol (Invitrogen, Mini Gel Tank). Two identical gels were run simultaneously to enable probing of phosphorylated and total ERK protein. Following electrophoresis (100 V for 60 minutes), protein was transferred onto poly(vinylidene fluoride) (PVDF) membrane (Bio-Rad, #1620264) according to the manufacturer's recommendations (Invitrogen, Mini Gel Tank) for 90 minutes at 20 V. Membranes were stained for total protein using No-Stain™ total protein stain reagent (Thermo Fisher, A44449) according to the manufacturer's recommendations. Membranes were washed in 1X TBST after visualizing total protein and blocked in 5% BSA in 1X TBST for 1 hour on a gyratory rocker at room temperature. All primary antibodies were purchased from Cell Signaling. Primary antibody solutions were resuspended in blocking buffer according to the following dilutions: pErk (1:500, 9101), Erk (1:1000, 9102). Membranes were incubated in the antibody solutions overnight at 4 °C on a gyratory rocker. On the following day, the membranes were incubated in secondary antibody solutions (HRP anti-rabbit IgG, 1:2000, Cell Signaling, 7074) and (HRP anti-mouse IgG, 1:4000, Cell Signaling, 7076) for 1 hour at room temperature. Chemiluminescence was used to detect proteins of interest (SuperSignal™ West Femto Maximum Sensitivity Substrate, ThermoFisher, 34096) and multiple exposures were taken to confirm that all samples were in the dynamic range. Total protein and antibody detection were analyzed using Bio-Rad Imager (Bio-Rad, Hercules, CA) and samples were normalized to total protein staining. Data are reported as the mean densitometry normalized to vehicle control ± SEM.

Bilateral Nodose Microinjection

All nodose microinjection surgeries were performed between 8 am and 2 pm. Mice were anesthetized with an intraperitoneal injection of ketamine/xylazine (80-100 mg/kg and 10 mg/kg, respectively, in 0.9% normal USP saline). Ophthalmic ointment was applied to both eyes prior to shaving the fur from the chin to the distal sternum. The surface was sterilized with povidone-iodine solution and 70% ethanol before making a 2 cm incision in the skin over the sternum. Blunt dissection was used to expose and retract the submandibular salivary glands, sternohyoid, and sternomastoid muscles and to expose the carotid artery and vagus nerve. The vagus nerve was followed to identify the nodose ganglion at the jugular foramen. A micropipette puller (Sutter Instruments, Model P-87) and microelectrode beveler (Sutter Instruments, #BV-10) were used to create capillary needles (Sutter Instruments, #BF100-50-10). Capillary needles were advanced into the ganglion and the solutions were injected (0.5 ul per ganglion, 40 psi, 15 sec; Picospritzer III, Parker Hannifin). We used CCK-conjugated saporin (400 ng/µL) (CCK-SAP, KIT-31, Advanced Targeting Systems) to ablate cells expressing CCK receptors, which has been successfully repeated in other studies[14,44]. We used AAV9-mGPR35 (AAV-m-GPR35-shRNA (shAAV-260635), Vector BioSciences) ($1e^{9}$-$1e^{11}$ genome copies (gc)/mL) to specifically knock down gene expression of GPR35 in VANs. For all studies, the nodose injection was repeated on the right side and the incision was closed using an interrupted suture (690G, Ethicon). The incision site was cleaned and postoperative analgesia was administered (carprofen, 5 mg/kg, subcutaneous). A reversal agent was administered following analgesia (atipamezole, 1 mg/kg, intramuscular), and the animals recovered in a warm cage until fully ambulatory.

Analgesics were administered daily for two days following the procedure. Food intake and body weight were measured every day for one week until feeding studies began.

Measuring Food Intake

Mice were housed in standard Allentown shoebox cages and food intake was measured twice per week to calculate average food intake per animal (kcal/day). Mice were acclimated to food-monitoring Allentown cages (BioDAQ, version 3, Research Diets, New Brunswick, NJ) for approximately 6 days before analyzing meal patterns. After housing mice in BioDAQ cages for 10 days, mice were returned to standard Allentown cages for the remaining feeding studies.

Measuring Drug-Induced Changes in Feeding Behavior

Drug-induced changes in cumulative food intake (e.g.,. CCK, devazepide, and zaprinast) were carried out in standard shoebox cages. For all feeding behavior studies, mice were fasted for 6 hours prior to the onset of the dark phase. Food was returned to mice immediately after CCK injections and 30 minutes after zaprinast, devazepide, or CID-2745687 injections. Mice were injected with CCK-8S or vehicle (0.9% saline), zaprinast or vehicle (4% DMSO, 2% Tween-80 in saline), devazepide or vehicle (0.2% DMSO, 0.2% Tween-80), or CID-2745687 or vehicle (0.5% DMSO) (10 uL/g BW).All feeding behavior studies were paired; treatments were randomized and each animal received either vehicle or treatment 48 hours apart.

Analysis of Meal Microstructure

Feeding events were defined as “meals” if one or more feeding bouts were separated by 5 minutes or less and their sum was at least 0.02 g. If two feeding events were separated by more than 5 minutes, they were considered separate meals. Meal parameters included cumulative calorie intake, meal size, meal duration, meal number, and rate of ingestion. Energy intake is reported in kcal.

Body Composition Analysis

The body composition of fat and lean mass of live mice was analyzed using an EchoMRI-100^{TM} (Echo Medical Systems). Lean and fat mass are reported in total grams. Body composition of mice was measured before initiating feeding behavior studies and repeated at the end of the study.

Oral Glucose Tolerance Testing

To determine if GPR35 knockdown in VANs affected glucose homeostasis, mice were fasted on paper bedding for 6 hours prior to an oral glucose tolerance test. Mice were provided *ad libitum* access to water during fasting. Mouse tails were anesthetized using oral viscous lidocaine before cutting 1 mm of the tail tip to measure glycemia. Blood glucose was measured in the tail blood using a glucometer (True Metrix, Trividia Health, For Lauderdale, Florida, USA). Baseline glycemia was measured before oral gavage with 50% USP glucose solution (2 g glucose/kg body weight) and was measured again at 15-, 30-, 60-, and 90-minutes post-gavage. All measurements were made in triplicate.

Quantitative PCR

Except for nodose ganglia, all tissues harvested for gene expression analyses were flash-frozen at necropsy. Total RNA was extracted using TRIzol (Cat #15596026, Life Technologies, Grand Island, New York, USA). Nodose ganglia from euthanized animals were collected into RNA Later (ThermoFisher, Waltham, Massachusetts, USA) and RNA was extracted using Qiagen RNEasy Micro Plus Kit (Cat #74034, Qiagen, Germantown, Maryland, USA). All purified RNA from all samples was reverse transcribed using the High-Capacity cDNA Reverse Transcription Kit (Cat # 4368814, Applied Biosystems, Waltham, Massachusetts, USA) according to the manufacturer's instructions. Real-time PCR was performed using the QuantStudio 6 Flex Real-Time PCR system (Thermo Fisher Scientific, Waltham, Massachusetts, USA) and SyberGreen PowerUp (Cat #A25778, Life Technologies, Grand Island, New York, USA) using custom primers (Table 2.1). The qPCR cycling conditions included an initial denaturation step at 95 °C for 10 minutes followed by 40 cycles consisting of a 95 °C-step for 15 seconds and a 60 °C-step for 30 seconds. Control samples included "no RNA template control" and "no reverse transcriptase control". Data were analyzed using the $2^{-\Delta\Delta CT}$ method[47]. Target gene expression for all data is expressed as the ratio to housekeeping gene expression (RPLP0)[48].

eGFP Immunohistochemistry

Mice were euthanized via carbon dioxide asphyxiation. Upon termination, mice were exsanguinated. To flush the remaining blood, a scalp vein set (21-gauge needle) was used to perfuse 10 mL 0.9% saline into the left ventricle. Nodose ganglia from AAV-injected mice and control animals were collected and post-fixed in 4% paraformaldehyde in normal PBS for 1 hour, then transferred to 30% sucrose. Nodose ganglia were frozen in OCT (Cat #23-730-571, Fisher, Waltham, Massachusetts, USA) directly on a cryosection specimen chuck. Nodose ganglia were sectioned at 20 µm and mounted onto SuperFrost Plus microscope slides (Cat #12-550-15, Fisher, Waltham, Massachusetts, USA). Mounted cryosections were stored at -20 °C until immunostaining. Tissue was rehydrated in 1X TBS-Tween (0.1%) (TBST) before blocking in 10% normal donkey serum (Cat #017-000-121, JacksonImmunoResearch Laboratories, Philadelphia, Pennsylvania, USA) in 1X TBST + TritonX-100 (0.2%) for 1 hour at room temperature. After blocking, tissues were incubated overnight at 4 °C in a staining solution containing anti-eGFP primary antibody (Cat #600-101-215, Rockland Immunochemicals, Pottstown, Pennsylvania, USA) (1:500) resuspended in 10% normal donkey serum in 1X TBST. The following day, slides were washed three times in 1X TBST for 5 mins/wash. The secondary antibody solution consisted of Alexa Fluor 633-conjugated donkey anti-rabbit antibody (1:500) (Invitrogen, A21082) resuspended in 10% normal donkey serum in 1X TBST for 1 hour at room temperature. Nuclei were stained with DAPI (1 µg/mL in 1X TBS) (Invitrogen, D1306) for 3 minutes at room temperature. Slides were treated with ProLong Diamond Antifade (Invitrogen, P36970) before mounting with rectangular #1.5 coverslips (#NC1034527, Fisher, Waltham,

Massachusetts, USA). Confocal images were acquired with a Leica TCS SP8 STED microscope using a 20X/0.75 oil lens.

Statistical Analysis

Randomization and blinding were used in the experimental design for all animal studies, imaging analysis, and analytical measurements. Differences between two groups were analyzed using GraphPad Prism using a two-tailed Student's t-test (e.g.,. paired for feeding studies, unpaired for endpoint studies). Differences among groups were analyzed by one- or two-way ANOVA as indicated in figure legends. Multiple comparisons tests for dose-response *in vivo* experiments were made using Dunnett's post hoc tests. Other multiple comparisons tests were made using Tukey's or Sidak's post hoc tests where appropriate. Simple linear regression analysis was used in Study 3 to determine if ingestion rate was dependent on GPR35 gene expression in nodose ganglia. Data are presented ±SEM unless indicated otherwise. *P*-values less than 0.05 were considered statistically significant.

3.4: Experimental Protocols

Study 1: Optimizing AAV-Mediated Knockdown of GPR35 Using sh-GPR35

In Study 1, we sought to determine the optimal concentration of AAV-shGPR35 required to significantly reduce GPR35 expression in VANs while minimizing off-target effects, such as tissue remodeling. AAV concentrations used were $1e^{9}$ (n=3), $1e^{10}$ (n=3), or $1e^{11}$ (n=7) genome copies (gc)/mL. All animals received bilateral injections at 0.5 µL/nodose. Mice were maintained on a normal chow diet for 2-4 weeks and food intake and body weight were measured twice per week. Mice were euthanized 2-4 weeks after nodose microinjection, according to scheduling described in previous studies[1]. Nodose were collected into RNAlater™ (ThermoFisher, AM7024) at necropsy and processed as described above for qPCR to determine the effects of each AAV-shGPR35 dose on gene expression of GPR35, enteroendocrine receptors, neuronal markers, and Iba1 (marker of satellite glia activation in VANs[49,50]).

Studies 2-4: Determining Food Intake During Light and Dark Periods Following Nodose Microinjection (AAV-shGPR35)

In Studies 2-4, we sought to investigate the effects of GPR35 knockdown in VANs on feeding behavior with a larger cohort of mice. Animals recovered for 2-3 weeks after nodose microinjection surgery before food intake was recorded in these studies. All animals were maintained on a normal chow diet during this study period. To determine food intake during the light periods in standard Allentown cages, food intake was measured approximately 1 hour before the onset of the dark period. Food intake was measured the following day at the onset of the light period to determine food intake during the dark period. This series of measurements were repeated for three

consecutive days to determine the average food consumption of animals during light and dark periods. This protocol was applied to AAV-shGPR35 Studies 2-4.

Study 3 and 4: Feeding Behavior Studies Following Nodose Microinjection (AAV-shGPR35)

Studies 3 and 4 were extended for a total period of 20 weeks following nodose microinjection. In both studies, mice were maintained on a normal chow diet for 5-6 weeks. We determined the effects of AAV-shGPR35 nodose microinjection on CCK-induced satiety (3 µg/kg BW, IP; Cat #1166, Tocris, Minneapolis, Minnesota, USA) and hyperphagia induced by the competitive CCK_AR antagonist, devazepide (600 µg/kg, IP; Cat #2304, Tocris) while mice were maintained on a chow diet in standard Allentown cages. Mice were injected with CCK-8S or vehicle (0.9% saline) or devazepide or vehicle (0.2% DMSO, 0.2% Tween-80) (10 uL/g BW). All studies were paired, and mice received either treatment or vehicle one week apart.

After CCK and devazepide feeding studies, mice were housed in BioDAQ cages for 10 days to determine the effects of AAV-shGPR35 nodose microinjection on feeding behaviors and meal microstructure. Following studies in BioDAQ cages, mice from Study 3 were counter-balanced and switched to HF or LF diet for the remainder of the study.

Mice were housed in standard Allentown cages and maintained on a HFD or LFD for 9 weeks prior to determining the effect of AAV-shGPR35 nodose microinjection on GPR35 agonist-induced satiety (zaprinast, 10 mg/kg, IP; Cat #0947 or vehicle (4% DMSO, 2% Tween-80 in saline) (10 µL/g BW). Mice were fasted for 6 hours before IP

injection and provided water *ad libitum* prior to feeding behavior studies. Mice were returned to BioDAQ cages to determine the effects of AAV-shGPR35 nodose microinjection on *ad libitum* feeding behavior.

Mice from Study 4 were maintained on a normal chow diet for the entire study. Mice were fasted for 6 hours before IP injection and provided water *ad libitum* prior to feeding behavior studies using devazepide and CCK. Zaprinast-induced satiety was not measured in Study 4 because we previously determined that zaprinast does not alter feeding behavior in LF-fed mice (Chapter 2).

Study 3: Gastric Emptying Following Nodose Microinjection of AAV-shGPR35

Acetaminophen is rapidly absorbed in the small intestine and its appearance in plasma is a clinically validated indicator for rates of gastric emptying[51,52]. We used acetaminophen to determine the effect of GPR35 knockdown on devazepide-enhanced gastric emptying. Mice were fasted overnight and provided ad libitum access to water. On the day of the experiment, liquid acetaminophen was resuspended in liquid meal replacement (10 mg/mL; Boost™, Nestle, Arlington, Virginia, USA). Mouse tails were anesthetized using oral viscous lidocaine (Hi-Tech Pharmacal Co. Inc, Amityville, New York, USA) before cutting 1 mm of the tail tip. Tail blood was collected using microcapillary tubes (Microvette® CB 300 with lithium heparin; Sarstedt, Newton, North Carolina, USA). Fifteen minutes before oral gavage with acetaminophen solution (100 mg/kg), animals were injected with either devazepide (Tocris, Minneapolis, Minnesota, USA; 600 µg/kg, IP) or vehicle (0.5% DMSO, 0.5% Tween-80 in USP 0.9% saline). Tail blood was collected at baseline and 15 minutes after IP injection. Samples were immediately stored on ice and centrifuged at 500 x g to separate plasma from whole blood. Mice were provided food after the final draw and cages were changed after the procedure. Plasma acetaminophen levels were measured using an ELISA (Acetaminophen-L3K; Sekisui Diagnostics, Burlington, Massachusetts, USA) according to the manufacturer's instructions.

3.5: Results

Effect of GPR35 Signaling on VAN Sensitivity to CCK *In Vitro*

To determine potential interactions between GPR35 and CCKAR, subthreshold concentrations of GPR35 agonists (zaprinast, KYNA, and LNT), established in previous experiments (see Chapter 2), were used on VANs *in vitro.* Treatment with either the GPR35 agonist zaprinast (10^{-9} M) or CCK (1-10 nM) alone had no significant effect on VAN activation relative to vehicle control, as measured by phosphorylation of ERK relative to total ERK (Figure 3.1, N=3). Simultaneous treatment with zaprinast (10^{-9} M) did not significantly increase VAN sensitivity to CCK (1 nM) relative to CCK alone (1 nM). However, zaprinast (10^{-9} M) significantly increased CCK (10 nM)-induced activation of VANs relative to CCK (10 nM) alone (Figure 3.1, $p<0.05$, N=3).

Figure 3.1: Effect of GPR35 agonist zaprinast on sensitivity of VANs to CCK, as measured by phosphorylation of ERK relative to total ERK (pERK/ERK). Neuronal activation as measured by phosphorylation of ERK relative to total ERK (pERK/ERK). A) Representative western blot of the effect of the GPR35 agonist zaprinast (10 nM) on increasing sensitivity of VANs to CCK (1-10 nM), as measured by pERK/ERK. B) Quantification of the effect of zaprinast or vehicle (0.1% DMSO) on CCK-induced activation of VANs. Two-way ANOVA, Tukey's multiple comparisons test, N=3. Different letters indicate statistically significant differences (p<0.05). All samples normalized to VEH (0.1% DMSO + 0.1% saline) control. Data are presented as ±SEM. VEH, vehicle. CCK, cholecystokinin. ZAP, zaprinast. PMA, phorbol 12-myristate 13-

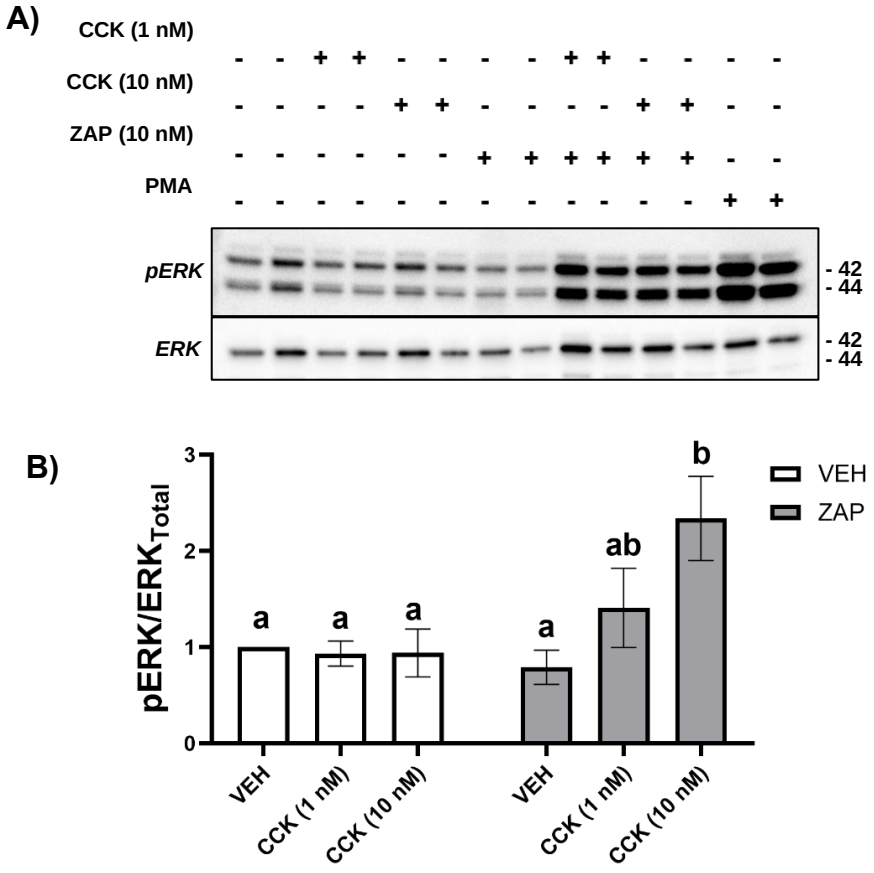

Acute treatment of VANs with KYNA or CCK (1, 10 nM) did not significantly increase VAN activation relative to vehicle control (Figure 3.2, N=5). However, simultaneous treatment of VANs with KYNA (1 µM) and CCK (1,10 nM) significantly increased pERK/ERK relative to CCK (1,10 nM) alone. This data indicates that KYNA increases the sensitivity of VANs to CCK *in vitro* (Figure 3.2, $p<0.05$, N=5).

Figure 3.2: Effect of GPR35 agonist KYNA on sensitivity of VANs to CCK, as measured by phosphorylation of ERK relative to total ERK (pERK/ERK). Representative western blot of the effect of the GPR35 agonist KYNA (1 μM) on increasing sensitivity of VANs to CCK (1-10 nM), as measured by pERK/ERK. Quantification of the effect of KYNA or vehicle (0.1% DMSO) on CCK-induced activation of VANs is shown underneath. Two-way ANOVA, Tukey's multiple comparisons test, N=5). Different letters indicate statistically significant differences (p<0.05). All samples normalized to VEH (0.1% DMSO + 0.1% saline) control. Data are presented as ±SEM. VEH, vehicle. CCK, cholecystokinin. KYNA, kynurenic acid. PMA, phorbol 12-myristate 13-acetate.

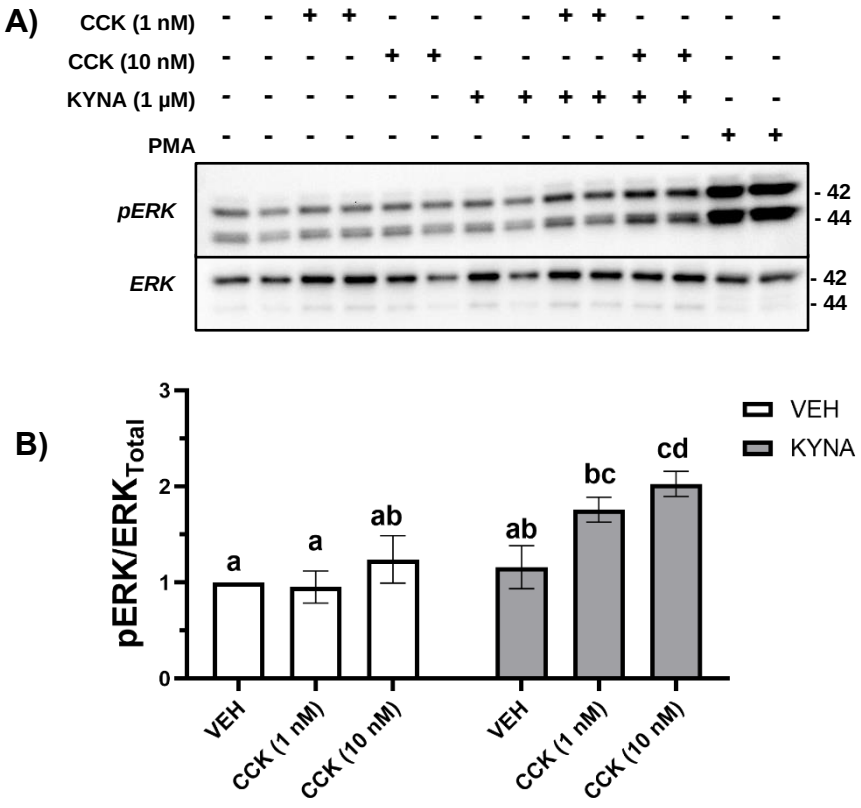

Our previous *in vitro* data from Chapter 2 demonstrated that the human milk oligosaccharide, L-N-tetraose (LNT), significantly increased VAN signaling via GPR35 *in vitro*. Treatment with either LNT (5 mM) or CCK (1-10 nM) alone failed to activate VANs *in vitro* (Figure 3.3, N=3). Similar to zaprinast and KYNA, simultaneous treatment of VANs with LNT (5 mM) and CCK (10 nM) significantly increased pERK/ERK relative to CCK (10 nM) alone (Figure 3.3, $p<0.05$, N=3). Although there was a trend of LNT to increase sensitivity to a lower concentration of CCK (1 nM) relative to LNT or CCK (1 nM) alone, this difference did not reach statistical significance.

Figure 3.3: Effect of GPR35 agonist LNT on sensitivity of VANs to CCK, as measured by phosphorylation of ERK relative to total ERK (pERK/ERK). Representative western blot of the effect of the GPR35 agonist LNT (5 mM) on increasing sensitivity of VANs to CCK (1-10 nM), as measured by pERK/ERK. Quantification of the effect of LNT on CCK-induced activation of VANs relative to vehicle is shown beneath the representative western blot. Two-way ANOVA, Tukey's multiple comparisons test, N=3). Different letters indicate statistically significant differences (p<0.05). All samples normalized to VEH (0.1% saline) control. Data are presented as ±SEM. VEH, vehicle. CCK, cholecystokinin. LNT, L-N-tetraose. PMA, phorbol 12-myristate 13-acetate.

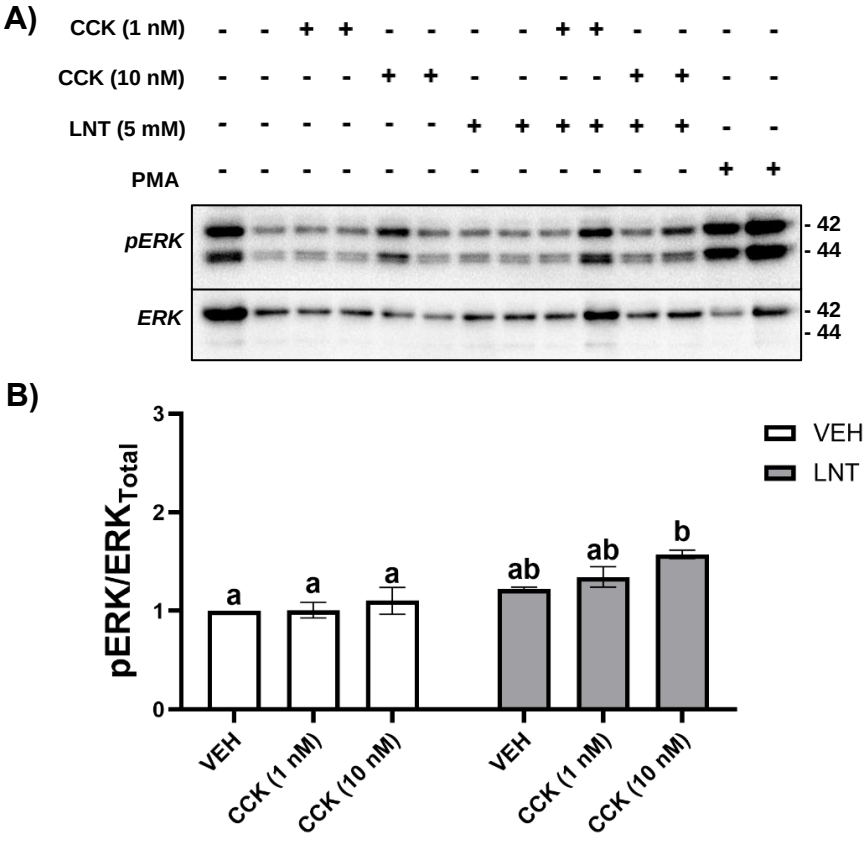

The GPR35 competitive antagonist CID-2745687 (CID; 50-100 μM) significantly reduced CCK (10 nM)-induced activation of VANs relative to vehicle control (Figure 3.4, $p<0.05$, N=5). The positive control of ERK phosphorylation, PMA (100 nM), also significantly increased pERK/ERK relative to vehicle control ($p<0.05$, N=5). The competitive GPR35 antagonist CID (50-100 μM) did not inhibit PMA-induced pERK/ERK, suggesting that CID specifically inhibits GPR35.

Figure 3.4: Effect of GPR35 antagonist on CCK-induced activation of VANs, as measured by phosphorylation of ERK relative to total ERK (pERK/ERK). Representative western blot of the effect of the GPR35 antagonist CID-7745687 (CID, 50 μM) on CCK-induced pERK/ERK in VANs. Positive control of pERK/ERK activation PMA (100 nM) is included. Quantification of inhibition by CID (50-100 μM) on CCK (10 nM)- or PMA-induced pERK/ERK activation relative to vehicle is shown beneath the representative western blot. Two-way ANOVA, Tukey's multiple comparisons test, N=4-5). Different letters indicate statistically significant differences (p<0.05). All samples normalized to VEH control. Data are presented as ±SEM. VEH, vehicle. CCK, cholecystokinin. CID, CID-2745687. PMA, phorbol 12-myristate 13-acetate.

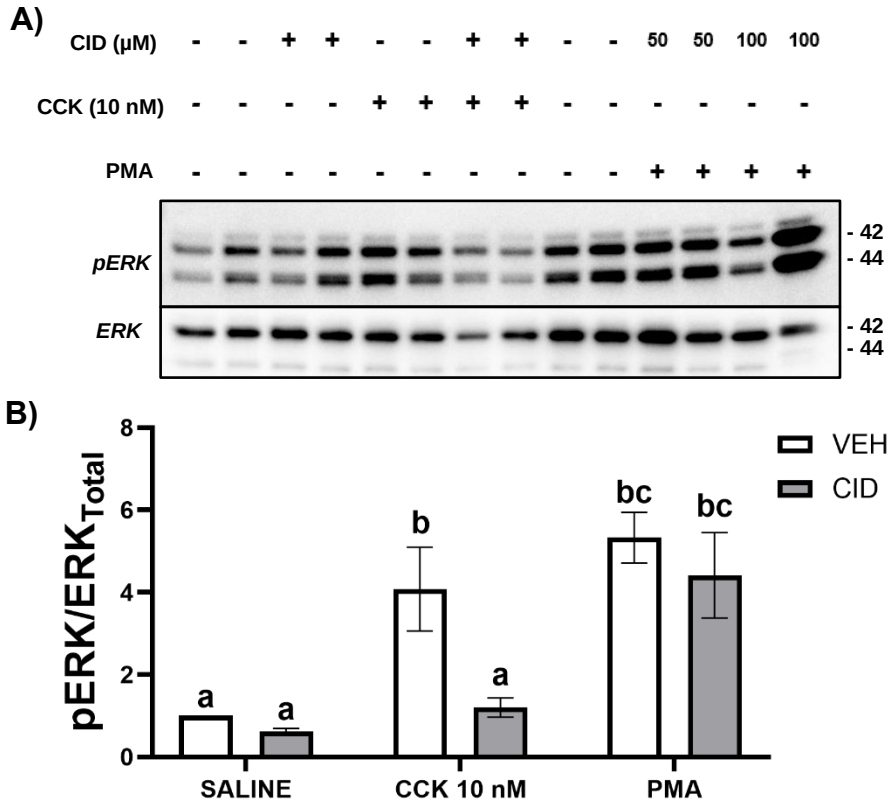

Effect of Ablating CCK-Sensing VANs on GPR35 Expression in Nodose Ganglia of Male Mice and Food Intake

We sought to verify previous data showing that CCK_AR and GPR35 are co-expressed on $Na_v1.8$-positive VANs in male mice[20] by ablating CCK-sensing VANs via nodose microinjection of CCK-conjugated saporin (CCK-SAP). The data show that CCK-SAP significantly reduced GPR35 gene expression in VANs relative unconjugated saporin and sham controls (Figure 3.5, $p<0.05$, N=6-11). CCK-SAP also significantly reduced gene expression of CCK_AR (Figure 3.5, $p<0.05$) relative to nodose injected with controls. Although there was a trend of CCK-SAP to decrease gene expression of NPY_2R and GLP-1R, which detect gut-derived enteroendocrine hormones PYY and GLP-1, respectively, these differences were not statistically significant. Relative to unconjugated saporin, CCK-SAP did not affect gene expression of the microbial metabolite receptor GPR41/FFAR3, which detects SCFAs and has been implicated in the satiety-enhancing effects of SCFAs on VAN signaling[24,53]. This observation supports previous findings showing that GPR41/FFAR3 is not expressed on VANs that express CCK_AR[20,22], which suggests that the satiety-enhancing effects of SCFAs may be attributed to the activation of hypothalamic anorexigenic circuitry[16] or another class of VANs. These data support previous findings showing that GPR35 is expressed on VANs that also detect CCK[20].

Nodose microinjection of CCK-saporin had no effect on cumulative food intake, meal patterns, or body weight in chow-fed mice relative to controls (data not shown). CCK-saporin has previously been shown to have no effect on *ad libitum* food intake in chow-fed rats relative to unconjugated saporin controls[14].

Figure 3.5: Effect of CCK-conjugated saporin on gene expression of receptors for enteroendocrine and microbial metabolites on VANs *in vivo*. Gene expression of CCKAR, GPR35, NPY2R, GLP1R, and GPR41 (FFAR3) in nodose ganglia of CCK-SAP injected mice relative to mice injected with unconjugated saporin and sham surgery controls. Different letters indicate significant differences *(*Two-way ANOVA, Tukey's multiple comparisons test, N=6-11*).* Different letters indicate significant differences *(p*<0.05*).* All samples normalized to sham control. Data are presented as ±SEM.

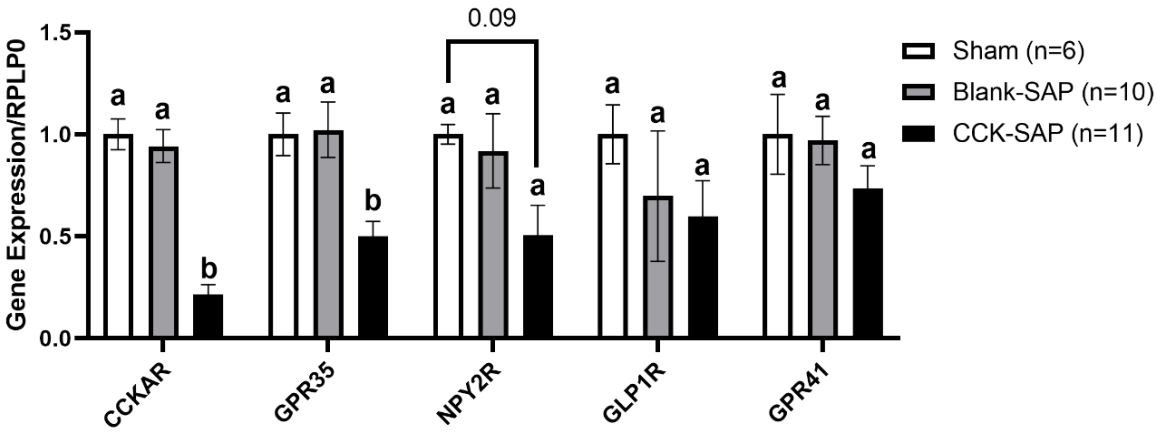

Study 1: Optimizing AAV-Mediated Knockdown of GPR35 Using sh-GPR35

We used a recombinant adenovirus to specifically knockdown GPR35 in VANs to better characterize the role GPR35 in VANs and feeding behavior in male mice. First, we determined the optimal dose of AAV9-shGPR35 ($1e^{11\text{-}13}$ gc/mL, 0.5 µL per nodose, bilateral) that specifically reduces GPR35 gene expression in VANs. Two weeks after injection, AAV-shGPR35 at $1e^{11}$ gc/mL and at $1e^{13}$ gc/mL reduced GPR35 gene expression in nodose ganglia but neither produced a statistically significant reduction (Figure 3.6, N=3-7/group, $p>0.05$). AAV-GPR35 ($1e^{11}$ and $1e^{13}$ gc/mL) significantly reduced gene expression of CCKAR and NPY2R, which are responsible for inducing satiety by gut-derived peptide hormones, CCK and PYY, respectively. AAV-shGPR35 did not affect gene expression of GHSR, which is the receptor on VANs proposed to be responsible for mediating the effects of gut-derived ghrelin[46]. Two weeks after nodose injection, all doses of AAV-shGPR35 significantly reduced gene expression of SCN10A, a marker for $Na_v1.8$-positive neurons, which are the major class of unmyelinated sensory neurons in the vagal pathway and responsible for relaying chemosensory information to the key satiety centers in the brain[54–56]. All doses of AAV-GPR35 also significantly increased the expression of Iba1, a marker of inflammation expressed by glial cells[49,50]. In Study 1, nodose microinjection with sh-GPR35 had no effect on cumulative food intake relative to sham controls.

Figure 3.6: Dose response of AAV-shGPR35 on gene expression of receptors, pan-neuronal, and non-neuronal markers on VANs *in vivo*. Dose response of changes in gene expression of GPR35, CCKAR, NPY2R, SCN10A, GHSR, and Iba1 in nodose ganglia following AAV-mediated knockdown of GPR35. Two-way ANOVA, Dunnett's multiple comparisons test, N=3-7. Different letters indicate significant differences from sham control *(p*<0.05). All samples normalized to sham control. Data are presented as ±SEM.

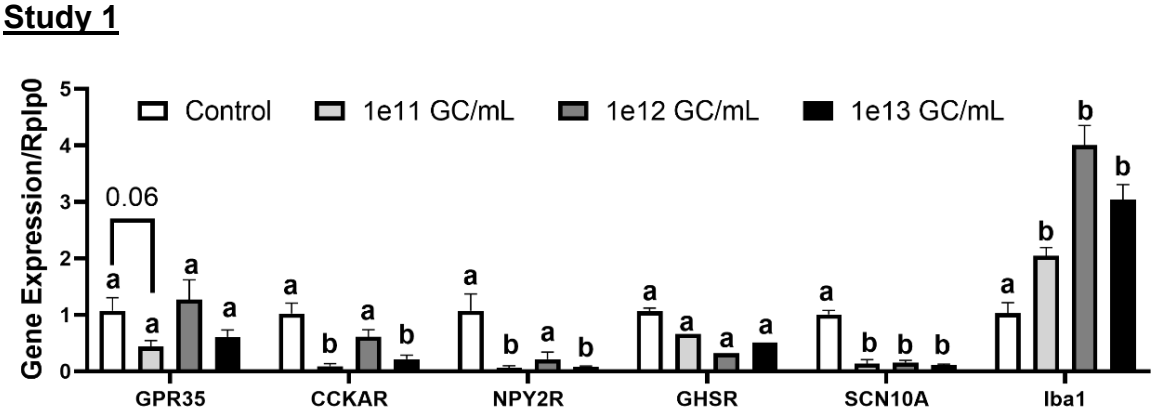

Study 2: Effect of Nodose Microinjection of shGPR35 on GPR35 Gene Expression on VANs and Short-term Changes in Cumulative Food Intake

In Study 2, we verified our observations that AAV-shGPR35 ($1e^{11}$ gc/mL) tends to reduce GPR35 expression on VANs and increased the sample size of all treatment groups. Considering that nodose microinjection could have induced reorganization of VANs[57], as measured by increases in gene expression of Iba1, we extended the period of recovery from two to three weeks in Study 2, which has been done in previous studies[1,3]. In this study, we microinjected one group of mice with a control vector containing a scrambled sequence of the anti-GPR35 shRNA to control for non-specific effects imposed by the AAV or vector (ref. sh-Scramble). The data shows that AAV shGPR35 ($1e^{11}$ gc/mL) significantly reduces gene expression of GPR35 on VANs relative to unoperated and sh-Scramble controls (Figure 3.7A, N=7-8/group, $p<0.05$). shGPR35 also significantly reduced gene expression of CCKAR ($p<0.05$) but it did not reduce expression of other receptors for gut-derived hormones, such as GLP1R and GHSR. Three weeks following nodose microinjection, AAV-shGPR35 did not significantly reduce the expression of pan-neuronal markers, such as SCN10A and TUBB3. The recombinant shRNA vectors used in these studies express an eGFP reporter; immunohistochemical staining shows positive eGFP staining in AAV-injected nodose relative to sham controls thereby verifying that the shGPR35 vector is expressed by VANs *in vivo* (Figure 3.7B).

Figure 3.7: Effect of AAV-shGPR35 or scramble vector control on gene expression of receptors, pan-neuronal, and non-neuronal markers on VANs in male mice. Effects of AAV-shGPR35 or scrambled shRNA vector (1e11 gc/mL per AAV type) on gene expression of GPR35, CCKAR, GLP1R, GHSR and pan-neuronal markers, SCN10A and TUBB3 in nodose ganglia following AAV microinjection. (Two-way ANOVA, Dunnet's multiple comparisons test, N=7-8). Different letters indicate significant differences from unoperated control *(p*<0.05). All samples normalized to unoperated control. Data are presented as ±SEM. B) Representative immunohistochemcial staining of eGFP (AAV-shGPR35 reporter) in nodose ganglia of AAV-injected and sham control mice. 'Secondary only' control also included to verify the specificity of secondary antibody to the anti-eGFP primary antibody.

Study 2

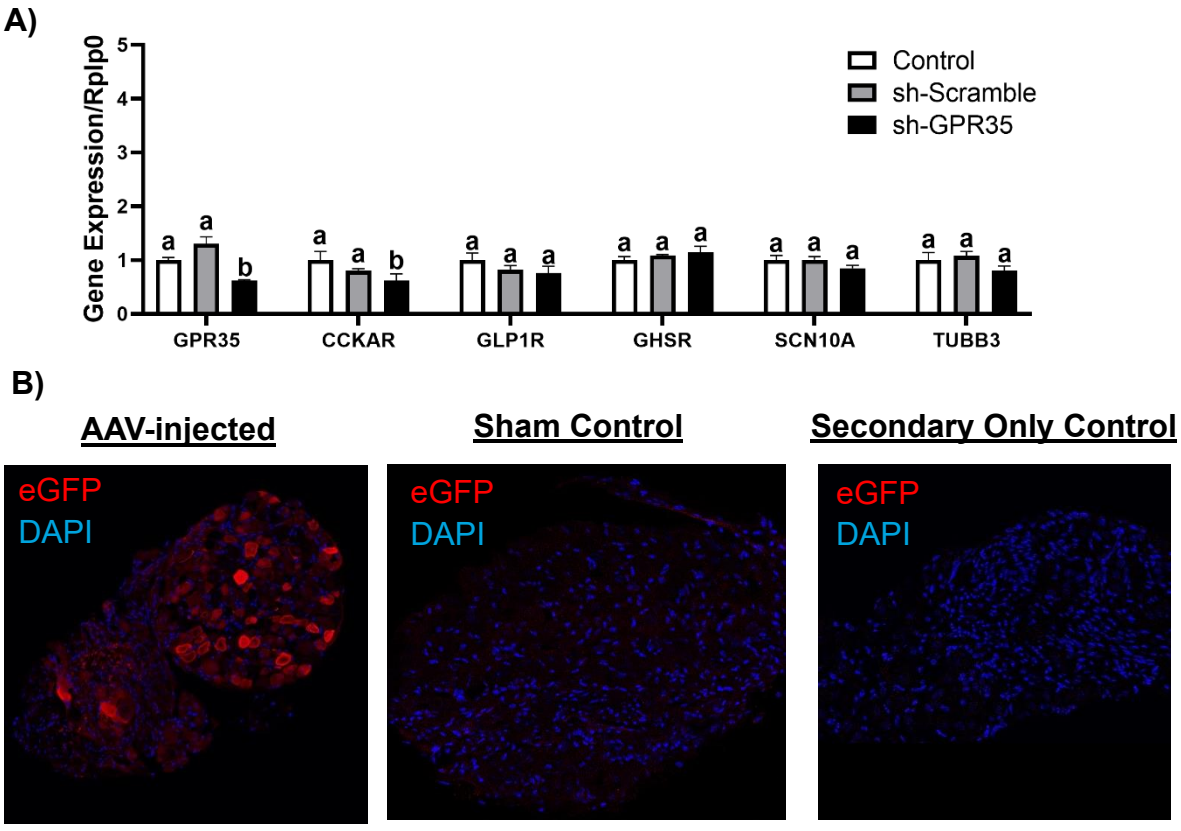

In Study 2, knockdown of GPR35 in VANs did not affect *ad libitum* food intake in standard shoebox cages relative to sham controls (Figure 3.8A). However, GPR35 knockdown in VANs was associated with a significant increase in food intake during the dark period in male mice relative to sham controls (Figure 3.8B, N=10-11, $^{**}p<0.01$). Although there was a trend for animals microinjected with sh-Scramble to increase food intake during the dark period relative to sham controls, this difference did not reach statistical significance ($p=0.23$), suggesting that the effects of sh-GPR35 on hyperphagia is due to knockdown of GPR35 in VANs and not due adverse effects to surgery nor vector integration. AAV-microinjection with either vector did not affect food intake during the light period relative to sham control. Nodose microinjection with sh-GPR35 or sh-Scramble did not significantly affect body weight relative to sham controls (Figure 3.8C), suggesting that GPR35 knockdown in VANs may increase hyperphagia three weeks from surgery, the reduction in GPR35 expression alone does not increase weight gain.

Figure 3.8: Effect of nodose microinjection of AAV-shGPR35 or scramble vector control (Study 2) on food intake of male mice during light and dark periods and body weight. A) Effects of nodose microinjection scrambled vector (sh-Scramble) and sh-GPR35 (1e11 gc/mL per AAV type) on daily food intake in standard cages over time. Blue arrow indicates when cages were changed and when food intake data was excluded from analysis. B) Effect of nodose microinjection scrambled vector (sh-Scramble) and sh-GPR35 (1e11 gc/mL per AAV type during the light and dark period over 3 consecutive days relative to sham controls (Two-way ANOVA, Tukey's multiple comparisons test, N=10-11, $^{**}p<0.01$). Data are presented as ±SEM. C) Effects of nodose microinjection with sh-Scramble and sh-GPR35 on body weight over time. Data are presented as ±SD.

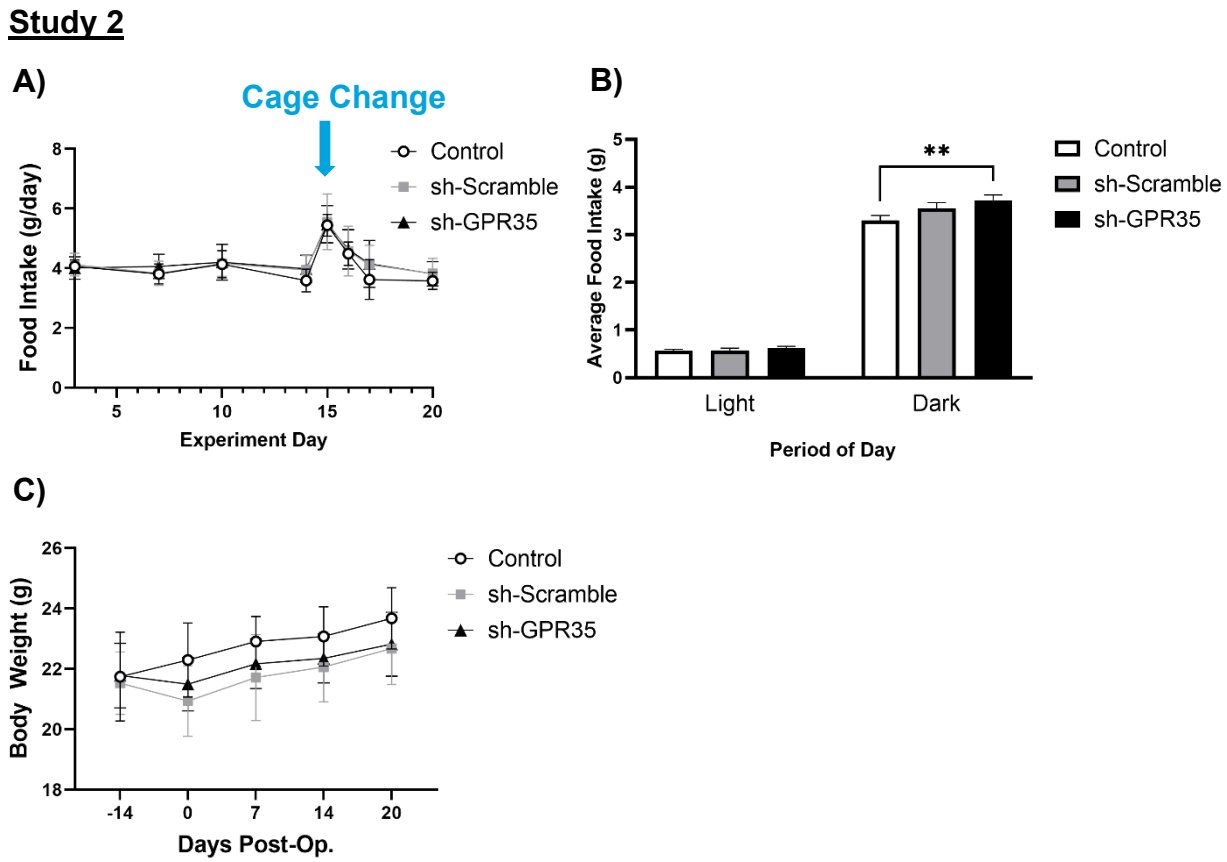

Study 3: Effect of Nodose Microinjection of shGPR35 on Feeding Behavior, Endogenous CCK Signaling, and Diet-Induced Weight Gain and GPR35 Gene Expression on VANs

Study 3 repeated Studies 1 and 2 but extended to 20 weeks to determine if nodose microinjection with sh-GPR35 (1) reduces endogenous CCK signaling in low-fat fed animals as measured by devazepide-induced hyperphagia and gastric emptying and (2) exacerbates diet-induced changes in feeding behavior.

Study 3: Effect of Microinjection of sh-GPR35 on Food Intake on Chow Diet

In Study 3, nodose microinjection of GPR35 did not significantly increase average daily food intake in chow-fed mice during the light or dark period as shown in Study 2. Relative to unoperated controls, microinjection with shRNA significantly increased average daily food intake in Study 3, regardless of the shRNA vector sequence (Figure 3.9, N=12-16/group, $*p<0.05$).

Figure 3.9: Effect of nodose microinjection of AAV-shGPR35 or scramble vector control (Study 3) on daily normal chow intake of male mice. A) Average daily food intake of male mice microinjected with scrambled vector (sh-Scramble) or sh-GPR35 relative to uninjected controls (Two-way ANOVA, Tukey's multiple comparisons test, N=12-16/group, *p<0.05*).* Data are presented as ±SEM.

Study 3

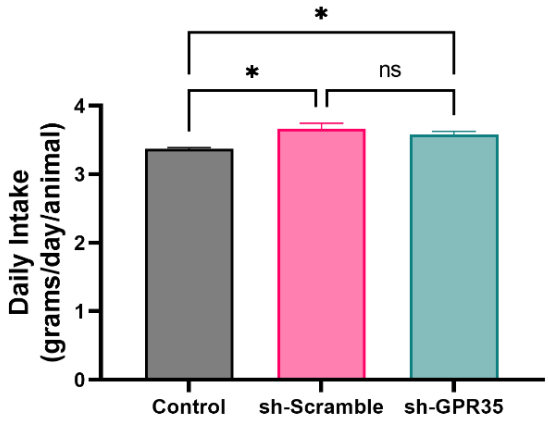

Study 3: Effect of sh-GPR35 on VAN-CCK$_A$R Signaling as Measured by Acute Administration of CCK

Acute administration of CCK (3 µg/kg, IP) significantly reduced cumulative food intake in sh-GPR35 animals and unoperated control mice relative to respective vehicle control groups up to 40 minutes (Figure 3.10, N=6-8; *p<0.05). CCK also decreased food intake in sh-Scramble mice relative to vehicle controls at the 20-minute timepoint but this difference did not reach statistical significance (p=0.053). These data suggest that GPR35 knockdown in VANs is not sufficient to reduce satiety induced by exogenous CCK.

Figure 3.10: Effect of nodose microinjection of AAV-shGPR35 or scramble vector control (Study 3) on CCK-induced satiety (3 µg/kg, IP) over 1-hour post-injection. Effects of nodose microinjection of sh-GPR35 on satiety following exogenous administration of CCK (3 µg/kg, IP). (Two-way ANOVA, Sidak's multiple comparisons test, N=6-8, paired; *p<0.05, **p<0.01, ***p<0.001). Data are presented as ±SEM. Each animal received either CCK or vehicle one week apart.

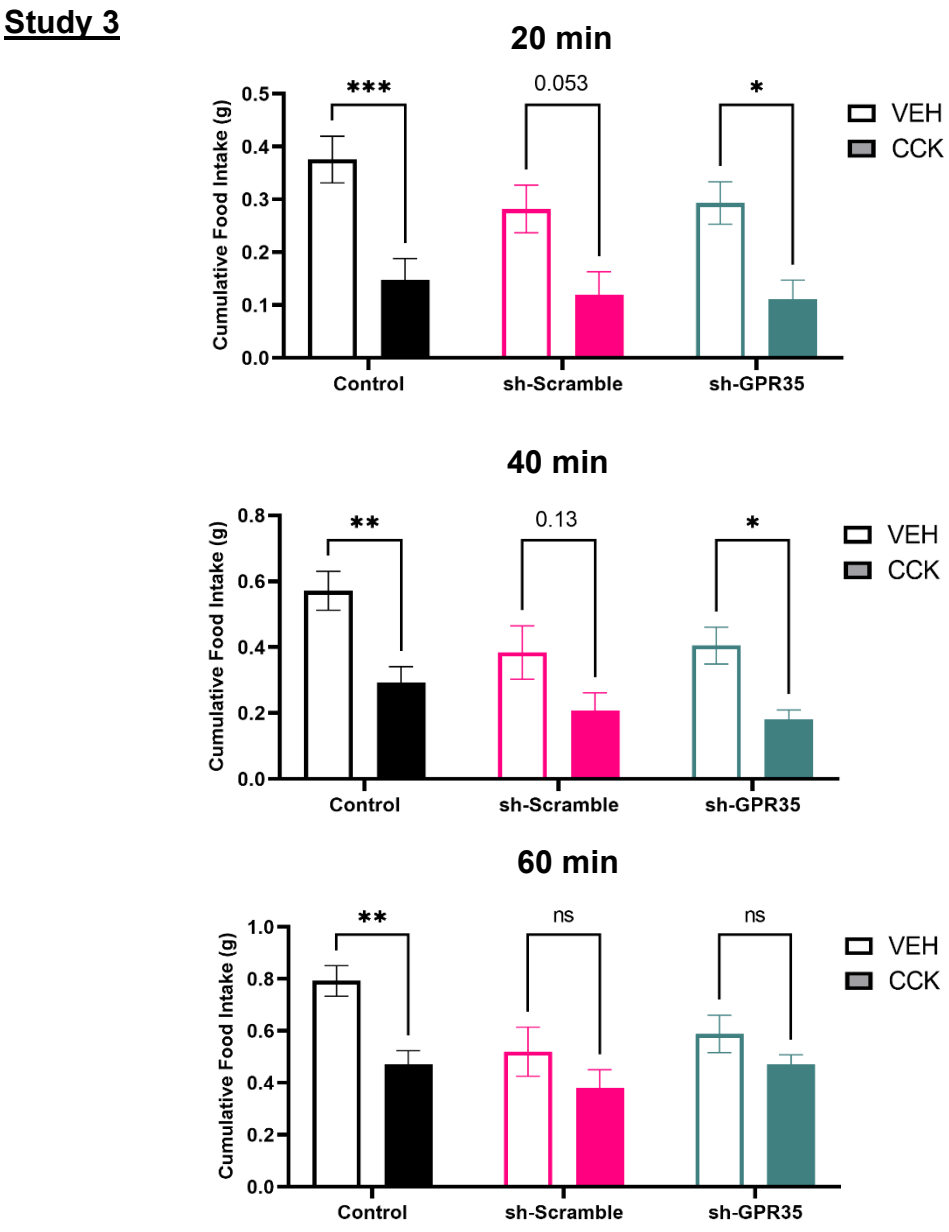

Study 3: Effect of sh-GPR35 on Endogenous VAN-CCK_AR Sensing as Measured by CCK_AR Blockade

Alternately, we tested if nodose microinjection of sh-GPR35 affects sensing of endogenous CCK, as measured by devazepide (would help to define this)-induced hyperphagia and gastric emptying. The data show that acute administration of devazepide (600 µg/kg, IP) significantly increased food intake in unoperated controls and sh-Scramble mice at 60 minutes in Study 3 but failed to significantly increase food intake in sh-GPR35 mice relative to vehicle controls (Figure 3.11, N=6-8). As expected, devazepide significantly increased gastric emptying in unoperated control animals (Figure 3.17, n=3, $p<0.05$) and tended to increase gastric emptying in sh-Scramble animals (n=3, $p=0.07$). However, devazepide failed to enhance gastric emptying in LF fed, sh-GPR35 microinjected animals relative to vehicle control (n=3, $p>0.05$). Relative to vehicle control, devazepide had no significant effect on gastric emptying in any treatment group maintained on an HF diet ($p>0.05$). Taken together, these data in lean animals suggest that GPR35 knockdown in VANs impairs VAN sensing of endogenous CCK.

Figure 3.11: Effect of nodose microinjection of AAV-shGPR35 or scramble vector control (Study 3) on impairment of endogenous CCK-induced satiety. Effects of nodose microinjection of sh-GPR35 on devazepide-induced hyperphagia (600 µg/kg, IP) relative to vehicle (0.2% DMSO, 0.2% Tween-80). Two-way ANOVA, Sidak's multiple comparisons test, N=6-8, paired *(*p*<0.05, ***p*<0.01. Data are presented as ±SEM. Each animal received either devazepide or vehicle one week apart.

Study 3

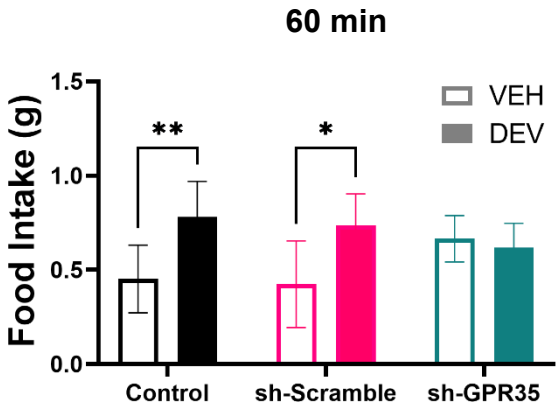

Study 3: Effect of sh-GPR35 on Diet-Induced Changes in Feeding Behavior and Body Weight

In Study 3, sh-GPR35 failed to increase body weight on a chow diet during the first 6 weeks of study (N=12-16) and did not exacerbate diet-induced weight gain, demonstrated by no significant increase in body weight after 8 weeks on a high-fat diet relative to unoperated controls (Figure 3.12, N=6-8).

Figure 3.12: Effect of nodose microinjection of AAV-shGPR35 or scramble vector control (Study 3) on diet-induced weight gain of male mice. A) Effects of nodose microinjection scrambled vector (sh-Scramble) and sh-GPR35 body weight on normal chow diet (1-6 weeks, N=12-16) and HFD or LFD (N=6-8/group). Data are presented as ±SEM.

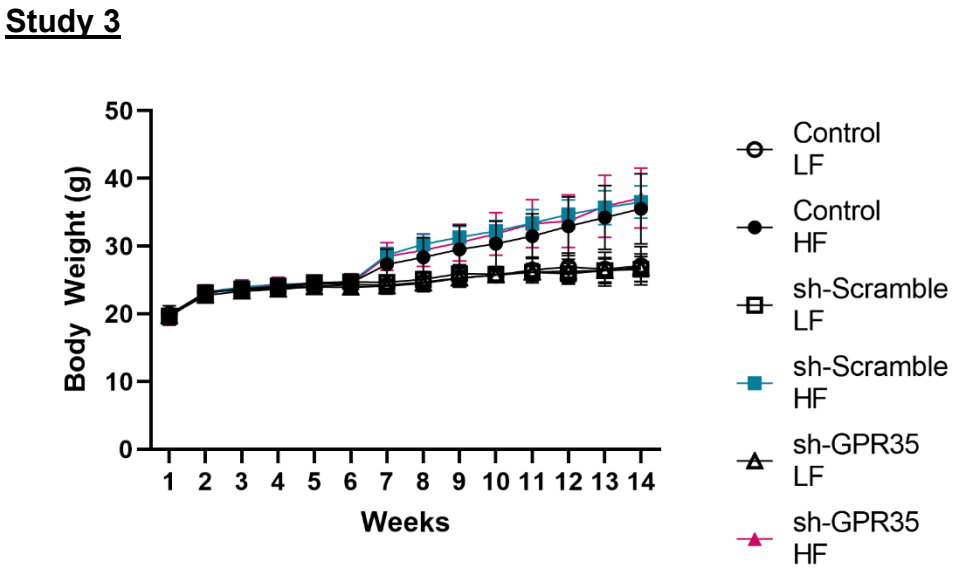

On average, HFD increased cumulative food intake relative to LF-fed mice throughout the dark period but not the light period in unoperated control mice (Figure 3.13, N=6-8, $p<0.05$). We observed differences among the average rates of food intake (kcal/ΔZT) within the first 6 hours of the light and dark periods, as indicated by the slopes of the lines (Figure 3.13). Relative to LF-fed mice, HFD increased cumulative food intake during the first 6 hours of the light and dark periods in unoperated and sh-Scramble control mice (Figure 3.13, N=6-8; *, $p<0.05$ Control LF vs. HF; †, $p<0.05$ sh-Scramble LF vs. HF). However, relative to LF-fed animals, HF-feeding did not significantly increase average cumulative food intake during the first 6 hours of the light and dark periods in sh-GPR35 mice. These data indicate that the knockdown of GPR35 in VANs may disrupt diurnal rhythms of VAN activity and satiety signaling reported in HF-fed mice[58–60].

Figure 3.13: Effect of nodose microinjection of AAV-shGPR35 or scramble vector control (Study 3) and diet on food intake. Effects of nodose microinjection and diet on cumulative food intake (kcal) across an average 24-hour cycle. Mixed-effects model, Tukey's multiple comparisons test, N=6-8/group (*, $p<0.05$ Control LF vs. HF; †, $p<0.05$ sh-Scramble LF vs. HF). Data are presented as ±SEM. Light phase extends from 6-18 ZT. Dark phase extends from 18-6 ZT, as indicated by the gray background.

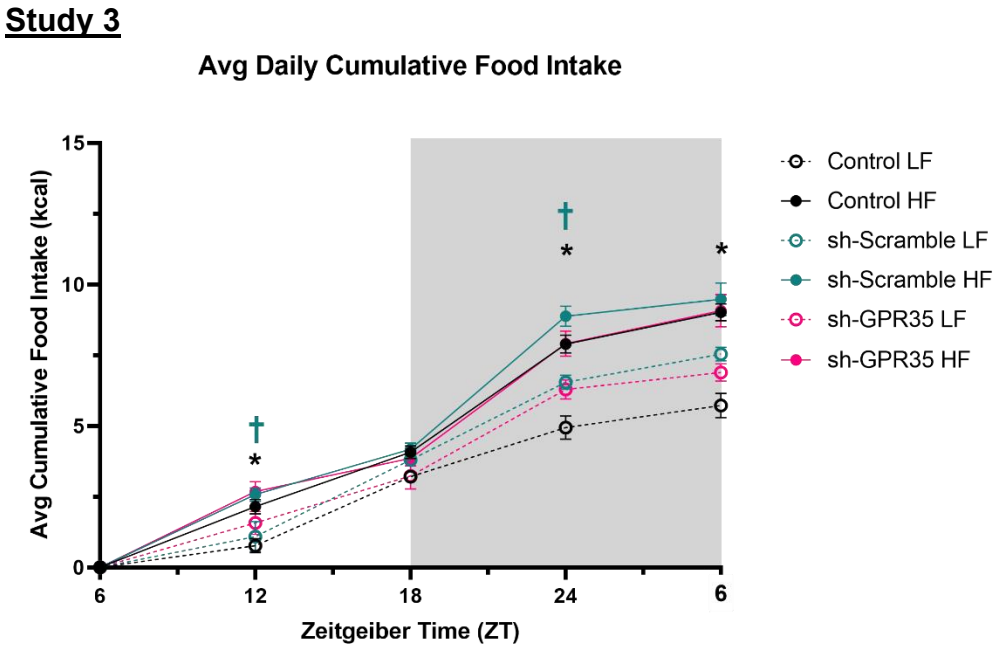

Meal microstructure analysis demonstrates that HF-feeding tended to increase meal size in the light but not dark periods across all groups (Figure 3.14A, N=6-8). HF-fed sh-Scramble mice tended to eat larger meals than LF-fed sh-Scramble mice in the light period, but this difference did not reach statistical significance (Figure 3.14A, N=6-8, p=0.17). GPR35 knockdown significantly increased average meal size in HF-fed animals in the light period relative to LF-fed sh-Scramble animals (Figure 3.14A, N=6-8, p<0.05). HF-fed sh-GPR35 mice tended to eat larger meals than HF-fed unoperated control mice, but this difference did not reach statistical significance (Figure 3.14A, N=6-8, p=0.19). Nodose microinjection of shRNA and diet had no effect on average meal size during the first 6 hours of either period (Figure 3.15A, N=6-8). Nodose microinjection of shRNA and diet had no effect on the average meal number (Figure 3.15D and 3.16D, N=6-8).

Figure 3.14: Effect of nodose microinjection of AAV-shGPR35 or scramble vector control (Study 3) on meal microstructure of male mice during light and dark periods. A) Effects of nodose microinjection scrambled vector (sh-Scramble) and sh-GPR35 and diet on the average A) meal size and B) meal duration during light and dark periods, averaged across 4 days. Mixed-effects model, Sidak's multiple comparisons test, N=6-8/group; * $p<0.05$, ** $p<0.005$, ***$p<0.0002$. Data are presented as ±SEM.

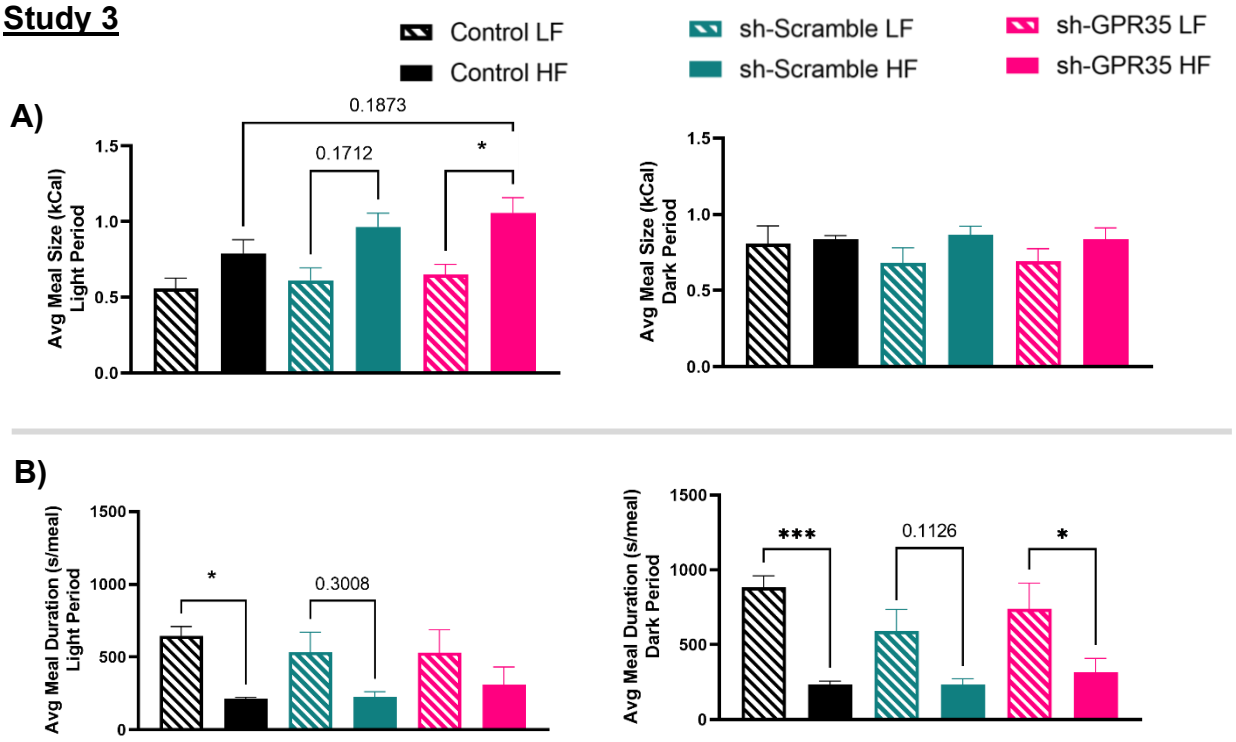

Figure 3.14: Effect of nodose microinjection of AAV-shGPR35 or scramble vector control (Study 3) on meal microstructure of male mice during light and dark periods. Effects of nodose microinjection scrambled vector (sh-Scramble) and sh-GPR35 and diet on the average C) ingestion rate and D) meal number during light and dark periods, averaged across 4 days. Mixed-effects model, Sidak's multiple comparisons test, N=6-8/group; * $p<0.05$, ** $p<0.005$, ***$p<0.0002$. Data are presented as ±SEM.

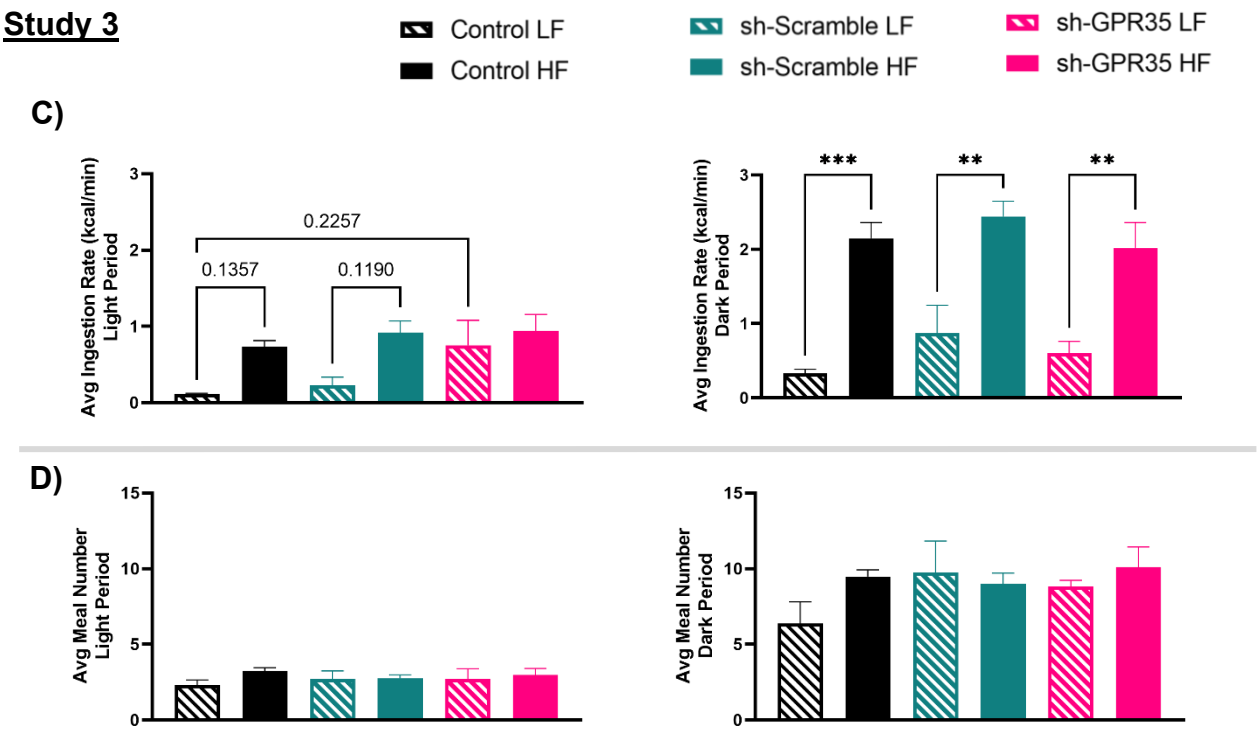

Figure 3.15: Effect of nodose microinjection of AAV-shGPR35 or scramble vector control (Study 3) on meal microstructure of male mice during the early periods of light and dark phases. Effects of nodose microinjection scrambled vector (sh-Scramble) and sh-GPR35 and diet on the average A) meal size and B) meal duration during the first 6 hours of light and dark period. Mixed-effects model, Sidak's multiple comparisons test, N=6-8/group; * $p<0.05$, ** $p<0.005$, ***$p<0.0002$, **** $p<0.0001$). Data are presented as ±SEM.

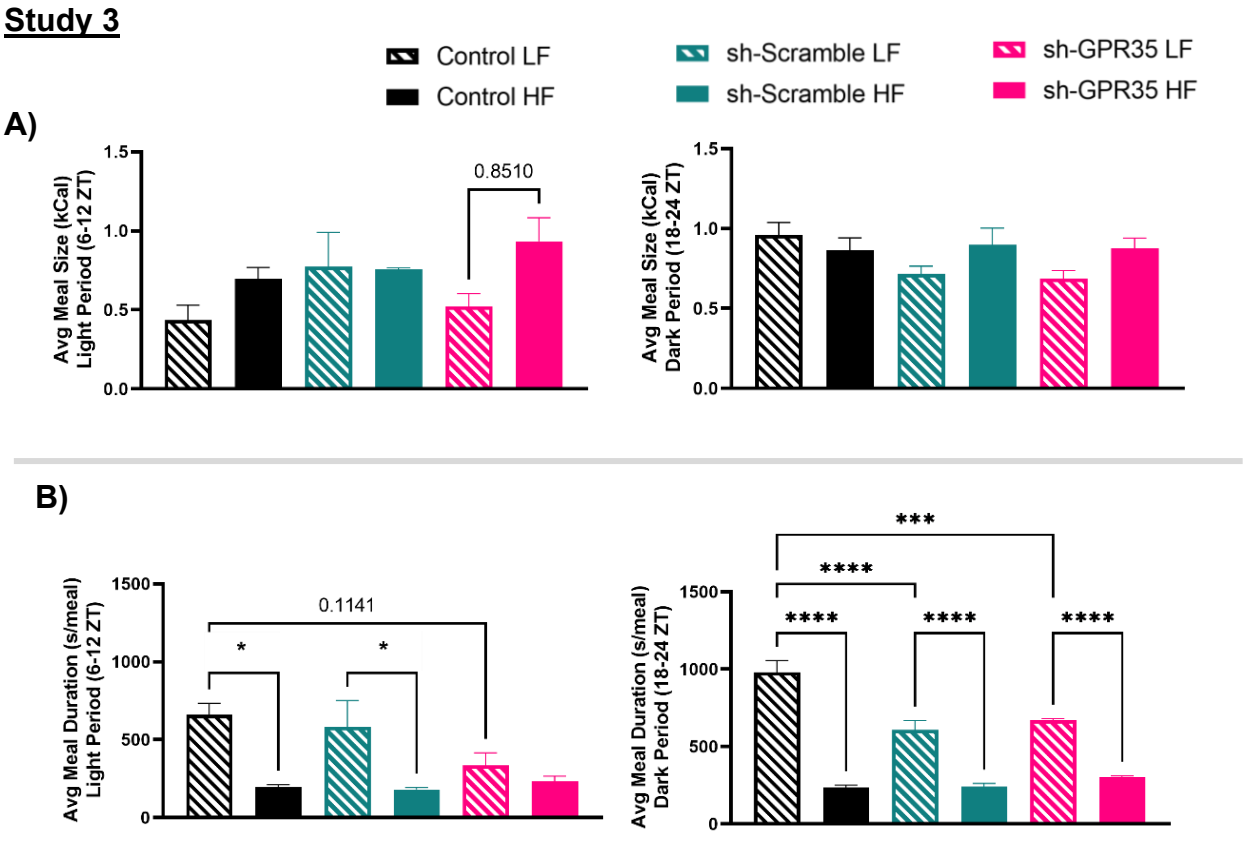

Figure 3.15: Effect of nodose microinjection of AAV-shGPR35 or scramble vector control (Study 3) on meal microstructure of male mice during the early periods of light and dark phases. Effects of nodose microinjection scrambled vector (sh-Scramble) and sh-GPR35 and diet on the average C) ingestion rate and D) meal number during the first 6 hours of light and dark period. Mixed-effects model, Sidak's multiple comparisons test, N=6-8/group; * $p<0.05$, ** $p<0.005$, *** $p<0.0002$, **** $p<0.0001$). Data are presented as ±SEM.

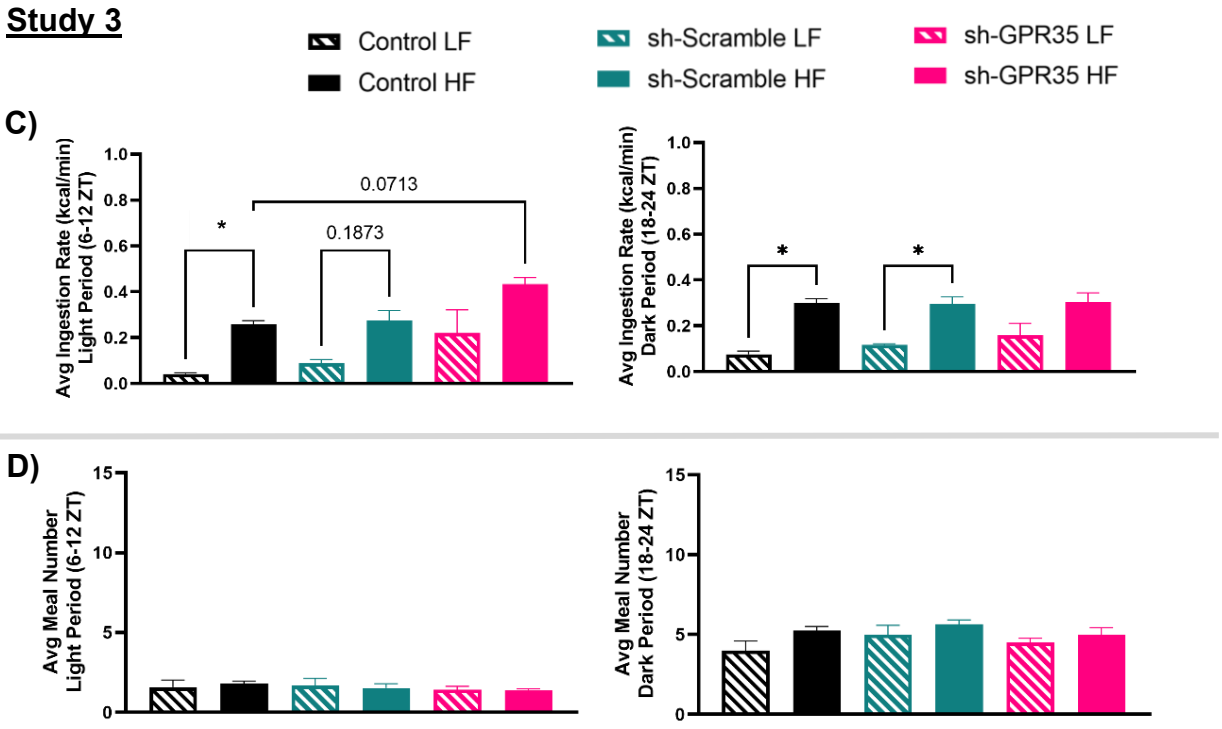

Relative to LF-fed controls, HFD significantly reduced the average meal duration during the light and dark periods in unoperated control mice (Figure 3.14B and 3.15B, N=6-8, $p<0.05$). HFD significantly decreased the average meal duration in sh-Scramble mice relative to LF-fed sh-Scramble mice within the first 6 hours of the light and dark periods (Figure 3.15B, N=6-8, $p<0.05$). sh-GPR35 decreased the average meal duration in the first 6 hours of the light period relative to LF-fed, unoperated controls, but this difference did not reach statistical significance (Figure 3.15B, N=6-8, $p=0.11$). Furthermore, sh-GPR35 microinjection reduced average meal duration in the early phase of the light period to a level not significantly different from HF-feeding (Figure 3.15B). Relative to LF-fed unoperated controls, nodose microinjection of sh-Scramble and sh-GPR35 reduced average meal duration during the first 6 hours of the dark period (Figure 3.15B, N=6-8, $p<0.05$), suggesting the nodose microinjection surgery may have unforeseen consequences on nocturnal feeding behavior, when the mice are most active[54,59].

During the first 6 hours of the light and dark periods, HF-feeding increased the average ingestion rate in unoperated controls relative to LF-fed mice (Figure 3.15C, N=6-8, $p<0.05$). HF-feeding also significantly increased the rate of ingestion in sh-Scramble mice relative to LF-fed sh-Scramble mice during the early phase of the dark period, but this difference did not reach statistical significance during the first 6 hours of the light period (Figure 3.15C, N=6-8, $p=0.19$). Unlike the other groups, HF-feeding did not significantly increase the rate of ingestion of sh-GPR35 mice in the first 6 hours of the light or dark periods relative to LF-fed sh-GPR35 mice (Figure 3.15C, N=6-8). Furthermore, HF-fed sh-GPR35 mice tended to eat faster than HF-fed unoperated

controls in the first 6 hours of the light period, but this difference did not reach statistical significance (Figure 3.15C, N=6-8, *p*=0.07). Taken together, these data suggest that GPR35 knockdown may alter feeding behavior in the early phases of both the light and dark periods perhaps by impairing vagal afferent activity and/or sensing of endogenous satiety signals[58]. These data may also suggest that GPR35 knockdown may exacerbate diet-induced increases in the rate of ingestion, which is also observed in obese humans[61].

Study 3: Effect of sh-GPR35 on GPR35 Agonist Zaprinast-Induced Satiety

Acute administration of the GPR35 agonist zaprinast (10 mg/kg, IP) had no significant effect on food intake in LF-fed mice relative to vehicle control (Figure 3.16, N=6-8). We previously showed that zaprinast-induced satiety is dependent on diet (Chapter 2). Zaprinast significantly reduced diet-induced hyperphagia in control and sh-GPR35 microinjected animals (Figure 3.16, N=6-8; *p<0.05). Although there was a trend of zaprinast to reduce food intake in HF-fed sh-Scramble mice, this difference did not reach statistical significance (p=0.17). These data suggest that GPR35 knockdown in VANs is not sufficient to prevent GPR35 agonist zaprinast-induced satiety.

Figure 3.16: Effect of nodose microinjection of AAV-shGPR35 or scramble vector control (Study 3) on GPR35 agonist-induced satiety. Effects of nodose microinjection of sh-GPR35 on cumulative food intake (kcal) following acute administration of GPR35 agonist zaprinast (10 mg/kg, IP) or vehicle (0.9% saline) at 90 minutes post-injection. Two-way ANOVA, Sidak's multiple comparisons test, N=6-8, paired, *p<0.05. Data are presented as ±SEM. Each animal received either zaprinast or vehicle one week apart.

Study 3

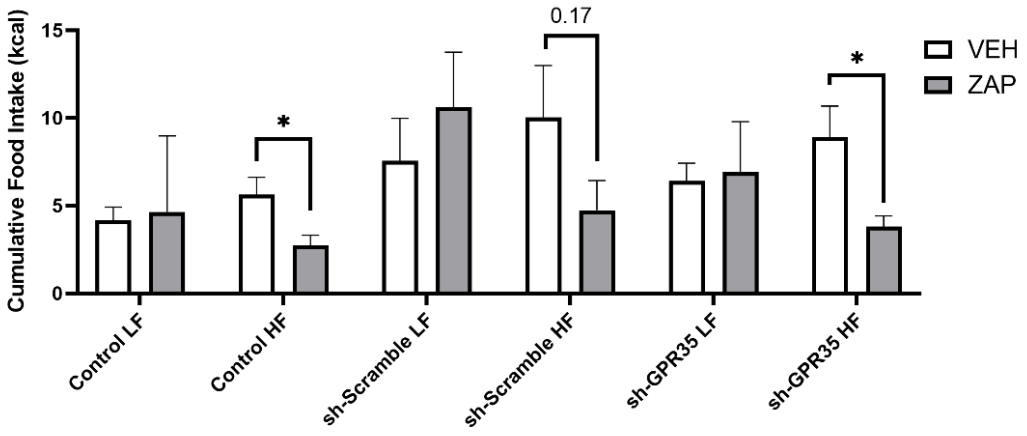

Study 3: Effect of sh-GPR35 on Devazepide-Enhanced Gastric Emptying

The CCK_AR antagonist devazepide (600 µg/kg, IP) increased gastric emptying in LF-fed unoperated mice relative to vehicle controls, as measured by plasma acetaminophen (Figure 3.17A, N=3; $p<0.05$). Devazepide also increased gastric emptying in LF-fed sh-Scramble mice relative to vehicle control, but this difference did not reach statistical significance (Figure 3.17A, N=3; $p=0.07$). Devazepide failed to significantly enhance gastric emptying in LF-fed sh-GPR35 mice relative to vehicle (Figure 3.17A, N=3). Vehicle control sh-GPR35 mice had slightly higher basal gastric emptying levels relative to the other LF-fed control groups, although this difference did not reach statistician significance (Figure 3.17A, N=3). Taken together, these gastric emptying data suggest that GPR35 knockdown in VANs impairs CCK_AR function on VANs (Figure 3.17A, N=3).

Devazepide failed to enhance gastric emptying in HF-fed mice relative to vehicle control mice in all surgical groups (Figure 3.17B, N=4-6). These data may suggest that HFD impairs the function of CCK_AR on VANs, which has been previously demonstrated by our lab and others[8,10,11]. We also observed that the range of plasma acetaminophen levels were approximately twice as large in HF-fed animals as LF-fed animals. These data may suggest that a HFD may reduce the accuracy of the colorimetric assay used in these studies, perhaps by interfering with the mechanism of acetaminophen detection.

Figure 3.17: Effect of AAV-shGPR35 or scramble vector control on devazepide-enhanced gastric emptying, as measured by plasma acetaminophen. A) Effect of CCK_AR antagonist devazepide (600 µg/kg) on plasma acetaminophen levels (µg/mL) in control, sh-Scramble, and sh-GPR35 male mice on low-fat diet or B) high-fat diet. Two-way ANOVA, Sidak's multiple comparisons test, N=3-6/group, paired, *p<0.05. All samples normalized to baseline levels. Data are presented as ±SD.

Study 3

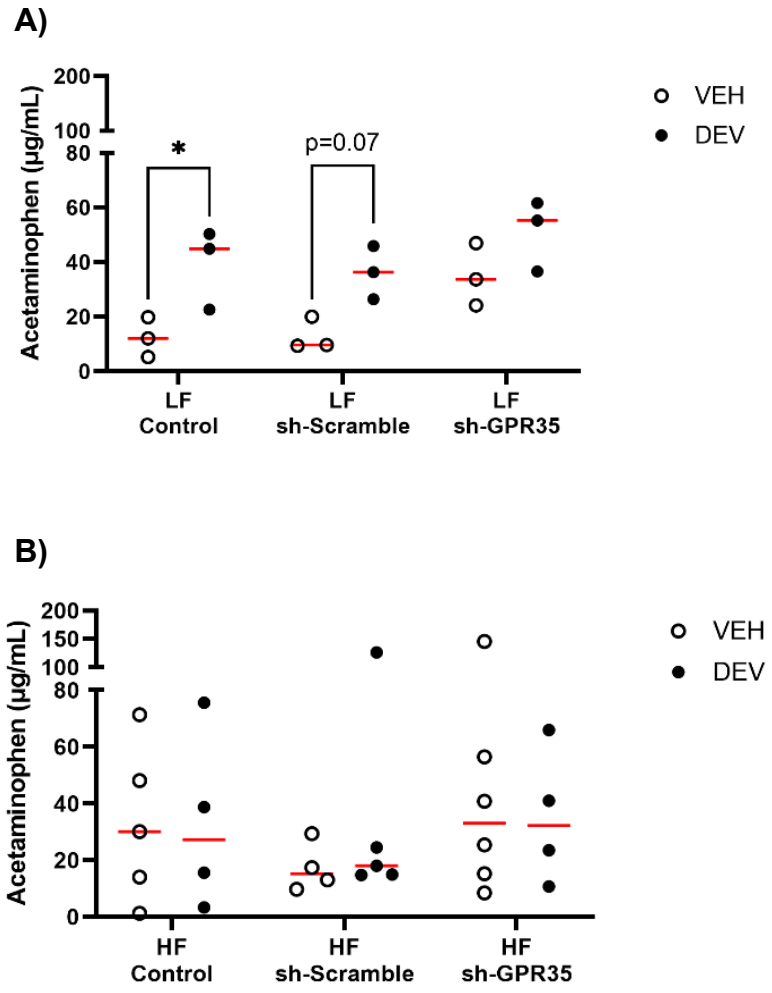

Study 3: Effect of sh-GPR35 on GPR35 Gene Expression in VANs

At 20 weeks, nodose microinjection with sh-GPR35 decreased the expression of GPR35, but this failed to reach statistical significance in mice relative to unoperated controls (Figure 3.18A, N=5-6, p=0.19). sh-GPR35 also reduced gene expression of CCK_AR and GLP1R in LF-fed mice (Figure 3.18B and 3.10C, respectively), but these differences also failed to reach statistical significance ($p \geq 0.2$). Relative to controls, sh-GPR35 did not reduce the gene expression of pan-neuronal markers, SCN10A and TUBB3 (Figures 3.19D and 3.10E), indicating that nodose injection did not result in neuronal loss relative to controls. Our previous data show that sh-GPR35 reduces GPR35 expression in nodose ganglia at 3 weeks post-injection. These data suggest that suppression of GPR35 gene expression by sh-GPR35 may decrease by 20 weeks post-injection. Injection with sh-Scramble control did not significantly affect the expression of any gut hormone receptors nor pan-neuronal markers surveyed (Figures 3.18A-E).

Figure 3.18: Effect of AAV-shGPR35 or scramble vector control on gene expression of receptors, pan-neuronal, and non-neuronal markers on VANs in male mice. Effects of AAV-shGPR35 or scrambled shRNA vector (1e11 gc/mL per AAV type) and diet on gene expression of A) GPR35, B) CCKAR, C) GLP1R, and pan-neuronal markers, D) SCN10A and E) TUBB3 in nodose ganglia following AAV microinjection. Two-way ANOVA, Sidak's multiple comparisons test, N=5-6, * $p<0.05$. All samples normalized to unoperated control. Data are presented as ±SEM.

Study 3

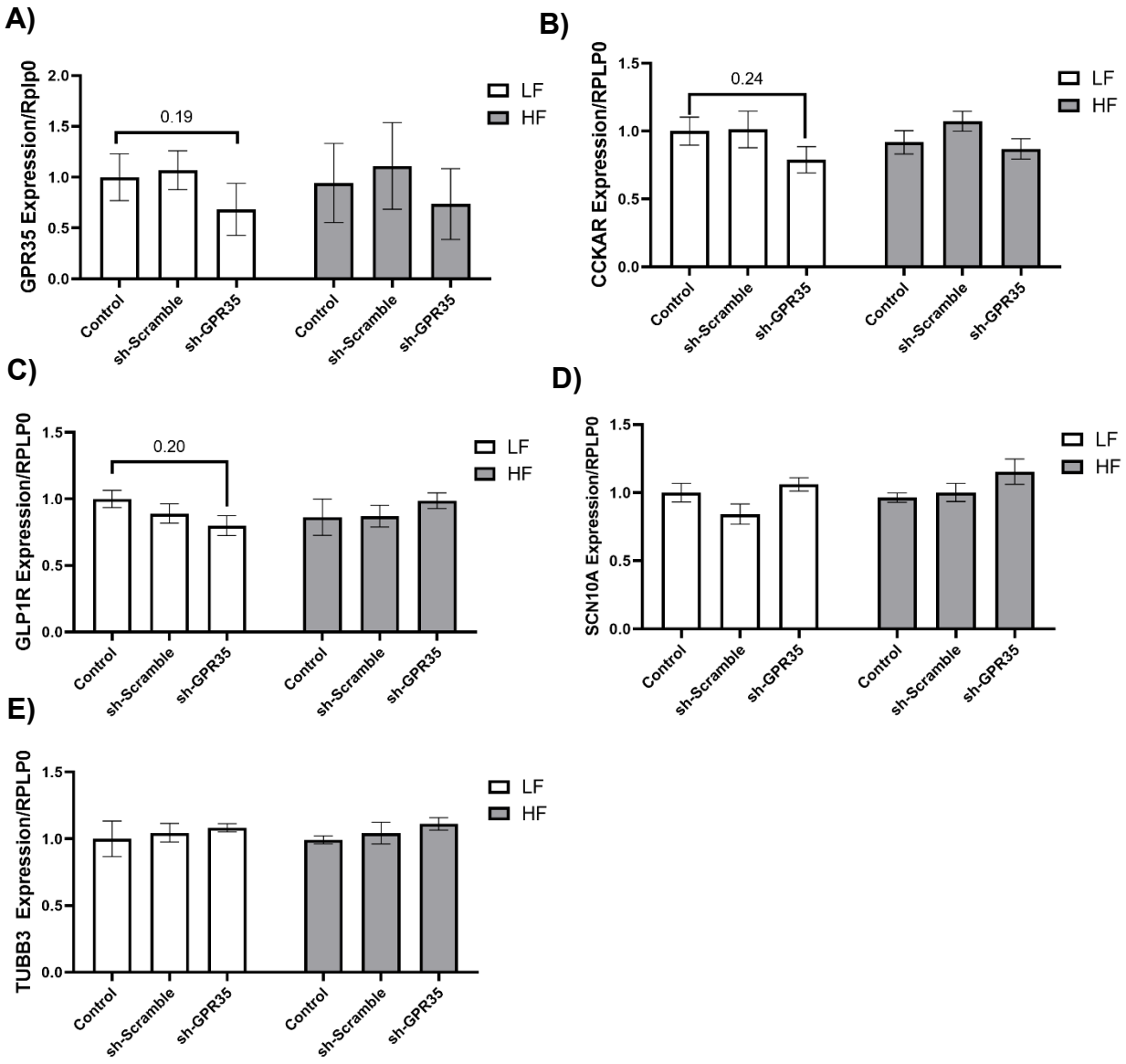

Simple linear regression analysis was used to determine if gene expression of GPR35 in nodose ganglia explained average ingestion rate in LF-fed mice in Study 3 (Figure 3.19). The results of the regression analysis indicate that GPR35 gene expression in nodose ganglia explained 36.21% of the variation in the average ingestion rate [$F(1,15)=8.513$, $p=0.0106$]. There was a small effect of surgery day on GPR35 knockdown, indicated by the modest aggregation of open circles in Figure 3.19 (colored by surgical group). Although sample size is limited, this data may suggest that there is an effect of surgery day and perhaps AAV aliquot on GPR35 knockdown. Taken together, these data suggest that reduction in the gene expression of GPR35 in nodose ganglia may increase the ingestion rate in LF-fed animals. However, these feeding behavior data also suggest that nodose microinjection of AAV-shRNA may impose unintended consequences on meal patterns in mice. The data from Studies 2 and 3 demonstrate that the efficacy or perhaps duration of knockdown induced by the sh-RNA vector varied across studies and individual animals.

Figure 3.19. Relationship between gene expression of GPR35 in nodose ganglia to average ingestion rate of LF fed-male mice. Simple linear regression was used to determine if relative expression of GPR35 in nodose ganglia determined average ingestion rate. N=5-6/group. “O” open circles represent animals whose surgeries were completed on the same day per group surgery day. Solid circles represent animals whose surgeries were completed on different days. Control LF animals did not undergo surgery.

Study 3

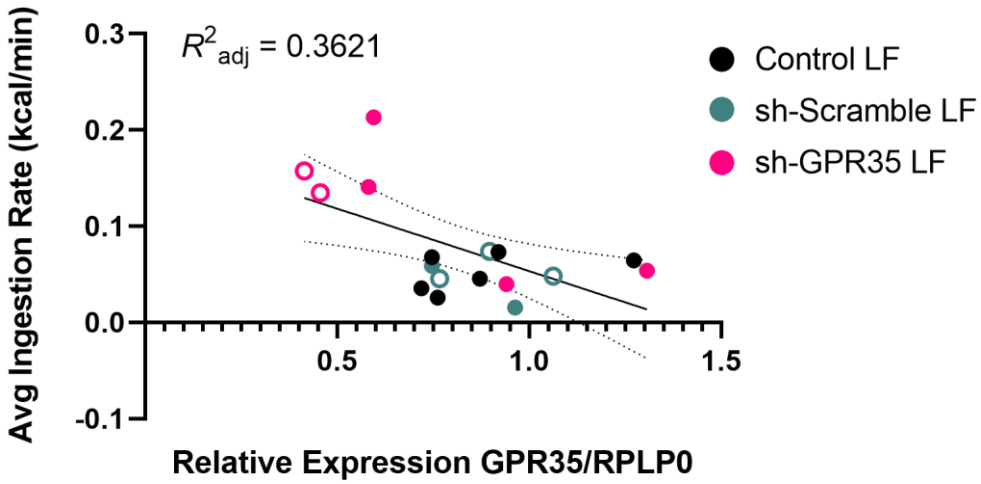

Study 4: Effect of Nodose Microinjection of shGPR35 on Feeding Behavior, Endogenous CCK Signaling, and GPR35 Gene Expression on VAN

Study 4 repeated the study design from Study 3 to expand the sample size and to determine if nodose microinjection with sh-GPR35 impairs endogenous CCK signaling in low-fat fed animals; diet challenges were excluded.

Study 4: Effect of Microinjection of sh-GPR35 on Feeding Behavior on Chow Diet

Relative to unoperated controls, nodose microinjection with sh-GPR35 failed to increase cumulative food intake on a chow diet, regardless of time of day (Figure 3.20, N=11, $p>0.05$). Study 4 also confirms that nodose microinjection with either shRNA vector sequence significantly increased meal size during the dark period but not during the light period (Figure 3.21, N=11, $^{**}p<0.01$), as observed in Study 3. This increase in meal size was accompanied by a commensurate reduction in meal number during the dark period in sh-GPR35-injected animals (Figure 3.21, N=11, $^{*}p<0.05$), resulting in no significant difference in cumulative food intake during the dark period in these animals. sh-GPR35-injection did not significantly increase meal duration during either period (Figure 3.21B).

Figure 3.20: Effect of nodose microinjection of AAV-shGPR35 or scramble vector control (Study 4) on food intake of male mice during light and dark periods. A) Effects of nodose microinjection scrambled vector (sh-Scramble) and sh-GPR35 on cumulative diet intake (chow) during light and dark periods in BioDAQ cages. One-way ANOVA, Tukey's multiple comparisons test, N=11/group. Data are presented as ±SEM.

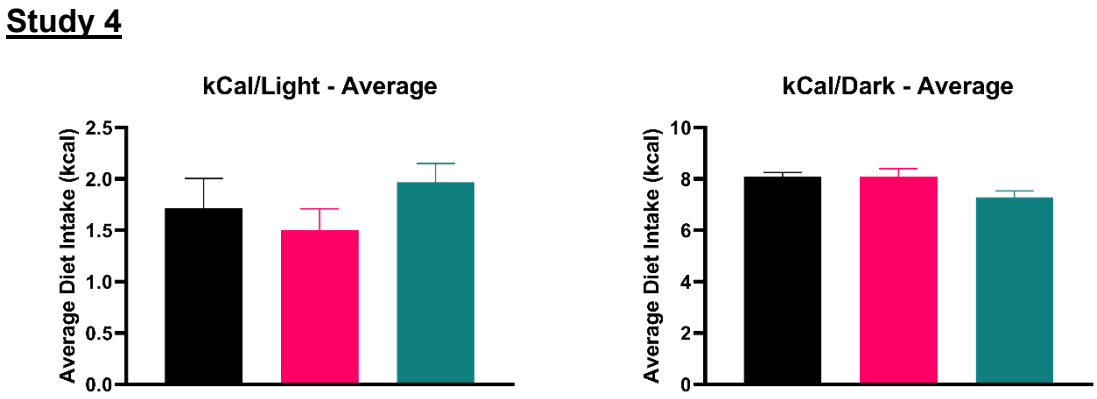

Figure 3.21: Effect of nodose microinjection of AAV-shGPR35 or scramble vector control (Study 4) on meal microstructure of male mice during light and dark periods. A) Effects of nodose microinjection scrambled vector (sh-Scramble) and sh-GPR35 on A) meal size, B) meal number, C) meal duration. One-way ANOVA, Tukey's multiple comparisons test, N=11/group, *p<0.05, **p<0.01. Data are presented as ±SEM.

Study 4

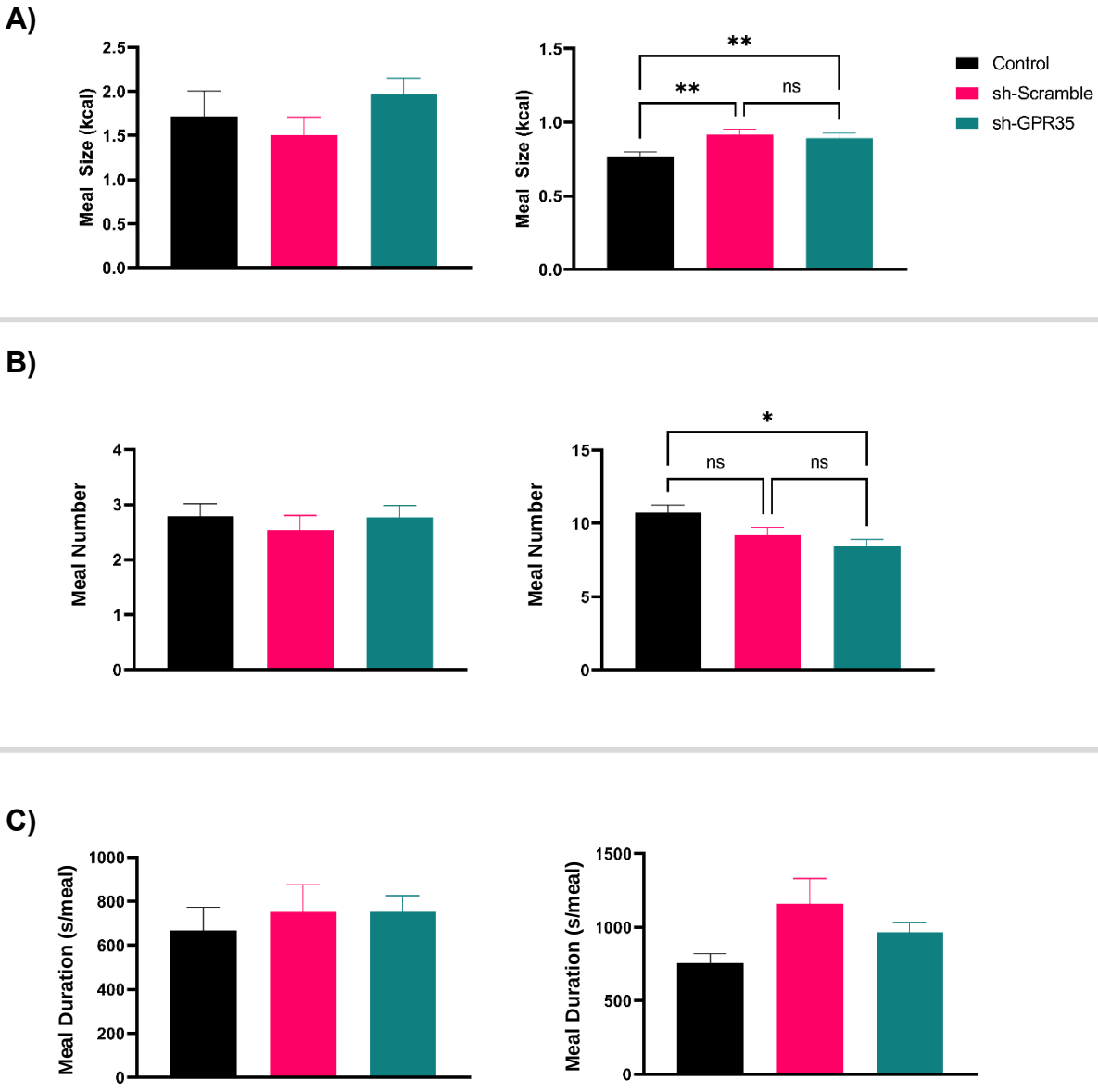

Study 4: Integrity of Endogenous VAN-CCK$_A$R Sensing by CCK$_A$R Blockade

Devazepide did not induce hyperphagia nor enhance gastric emptying in any group of mice in this cohort relative to vehicle control (data not shown). This was unexpected because devazepide increased food intake in the first cohort of mice from Study 3 (Figure 3.11) just two weeks prior. Careful technical precautions were taken to use frozen aliquots from the same stocks across Studies 3 and 4, eliminating the risk of lot-to-lot variations in drug processing. This feeding behavior experiment was repeated a total of three times in Study 4 and devazepide did not increase food intake relative to vehicle control in any trail in Study 4. Although these studies were separated by only two weeks, these data suggests that this may have been a cohort of unresponsive mice. Recent studies have demonstrated that the gut microbiome can influence drug activity and metabolism[62]. Furthermore, published and unpublished work from our lab shows that differences in bacterial abundance between cohorts of mice can introduce variability that can influence metabolic outcomes[63]. Despite taking every reasonable measure to reduce variations in animal sourcing, housing, environment, and study design, the mice in Study 4 failed to respond to drug-induced changes in feeding behavior and gastric emptying.

Study 4: Effect of Microinjection of sh-GPR35 on GPR35 Gene Expression in VANs

In Study 4, sh-GPR35 failed to reduce GPR35 gene expression, or any other gene surveyed relative to control groups (Figure 3.22, N=11). Considering that these surgeries in Study 4 were completed only two weeks after the cohort from Study 3 and that the animals from Study 4 did not respond to any treatment throughout the study period, we suspect this lack of response to sh-RNA may be attributed to either a cohort

effect, as described in a previous study from our lab[63], or to the reduction of shRNA-induced suppression over time.

Figure 3.22: Effect of AAV-shGPR35 or scramble vector control on gene expression of receptors, pan-neuronal, and non-neuronal markers on VANs in male mice (Study 4). Effects of AAV-shGPR35 or scrambled shRNA vector (1e11 gc/mL per AAV type) on gene expression of GPR35, CCKAR, GLP1R, and pan-neuronal markers, SCN10A and TUBB3 in nodose ganglia following AAV microinjection. Two-way ANOVA, Tukey's multiple comparisons test, N=11/group. All samples normalized to unoperated control. Data are presented as ±SEM.

Study 4

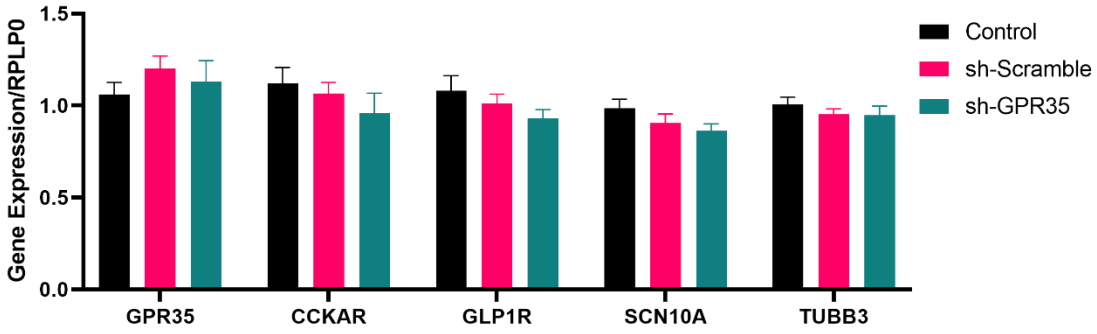

3.6: Discussion

Hyperphagia is an early adaptation to chronic consumption of calorie-dense foods[14,54,64,65]. Currently, the most successful treatment for increasing satiety and reducing body weight are gastric bypass and incretin mimetics[66–68], which act in part by activating gut hormone receptors located on VAN termini embedded within the gut wall, resulting in reduced gastric motility and appetite[69]. The development of other gut hormone mimetics is currently underway[70–72] (e.g., PYY) and there is some success in reducing food intake in nonhuman primates[73]. While expanding the pharmaceutical repertoire of incretin mimetics is an accelerating trend in the field, another approach to reducing energy intake is to increase sensitivity to endogenous satiety hormones.

GPR35 is a metabolite receptor for kynurenic acid, a tryptophan metabolite abundant in the gut lumen, and is highly expressed by VANs and co-expressed with CCK_AR in the mouse[20]. Recent evidence has demonstrated the potential role of GPR35 in regulating energy balance[41,74,75] However, the impact of GPR35 on CCK_AR signaling in VANs has not been studied. Therefore, we sought to better characterize the functional relationship of CCK_AR and GPR35 on VANs and its role in post-prandial metabolism and feeding behavior in mice.

The data show that endogenous and synthetic GPR35 agonists increase the sensitivity of VANs to CCK *in vitro.* In the context of these experiments, pERK/ERK served as a measure of VAN activation, as in our previous published work[45,46,76]. This data is further supported by unpublished *in vivo* work in our group demonstrating that chronic administration of a human milk oligosaccharide and GPR35 agonist, LNT, reduces diet-induced hyperphagia relative to HFD controls (Goodson and Vang). Data

from those studies show that nodose ganglia from mice supplemented with LNT have increased CCK-induced *fos* expression relative to nodose ganglia from CCK-treated, unsupplemented controls. Taken together, these data suggest that GPR35 agonists may act on GPR35 expressed on VANs to reduce HFD-induced hyperphagia. These data support previous findings demonstrating that administration of natural GPR35 agonists, such as KYNA, suppresses diet-induced hyperphagia and weight gain in mouse models of diet-induced obesity[41,42].

Alternately, we tested the hypothesis that inhibition of GPR35 reduces sensitivity to CCK using the GPR35 competitive antagonist, CID-2745687 (CID), and GPR35 knockdown. The data shows that inhibiting GPR35 reduces CCK-induced pERK/ERK in VANs *in vitro*. CID did not affect the response of VANs to our positive control, suggesting that GPR35 signaling impacts CCK_AR signaling on VANs.

We used a CCK-conjugated saporin to confirm that GPR35 is expressed on the same neurons as CCK_AR. This work verifies previous observations that GPR35 is co-expressed with CCK_AR on unmyelinated, $Na_V1.8$-positive VANs in male mice[20]. Microinjection of CCK-conjugated saporin resulted in a significant reduction in gene expression of GPR35 and CCK_AR in VANs. This class of unmyelinated VANs has also been shown to express receptors for gut hormones, such as GLP1R and NPY2R, and metabolite receptors, such as GPR41/FFAR3. Although CCK-conjugated saporin did not significantly reduce the gene expression of GLP1R and NPY2R, we must note that the variance is relatively high in these data, suggesting a technical issue. Considering the sample size is sufficiently high and the variance is sufficiently low, we may conclude that GPR41 may not be co-expressed on CCK-sensing VANs. This data also suggests

that the endogenous agonist for GPR41/FFAR3, bacteria-derived butyrate, may enhance satiety signaling[53,63,80] by an indirect method rather than direct stimulation of VANs.

Our *in vitro* data and our previous data showing that the GPR35 agonist zaprinast increased satiety signaling in mice led us to test the hypothesis that acute administration of the GPR35 antagonist (CID) would increase food intake relative to vehicle control. However, the GPR35 antagonist had no effect on food intake (data not shown). We suspect this may be due in part to the highly hydrophobic nature of CID; prior to administration, we observed precipitate clinging to the walls of the CID syringes compared to vehicle control (personal observations). This observation suggests that a sufficient concentration of CID may have not been administered to the animals to accurately determine the effect of systemic inhibition of GPR35 on feeding behavior. Therefore, knockdown approach to determine the effect of GPR35 signaling on feeding behavior in mice.

We used AAV-mediated shRNA knockdown of GPR35 to further investigate the role of GPR35 on VAN satiety signaling *in vivo.* In Study 2, relative to sham operated controls, GPR35 knockdown significantly increased cumulative food intake during the dark period. In Study 3, nodose microinjection of sh-GPR35 did not exacerbate diet-induced weight gain or hyperglycemia (data not shown) in male mice. However, in Study 3, relative to LF-fed unoperated controls, we observed that LF-fed sh-GPR35 mice had a higher rate of ingestion in the first 6 hours of the light and dark periods. Furthermore, the rate of ingestion of LF-fed sh-GPR35 mice was not significantly different from HF-fed sh-GPR35 mice during the light period. These data may suggest

that GPR35 knockdown in VANs may disrupt diurnal rhythms in vagal afferent activity, as previously reported in mouse models of diet-induced obesity[58–60].

In Studies 2-4, the effects of shGPR35 on knockdown of GPR35 on VANs and cumulative *ad libitum* feeding behavior varied significantly. In Studies 2-4, all mice were maintained on a chow diet for the first period of the study (3-6 weeks). In Study 2, relative to sham controls, shGPR35 significantly decreased gene expression of GPR35 in nodose ganglia and increased cumulative food intake within three weeks of nodose microinjection. In Study 3, the sample size of all groups was increased by 50-100% to improve the accuracy of our estimates and we found that sh-GPR35 significantly increased food intake relative to unoperated controls. However, this difference in cumulative food intake of sh-GPR35 mice was not significant from food intake of sh-Scramble mice, which suggests that nodose microinjection with AAV-shRNA likely causes unintended effects on feeding behavior. However, in Study 3, LF-fed shGPR35 mice ate significantly faster than unoperated controls in the early phases of the light period, suggesting that GPR35 knockdown on VANs may change meal patterns but may not be sufficient to significantly increase cumulative food intake. In Study 4, sh-GPR35 had no significant effect on cumulative food intake relative to controls.

Studies have shown that GPR35 inhibition may disrupts metabolism and energy homeostasis[41,77–79]. Previous work using short-interfering RNA (siRNA) demonstrates that GPR35 inhibition exacerbates HFD-induced accumulation of lipids within hepatocytes[77,78]. These studies are supported by other work utilizing a global knockout mouse model, which shows that GPR35 knockout increases weight gain of male mice on a normal chow diet[41]. To our knowledge, our studies are the first to use shGPR35 *in*

vivo to evaluate the role of GPR35 in satiety signaling in mice. Although nodose microinjection of sh-GPR35 did not reduce satiety evoked by exogenous CCK, it did impair endogenous CCK-induced satiety. The differences in the outcomes among Studies 2-4 may indicate an unexpected technical limitation of this viral vector. Considering sh-GPR35 significantly reduced GPR35 expression in VANs in Study 2 (3 weeks post-surgery) and sh-GPR35 microinjection diminished hyperphagia and gastric emptying induced by administration of a competitive CCK_AR blocker in Study 3 (6-7 weeks post-surgery), these data may suggest that sh-GPR35 induced suppression of GPR35 gene expression is time-limited.

In Study 4, we were unable to replicate any of our previous observations seen in Studies 2 and 3, including GPR35 knockdown in VANs and impairment of CCKAR blockade. In addition, the unoperated control mice failed to exhibit devazepide-induced hyperphagia. Furthermore, Studies 3 and 4 were executed within two weeks of each other. These data highlight important technical limitations of using a knockdown approach in studying the functional relationship of GPR35 and CCKAR on peripheral satiety signaling in vivo. When these studies were conducted, no GPR35-flox mouse or VAN-specific GPR35 knockout mouse had been developed. Taken together, these data suggest that GPR35 on vagal sensory neurons may play an important role in peripheral sensing of CCK and satiety signaling.

Notable Observations to Inform Exclusion of Outliers

We observed unexpected changes in animals' feeding behaviors during Studies 2 and 3 following cage changes and housing in the BioDAQ. Cage changes occurred every two weeks. Following cage change on day 14 (Figure 3.10A), there was a sharp increase in food intake across all groups, although this difference did not reach statistical significance. We suspect this increase in energy intake was due to an increase in energy expenditure (i.e., nest building observed) and stress. Food intake returned to baseline approximately 3 days after the cage change. This abrupt change in mouse feeding behavior was taken into consideration when planning feeding behavior studies.

3.7: Conclusion

This work demonstrates that GPR35 agonists increase the sensitivity of VANs to CCK and that GPR35 inhibition impairs normal CCK_AR signaling on VANs. Taken together, these data demonstrate a functional role for GPR35 in the peripheral sensing of endogenous CCK and reveal a potential peripheral target for increasing sensitivity to CCK to reduce diet-induced hyperphagia. Considering the technical limitations of our GPR35 knockdown model, future work must include the development and characterization of VAN-specific GPR35-knockout cell systems and animals to determine the mechanism by which GPR35 influences CCK_AR signaling.

3.8: References

1. Bai, L. *et al.* Genetic Identification of Vagal Sensory Neurons That Control Feeding. *Cell* **179**, 1129-1143.e23 (2019).
2. Berthoud, H. R. & Neuhuber, W. L. Functional and chemical anatomy of the afferent vagal system. *Auton. Neurosci. Basic Clin.* **85**, 1–17 (2000).
3. Han, W. *et al.* A Neural Circuit for Gut-Induced Reward. *Cell* 1–14 (2018) doi:10.1016/j.cell.2018.08.049.
4. Wang, Y. B., de Lartigue, G. & Page, A. J. Dissecting the Role of Subtypes of Gastrointestinal Vagal Afferents. *Front. Physiol.* **11**, (2020).
5. Grabauskas, G. & Owyang, C. Plasticity of vagal afferent signaling in the gut. *Medicina (Mex.)* (2017).
6. Loper, H. *et al.* Both high fat and high carbohydrate diets impair vagus nerve signaling of satiety. *Sci. Rep.* **11**, 10394 (2021).
7. De Lartigue, G., Barbier, C., Serre, L. & Raybould, H. E. Vagal afferent neurons in high fat diet-induced obesity; intestinal microflora, gut inflammation and cholecystokinin. *Physiol. Behav.* **105**, 100–5 (2011).
8. De Lartigue, G., Barbier De La Serre, C., Espero, E., Lee, J. & Raybould, H. E. Diet-induced obesity leads to the development of leptin resistance in vagal afferent neurons. *Am J Physiol Endocrinol Metab* **301**, 187–195 (2011).
9. Little, T. J., Horowitz, M. & Feinle-Bisset, C. Modulation by high-fat diets of gastrointestinal function and hormones associated with the regulation of energy intake: Implications for the pathophysiology of obesity. *Am. J. Clin. Nutr.* **86**, 531–541 (2007).
10. Covasa, M. & Ritter, R. C. Adaptation to high-fat diet reduces inhibition of gastric

emptying by CCK and intestinal oleate. *Am J Physiol Regul. Integr. Comp Physiol* **278**, 166–170 (2000).

11. Covasa, M., Grahn, J. & Ritter, R. C. High fat maintenance diet attenuates hindbrain neuronal response to CCK. *Regul. Pept.* **86**, 83–88 (2000).
12. de La Serre, C. B. *et al.* Propensity to high-fat diet-induced obesity in rats is associated with changes in the gut microbiota and gut inflammation. *AJP Gastrointest. Liver Physiol.* **299**, G440–G448 (2010).
13. Madden, C. J. & Morrison, S. F. A high-fat diet impairs cooling-evoked brown adipose tissue activation via a vagal afferent mechanism. *Am. J. Physiol. - Endocrinol. Metab.* **311**, E287–E292 (2016).
14. McDougle, M. *et al.* Intact vagal gut-brain signalling prevents hyperphagia and excessive weight gain in response to high-fat high-sugar diet. *Acta Physiol.* **00**, (2020).
15. Lee, S. *et al.* 2'-Fucosyllactose Supplementation Improves Gut-Brain Signaling and Diet-Induced Obese Phenotype and Changes the Gut Microbiota in High Fat-Fed Mice. *Nutrients* **12**, (2020).
16. Frost, G. *et al.* The short-chain fatty acid acetate reduces appetite via a central homeostatic mechanism. *Nat. Commun.* **5**, 1–11 (2014).
17. Del Prato, S., Gallwitz, B., Holst, J. J. & Meier, J. J. The incretin/glucagon system as a target for pharmacotherapy of obesity. *Obes. Rev.* **23**, e13372 (2022).
18. Berthoud, H. R. & Neuhuber, W. L. Vagal mechanisms as neuromodulatory targets for the treatment of metabolic disease. *Ann. N. Y. Acad. Sci.* **1454**, 42–55 (2019).
19. Gautron, L. The Phantom Satiation Hypothesis of Bariatric Surgery. *Front. Neurosci.*

15, 22 (2021).

20. Egerod, K. L. *et al.* Profiling of G protein-coupled receptors in vagal afferents reveals novel gut-to-brain sensing mechanisms. *Mol. Metab.* **12**, 62–75 (2018).
21. Lund, M. L. *et al.* Enterochromaffin 5-HT cells – A major target for GLP-1 and gut microbial metabolites. *Mol. Metab.* **11**, 70–83 (2018).
22. Kupari, J., Hä Ring, M., Agirre, E., Alo Castelo-Branco, G. & Ernfors, P. An Atlas of Vagal Sensory Neurons and Their Molecular Specialization Cell Reports Resource An Atlas of Vagal Sensory Neurons and Their Molecular Specialization. *CellReports* **27**, 2508-2523.e4 (2019).
23. Goswami, C., Iwasaki, Y. & Yada, T. Short-chain fatty acids suppress food intake by activating vagal afferent neurons. *J. Nutr. Biochem.* **57**, 130–135 (2018).
24. Cook, T. M. *et al.* Vagal neuron expression of the microbiota-derived metabolite receptor, free fatty acid receptor (FFAR3), is necessary for normal feeding behavior. *Mol. Metab.* **54**, 101350 (2021).
25. Akbarali, H. I. *et al.* The Gut Microbiota, Kynurenine Pathway, and Immune System Interaction in the Development of Brain Cancer. (2020) doi:10.3389/fcell.2020.562812.
26. Foata, F., Sprenger, N., Rochat, F. & Damak, S. Activation of the G-protein coupled receptor GPR35 by human milk oligosaccharides through different pathways. *Sci. Rep.* **10**, 1–9 (2020).
27. Boets, E. *et al.* Systemic availability and metabolism of colonic-derived short-chain fatty acids in healthy subjects: a stable isotope study. *J. Physiol.* **595**, 541–555 (2017).

28. Blaak, E. E. *et al.* Short chain fatty acids in human gut and metabolic health. *Benef. Microbes* **11**, 411–455 (2020).
29. Kuc, D., Zgrajka, W., Parada-Turska, J., Urbanik-Sypniewska, T. & Turski, W. A. Micromolar concentration of kynurenic acid in rat small intestine. *Amino Acids* **35**, 503–505 (2008).
30. Liu, B. *et al.* Characterizing the influence of gut microbiota on host tryptophan metabolism with germ-free pigs. *Anim. Nutr.* **11**, 190–200 (2022).
31. Cheng, D. *et al.* Tiansi Liquid modulates gut microbiota composition and tryptophan–kynurenine metabolism in rats with hydrocortisone-induced depression. *Molecules* **23**, (2018).
32. Dehhaghi, M., Kazemi Shariat Panahi, H. & Guillemin, G. Microorganisms, Tryptophan Metabolism, and Kynurenine Pathway: A Complex Interconnected Loop Influencing Human Health Status. *Int. J. Tryptophan Res.* **12**, 1–10 (2019).
33. Daly, D. M., Park, S. J., Valinsky, W. C. & Beyak, M. J. Impaired intestinal afferent nerve satiety signalling and vagal afferent excitability in diet induced obesity in the mouse. *J. Physiol.* **589**, 2857–2870 (2011).
34. Cheng, D. *et al.* In Silico Prediction of the Anti-Depression Mechanism of a Herbal Formula (Tiansi Liquid) Containing Morinda officinalis and Cuscuta chinensis. *Mol. J. Synth. Chem. Nat. Prod. Chem.* **22**, 1614 (2017).
35. Bernard, A. *et al.* The Tryptophan/Kynurenine Pathway: A Novel Cross-Talk between Nutritional Obesity, Bariatric Surgery and Taste of Fat. *Nutrients* **13**, 1366 (2021).
36. Favennec, M. *et al.* The kynurenine pathway is activated in human obesity and

shifted toward kynurenine monooxygenase activation. *Obesity* **23**, 2066–2074 (2015).

37. Wang, D. *et al. GPR35-mediated Kynurenic Acid Sensing Acts as a Defender Against Gut Microbiota Disorder in Ulcerative Colitis*. https://www.researchsquare.com/article/rs-2162768/v1 (2022) doi:10.21203/rs.3.rs-2162768/v1.
38. Fang, H. *et al.* Effects of High-Fat Diet on the Gut Microbiota of Renalase Gene Knockout Mice. *Obesities* **2**, 303–316 (2022).
39. Murphy, E. A., Velazquez, K. T. & Herbert, K. M. Influence of High-Fat-Diet on Gut Microbiota: A Driving Force for Chronic Disease Risk. *Curr. Opin. Clin. Nutr. Metab. Care* **18**, 515–520 (2015).
40. Turnbaugh, P. J. *et al.* An obesity-associated gut microbiome with increased capacity for energy harvest. doi:10.1038/nature05414.
41. Agudelo, L. Z. *et al.* Kynurenic Acid and Gpr35 Regulate Adipose Tissue Energy Homeostasis and Inflammation. *Cell Metab.* **27**, 378-392.e5 (2018).
42. Li, J. *et al.* The Beneficial Effects of Edible Kynurenic Acid from Marine Horseshoe Crab (Tachypleus tridentatus) on Obesity, Hyperlipidemia, and Gut Microbiota in High-Fat Diet-Fed Mice. *Oxid. Med. Cell. Longev.* **2021**, (2021).
43. Roberts, A. *et al.* Modulation of vagal afferent signalling by the amino acid metabolite sensor GPR35. in *Endocrine Abstracts* vol. 65 (Bioscientifica, 2019).
44. Diepenbroek, C. *et al.* Validation and characterization of a novel method for selective vagal deafferentation of the gut. *Am J Physiol Gastrointest Liver Physiol* **313**, 342–352 (2017).

45. de La Serre, C. B., de Lartigue, G. & Raybould, H. E. Chronic exposure to Low dose bacterial lipopolysaccharide inhibits leptin signaling in vagal afferent neurons. *Physiol. Behav.* **139**, 188–194 (2015).
46. de Lartigue, G. *et al.* EGR1 Is a target for cooperative interactions between cholecystokinin and leptin, and inhibition by ghrelin, in vagal afferent neurons. *Endocrinology* **151**, 3589–99 (2010).
47. Livak, K. J. & Schmittgen, T. D. Analysis of Relative Gene Expression Data Using Real-Time Quantitative PCR and the 2−ΔΔCT Method. *Methods* **25**, 402–408 (2001).
48. Fan, X. *et al.* High-Fat Diet Alters the Expression of Reference Genes in Male Mice. *Front. Nutr.* **7**, (2020).
49. Waise, T. M. Z. *et al.* One-day high-fat diet induces inflammation in the nodose ganglion and hypothalamus of mice. *Biochem. Biophys. Res. Commun.* **464**, 1157–1162 (2015).
50. Kim, J. S. *et al.* Gut microbiota composition modulates inflammation and structure of the vagal afferent pathway. *Physiol. Behav.* **225**, 113082 (2020).
51. Clements, J. A., Heading, R. C., Nimmo, W. S. & Prescott, L. F. Kinetics of acetaminophen absorption and gastric emptying in man. *Clin. Pharmacol. Ther.* **24**, 420–431 (1978).
52. Berg, J. K., Kim, E. H., Li, B., Joelsson, B. & Youssef, N. N. A randomized, double-blind, placebo-controlled, multiple-dose, parallel-group clinical trial to assess the effects of teduglutide on gastric emptying of liquids in healthy subjects. *BMC Gastroenterol.* **14**, 25 (2014).

53. Li, Z. *et al.* Butyrate reduces appetite and activates brown adipose tissue via the gut-brain neural circuit. *Gut* **67**, 1269–1279 (2018).
54. de Lartigue, G., Ronveaux, C. C. & Raybould, H. E. Deletion of leptin signaling in vagal afferent neurons results in hyperphagia and obesity. *Mol. Metab.* **3**, 595–607 (2014).
55. Serlin, H. K. & Fox, E. A. Abdominal vagotomy reveals majority of small intestinal mucosal afferents labeled in nav1.8cre-rosa26tdTomato mice are vagal in origin. *J. Comp. Neurol.* **528**, 816–839 (2020).
56. Udit, S. *et al.* Nav1.8 neurons are involved in limiting acute phase responses to dietary fat. *Mol. Metab.* **6**, 1081–1091 (2017).
57. Ballsmider, L. A. *et al.* Sleeve Gastrectomy and Roux-en-Y Gastric Bypass Alter the Gut-Brain Communication. **2015**, (2015).
58. Kentish, S. J., Vincent, A. D., Kennaway, D. J., Wittert, G. A. & Page, A. J. High-Fat Diet-Induced Obesity Ablates Gastric Vagal Afferent Circadian Rhythms. *J. Neurosci. Off. J. Soc. Neurosci.* **36**, 3199–3207 (2016).
59. Kentish, S. J., Frisby, C. L., Kennaway, D. J., Wittert, G. A. & Page, A. J. Circadian variation in gastric vagal afferent mechanosensitivity. *J. Neurosci. Off. J. Soc. Neurosci.* **33**, 19238–19242 (2013).
60. Page, A. J. Gastrointestinal vagal afferents and food intake: Relevance of circadian rhythms. *Nutrients* **13**, 1–17 (2021).
61. Simon, S. L. *et al.* Body mass index and variability in meal duration and association with rate of eating. *Front. Nutr.* **9**, (2022).
62. Dhurjad, P., Dhavaliker, C., Gupta, K. & Sonti, R. Exploring Drug Metabolism by the

Gut Microbiota: Modes of Metabolism and Experimental Approaches. *Drug Metab. Dispos.* **50**, 224–234 (2022).

63. Lee, S. *et al.* Metabolic Responses to Butyrate Supplementation in LF-and HF-Fed Mice Are Cohort-Dependent and Associated with Changes in Composition and Function of the Gut Microbiota. *Nutrients* **12**, 3524 (2020).
64. Souza, G. F. P. *et al.* Defective regulation of POMC precedes hypothalamic inflammation in diet-induced obesity. *Sci. Rep.* **6**, 1–9 (2016).
65. Andrich, D. E. *et al.* Altered Feeding Behaviors and Adiposity Precede Observable Weight Gain in Young Rats Submitted to a Short-Term High-Fat Diet. *J. Nutr. Metab.* **2018**, e1498150 (2018).
66. Iwasaki, Y. *et al.* GLP-1 release and vagal afferent activation mediate the beneficial metabolic and chronotherapeutic effects of D-allulose. *Nat. Commun.* **9**, 113 (2018).
67. Herman, G. A. *et al.* Effect of single oral doses of sitagliptin, a dipeptidyl peptidase-4 inhibitor, on incretin and plasma glucose levels after an oral glucose tolerance test in patients with type 2 diabetes. *J. Clin. Endocrinol. Metab.* **91**, 4612–4619 (2006).
68. Vilsbøll, T., Christensen, M., Junker, A. E., Knop, F. K. & Gluud, L. L. Effects of glucagon-like peptide-1 receptor agonists on weight loss: systematic review and meta-analyses of randomised controlled trials. *BMJ* **344**, d7771 (2012).
69. HEISE, T. *et al.* 338-OR: Tirzepatide Reduces Appetite, Energy Intake, and Fat Mass in People with T2D. *Diabetes* **71**, 338-OR (2022).
70. Lear, S. *et al.* Engineering of a Potent, Long-Acting NPY2R Agonist for Combination with a GLP-1R Agonist as a Multi-Hormonal Treatment for Obesity. *J. Med. Chem.* **63**, 9660–9671 (2020).

71. Milliken, B. T. *et al.* Design and Evaluation of Peptide Dual-Agonists of GLP-1 and NPY2 Receptors for Glucoregulation and Weight Loss with Mitigated Nausea and Emesis. *J. Med. Chem.* **64**, 1127–1138 (2021).
72. Østergaard, S., Paulsson, J. F., Kjærgaard Gerstenberg, M. & Wulff, B. S. The Design of a GLP-1/PYY Dual Acting Agonist. *Angew. Chem. Int. Ed.* **60**, 8268–8275 (2021).
73. Rangwala, S. M. *et al.* A Long-Acting PYY3–36 Analog Mediates Robust Anorectic Efficacy with Minimal Emesis in Nonhuman Primates. *Cell Metab.* **29**, 837-843.e5 (2019).
74. Lemieux, G. A. *et al.* Kynurenic Acid Is a Nutritional Cue that Enables Behavioral Plasticity. *Cell* **160**, 119–131 (2015).
75. Schlittler, M. *et al.* Endurance exercise increases skeletal muscle kynurenine aminotransferases and plasma kynurenic acid in humans. *Am. J. Physiol. - Cell Physiol.* **310**, C836–C840 (2016).
76. Ehrlich, A. M. *et al.* Indole-3-lactic acid associated with Bifidobacterium-dominated microbiota significantly decreases inflammation in intestinal epithelial cells. *BMC Microbiol.* (2020).
77. Nam, S.-Y., Park, S.-J. & Im, D.-S. Protective effect of lodoxamide on hepatic steatosis through GPR35. *Cell. Signal.* **53**, 190–200 (2019).
78. Kim, M.-J., Park, S.-J., Nam, S.-Y. & Im, D.-S. Lodoxamide Attenuates Hepatic Fibrosis in Mice: Involvement of GPR35. https://www.ncbi.nlm.nih.gov/pmc/articles/PMC6939691/pdf/bt-28-092.pdf.
79. Zhang, X., Wu, X. & Chen, S. GPR35 Deficiency Aggravates NAFLD via

Remodeling The Gut Microbiome. in vol. 71 A15–A17 (Gut, 2022).

80. Gao, Z. *et al.* Butyrate improves insulin sensitivity and increases energy expenditure in mice. *Diabetes* **58**, 1509–1517 (2009).

Chapter 4:

Characterizing Rat Nodose Ganglia Culture for the Development of a Microfluidic Model of the Gut-Brain Axis

4.1: Abstract

Vagal afferent neurons (VANs) represent the primary neurosensory branch of the gut-brain axis (GBA) and communicate chemosensory signals from the viscera to the central nervous system to regulate the autonomic control of digestion, metabolism, and feeding behavior. VANs are critical for detecting gut-derived hormones and have also been shown to mediate the therapeutic effects of dietary and microbial-derived metabolites. However, our understanding of the metabolites that can impact the function of VANs in situ is lacking. Although animal models enable us to measure acute changes in VAN activity, *in situ* models are invasive, have low throughput, and do not support longitudinal monitoring of VAN activity. Ultimately, confounding factors present in *in vivo* models prevents experiments from elucidating precise mechanisms of action. Recent advancements have been made in microfluidic models of organ systems to address these technical challenges. In this chapter, our aims were (1) to characterize the morphology and response of VANs to known activators, such as the enteroendocrine hormone, cholecystokinin, and (2) to optimize a method for culturing VANs in a novel microfluidic platform. The custom platform consists of two chambers with interconnecting microchannels for facilitating axonal connectivity between the two chambers. The data in this chapter demonstrate that this new platform is capable of supporting VANs that express functional CCK receptors, a sensor for a key peripheral satiety hormone. We have also demonstrated that serum source has a modest effect on VAN viability, which should be considered when culturing VANs. Additionally, we optimized the concentration of a mitotic inhibitor to prevent glia overgrowth in nodose ganglia cultures. These optimized cultures were introduced into a microfluidic device, which will be used in future studies to establish a gut-brain axis “on-a-chip”, capable of

screening physiologically relevant metabolites and characterizing effects on VANs using IHC and microelectrode arrays. These methods are likely compatible with co-culturing methods and future work will incorporate organoids into the neighboring chamber to provide a physiologically relevant interface for screening therapeutic compounds.

4.2: Introduction

Previously known as a branch of the "great abdominal brain"[1], the vagus nerve is the primary neural pathway of the microbiota-gut-brain axis (MGBA), which describes the bidirectional communication between the gut microbiota, viscera, and central nervous system. Cell bodies of the vagus are contained within the nodose ganglia, located at the base of the skull. The sensory terminals of the vagal afferent neurons (VANs) innervate the gastrointestinal tissue and relay chemosensory information in the form of enteroendocrine hormones to the CNS to regulate gastrointestinal physiology and modulate behavior. Earlier work in the field using *in vivo* models established foundational knowledge of the neural regulation of digestion and feeding behavior[2–4]. The development of primary cell culture methods has provided researchers with the necessary tools to control variables and elucidate the mechanisms of actions of these hormones on VANs[5–7]. Furthermore, the advancement and combination of sequencing technologies and knockout models have been used in recent studies and reveal that VANs express receptors on their sensory terminals for not only gut-derived hormones but also for dietary and microbial metabolites[8,9]. These studies demonstrate that the therapeutic effects of beneficial dietary and microbial end-products, such as tryptophan metabolites and short-chain fatty acids, are likely mediated by VANs[10–12]. In addition, our laboratory has shown that the microbial-derived, pro-inflammatory metabolite, lipopolysaccharide (LPS), can obstruct VAN satiety signaling and may contribute to diet-induced hyperphagia[13,14]. While these studies reveal important information about how the microbiota and host communicate with each other, these studies only demonstrate correlation and not causation and this may be addressed using a new model.

In vitro models are an important tool in establishing mechanisms of action partly because they enable researchers to define and manipulate the fundamental constituents of the system. The platforms for establishing these models often consist of a two-dimensional glass coverslip or polystyrene dish and a defined cell culture media, which contains the essential nutrients and vitamins to maintain cell viability. *In vitro* models have enabled researchers to isolate and study aspects of cellular physiology, such as calcium homeostasis, which help establish foundational knowledge for clinical applications[5,6,15,16]. However, these traditional *in vitro* models lack critical physiological features for modeling and studying interactions at an epithelial interface, such as cell-cell interactions and a third dimension. Transwell systems are another two-dimensional platform, which consists of a microporous membrane insert suspended over a standard cell culture well. Unlike traditional cell culture systems, transwell apparatuses can support paracrine and direct cell-to-cell interactions of two known cell types. However, none of the available systems are capable of modeling nor studying the complex interactions at the vagal afferent arm of the gut-brain axis.

Microfluidic *in vitro* models provide a new approach to modeling inter-organ interactions and investigating mechanisms of action *in situ*, which are not feasible with *in vivo* models. Most of these models use either biocompatible thermoplastic or polydimethylsiloxane (PDMS) to create a biomimetic interface that can support long-term two- or three-dimensional primary cell culture[17–21]. In addition, many of these platforms are comparable to common *in vitro* techniques, in that they are compatible with inverted microscopy and effluent can be monitored throughout the culture. Although this technology has emerged within the past 10 years, microfluidic models of the gut

and the microbiota-gut axis are in development and include short-term co-culturing of gut bacteria and intestinal epithelial cells[17,18]. Importantly, these models support longitudinal measurements and enable researchers to demonstrate causation. However, at the time of this article, no work has been published on a microfluidic model of the gut-brain axis using primary vagal afferent neurons.

The aims of this study were (1) to optimize a method to culture primary VANs within a custom microfluidic device and (2) to characterize the morphology, baseline activity, and viability of the primary cultures. To address these aims, we optimized an established model of the short-term culture of VANs[13,22] to maximize VAN retention. We measured resting intracellular calcium levels and also used CCK-conjugated saporin to confirm that the culture methods supported VANs of interest (i.e., CCK-sensing VANs). We also optimized the culture for long-term studies by limiting gliosis using a mitotic inhibitor, arabinose cytosine. Finally, we worked with our collaborators to optimize the design of the microfluidic platform to support the culture of VANs. Our collaborators have also developed microelectrode arrays to monitor the spontaneous and evoked activity of VANs over time, but this is not discussed in this thesis.

VANs innervate virtually every visceral organ and are a critical parasympathetic regulator of metabolism; a microfluidic platform for studying VANs would support our understanding of how they monitor and respond to biologically relevant metabolites. Since VANs to do physically project into the gastrointestinal lumen, this microfluidic device is an improvement on currently available platforms partly because it fluidically isolates VANs from co-culturing tissue[23]. This data demonstrates that primary VANs can be reliably cultured and maintained in this microfluidic platform, but we recognize that

this model is in the earliest stages of development. However, this microfluidic model could also be used to model interactions between VANs and other physiologically relevant tissues, such as pulmonary epithelium, cardiomyocytes, and lymphoid tissues, whose primary culture conditions have already been optimized. Understanding and applying the optimized practices to VAN primary culture may also support advancements in these adjacent fields.

4.3: Methods

Animals and Housing

All experiments were approved by the University of California Davis Institutional Animal Care and Use Committees. All animals were maintained at 25 °C under a 12-h:12-h light-dark cycle (light 7 AM to 7 PM) with ad libitum access to water and food. For nodose cultures, 4-8-week-old adult male Wistar rats (Envigo, Hayward, CA) were housed in pairs in a separate facility and were provided ad libitum access to water and chow (Teklad #2018, Envigo, Indianapolis; IN). Rats were chosen over mice to reduce the number of animals required to achieve statistical significance and experimental requirements for robustness and reproducibility.

Preparing Culture Chambers for Nodose Ganglia Primary Culture

Prior to nodose dissection, sterile working solutions of poly-D-lysine (Sigma-Aldrich P6407) were resuspended at 0.1 mg/mL in sterile cell culture grade water (Invitrogen, 10977015) in a Class II biosafety cabinet. Round coverslips (25 mm) (Fisher, 12-245-102) were placed in a cover slip rack and treated with a plasma cleaner (Harrick Plasma, ionized ambient air at 10 W) for 7 minutes. Coverslips were immediately transferred in a sterile container to a Class II biosafety cabinet and transferred to a 6-well tissue culture dish (Fisher, 140675)**.** The rims of sterile cloning cylinders (Sigma, CLS31668) were lightly coated with sterilized vacuum lubricant (Dow Corning, 1597418) and adhered to sterile coverslips using sterile forceps. Poly-D-lysine (100 µL, 0.1 mg/mL) was applied to the center of the cloning cylinders to stabilize the hydrophilicity of the plasma-treated coverslips and incubated for 30 minutes at room temperature. Finally, coverslips were coated with Matrigel (Corning, 354262; 150 µg/ml) by applying a working solution to the center of the cloning cylinders before beginning nodose ganglia dissection. The dead space between wells of the tissue culture plate was filled with sterile cell culture grade water (Invitrogen, 10977015) to prevent evaporation from VAN culture chambers.

Generation of Heat-Inactivated Rat Serum

Wistar rats were euthanized by carbon dioxide asphyxiation. The ventral surface of the animal was sterilized and the skin was transected directly beneath the xiphoid process to expose the heart. Approximately 5 mL of blood was collected via cardiac puncture and centrifuged at 1,500 x g for 15 minutes at 4 °C to separate serum from

whole blood and transferred to a Class II biosafety cabinet. Under sterile conditions, serum was collected and centrifuged for an additional 10 minutes at 20,000 x g at 4 °C to remove any remaining cell debris. The remaining 2 mL serum was distributed to 1.5 mL microcentrifuge tubes and heat-inactivated for 30 minutes at 56 °C in a heating block. Following heat inactivation, the serum was incubated in ice for 10 minutes to complete heat inactivation. The final serum was centrifuged for 10 minutes at 20,000 x g before sterile filtration using a 0.2 µm syringe filter.

Nodose Ganglia Dissection and Primary Cultures

Rat nodose ganglia were identified by following the vagus nerve to the jugular foramen and dissected under aseptic conditions. Nodose ganglia were collected into 1 mL sterile calcium-, magnesium-, and phenol red-free ice-cold Hanks Buffered Saline Solution (HBSS) (Gibco, 14175095). Nerve fibers were cut away and desheathed using sterile Dumont forceps and scalpel. The ganglia were pre-digested with 2 mg/ml collagenase type 4 (Worthington-Biochem, LS004188) and 2.4 mg/ml dispase II (Roche, 4942078001) for 5 minutes at 37 °C. Following pre-digestion, ganglia were incubated in 22 U/mL papain (Worthington-Biochem, LS003126) resuspended in a solution of HBSS, L-cysteine (Sigma, C6852; 0.4 mg/mL), 0.5 mM EDTA, and 1.5 mM $CaCl_2$ for 30 minutes at 37 °C in a 5 cm-diameter Petri dish. Dissociated ganglia were transferred to a 15 mL centrifuge tube and centrifuged at 400 x g for 3 minutes before final digestion in collagenase (1 mg/mL) and dispase (1.2 mg/ml) for 30 minutes at 37 °C in a 5 cm-diameter Petri dish. Ganglia were mechanically dissociated before final centrifugation at 500 x g for 5 minutes. Nodose cultures were resuspended in 300 µL media consisting of DMEM base media (Sigma-Aldrich, D5030) supplemented with 0.5 mM L-glutamine,

10mM HEPES, 2.2g/L sodium bicarbonate, 0.227 mM sodium pyruvate, 5 mM glucose, and 10% heat-inactivated rat serum (method included below) or fetal bovine serum (FBS; HyClone, SH30071.03, Lot AF29485596, Bottle #01574). 50 µL DMEM base media with 10% serum was added to each cloning cylinder prior to cell seeding. 50 µL of the culture suspension was added into each pre-filled cloning cycling onto plasma-treated, Matrigel-coated coverslips within a 6-well tissue culture dish. Nodose cultures were maintained at 37 °C, 5% CO2 for 24-72 hours prior to experiments. Each nodose culture consisted of pooled nodose ganglia (left and right) collected from two rats.

Viability Assessment of Rat VANs *In Vitro*

To determine the effect of serum source on culture viability, nodose ganglia cultures were maintained in VAN media supplemented with either 10% heat-inactivated rat serum or 10% FBS (HyClone, SH30071.03, Lot AF29485596, Bottle #01574) at 37 °C, 5% CO_2 for 24 hours prior to assessing cell viability. The working solution of the fluorescent viability stain was comprised of calcein acetoxymethyl (AM) (2 µM; Sigma, #I7783) and ethidium homodimer-1 (4 µM; Sigma, #E1903) in DMEM base media without serum. The working solution of the viability stain was applied to cells (100 µL) for 30 minutes in a cell culture incubator at 37 °C, 5% CO_2. After incubation, the working solution was carefully aspirated and cultures were washed with phenol red-free HBSS (Gibco, 14025092). Cultures were imaged on a confocal microscope (Leica TCS SP8 STED microscope) using a 40X/1.1 water lens.

Limiting Mitotic Proliferation in Nodose Ganglia Cultures with Cytosine β-D-Arabinofuranoside

Nodose cultures were treated with cytosine β-D-arabinofuranoside (Ara-C; Sigma-Aldrich, C1768) (0-10 μM) 24 hours after plating to determine the minimum effective concentration to reduce glia proliferation. Working solutions of treatments were resuspended in 0.9% normal saline. Cultures were maintained at 37 °C, 5% CO2 in control media with 1% penicillin-streptomycin (PenStrep; ThermoFisher, 15140122), 10% FBS (HyClone, SH30071.03, Lot AF29485596, Bottle #01574), and Ara-C or vehicle for 72 hours. Cultures were washed with cold 1X PBS before fixation in 4% paraformaldehyde for 20 minutes and prepared for immunocytochemical probing of β-tubulin III (neuronal marker), Iba-1 (glial marker), and DAPI. Although Iba-1 (ionized calcium-binding adapter molecule 1) is considered to be a marker of activated macrophages, satellite glial cells within the nodose ganglia have also been shown to express Iba-1[24]. In the immunofluorescent studies conducted in these chapters and in the previous work in our lab[25], Iba-1 is the most robust marker of satellite glia within mouse and rat nodose ganglia.

Immunocytochemistry

After fixation, cultures were washed in 1X Tris-buffered saline with 0.01% Tween-20 (TBST) and blocked in blocking buffer (10% goat serum (Jackson ImmunoResearch Laboratories, 005-000-121) in 1X TBST) for 1 hour at room temperature. Primary antibody solutions were resuspended in blocking buffer according to the following dilutions: mouse anti-β-tubulin III (1:500, BioLegend, 801202; or Thermo rabbit anti-Iba-1 (1:500; Wako, 019-19741). After blocking, cultures were incubated overnight at 4 °C in primary antibody solutions. The following day, coverslips were washed three times in 1X TBST for 5 mins/wash. Secondary antibody solution consisted of Alexa Fluor 647-conjugated goat anti-rabbit antibody (1:500) (Invitrogen, A21244, Lot 1834794) and Alexa Fluor 488-conjugated goat anti-mouse (Invitrogen, 11001, Lot 477591) resuspended in 10% normal goat serum in 1X TBST for 1 hour at room temperature. Nuclei were stained with DAPI (1 µg/mL in 1X TBS) (Invitrogen, D1306) for 2 minutes at room temperature. Coverslips were treated with ProLong Diamond Antifade mountant (Invitrogen, P36970) before mounting onto SuperFrost Plus™ microscope slides (Fisher, #12-550-15). Slides were maintained at room temperature in a slide carrier for 24-72 hours before imaging to allow the mountant to cure. Mountant was not used for imaging VANs in aqueous solutions (e.g.,. fluorescent viability stain and microfluidic devices). Confocal images were acquired with a Leica TCS SP8 STED microscope using a 40X/1.3 oil lens for coverslips cured with mountant and a 40X/1.1 water lens for imaging VANs in aqueous solutions.

Calcium Imaging of Nodose Cultures

After cell seeding, cultures were maintained in VAN media with 10% serum at 37º C in 5% CO_2 for 24-72 hours prior to experiments. On the day of the experiment, nodose cultures were washed with 100 µL VAN media without serum. VAN cultures were loaded for 45 minutes at 37º C with the non-ratiometric dye Fluro-4 acetoxy-methyl ester (AM) (10 µM) (Invitrogen, F14201) in a solution of DMSO (0.5%) and Pluronic-F127 (0.002%). At the end of the incubation, cells were washed with phenol red-free HBSS (Gibco, 14025092). A single coverslip was mounted onto a closed imaging chamber at a time (Warner Instruments, RC-21BR). For all calcium imaging experiments, Fluo-4-loaded cultures were excited at a wavelength of 488 nm, and emitted light was detected at 525 nm. Vagal afferent neurons were identified based on their globe-like appearance (Figure 4.2A) and an observable increase in fluorescence upon a brief stimulation with 45 mM KCl on a test sample followed by a 15-minute washout before measuring Ca^{2+}_i flux to quickly evaluate cell excitability. Cells that did not satisfy these criteria were rejected from the experiment. Each test was concluded with a final depolarization using 60 mM KCl. This procedure was repeated for each condition, regardless of the microscope. Background fluorescence was subtracted from all measurements to account for any differences in autofluorescence between samples as shown in Figure 4.2B. Acquired images were analyzed using Fiji image processing software[26].

Measuring Baseline Intracellular Calcium

Baseline levels of intracellular calcium ($[Ca^{2+}_i]$) of VANs were determined in the Advanced Imaging Facility (HSDAIF) using the Leica TCS SP8 STED 3X confocal microscope with a 40x/1.1 water HC PL APO CS2 objective. After cell seeding, cultures were maintained in VAN media with 10% heat-inactivated rat serum at 37º C in 5% CO_2 for 24 prior to calcium imaging. After cells were loaded with Fluo-4 AM and washed with phenol red-free HBSS, coverslips were loaded into the imaging chamber as aforementioned. Solutions were carefully exchanged via micropipette. VANs in phenol red-free HBSS are referred to as “baseline”. A calcium calibration kit (C3008MP, Invitrogen) was used to determine the baseline levels of intracellular calcium (0-10 mM). All calibration solutions contained ionomycin (1 µM in 0.1% DMSO; Sigma, I9657), an ionophore used to manipulate transmembrane calcium flux. Baseline measurements did not contain ionomycin and were followed by treatment with 45 mM KCl to confirm excitability. Fluorescent images were acquired at a frame rate of 1 Hz for 60 seconds for each calcium concentration tested.

Measuring CCK-Induced Intracellular Calcium Flux in VANs

Nodose ganglia cultures for measuring CCK-induced Ca^{2+}_i were maintained in media supplemented with 10% FBS (HyClone, SH30071.03, Lot AF29485596, Bottle #01574) for 72 hours before experiments. For these experiments, a Nikon High Content spinning disk confocal microscope with a 40X objective was used to measure CCK-induced fluctuations in intracellular calcium (Ca^{2+}_i) (frame rate of 2 Hz for 60 seconds). Cloning cylinders were removed prior to mounting the enclosed imaging chamber onto the microscope stage. For these experiments, the chamber was filled with ambient control solution (140 mM NaCl, 3 mM KCl, 2.4 mM $CaCl_2$, 1.3 mM $MgCl_2$, 10 mM HEPES, and 10 mM glucose; pH of 7.4) and set to acclimate for 15 minutes under perfusion (1 mL/min) before calcium imaging[27,28]. Timelapse imaging began before perfusion to acquire baseline fluorescence prior to treatment (F_{min}). Changes in intracellular fluorescence intensity were expressed as $\Delta F/F_{max}$, where ΔF represents the difference between maximum fluorescence intensity per stimulus and baseline fluorescence (F_{min}), and F_{max} represents the maximum fluorescence intensity evoked by final depolarization with 60 mM KCl, normalized to baseline fluorescence.

These initial calcium imaging experiments were conducted early in the process of culture optimization (early 2019; before COVID-19) and were cultured in 10% FBS rather than rat serum. Results from nodose ganglia cultures using 10% FBS versus rat serum were considered separate conditions and the results were not pooled together.

CCK-Saporin Elimination of Rat VANs *In Vitro*

Nodose ganglia cultures were maintained at 37 °C, 5% CO_2 in control media including 1% penicillin-streptomycin (ThermoFisher, 15140122) and 10% FBS (Hyclone, SH30071.03, Lot AF2948556, Bottle #01574) for 72 hours. Nodose cultures were treated with CCK-conjugated saporin (Advanced Targeting Systems, KIT-31; 15-150 ng/µL) or unconjugated saporin control (150 ng/µL) resuspended in control media for 24 hours at 37 °C, 5% CO_2. Conditions of CCK saporin were based on the previous literature[22,29]. Cultures were washed with cold 1X PBS before fixation in 4% paraformaldehyde for 20 minutes and prepared for immunocytochemical probing of β-tubulin III (neuronal marker), Iba-1 (glial marker), and DAPI.

Soft Lithography, Microfluidic Device Assembly, and Design Optimization

Master molds were created by our collaborators in the Department of Electrical and Computer Engineering at the University of California, Davis (Laboratory of Professor Erkin Şeker). Details of device design and assembly have been detailed in previous publications by our collaborators[23,30]. We have included details of fabrication that are most relevant to the work discussed in this thesis chapter. In brief, master molds were fabricated by patterning two layers of SU-8 (Kayaku Advanced Materials) on a silicon wafer. The first layer contained the interconnecting microchannels and the second layer contained the cell culture chambers. Master molds were hard-baked for 1 hour at 250 °C. The master molds were placed in a Petri dish (100 mm) and premixed (1 : 10 w/w curing agent to base) polydimethylsiloxane (PDMS; Sylgard 184, Dow Corning) was poured over the mold and degassed in a vacuum chamber to remove any bubbles. The PDMS was cured for 2.5 hours at 90 °C on a hotplate. The PDMS platforms were removed from the master mold and fluidic ports to access the cell culture chambers were opened using a 3 mm biopsy punch. The PDMS platforms were temporarily bonded to poly-L-lysine (PLL) coated glass coverslips (0.5 mg/mL PLL (Sigma) resuspended in B-buffer (3.1 mg/mL boric acid and 4.75 mg/mL borax (Sigma)) for 4 hours at 37 °C and 5% CO_2. The coverslips were then washed with sterile deionized water and dried under ambient conditions. To produce reversibly bonded devices, the PDMS platforms were sterilized with 70% EtOH followed by treatment in an air plasma cleaner at 10 W for 2 min. These treatments prepare the surfaces of the glass and PDMS hydrophilic for bonding/sealing and also make the surfaces hydrophilic. Finally,

glass cloning cylinders (8 mm × 6 mm inner, Sigma) were fixed over each of the fluidic ports using sterile vacuum grease to form the final device.

The aforementioned procedure was used to generate all microfluidic devices used in this thesis chapter. All microfluidic device channels in all devices used were 10-25 µm wide. In the first prototype device, the length of interconnecting channels was between 500-1000 µm. The chambers were on either side of the channels and the chamber volumes were approximately 500 µL/chamber (Figure 4.6). The second prototype device featured concentric culture chambers (Figure 4.7) (150 µL/chamber) connected by 500-µm long, 15 µm-wide channels.

Seeding Primary Nodose Ganglia Cultures into Microfluidic Devices

Following nodose ganglia dissection, primary cultures were consistently resuspended in 300 µL VAN base media with 10% FBS. Before seeding, device chambers were coated with diluted Matrigel solution (150 µg/ml) as described in the previous section. After Matrigel-coating, solutions were aspirated and devices were filled with VAN media with 10% FBS and left to equilibrate in a cell culture incubator before seeding (37 °C, 5% CO_2).

For the first prototype device, VAN media was aspirated and replaced with 100 µL VAN media with 10% FBS immediately before seeding. The design changes in the second prototype device rendered this step unnecessary. For both devices, 100 µL of culture suspension was added in the VAN chamber (in the second prototype drive, this is noted as chamber “N” in Figure 4.7A). Cultures were left for seeded cells to adhere for 24 hours before media exchange. 24 hours after cell seeding, spent media was

aspirated and replaced with VAN media + 10% FBS + Ara-C (2 μM). Media was exchanged every 2 days and cultures were maintained for 5 days at 37 °C, 5% CO_2.

Statistical Analysis

Randomization and blinding were used in the experimental design for imaging analysis. Differences among groups were analyzed by one- or two-way ANOVA as indicated in figure legends. Multiple comparisons tests were made using Tukey's or Sidak's post hoc tests where appropriate. Differences between two groups were analyzed by unpaired t-tests. Data are presented as mean ± SEM unless indicated otherwise. *P*-values less than 0.05 were considered statistically significant.

4.4: Results

Basal Intracellular Calcium (Ca^{2+}_i) Levels in VANs *In Vitro*

A total of 26 VANs from two separate experiments satisfied the criteria described in the Methods section. VANs were identified based on their globe-like soma, as represented in Figure 4.1A. 24 hours after seeding, the basal Ca^{2+}_i levels in VANs acclimated in HBSS were 86.88 nM ±19.05 (Figure 4.1C, 95% CI [79.18, 94.57]; n=26), as measured by calibrated Fluo-4 AM fluorescence. These levels are also supported visually in Figure 4.1B, which shows a representative image of a VAN in "baseline" HBSS in between "0 nM Ca^{2+}" and "100 nM Ca^{2+}"; "baseline" fluorescence of the selected VAN is between the two concentrations. These intracellular levels of calcium are within the range of published data[27,31]**.** Glia were excluded from these measurements.

Figure 4.1: Baseline intracellular calcium concentrations (Ca^{2+}_i) in VAN cultures, calibrated using Fluo-4 AM. A) Representative brightfield image of VANs (indicated by black arrows) and glia (indicated by white arrows) within nodose ganglion cultures. Scales = 20 μm B) Representative fluorescent images of VANs (indicated by yellow circles) within nodose culture at 0 nM Ca^{2+}_i, baseline, and 100 nM Ca^{2+}_i. Green circles represent samples of background fluorescence. C) Quantitation of resting average Ca^{2+}_i in rat VAN cultures (n=26).

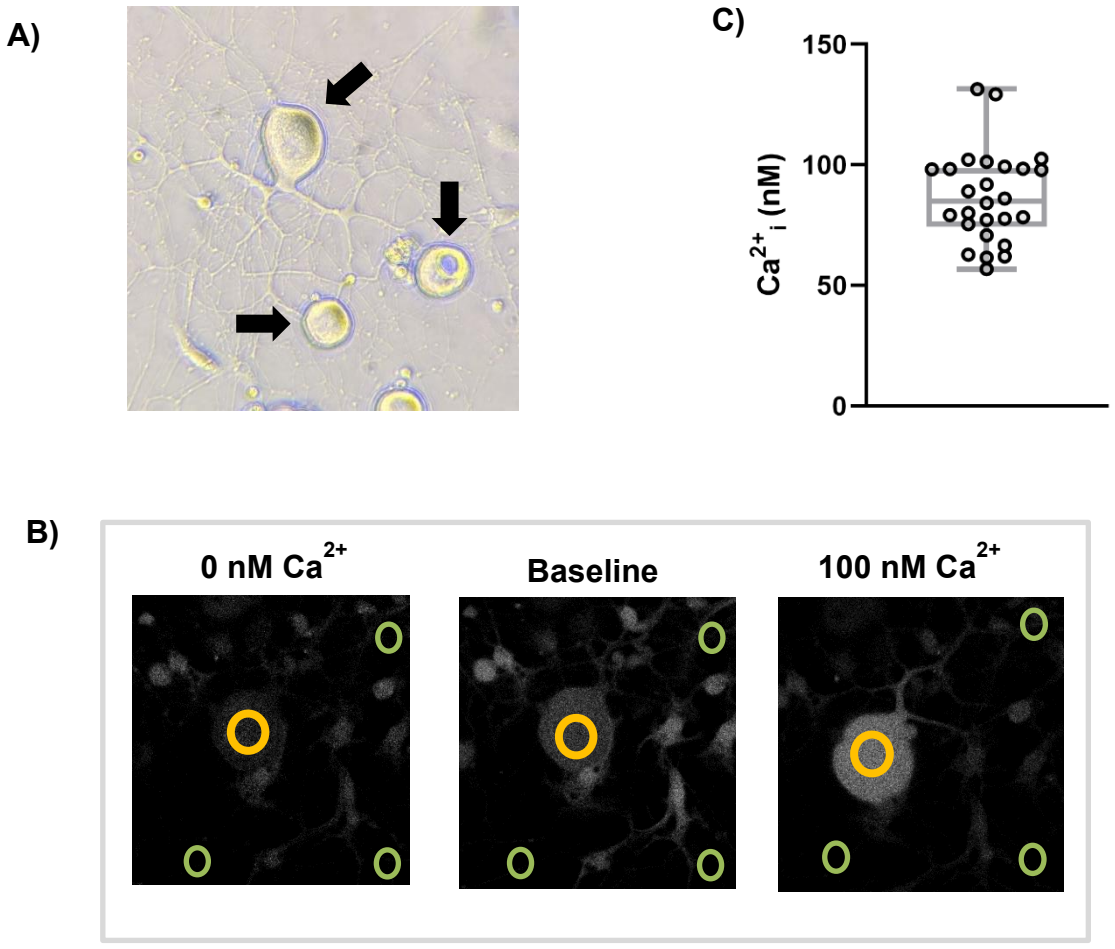

Dose-Dependent Effects of CCK-8S on Ca^{2+}_i in VANs *In Vitro*

CCK-8S (0.01-10 nM) increased Ca^{2+}_i in a concentration-dependent manner (Figure 4.2, R^2=0.8392; n=1-3/treatment), as measured by Fluo-4 AM fluorescence intensity normalized to maximum depolarization by 60 mM KCl. Across three experiments, only 6 cells in total satisfied the selection criteria for analysis (i.e., two separate events of KCl-induced depolarization bordering CCK-induced calcium flux). Glia were identified based on their spindle-like shape and were excluded from these measurements.

Figure 4.2: Dose response of CCK (0.1-10 nM) on intracellular fluorescence intensity in rat nodose ganglia cultures. Quantitation of CCK-induced flux in Fluo-4 AM fluorescence intensity in rat VANs relative to maximum depolarization with 60 mM KCl (ΔF/Fmax). n=1-3 per treatment.

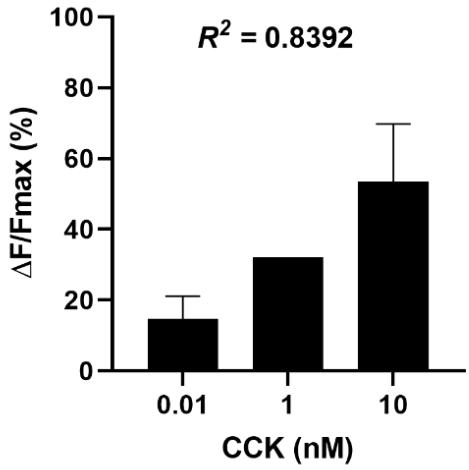

Effect of CCK-Conjugated Saporin on VAN Abundance *In Vitro*

Relative to unconjugated saporin (Blank-SAP), CCK-conjugated saporin significantly reduced the relative abundance of VANs within nodose ganglia cultures, as indicated by β-tubulin III protein expression (Figure 4.3, n=3/treatment, $p<0.05$). CCK-saporin significantly reduced the abundance of VANs at the same concentration as unconjugated saporin (150 ng/µL) and at concentrations ten times less than Blank-SAP (15 ng/µL), indicating that CCK-saporin is specific to VANs and that unconjugated saporin does not get incorporated into VANs, as others have noted[22]. There was no significant difference in the reduction of VANs between CCK-SAP treatments, suggesting that the effective concentration for ablating CCK receptor-expressing cells could be less than or equal to 15 ng/µL (Figure 4.3, n=3/treatment, $p>0.05$).

Figure 4.3: Effect of CCK-conjugated saporin on viability of rat VANs *in vitro,* as measured by abundance of β-tubulin III-positive cells after 24-hour treatment. Quantitation of VAN viability following 24-hour treatment with CCK-conjugated saporin relative to unconjugated control saporin, as measured by relative abundance of β-tubulin III-positive cells, a neuron-specific marker. One-way ANOVA with Tukey's multiple comparisons test (n=3/treatment, $p<0.005$). Different letters indicate significant differences among groups.

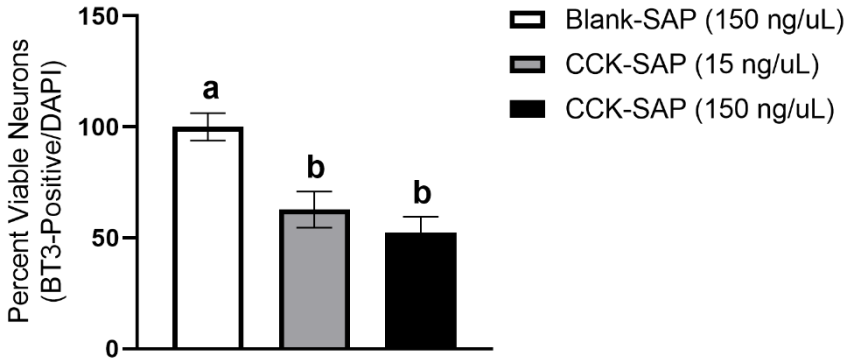

Effects of Serum Source on Nodose Ganglia Culture Viability *In Vitro*

Rat serum significantly increased the viability of nodose ganglia cultures, as measured by the relative percentage of cells stained with calcein-AM, relative to cells cultured in 10% FBS (Figure 4.4A, N=3, $p<0.0001$). Correspondingly, rat serum decreased the percentage of dead or dying cells relative to FBS (Figure 4.4B, N=3, $p<0.0001$). The relative density of viable cells (VANs and glia; cells/μm^2) retained after 24 hours *in vitro* did not differ significantly between treatments (Figure 4.4D, N=3, $p=0.585$).

Figure 4.4: Effect of serum source on viability of rat nodose ganglia (VAN) cultures. Representative images of VANs indicating viability of cultures after 24 hours *in vitro*, as measured by fluorescence of calcein-AM (CaAM, green; indicating viable cells) or ethidium homodimer-1 (Eth-D1, red; indicating dead/dying cells) when cultured in either 10% v/v heat-inactivated A) fetal bovine serum (FBS) or B) rat. Scales = 100 µm. Pie charts representing average percentage of live and dead cells per treatment are pictured beside representative images. Two-Way ANOVA with Sidak's multiple comparisons test (N=3 experiments.****p<0.0001).

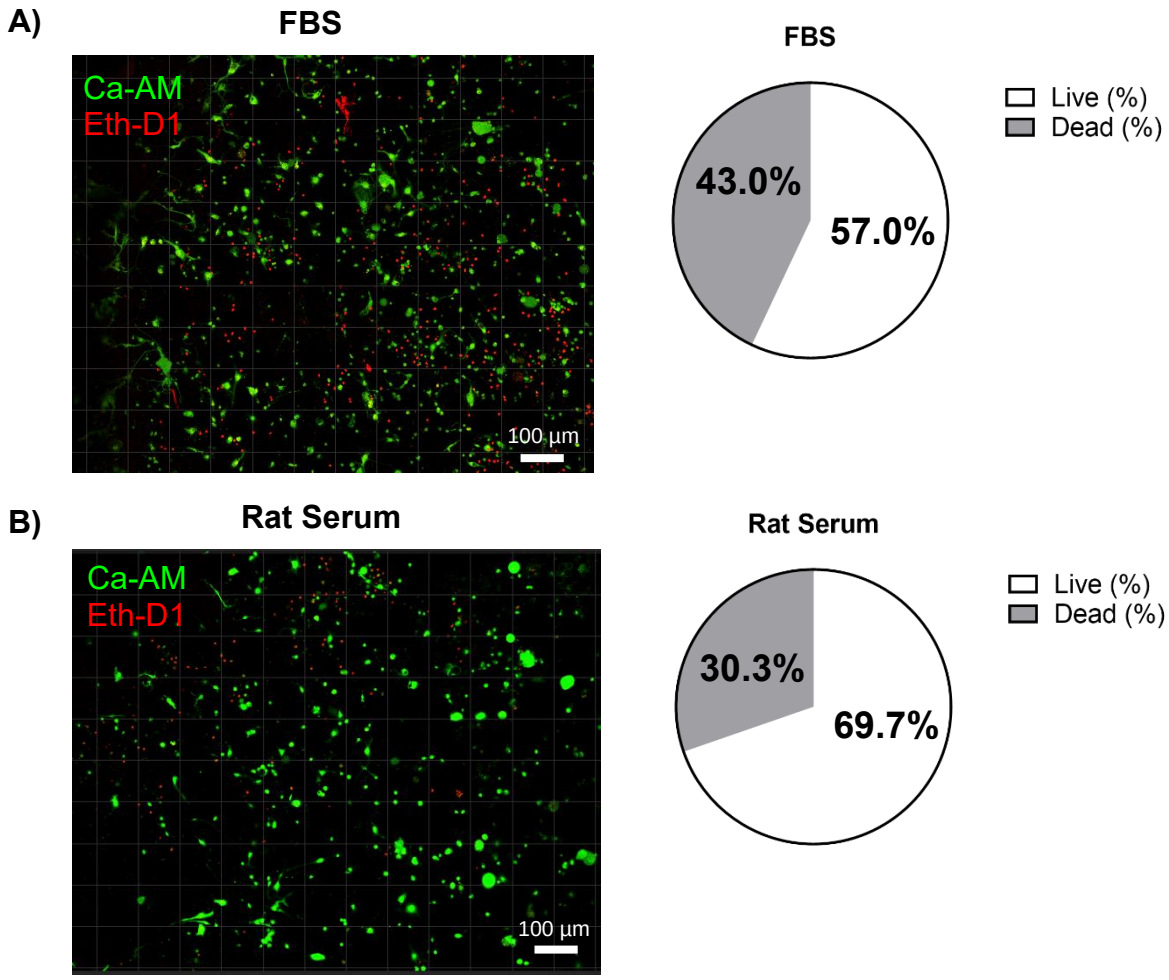

Figure 4.4: Effect of serum source on viability of rat nodose ganglia (VAN) cultures. C) Quantification of effect of serum of culture viability. Two-Way ANOVA with Sidak's multiple comparisons test (N=3 experiments.****p<0.0001).

D) Quantification of relative density of viable VANs 24 hours after seeding. Unpaired t-test (N=3 experiments).

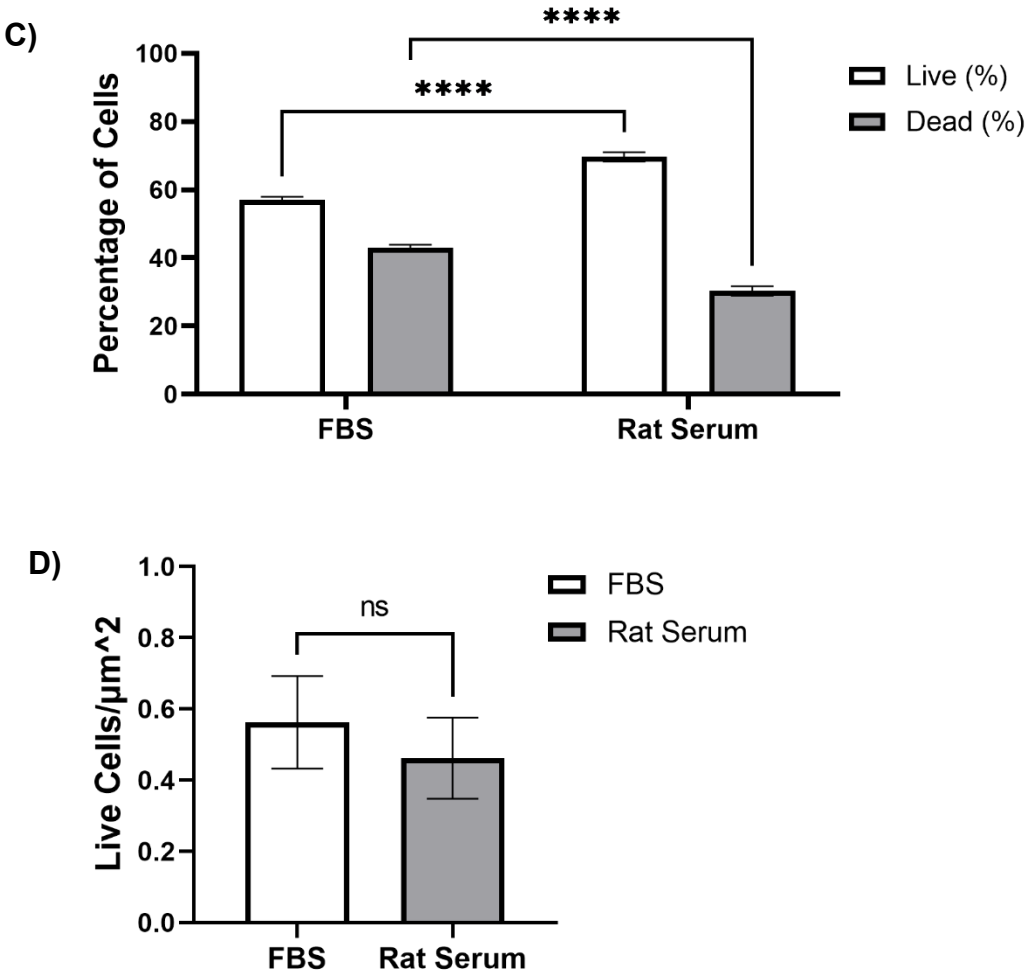

Effects of Cytosine β-D-Arabinofuranoside on Nodose Culture Proliferation *In Vitro*

24-hour treatment with cytosine β-D-Arabinofuranoside (AraC; 1-10 µM) significantly decreased cell proliferation relative to vehicle, as measured by relative cell density (Figure 4.5C, N=3, $P<0.05$). There was no statistically significant difference between mitotic inhibition by Ara-C 1 µM or 5 µM (Figure 4.5A). However, we did observe a slight decrease in B-tubulin III abundance Ara-C at 10 µM further reduced the relative cell density beyond that of lower concentrations.

Figure 4.5: Effect of arabinose cytosine (Ara-C) on cell proliferation in nodose ganglia cultures. A) Representative images of nodose ganglia cultures after 72 hours of treatment with Ara-C (0-10 μM). VANs stained with B-tubulin III (BT3, red), glia stained with Iba1 (red), and nuclei with DAPI (blue). Scales = 200 μm.

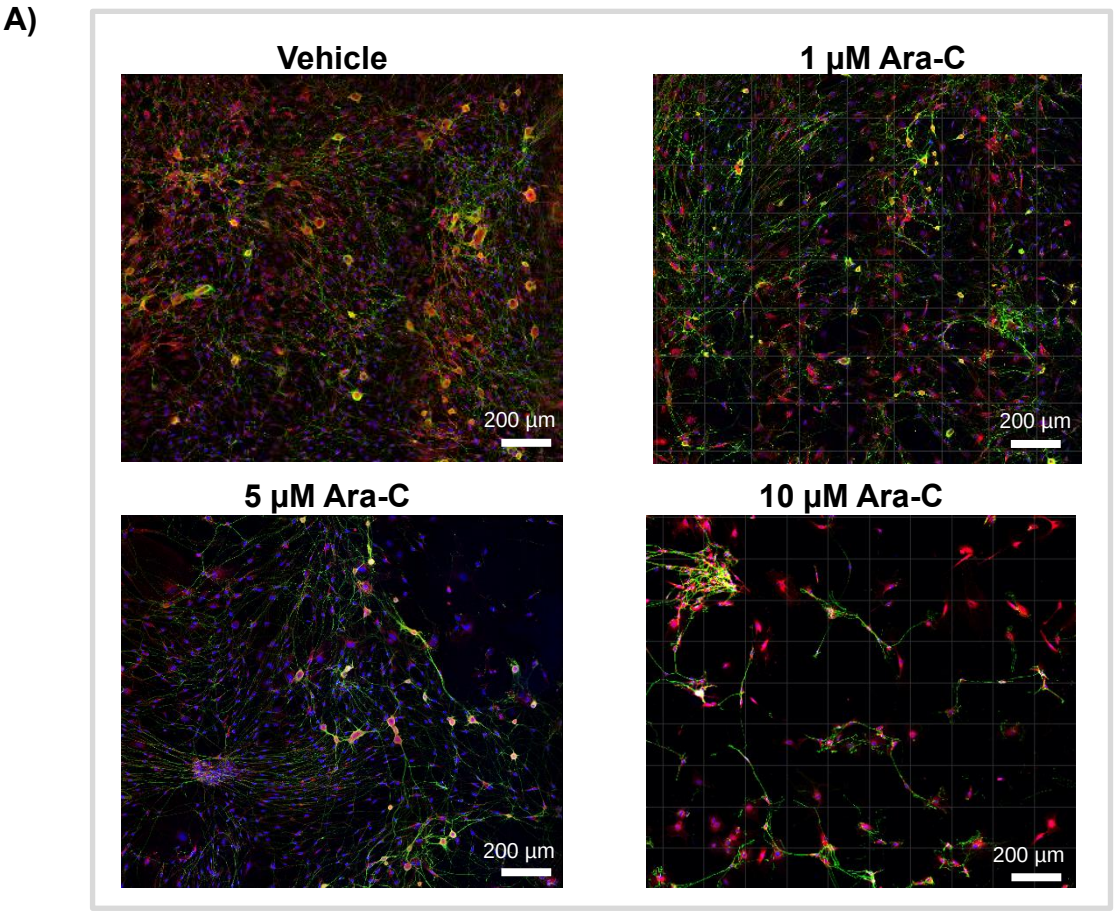

Figure 4.5: Effect of arabinose cytosine (Ara-C) on cell proliferation in nodose ganglia cultures. B) B) Quantitation of Ara-C inhibition of cellular proliferation relative to vehicle control, as measured by relative cell density. One-way ANOVA with Tukey's multiple comparisons (N=3 experiments). Different letters indicate significant differences among groups.

B)

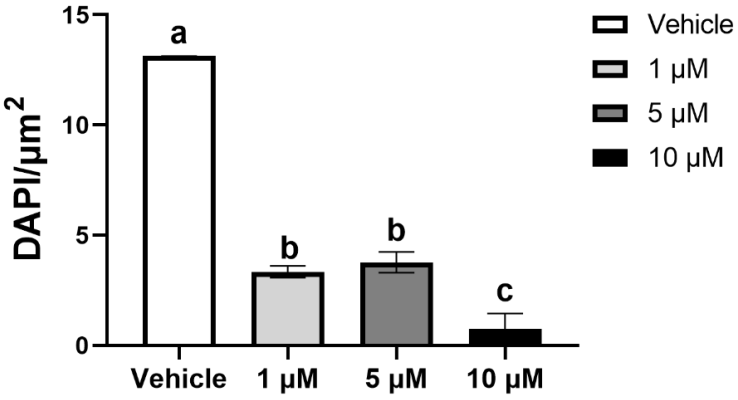

Optimizing Microfluidic Device Geometry to Support Short-Term Culture of Primary Nodose Ganglia and the Development of a Novel Gut-Brain Axis Model

In the first prototype device, immunohistochemistry data demonstrates that VAN neurites enter and project through the 750-1000 μm channels within 5 days (Figure 4.6A and B). These channels largely exclude VANs from transmigrating into the second chamber. However, we observed DAPI staining in Chamber 2, indicating that cells from the nodose ganglia cultures were not excluded by the channels.

Figure 4.6: Nodose ganglia cultures spanning chambers in first prototype device after 5 days in culture (DIV 5). A) Representative fluorescence images of nodose ganglia cultures within first prototype device showing VAN fibers entering (“Entry”) and exiting channels (“Exit”) on both sides of a CAD rendering of first prototype device. VANs stained with B-tubulin III (BT3, red) and nuclei with DAPI (blue). Scales = 100 µm.

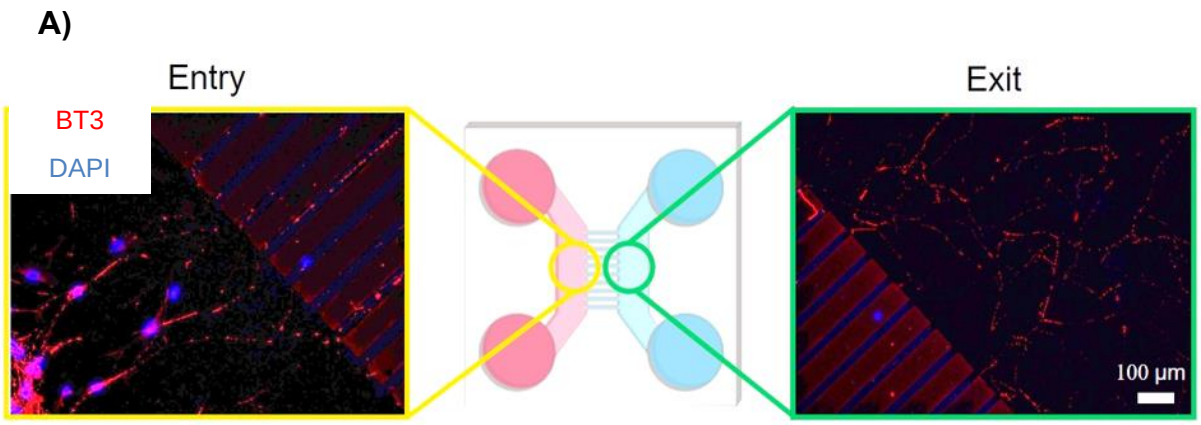

Figure 4.6: Nodose ganglia cultures spanning chambers in first prototype device after 5 days in culture (DIV 5). B) Representative fluorescent image of nodose ganglia cultures grown within prototype device with 1000 µm channel length and 25 µm channel width. VANs stained with BT3 (green), glia stained with Iba1 (red), and nuclei with DAPI (purple). Chambers are labeled to indicate where cultures are introduced (VAN = rat nodose ganglia cultures, Chamber "2" = area where cultures can be introduced to be innervated by VANs). N = 6 devices. Scales = 100 µm.

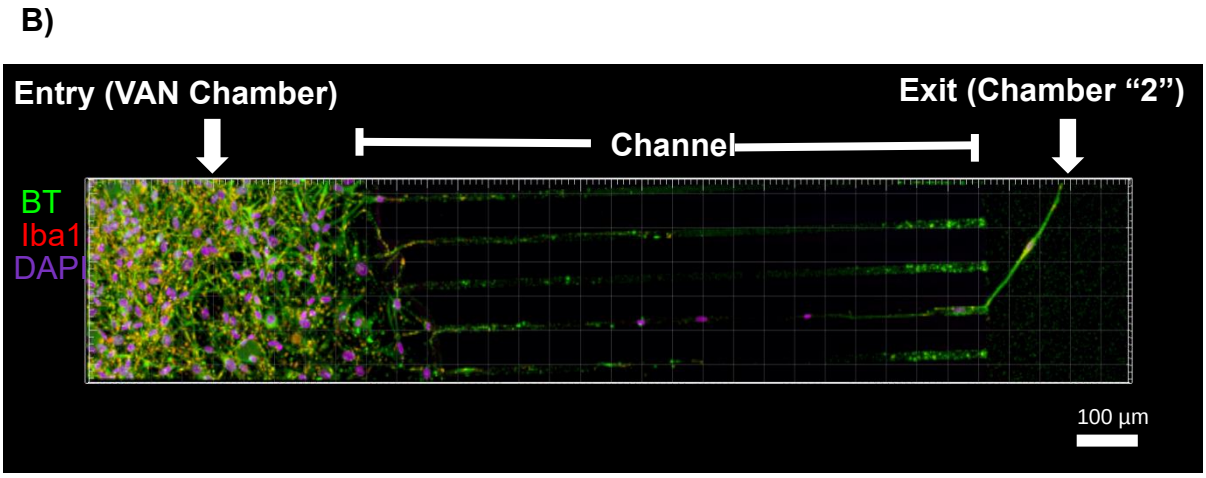

In the second prototype device (Figure 4.7A), brightfield images show that cells from the nodose ganglia culture entered channels within 3 days post-seeding (Figure 4.7B). Given their size and morphology (spindle-like appearance), they are likely glia and are presumed to be guiding VAN neurites[32] across the channels into the second chamber. Upon fixing cultures within the devices 5 days after seeding, we observed nearly every channel was populated with β-tubulin III-positive cells, indicative of VANs (Figure 4.7C). We also observed Iba1-positive cells within the channels and in the other chamber, indicating that glia are not excluded by 15 µm-wide channels. However, we did not observe β-tubulin III positive globe-like cell bodies in the opposite chamber, indicating that these channels predominately restrict VANs from entering the opposing chamber.

These preliminary data demonstrate that these microfluidic platforms can maintain primary nodose ganglia cultures for up to 5 days *in vitro*. Although both devices can support the growth of VANs *in vitro*, our preliminary data in the second prototype device suggest that changing device geometry can accelerate the rate at which cells enter the microfluidic channels. These data suggest that microfluidic platforms could facilitate the development of relevant co-culture models in future studies.

Figure 4.7: Nodose ganglia cultures span chambers in circular prototype device within 3 days in culture (DIV 3). A) Representative image of circular microfluidic device where concentric chambers, “N” (neuronal) and “E” (epithelial), are filled with blue dye. Blue dye from Chamber “N” fills channels when fluid is removed from Chamber “E”, as indicated by yellow arrow. B) Representative brightfield image of nodose ganglia cultures 3 days after seeding into Chamber “N” within circular prototype. Black arrows indicate cells that have entered channels by DIV 3. N = 3 devices. Scale = 50 µm.

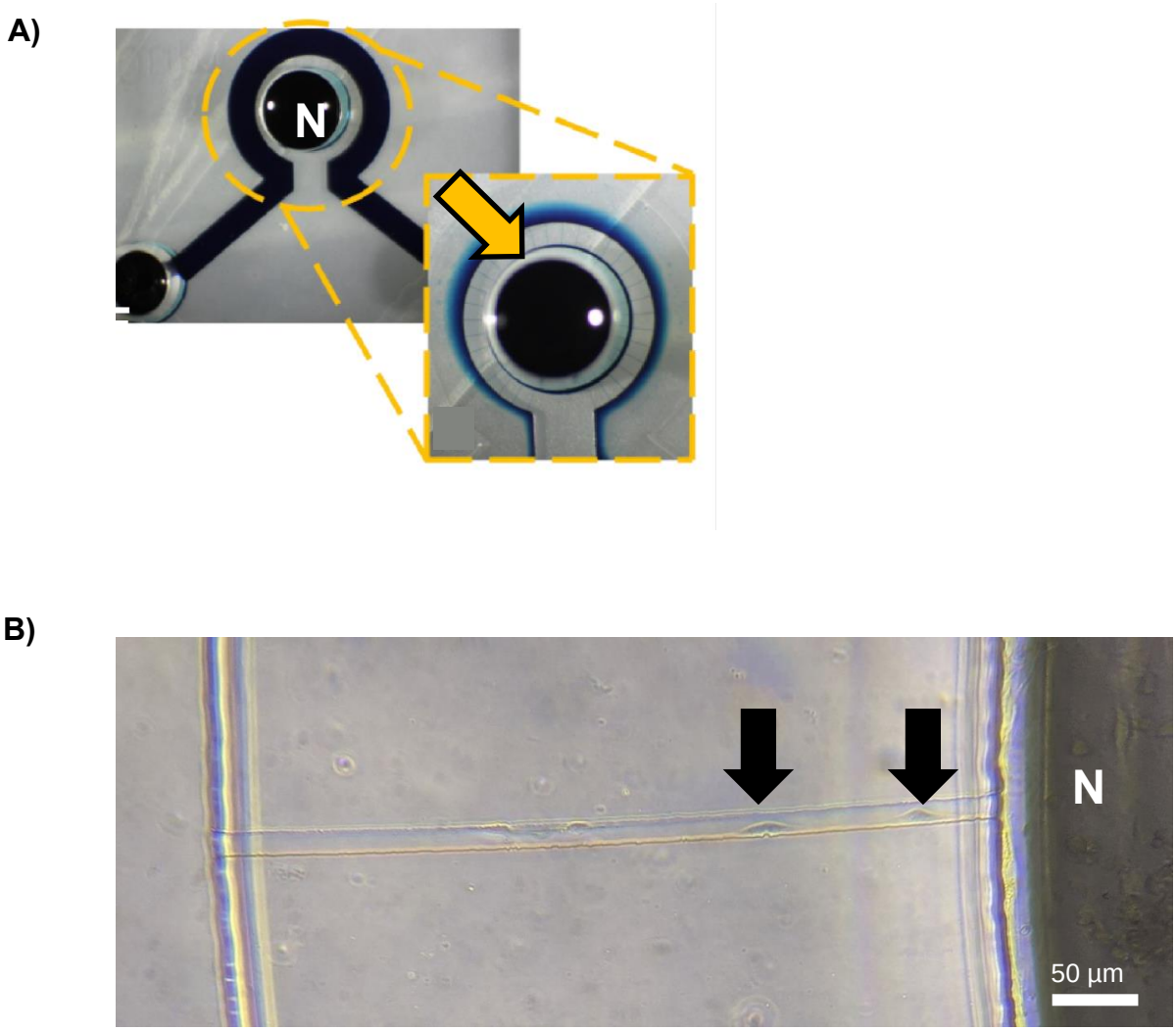

Figure 4.7: Nodose ganglia cultures span chambers in circular prototype device within 3 days in culture (DIV 3). C) Representative fluorescence image of circular prototype with 500 µm channel length (outlined by dashed white lines) and 15 µm channel width. VANs stained with B-tubulin III (BT3, red), glia stained with Iba1 (red), and nuclei with DAPI (purple). Chambers are labeled to indicate where neuronal cultures are introduced ("N" = rat nodose ganglia cultures, "E" = area where epithelial/organoid cultures can be introduced). N=3 devices. Scale = 200 µm.

C)

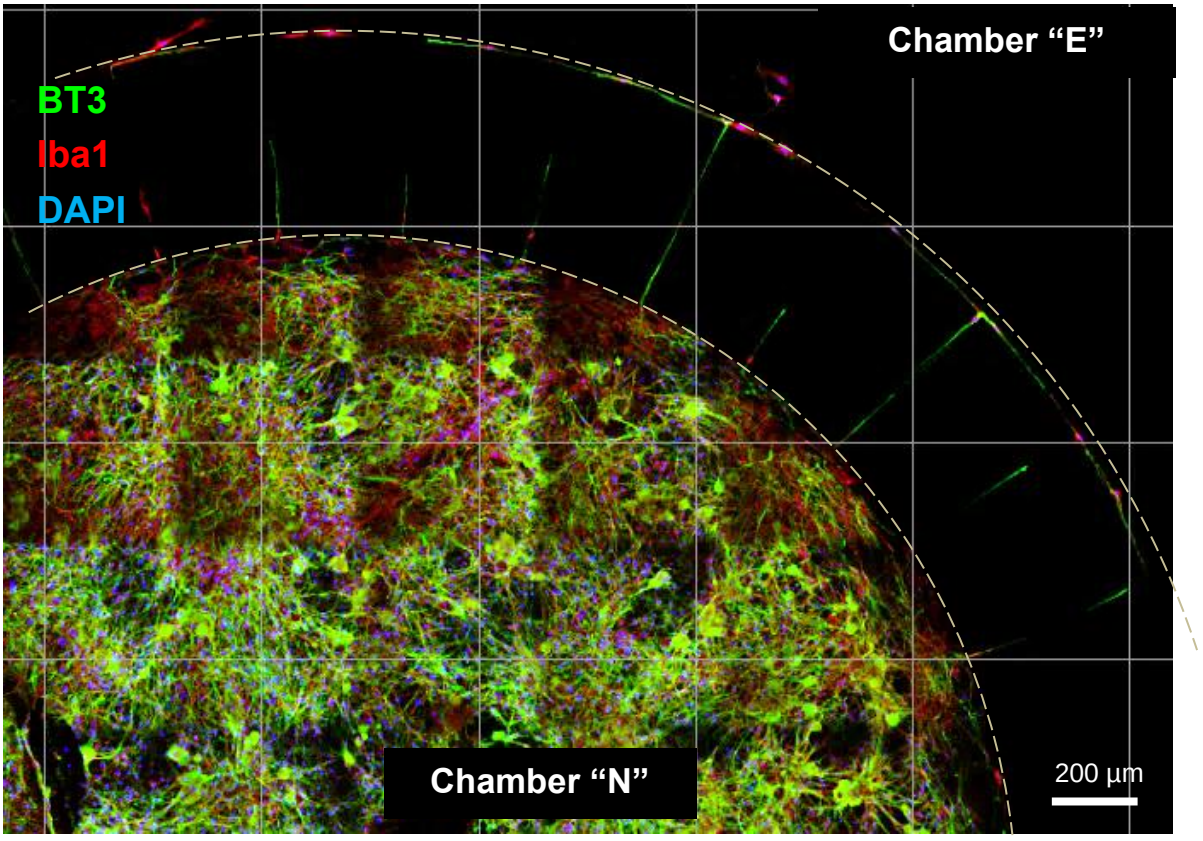

4.5: Discussion

The success of the best pharmaceutical strategies for treating obesity are primarily attributed to a reduction in food intake, which is due, in part, to the increased signaling of vagal afferent neurons (VANs)[33–35]. Current methods for screening new therapies to increase VAN activity are limited to animal models of obesity; there are no immortalized cell line models of VANs at the time this dissertation was written. In this chapter, we have demonstrated (1) an optimized method for culturing VANs *in vitro* and (2) applied this method for culturing VANs in a novel microfluidic platform. The goal of this collaborative project is to develop a scalable platform for *in situ* screening of neuroactive metabolites that increase VAN signaling, which will be accomplished in future studies.

In our first experiments for optimizing primary nodose ganglia cultures, we measured the response of VANs to CCK *in vitro*[27,28]. CCK-8S increased Ca^{2+}_i in VANs in a dose-dependent manner, indicating that these cultures are responsive to physiologically relevant levels of CCK-8S. It is important to note that these experiments measuring CCK-induced Ca^{2+}_i were some of our earliest *in vitro* experiments using VANs; they were conducted between 2019-2020 and just before our facilities were closed due to shelter-in-place orders during the COVID pandemic. We conducted baseline intracellular calcium measurements approximately one year after measuring CCK-induced intracellular calcium flux. In these later experiments, the average intracellular calcium (Ca^{2+}_i) levels in VANs was 86.88 nM ±19.05, which falls within the range of "textbook" levels of Ca^{2+}_i for neurons (~100 nM). In addition to the gap in time between these experiments, there were also some key differences in culturing conditions between these two projects:

1) VANs for measuring CCK-induced Ca^{2+}_i flux were maintained in 10% FBS whereas VANs for measuring baseline Ca^{2+}_i levels were maintained in 10% rat serum

2) Measurements of CCK-induced Ca^{2+}_i flux were conducted 72 hours after cell seeding versus measurements of CCK-induced Ca^{2+}_i flux were conducted 24 hours after cell seeding

Due to these significant differences in culturing methods, data from these experiments were not pooled, but instead treated as different experiments. Data from a single set of three experiments shown in Figure 4.4 demonstrate that rat serum significantly increases the viability of VANs relative to FBS. Taken together, these data suggest that time and serum sources should be considered when using VANs *in vitro* for research and testing effector molecules.

Fetal bovine serum (FBS) is a commonly used component in cell culture practices. It has been used since the mid-19th century in culturing cells when it was introduced by Theodore Puck[36] and is nearly ubiquitous in cell culture to this day[37]. However, its complex composition and lot-to-lot variations make it difficult to determine its role in supporting cells *in vitro*[38]*.* Furthermore, others have shown that differences between hosts of the cells and serum can be a major contributing factor to cell culture challenges[38]**.** We tested the effect of serum source on VANs by comparing the viability of rat VANs 24 hours after culturing in either commercial FBS or rat serum. For all experiments, cultured nodose ganglia and serum were harvested from the same rats. Compared to FBS, rat serum significantly improved the viability of nodose ganglia

cultures, as measured by calcein-AM and ethidium homodimer-1. Calcein-AM is a dye rendered fluorescent after it is actively transported across cell membranes thereby identifying living cells. Ethidium homodimer-1 is excluded by live cells and can only bind to the nucleus of cells with a compromised plasma membrane (i.e., dead or dying cells).

Calcein-AM also highlights viable cells in their entirety, which enables users to make gross estimates of cell morphology, such as cell size and shape. When comparing the viability of nodose ganglia cultures in FBS versus rat serum, we frequently noticed more multipolar live cells in FBS-containing media than in rat serum (qualitative observations and examples in Figure 4.4A). VANs are pseudounipolar neurons, have a globe-like cell body (examples shown in Figures 4.1A and 4.1B), and have a single proximal axon that diverges into two terminals, one sensory terminal with receptor endings and one terminal that synapses in the central nervous system. Although these multipolar cells could be a type of glia from nodose ganglia, these multipolar cells had relatively large cell bodies and had globe-like soma, which are indicative of VANs. Furthermore, these globe-shaped cells were slightly more prevalent in cultures maintained in rat serum than in cultures in FBS (qualitative observations). Even though these simple viability stains limit us from making definitive conclusions about the identity of the cells within these nodose cultures, these data suggest that culturing rat VANs in the serum of the same host increases viability and maintains native morphology of these vagal sensory neurons *in vitro*. This is important to the field because many researchers in the field using VANs *in vitro* use FBS[13,22,31]. Therefore, replacing FBS with rat serum in VAN culturing protocols may help bridge the gap between *in vitro* and *in vivo* studies thereby supporting our understanding of VANs in detecting chemosensory signals relevant to

metabolic health and disease. Future work could include characterizing the gene and protein expression profiles of VANs cultured in these different media and compare these profiles to what is observed *in vivo*.

We used CCK-conjugated saporin (CCK-SAP) as another method to determine if functional CCK receptors were expressed by VANs *in vitro.* CCK-SAP significantly reduced the relative abundance of VANs relative to unconjugated-saporin (Blank-SAP) at the same concentration (150 ng/µL), as indicated by the relative abundance of B-tubulin III, a neuron-specific marker, to DAPI. We also demonstrated that CCK-SAP was also effective at eliminating VANs at 15 ng/µL, which strongly suggests that unconjugated saporin has no effect on VANs *in vitro*; these interpretations are supported by previous findings in the literature[22]. These data support our previous observations that CCK activates VANs at physiologically relevant concentrations, as measured via calcium imaging. These data demonstrate that our method of culturing VANs supports CCK receptor-expressing cells, which is critical for our downstream applications within the microfluidic device.

Uncontrolled mitotic proliferation is a common concern when culturing primary neuronal tissue and we considered this would also present an issue in our nodose ganglia cultures within the microfluidic devices. To prevent glia from overtaking VANs in long-term primary nodose ganglia cultures (>3-day culture), we determined the minimal concentrations of cytosine β-D- (Ara-C) required to significantly reduce glia proliferation. We determined that Ara-C (1-5 µM) significantly reduced cell density relative to vehicle control. However, unlike the highest concentration tested (10 µM), Ara-C at 1-5 µM did not alter the abundance of VANs, indicated by the relative intensity of β-tubulin III

staining. These data suggest that there may be a critical threshold of glia required to support VAN growth and viability *in vitro*. Future studies could determine the effects of the density of peripheral glia on VAN excitability within the microfluidic device.

Our collaborators and others have shown that the geometry of the first microfluidic device supports the co-culture of primary cortical neuron cultures and other types of neuronal tissue[23,30,39–41]. Dissections of cortical tissue in our collaborator's lab typically yields tens of millions of cells[23,30]. However, we discovered early in the development process of a "gut-brain axis" model that the yield of primary nodose ganglia cultures is approximately 100 times lower than cortical dissections; our primary nodose ganglia harvest protocol from two rats typically yields approximately 10-40,000 total VANs, which is also supported by the literature[42]. Low cell density presented a technical obstacle in developing this model and was first addressed by increasing cell seeding density into the devices. Although the cell seeding density was still too low to fill all channels between the two chambers in the original device, the VAN neurites reached the adjacent chamber within 5 days after cell seeding. Considering the inherent limitations of the nodose cultures, a second prototype device was created that reduced chamber volumes by half and reduced channel length by half, which facilitated cells and/or neurites to enter the channels within 3 days after seeding.

Immunofluorescence confirmed that VAN neurites also crossed the channels and projected into the adjacent chamber within 5 days. Most importantly, we observed that nearly every channel of the second prototype device enclosed β-tubulin III-positive cells, indicating the presence of neuronal tubulin. Furthermore, a ring of B-tubulin III staining was observed along the inner wall of the adjacent chamber (Chamber "E"), suggesting

that future cultures seeded within Chamber “E” have the potential to be innervated. Although we have yet to seed Chamber “E” with intestinal organoids or other cultures of interest, these data show that this microfluidic model of the “gut-brain axis” is capable of supporting VANs for up to 5 days and could likely innervate primary cultures of interest.

4.6: Conclusion

This work demonstrates one method for optimizing culturing conditions of primary rat nodose ganglia. Through close collaboration with the Şeker Lab, we have applied these optimized techniques to support the development of the first microfluidic model of the “gut-brain axis” that includes vagal afferent neurons. Future work will include incorporating a micro-electrode array within the optimized device and using VANs to screen neuroactive chemical effectors relevant to animal health.

4.7: References

1. Lewandowska-Pietruszka, Z., Figlerowicz, M. & Mazur-Melewska, K. The History of the Intestinal Microbiota and the Gut-Brain Axis. *Pathog. Basel Switz.* **11**, 1540 (2022).
2. Stanton Stavney, L., Kato, T., Griffith, C. A., Nyhus, L. M. & Harkins, H. N. A physiologic study of motility changes following selective gastric vagotomy. *J. Surg. Res.* **3**, 390–394 (1963).
3. Smith, G. P., Jerome, C. & Norgren, R. Afferent axons in abdominal vagus mediate satiety effect of cholecystokinin in rats. *Am. J. Physiol.-Regul. Integr. Comp. Physiol.* **249**, R638–R641 (1985).
4. Raybould, H. E. *et al.* Detection of macronutrients in the intestinal wall. *Auton. Neurosci. Basic Clin.* **125**, 28–33 (2006).
5. Peters, J. H., Ritter, R. C. & Simasko, S. M. Leptin and CCK modulate complementary background conductances to depolarize cultured nodose neurons. *Am J Physiol Cell Physiol* **290**, 427–432 (2006).
6. de Lartigue, G. *et al.* EGR1 Is a target for cooperative interactions between cholecystokinin and leptin, and inhibition by ghrelin, in vagal afferent neurons. *Endocrinology* **151**, 3589–99 (2010).
7. Wang, Y. B., de Lartigue, G. & Page, A. J. Dissecting the Role of Subtypes of Gastrointestinal Vagal Afferents. *Front. Physiol.* **11**, (2020).
8. Egerod, K. L. *et al.* Profiling of G protein-coupled receptors in vagal afferents reveals novel gut-to-brain sensing mechanisms. *Mol. Metab.* **12**, 62–75 (2018).
9. Bai, L. *et al.* Genetic Identification of Vagal Sensory Neurons That Control Feeding. *Cell* **179**, 1129-1143.e23 (2019).

10. Goswami, C., Iwasaki, Y. & Yada, T. Short-chain fatty acids suppress food intake by activating vagal afferent neurons. *J. Nutr. Biochem.* **57**, 130–135 (2018).
11. Li, Z. *et al.* Butyrate reduces appetite and activates brown adipose tissue via the gut-brain neural circuit. *Gut* **67**, 1269–1279 (2018).
12. Lee, S. *et al.* Metabolic Responses to Butyrate Supplementation in LF-and HF-Fed Mice Are Cohort-Dependent and Associated with Changes in Composition and Function of the Gut Microbiota. *Nutrients* **12**, 3524 (2020).
13. de La Serre, C. B., de Lartigue, G. & Raybould, H. E. Chronic exposure to Low dose bacterial lipopolysaccharide inhibits leptin signaling in vagal afferent neurons. *Physiol. Behav.* **139**, 188–194 (2015).
14. De Lartigue, G., Barbier De La Serre, C., Espero, E., Lee, J. & Raybould, H. E. Diet-induced obesity leads to the development of leptin resistance in vagal afferent neurons. *Am J Physiol Endocrinol Metab* **301**, 187–195 (2011).
15. De Lartigue, G., Barbier De La Serre, C., Espero, E., Lee, J. & Raybould, H. E. Leptin Resistance in Vagal Afferent Neurons Inhibits Cholecystokinin Signaling and Satiation in Diet Induced Obese Rats. *PLoS ONE* **7**, (2012).
16. Psichas, A. *et al.* The short chain fatty acid propionate stimulates GLP-1 and PYY secretion via free fatty acid receptor 2 in rodents. *Int. J. Obes.* **39**, 424–429 (2015).
17. Shim, K. Y. *et al.* Microfluidic gut-on-a-chip with three-dimensional villi structure. *Biomed. Microdevices* **19**, (2017).
18. Bein, A. *et al.* Microfluidic Organ-on-a-Chip Models of Human Intestine. *Cmgh* **5**, 659–668 (2018).
19. Moossavi, S., Arrieta, M.-C., Sanati-Nezhad, A. & Bishehsari, F. Gut-on-chip for

ecological and causal human gut microbiome research. *Trends Microbiol.* **30**, 710–721 (2022).

20. Kasendra, M. *et al.* Development of a primary human Small Intestine-on-a-Chip using biopsy-derived organoids. *Sci. Rep.* **8**, 1–14 (2018).
21. Kim, H. J., Li, H., Collins, J. J. & Ingber, D. E. Contributions of microbiome and mechanical deformation to intestinal bacterial overgrowth and inflammation in a human gut-on-a-chip. *Proc. Natl. Acad. Sci.* **113**, E7–E15 (2016).
22. Diepenbroek, C. *et al.* Validation and characterization of a novel method for selective vagal deafferentation of the gut. *Am J Physiol Gastrointest Liver Physiol* **313**, 342–352 (2017).
23. Goshi, N. *et al.* Influence of microchannel geometry on device performance and electrophysiological recording fidelity during long-term studies of connected neural populations. *Lab. Chip* **22**, 3961–3975 (2022).
24. Waise, T. M. Z. *et al.* One-day high-fat diet induces inflammation in the nodose ganglion and hypothalamus of mice. *Biochem. Biophys. Res. Commun.* **464**, 1157–1162 (2015).
25. Lee, S. *et al.* 2'-Fucosyllactose Supplementation Improves Gut-Brain Signaling and Diet-Induced Obese Phenotype and Changes the Gut Microbiota in High Fat-Fed Mice. *Nutrients* **12**, (2020).
26. Schindelin, J. *et al.* Fiji: an open-source platform for biological-image analysis. *Nat. Methods* **9**, 676–682 (2012).
27. Simasko, S. M., Wiens, J., Karpiel, A., Covasa, M. & Ritter, R. C. Cholecystokinin increases cytosolic calcium in a subpopulation of cultured vagal afferent neurons.

Am. J. Physiol. - Regul. Integr. Comp. Physiol. **283**, R1303–R1313 (2002).

28. Rogers, R. C. & Hermann, G. E. Mechanisms of action of CCK to activate central vagal afferent terminals. *Peptides* **29**, 1716–1725 (2008).
29. McDougle, M. *et al.* Intact vagal gut-brain signalling prevents hyperphagia and excessive weight gain in response to high-fat high-sugar diet. *Acta Physiol.* **00**, (2020).
30. Goshi, N., Kim, H., Girardi, G., Gardner, A. & Seker, E. Electrophysiological Activity of Primary Cortical Neuron-Glia Mixed Cultures. *Cells* **12**, 821 (2023).
31. Peters, J. H., Karpiel, A. B., Ritter, R. C. & Simasko, S. M. Cooperative Activation of Cultured Vagal Afferent Neurons by Leptin and Cholecystokinin. *Endocrinology* **145**, 3652–3657 (2004).
32. Lago-Baldaia, I., Fernandes, V. M. & Ackerman, S. D. More Than Mortar: Glia as Architects of Nervous System Development and Disease. *Front. Cell Dev. Biol.* **8**, (2020).
33. HEISE, T. *et al.* 338-OR: Tirzepatide Reduces Appetite, Energy Intake, and Fat Mass in People with T2D. *Diabetes* **71**, 338-OR (2022).
34. Herman, G. A. *et al.* Effect of single oral doses of sitagliptin, a dipeptidyl peptidase-4 inhibitor, on incretin and plasma glucose levels after an oral glucose tolerance test in patients with type 2 diabetes. *J. Clin. Endocrinol. Metab.* **91**, 4612–4619 (2006).
35. Iwasaki, Y. *et al.* GLP-1 release and vagal afferent activation mediate the beneficial metabolic and chronotherapeutic effects of D-allulose. *Nat. Commun.* **9**, 113 (2018).
36. van der Valk, J. *et al.* Fetal Bovine Serum (FBS): Past - Present - Future. *ALTEX* **35**, 99–118 (2018).

37. Pilgrim, C. R. *et al.* A Review of Fetal Bovine Serum in the Culture of Mesenchymal Stromal Cells and Potential Alternatives for Veterinary Medicine. *Front. Vet. Sci.* **9**, (2022).
38. Gstraunthaler, G., Lindl, T. & van der Valk, J. A plea to reduce or replace fetal bovine serum in cell culture media. *Cytotechnology* **65**, 791–793 (2013).
39. Dai, C., Liu, X., Tang, R., He, J. & Arai, T. A Review on Microfluidic Platforms Applied to Nerve Regeneration. *Appl. Sci.* **12**, 3534 (2022).
40. Taylor, A. M. *et al.* A microfluidic culture platform for CNS axonal injury, regeneration and transport. *Nat. Methods* **2**, 599–605 (2005).
41. Seker, E. *et al.* The fabrication of low-impedance nanoporous gold multiple-electrode arrays for neural electrophysiology studies. (2010) doi:10.1088/0957-4484/21/12/125504.
42. Gil, K., Bugajski, A., Skowron, B. & Thor, P. Increased c-fos expression in nodose ganglion in rats with electrical vagus nerve stimulation. *Folia Med. Cracov.* **51**, 45–58 (2011).

Chapter 5:

Discussion and Conclusion

5.1: Introduction

Vagal afferent neurons (VANs) innervate the gut and relay peripheral chemosensory signals in the form of enteroendocrine hormones to the brain to regulate appetite, digestion, and feeding behavior[1–3]. Hyperphagia is an early behavioral adaptation in diet-induced obesity and is associated with peripheral changes in gut hormone signaling[4–7]. Recent innovations in obesity treatment have targeted the vagal pathway to increase satiety signaling, reduce food intake, and improve energy balance[8–12].

Successful strategies for treating obesity improve metabolic outcomes in part by promoting appetite suppression and reducing food intake. These increases in satiety are also associated with an increase in the abundance of beneficial microbial metabolites, such as tryptophan metabolites and short-chain fatty acids[13–16]. Previous work shows that VANs can detect these microbial metabolites via cell surface and nuclear receptors[17–19]. Recent studies also show that these microbial metabolites may increase satiety signaling by upregulating enteroendocrine hormone signaling pathways within the cell bodies of VANs, located within the nodose ganglia[20]. However, there is still a gap in our understanding of how beneficial microbial metabolites likely contribute to the success of weight-loss strategies. Investigating the interacting mechanisms between gut-derived hormones and microbial metabolites could support the development of new therapies for treating diet-induced hyperphagia and consequent metabolic disease.

Recent studies have revealed GPR35, a receptor for the microbial metabolite kynurenic acid (KYNA), is highly expressed by VANs and co-expressed with CCK_AR, a receptor for a key satiety hormone, cholecystokinin (CCK)[17]. Previous studies show that a high-fat diet (HFD) reduces plasma levels of KYNA[21–24] and that administration of

KYNA to diet-induced animals reduces hyperphagia, weight gain, and adiposity[23,24]. However, the role of GPR35 expressed by VANs in satiety signaling has yet to be studied. Here, an *in vitro* model and animal model of diet-induced obesity were used to determine the effects of GPR35 agonists on VAN activation and satiety signaling.

5.2 Main Findings

In Chapter 2, we determined the effects of synthetic and endogenous GPR35 agonists on VAN signaling *in vitro*. GPR35 agonists, zaprinast, kynurenic acid (KYNA), and L-N-tetraose (LNT), increased VAN signaling *in vitro* as measured by phosphorylation of ERK, and this was prevented by the GPR35 antagonist, CID-2754687. We demonstrated that acute administration of the GPR35 agonist zaprinast reduced food intake in male and female diet-induced obese mice, but not their low-fat-fed counterparts. Acute administration of zaprinast also increased the gene expression of *fos*, an early marker of neuronal activation[25,26], in the nodose ganglia of obese mice relative to vehicle control. Notably, zaprinast increased *fos* expression in the nodose of diet-induced obese mice despite an HFD-induced increase in gene expression of *KCNK3*, which has been implicated in diet-induced desensitization of VANs to peripheral satiety signals[27]. These data are significant because they suggest that zaprinast-induced satiety is dependent on diet and perhaps metabolic phenotype, but not on sex. Furthermore, these observations support previous findings showing that the administration of other GPR35 agonists, such as KYNA, reduces HFD-induced hyperphagia[25,26]. Taken together, this evidence provides a mechanism by which acute administration of GPR35 agonists suppresses diet-induced hyperphagia.

In Chapter 3, we demonstrated that GPR35 agonists, zaprinast, KYNA, and LNT increase the sensitivity of VANs to CCK, thereby demonstrating that subthreshold levels of GPR35 agonists may reduce the threshold of CCK_AR activation. This hypothesis was alternately tested *in vivo* using shRNA microinjection into the nodose ganglia to reduce GPR35 gene expression in VANs. Across three studies, we demonstrated that nodose microinjection of sh-GPR35 may not increase cumulative food intake but may alter meal patterns that are similar to early changes in diet-induced obesity. In Study 3, we found that sh-GPR35 increases the rate of ingestion during the first 6 hours of the light and dark periods to levels not significantly different from HF feeding. These data suggest that sh-GPR35 may disrupt diurnal rhythms of vagal activity as previously observed in other mouse models of diet-induced obesity. We showed that sh-GPR35 microinjection suppresses endogenous sensing of CCK, as measured by hyperphagia and gastric emptying stimulated by the CCK_AR antagonist devazepide. However, GPR35 knockdown was not sufficient to prevent GPR35 agonist zaprinast-induced satiety. This evidence suggests that GPR35 may be involved in the endogenous signaling of CCK_AR on VANs. Our data show that GPR35 knockdown was not sufficient to suppress satiety induced by acute administration of CCK_AR and GPR35 agonists, which suggests that knockdown models may not be sufficient to determine the necessity of GPR35 on VANs for detecting these agonists.

In Chapter 4, we optimized a method for culturing primary rat nodose ganglia cultures in a microfluidic platform as one leap towards developing a novel *in vitro* model of the gut-brain axis. We validated our culturing method using viability stains, calcium imaging, and immunohistochemistry and determined that primary noose ganglia can be

cultured for at least 5 days after dissection. Protocol optimization also helped direct the design of the second generation of the device, which will aid in increasing throughput. Future studies will include co-culturing with organoids and short-term exposure to gut microbiota or their derived metabolites.

5.3: Limitations

Primary nodose ganglia cultures are an established technique in our lab and have been reproduced by others[28–31]. Over the past decade, studies in the Raybould lab have been designed to improve this technique to maximize cell retention and optimize neuron-to-glia ratios and cell culture media formulation (Ehrlich and Raybould). Despite the best efforts of our lab and others to standardize culture quality and maximize cell viability, cell density is a persistent problem in primary peripheral ganglia culture. Culture quality and viability significantly impacted the output rate and quality of the data collected from these *in vitro* models and represent a significant source of variance in these experiments. In addition, cell density was a limiting factor in what experiments we could feasibly conduct *in vitro* (e.g., sh-GPR35 knockdown).

Rats were used in primary nodose ganglia cultures instead of mice to reduce the number of animals needed to sufficiently power a study; rat nodose ganglia contain significantly more neurons than mouse nodose ganglia[32]. However, the *in vivo* studies in this thesis examining the effects of GPR35 on feeding behavior were conducted in mice. Therefore, experiments were designed to prevent generalizing the function of GPR35 on VANs across species. Both models had their inherent limitations. For example, knockdown of GPR35 using shRNA was concentration-dependent, which prevented us from reducing GPR35 expression *in vitro*. On the other hand, the GPR35 antagonist

CID-274567 had limited solubility in aprotic solvents, which prevented us from accurately testing the effects of acute GPR35 inhibition on food intake in mice. Despite these inherent and different limitations in both models, our independent observations across these two models demonstrate that effective GPR35 inhibition impairs not only the activation of GPR35 but also CCK_AR. In this case, the inherent limitations of the two models discussed in Chapter 2 strengthened our interpretation of the data.

Perhaps the most significant limitation in this thesis is the efficacy and reliability of shRNA to reduce the gene expression of GPR35 (sh-GPR35). When these experiments were conducted, no VAN-specific GPR35 knockout mouse model was available. Therefore, nodose microinjection of sh-GPR35 was the best available method to determine the effects of GPR35 signaling on satiety in mice. Although the manufacturer had determined the efficacy of the vector *in vitro*, there were no published studies in the literature regarding its efficacy or side effects *in vivo*. Previous studies demonstrate that nodose microinjection of shRNA reduces the expression of other G-protein coupled receptors *in vivo*[33]. However, the studies described in this thesis are the first to evaluate the efficacy of sh-GPR35 *in vivo*. Our data suggest that the shRNA vector may induce acute inflammation in the nodose ganglia of mice following injection, as measured by *Iba-1* upregulation, which subsides within four weeks of surgery. Furthermore, there was significant variation in the level of GPR35 knockdown in the nodose ganglia between Studies 2-4. Our data from Study 3 show that this is primarily due to variability on the individual level and may be attributed to either the efficacy or durability of the shRNA vector. Due to limitations in sample size, we did not pursue RNA sequencing of these nodose ganglia following knockdown to determine how GPR35 knockdown

influenced other pathways, such as CCK_AR signaling pathways. Finally, our interpretations of GPR35 knockdown on feeding behavior and satiety signaling in mice are limited to male mice.

5.4: Future Directions

To our knowledge, we conducted the first experiments testing the satiating effects of the GPR35 agonist zaprinast on diet-induced obese mice. Our priorities in these studies were to determine the effects of zaprinast on HF-induced hyperphagia. Since there was very little data regarding its tolerability in mice, we refrained from testing the effects of repeated zaprinast injection on inhibiting diet-induced weight gain. Previous unpublished work in our lab shows that chronic administration of water-soluble GPR35 agonists reduces diet-induced weight gain in male mice. Therefore, future studies could use a modified method, such as implantable osmotic pumps, to determine the effects of chronic zaprinast administration on inhibiting diet-induced weight gain and hyperphagia in mice.

The largest technical hurdle in these *in vivo* studies was the GPR35 knockdown studies. Although we carefully considered and controlled for variability in housing, surgery, and treatment, our data suggest that the shRNA vector changes animal feeding behavior and diet-induced hyperphagia. Future studies could include the development of an inducible VAN- or $Na_V1.8$-specific knockout of GPR35. An inducible tissue specific GPR35 knockout would eliminate not only the effects of surgery on feeding behavior but also the effects of maternal microbiota on animal behavior. This method would also enable us to accurately determine the effects of GPR35 on VANs in age-matched female mice from the same litters.

The microfluidic model of the “gut-brain axis” is the first of its kind to include VANs. Challenges with optimizing cell density optimization and throughput could be addressed by reducing the culture surface area and increasing the replicates per platform. Important follow-up studies could also characterize the lifetime of primary VAN cultures on the microfluidic platform to determine the timeline of longitudinal studies.

5.5: Conclusion

The findings of these studies demonstrate that GPR35 plays a role in peripheral satiety signaling at the level of vagal afferent neurons (VANs). The first data chapter demonstrates that GPR35 agonists increase satiation in mice with diet-induced hyperphagia, regardless of sex. The second data chapter validates the findings of previous literature showing that GPR35 is co-expressed with CCK_AR on VANs in mice and also demonstrates that GPR35 may be involved in peripheral sensing of endogenous CCK to modulate feeding behaviors in male mice. In an interdepartmental collaboration presented in the third chapter, we demonstrated that this *in vitro* model of VANs can be adapted to a microfluidic platform for the identification and characterization of neuroactive metabolites. Overall, these studies have helped characterize GPR35 on VANs in the context of satiety signaling and have contributed to the development of a novel microfluidic model of VANs for screening neuroactive metabolites for the treatment of diet-induced obesity.

5.6: References

1. Berthoud, H. R. & Neuhuber, W. L. Functional and chemical anatomy of the afferent vagal system. *Auton. Neurosci. Basic Clin.* **85**, 1–17 (2000).
2. Wang, Y. B., de Lartigue, G. & Page, A. J. Dissecting the Role of Subtypes of Gastrointestinal Vagal Afferents. *Front. Physiol.* **11**, (2020).
3. Han, W. *et al.* A Neural Circuit for Gut-Induced Reward. *Cell* 1–14 (2018) doi:10.1016/j.cell.2018.08.049.
4. Abarca-GÃ, L. *et al.* Worldwide trends in body-mass index, underweight, overweight, and obesity from 1975 to 2016: a pooled analysis of 2416 population-based measurement studies in 128·9 million children, adolescents, and adults NCD Risk Factor Collaboration (NCD-RisC)*. *The Lancet* **390**, 2627–2642 (2017).
5. Bellisle, F. & Blundell, J. E. Satiation, satiety: Concepts and organisation of behaviour. in *Satiation, Satiety and the Control of Food Intake* 3–11 (Elsevier Ltd., 2013). doi:10.1533/9780857098719.1.3.
6. Berthoud, H.-R. The vagus nerve, food intake and obesity. *Regul. Pept.* **149**, 15–25 (2008).
7. de Lartigue, G., Ronveaux, C. C. & Raybould, H. E. Deletion of leptin signaling in vagal afferent neurons results in hyperphagia and obesity. *Mol. Metab.* **3**, 595–607 (2014).
8. HEISE, T. *et al.* 338-OR: Tirzepatide Reduces Appetite, Energy Intake, and Fat Mass in People with T2D. *Diabetes* **71**, 338-OR (2022).
9. Sisley, S. *et al.* Neuronal GLP1R mediates liraglutide's anorectic but not glucose-lowering effect. *J. Clin. Invest.* **124**, 2456–2463 (2014).
10. Lear, S. *et al.* Engineering of a Potent, Long-Acting NPY2R Agonist for Combination

with a GLP-1R Agonist as a Multi-Hormonal Treatment for Obesity. *J. Med. Chem.* **63**, 9660–9671 (2020).

11. Wang, L. *et al.* Engineered Bacteria of MG1363-pMG36e-GLP-1 Attenuated Obesity-Induced by High Fat Diet in Mice. *Front. Cell. Infect. Microbiol.* **11**, (2021).
12. Irwin, N., Pathak, V. & Flatt, P. R. A Novel CCK-8/GLP-1 Hybrid Peptide Exhibiting Prominent Insulinotropic, Glucose-Lowering, and Satiety Actions With Significant Therapeutic Potential in High-Fat–Fed Mice. *Diabetes* **64**, 2996–3009 (2015).
13. Schlittler, M. *et al.* Endurance exercise increases skeletal muscle kynurenine aminotransferases and plasma kynurenic acid in humans. *Am. J. Physiol. - Cell Physiol.* **310**, C836–C840 (2016).
14. Schubert, M. M., Sabapathy, S., Leveritt, M. & Desbrow, B. Acute exercise and hormones related to appetite regulation: A meta-analysis. *Sports Med.* **44**, 387–403 (2014).
15. Arakawa, R. *et al.* Prospective study of gut hormone and metabolic changes after laparoscopic sleeve gastrectomy and Roux-en-Y gastric bypass. *PLOS ONE* **15**, e0236133 (2020).
16. Paganelli, F. L. *et al.* Roux-Y Gastric Bypass and Sleeve Gastrectomy directly change gut microbiota composition independent of surgery type. *Sci. Rep.* **9**, 10979 (2019).
17. Egerod, K. L. *et al.* Profiling of G protein-coupled receptors in vagal afferents reveals novel gut-to-brain sensing mechanisms. *Mol. Metab.* **12**, 62–75 (2018).
18. Bai, L. *et al.* Genetic Identification of Vagal Sensory Neurons That Control Feeding. *Cell* **179**, 1129-1143.e23 (2019).

19. Kupari, J., Hä Ring, M., Agirre, E., Alo Castelo-Branco, G. & Ernfors, P. An Atlas of Vagal Sensory Neurons and Their Molecular Specialization Cell Reports Resource An Atlas of Vagal Sensory Neurons and Their Molecular Specialization. *CellReports* **27**, 2508-2523.e4 (2019).
20. Cook, T. M. *et al.* Vagal neuron expression of the microbiota-derived metabolite receptor, free fatty acid receptor (FFAR3), is necessary for normal feeding behavior. *Mol. Metab.* **54**, 101350 (2021).
21. Poulain-Godefroy, O. *et al.* Induction of TDO2 and IDO2 in Liver by High-Fat Feeding in Mice: Discrepancies with Human Obesity. *Int. J. Tryptophan Res. IJTR* **6**, 29–37 (2013).
22. Lee, K.-J. *et al.* High-Fat Diet and Voluntary Chronic Aerobic Exercise Recover Altered Levels of Aging-Related Tryptophan Metabolites along the Kynurenine Pathway. *Exp. Neurobiol.* **26**, 132–140 (2017).
23. Agudelo, L. Z. *et al.* Kynurenic Acid and Gpr35 Regulate Adipose Tissue Energy Homeostasis and Inflammation. *Cell Metab.* **27**, 378-392.e5 (2018).
24. Li, J. *et al.* The Beneficial Effects of Edible Kynurenic Acid from Marine Horseshoe Crab (Tachypleus tridentatus) on Obesity, Hyperlipidemia, and Gut Microbiota in High-Fat Diet-Fed Mice. *Oxid. Med. Cell. Longev.* **2021**, (2021).
25. Zittel, T. T. *et al.* C-fos protein expression in the nucleus of the solitary tract correlates with cholecystokinin dose injected and food intake in rats. *Brain Res.* **846**, 1–11 (1999).
26. Wang, L., Martínez, V., Barrachina, M. D. & Taché, Y. Fos expression in the brain induced by peripheral injection of CCK or leptin plus CCK in fasted lean mice. *Brain*

Res. **791**, 157–166 (1998).

27. Park, S. J. *et al.* Increased TASK channel-mediated currents underlie high-fat diet induced vagal afferent dysfunction. *Am. J. Physiol.-Gastrointest. Liver Physiol.* **315**, G592–G601 (2018).
28. de Lartigue, G. *et al.* EGR1 Is a target for cooperative interactions between cholecystokinin and leptin, and inhibition by ghrelin, in vagal afferent neurons. *Endocrinology* **151**, 3589–99 (2010).
29. Diepenbroek, C. *et al.* Validation and characterization of a novel method for selective vagal deafferentation of the gut. *Am J Physiol Gastrointest Liver Physiol* **313**, 342–352 (2017).
30. Peters, J. H., Ritter, R. C. & Simasko, S. M. Leptin and CCK modulate complementary background conductances to depolarize cultured nodose neurons. *Am J Physiol Cell Physiol* **290**, 427–432 (2006).
31. Peters, J. H., Karpiel, A. B., Ritter, R. C. & Simasko, S. M. Cooperative Activation of Cultured Vagal Afferent Neurons by Leptin and Cholecystokinin. *Endocrinology* **145**, 3652–3657 (2004).
32. Kaelberer, M. M. & Jordt, S.-E. A Method to Target and Isolate Airway-innervating Sensory Neurons in Mice. *J. Vis. Exp. JoVE* 53917 (2016) doi:10.3791/53917.
33. Krieger, J.-P. *et al.* Knockdown of GLP-1 Receptors in Vagal Afferents Affects Normal Food Intake and Glycemia. *Diabetes* **65**, 34–43 (2016).